

Department of Earth and Environmental Sciences

PhD program: Chemical, Geological and Environmental Sciences, Cycle XXXVI

Curriculum: Geological Sciences

CENOZOIC BENTHIC FORAMINIFERAL ASSOCIATIONS AS TOOLS FOR PALAEOENVIRONMENTAL AND STRATIGRAPHIC RECONSTRUCTIONS

Surname: Mariani Name: Luca

Registration number: 789314

Tutor: Prof. Marco Giovanni Malusà

Co-tutors: Dott. Giovanni Coletti; Prof. Guillem Mateu Vicens

Supervisor: Prof.ssa Elisa Malinverno

Coordinator: Prof. Marco Giovanni Malusà



INDEX

1- Introduction and aim of the work.....	7
2- Modern shallow water carbonates. Global neritic carbonate sediment distribution: allochem continuum along an energy gradient.....	9
2.1- Abstract.....	9
2.2- Introduction.....	10
2.3- Methodology.....	10
2.4- Results and discussion.....	12
2.5- Conclusions.....	14
3- Cenozoic Shallow water carbonates. Palaeocene to Miocene southern Tethyan carbonate factories: a meta-analysis of the successions of South-western and Western Central Asia.....	18
3.1- Abstract.....	18
3.2- Introduction.....	19
3.3- Geological context.....	20
3.4- Materials and methods.....	21
3.5- Results.....	23
3.5.1- Epochs.....	24
3.5.2- Rupelian–Burdigalian detailed analysis.....	26
3.5.3- Statistical analysis.....	27
3.6- Discussion.....	29
3.6.1- Carbonate factories evolution.....	29
3.6.2- Regional and global implications.....	36
3.7- Conclusions.....	39
4- Foraminifera.....	49
4.1- Introduction.....	49
4.2- Foraminiferal biology.....	50
4.3- Ecology of small benthic foraminifera.....	53
4.4- Ecology of large benthic foraminifera.....	55
4.4.1- Distribution of large benthic foraminifera.....	61
5- Epiphytic foraminifera. Testing an indirect palaeo-seagrass indicator: Benthic foraminifera from the Lower Pleistocene <i>Posidonia</i> meadow of Fauglia (Tuscany, Italy).....	65
5.1- Abstract.....	65
5.2- Introduction.....	66

5.3- Geological setting.....	68
5.4- Materials and methods.....	71
5.5- Results.....	75
5.5.1- Field observations and stratigraphic section.....	75
5.5.2- Foraminiferal analysis.....	75
5.5.2.1- Mode-1: Classification with miliolids.....	77
5.5.2.2- Mode-2: Classification without miliolids.....	78
5.5.2.3 Keeled/Rounded ratio.....	78
5.6- Discussion.....	87
5.6.1- The exceptional preservation of <i>Posidonia oceanica</i> and the diagenetic imprint on the foraminiferal association.....	87
5.6.2- Epiphytic foraminifera analysis.....	89
5.7- Conclusions.....	94
6- Epiphytic foraminifera. Benthic foraminifera as proxy for fossil seagrass from the Lower Pleistocene deposits of the Stirone River (Emilia-Romagna, Italy).....	102
6.1- Abstract.....	102
6.2- Introduction.....	102
6.3- Geological setting.....	106
6.4- Materials and methods.....	108
6.4.1- Field work.....	108
6.4.2- Sediments and foraminiferal analysis.....	108
6.4.2.1- Granulometry and foraminiferal assemblages.....	108
6.4.2.2- Environmental indices.....	109
6.5- Results.....	113
6.5.1- Field observations and stratigraphic section.....	113
6.5.2- Foraminiferal analysis and skeletal assemblage.....	113
6.6- Discussion.....	118
6.6.1- Foraminiferal assemblages in a seagrass-related environment.....	118
6.6.2- Comparison with a similar study site: the case of Fauglia.....	124
6.6.3- The usefulness of K/R _{EXT} index: insights and perspectives.....	126
6.7- Conclusions.....	127

7- Palaeoenvironmental and stratigraphic reconstruction of the Lower-Middle Eocene Foraminiferal Limestone of Pag Island (Croatia).....	135
7.1- Abstract.....	135
7.2- Introduction.....	136
7.3- Geological setting.....	138
7.3.1- The Dinaric Foreland Basin.....	138
7.3.2- Pag Island sequence.....	140
7.4- Materials and methods.....	142
7.4.1- Field work.....	142
7.4.2- Laboratory analysis.....	143
7.5- Results.....	145
7.5.1- Field work.....	145
7.5.2- Microfacies analysis.....	149
7.6- Discussion.....	156
7.6.1- Biostratigraphy.....	156
7.6.2- Facies interpretation and palaeoenvironmental reconstruction.....	157
7.6.3- Calculated parameters.....	163
7.6.4- The advantages of quantitative analysis.....	164
7.7- Conclusions.....	165
8- Skeletal assemblages and terrigenous input in the Eocene carbonate systems of the Nummulitic Limestone (NW Europe).....	172
8.1- Abstract.....	172
8.2- Introduction.....	172
8.3- Geological setting.....	174
8.3.1- The Paleogene succession.....	174
8.3.2- Stratigraphic ages.....	178
8.4- Materials and methods.....	178
8.5- Results.....	180
8.5.1- Mortola.....	181
8.5.2- Loreto.....	186
8.5.3- Braux.....	192
8.5.4- Lauzanier.....	196

8.6- Discussion.....	198
8.6.1- Biostratigraphy of the Nummulitic Limestone.....	198
8.6.2- Facies interpretation and paleoenvironmental reconstruction.....	200
8.6.3- Controls on carbonate factories distribution.....	202
8.7- Conclusions.....	204
9- Discussion and conclusions.....	211

1. Introduction and aim of the work

The aim of this doctoral thesis is the detailed palaeontological study of different benthic foraminiferal associations characteristic of various localities, but all framed within shallow-water carbonate successions deposited during the Cenozoic. Combining the analysis of large and small benthic foraminifera with the analysis of the other organisms preserved in the fossil record, it is possible to obtain a more detailed understanding of the palaeoenvironment and, where possible, of the stratigraphy. As will be shown later in this thesis, the majority of the associations studied are related to seagrass environments. Therefore, special attention has been given to this type of environment, whose clear identification in the geological record can often be challenging.

Shallow water carbonate-producing environments consist of exceptionally diverse and effective carbon sinks on Earth. Nevertheless, the impact of alterations in ocean chemistry and climate on these settings is a subject of intense debate. Examining Earth's geological records provides a crucial perspective on how these systems might respond to significant changes. However, these environments have limitations in preserving geochemical signals, emphasizing the significance of microfacies (i.e., the comprehensive sedimentological and paleontological data derived from thin sections, peels, polished slabs, or rock samples) as a crucial investigative approach. Furthermore, the study of modern oceans and of more recent environments (e.g., Quaternary) is essential to calibrate the tools used for the reconstruction of older environments (e.g., Palaeogene). In the context of my research, these tools consist mainly of quantitative experimental parameters derived from i) the counting of benthic foraminifera (specially separated into different groups to make standardized counts), and ii) the point counting analysis conducted on the entire skeletal assemblage. These analyses can provide valuable information on the characteristics of depositional paleoenvironments in terms of paleobathymetry, paleotemperature, nutrients, transport etc.

Benthic foraminifera are particularly suited for quantitative palaeoenvironmental analyses: i) they are widespread, ii) they are present in large quantities even in small-sized samples, which makes them particularly convenient to sample and analyse, iii) they are easily preserved in the fossil record (except for specific diagenetic conditions), iv) they provide reliable palaeoecological and stratigraphic information, and v) they can be recognized quite easily at genera/species level. Thus, the research that I carried out focuses on the study of large and small benthic foraminifera that are present in different carbonate and mixed carbonate/terrigenous successions dating back to a time interval between the early Eocene and the Holocene. Moreover, considering such an extended time interval throughout the Cenozoic has given the opportunity to obtain information and acquire knowledge about the evolution and differentiation of this category of organisms over time.

This thesis unfolds in the following manner. Initially, two introductory review papers, for which I have collaborated, will be presented and will serve as an introduction and general context. These papers discuss the distribution of carbonate-producing organism relative to modern and fossil environments. This type of information is important to understand how carbonate producers respond, and responded, to various ecological parameters and to provide a global, quantitative and standardised overview of this, in particular focusing on shallow-water carbonates. Subsequently, the focus will shift to seagrass environments, emphasizing the importance of the analysis of this type of settings, even in paleontology, with the aim of understanding how these might evolve in the future in response to changes in climate conditions. At this point, benthic foraminifera will be introduced, specifically the epiphytic ones, stressing their importance as environmental and palaeo-seagrass proxies. In this regard, the focus will be given to two Pleistocene settings, i) Fauglia (Tuscany, Italy) and ii) Stirone River (Emilia-Romagna, Italy); and to five Eocene successions exposed at iii) Pag Island (Croatia), and iv) Western Liguria (Italy) and South-Eastern France. Furthermore, a concluding chapter will address, in the light of the obtained results, the significance of benthic foraminifera as environmental and stratigraphic indicators, potential avenues for further research, and the possible application of these findings in analysing the future evolution of shallow-water carbonate environments.

2. Modern shallow water carbonates. Global neritic carbonate sediment distribution: allochem continuum along an energy gradient

This chapter is taken from the scientific paper:

Bialik, O. M., Coletti, G., Mariani, L., Commissario, L., Desbiolles, F., Niyonkuru Meroni, A. (2023). Global neritic carbonate sediment distribution: allochem continuum along an energy gradient. *Scientific Reports*, submitted.

2.1 Abstract

The study of carbonate rocks is primarily reliant on microfacies analysis, which is strongly based on the comparison with modern allochem assemblages. Despite the existence of several models aimed at comprehensively explaining, on the basis abiotic factors, the distribution of carbonate-producing organisms, a global, quantitative and standardised overview of the composition of shallow-water carbonate sediments is still missing. Aiming to address this gap in knowledge, the current study provides a global database of the available quantitative data on neritic carbonate sediments. This is paired with satellite-based observations for the abiotic parameters. The results highlight a non-linear, multi-variable, dependence in the distribution of allochems and suggest that depth, temperature and trophic state are, to a certain extent, interchangeable. The implication of which is a level of non-uniqueness for paleoenvironmental interpretation. The resulting distribution is rather continuous and stretches along an energy gradient. A gradient extending from solar energy, with autotrophs and symbiont-bearing organisms to chemical energy with heterotrophs. Further, quantitative data from modern oceans are still required to disentangle the remaining elements of uncertainty.

2.2 Introduction

Shallow water carbonate-producing settings are some of the most diversity-rich and carbon-absorbing localities on Earth. Yet their fate in light of changes to ocean chemistry and climate is highly debated^{1,2}. The Earth's past is a key window into how these systems will respond to such dramatic changes. However, these environments do not preserve geochemical signals well, making inferences from the constituents and texture - i.e. microfacies - a critical means of investigation³⁻⁵. A microfacies is the total of all sedimentological and paleontological data that can be inferred from thin sections, peels and polished slabs or rock samples⁶. The interpretation of these microfacies is, supposedly, based on the comparison with the modern ocean. Initially, allochem assemblages were classed together into large boxes such as chlorozoan or foramol⁷. As more data became available, further segmentation was required to account for the wide variability observed in nature^{8,9}. More recently, various conceptual models, aimed at comprehensively explaining allochem assemblages based on the main abiotic factors, were proposed by several authors¹⁰⁻¹³. This is despite detailed examinations of facies

together with abiotic parameters often suggesting that there is no clear differentiation based on composition¹⁴. The current approach has been either to look at the end members through a broad qualitative view, or to investigate a local dataset and infer from it on a global scale. The former without examining the details; the latter without properly accounting for the existing variability displayed by global carbonate-producing assemblages. Data on modern allochem assemblages is actually very rarely reported in a detailed fashion with open data. Often, only the information relative to the facies is provided. This results in an artificial reduction of the internal variability of any examined system. Meanwhile, biological/ecological datasets are challenging to compare to sedimentary assemblages due to the high abundance of organic mass in the former. Combined, these problems significantly hinder large-scale analysis and make robust tests of facies models difficult. Several attempts have been made to glean insights on the future evolution of marine environments from the global record of past shallow-water carbonates^{15–18}. However, our limitations in the comprehension of modern systems and the absence of quantitative data greatly hinder these efforts. To address these issues, this study attempts to compile and standardise a comprehensive database, one which encompasses as much available information on modern marine neritic carbonate sediments. Taking into account as much as possible of the total variability of these systems, this work aims to inform on the mechanisms that regulate allochem assemblages, without any pre-existing expectations or a priori assumptions.

2.3 Methodology

Information on carbonate sediments composition from modern marine environments was aggregated from multiple sources, including data repositories, peer-reviewed papers, books, theses and reports. In total 3730 samples were identified (Figure 2.1). For 2264 of them, clear quantitative information on the grain composition could be extracted. In total 2062 were within the depth bracket of euphotic and mesophotic zones (here set to 200 m). Of these 2034 localities were paired with satellite-based time series to assess the effect of the abiotic factors. Satellite-based abiotic parameters tested here include: sea surface temperature (SST), chlorophyll α concentrations (Chl α), light attenuation coefficient for a wavelength of 490 nm (KD), and available light at depth (SW). In addition, water depth (WD) and latitude (LAT) were included as abiotic parameters. Multiple sources did not have the information in tabular form but rather as graphical representation (pie charts, column charts, map symbols etc.). These and non-digital tables in older sources have been manually digitised and integrated into the database. The different sources had no consistency in the categories reported, with different elements separated, lumped or completely unreported. In order to minimise zeros in the allochem variables, we grouped observative data into 9 consistent allochem categories, which could

be established for most data sources: Molluscs (Mol), symbiont-bearing colonial corals (SBCC), red calcareous algae (RCA), foraminifera (For), *Halimeda* (Hal), Echinodermata (Ech), sessile benthic filter feeders (SBFF; including bryozoans, barnacles, serpulids, brachiopods and deep-water corals), mobile arthropoda (MA), bioclasts (BC; other types of carbonate producers) and non-skeletal grains (NSG). Multivariate statistical analysis of these allochem categories and abiotic parameters was then performed. Since the distributions of the abiotic parameters were not normal, the median of the seasonal cycle was used as the centrality index rather than the mean. Analyses were implemented to the dataset using R and PAST softwares^{19,20}. Additional spatial analyses were performed with QGIS. Data preparation followed the recommended workflow outlined in Bialik et al.²¹. A detailed explanation of the methods and methodology is provided in Supplement 1. It should be stressed that this dataset is imperfect. Different reporting approaches between the different sources (Supplement 2) resulted on some elements not always being reported. These notably include grain size, fish detritus, terrigenous fraction, and lime mud abundance. The latter two are particularly relevant given the influence of terrigenous supply on benthic carbonate producers²² and the importance of lime mud as a possible marker of high-temperature / high alkalinity^{23,24}. These different ways of reporting data also introduce biases to the dataset which are hard to account for or may be unknown. An additional bias relates to sample distribution, with only 16% of samples collected north or south of 30° and many areas (e.g., Persian Gulf, Red Sea, South China Sea, Gulf of California) being under-sampled.

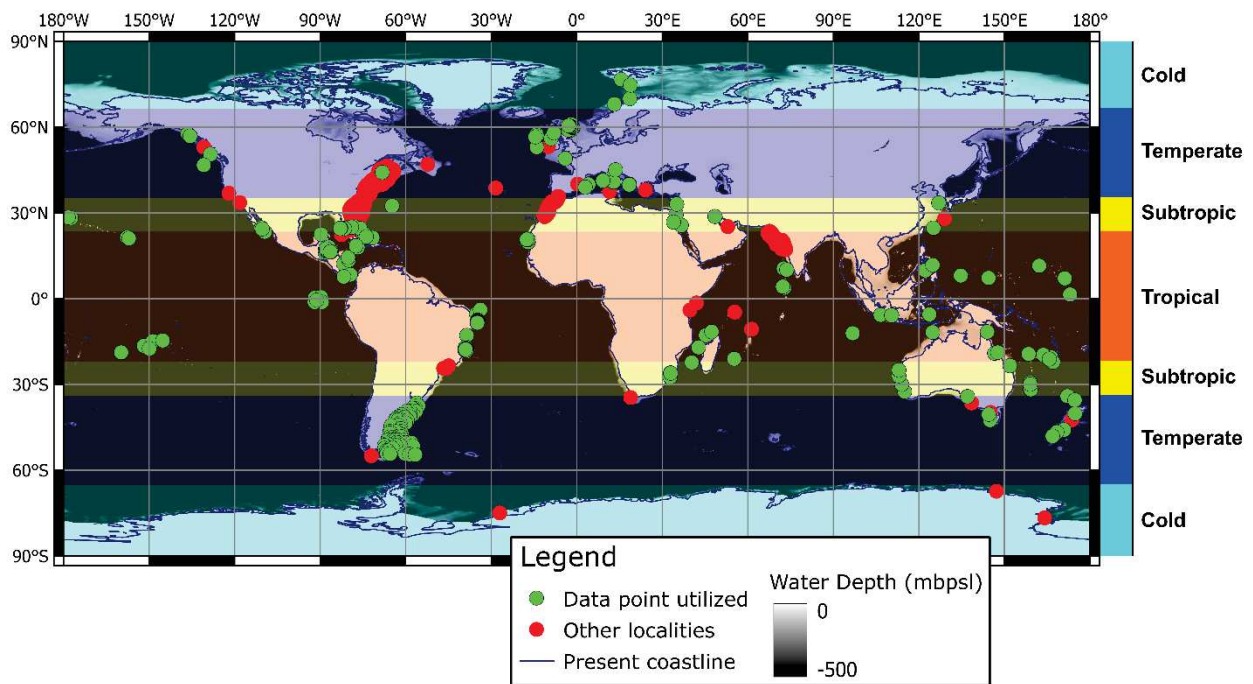


Figure 2.1 Location map of data points aggregated for this study and delineation of the climate belts discussed in the text. Green points are locations for which sufficient information was available; red points are locations for which some description exists, but no quantitative data.

2.4 Results and discussion

The dataset represents information on allochem assemblages from all continents (excluding Antarctica, Figure 2.1) and a wide range of environmental conditions, from very cold to very warm ($-0.2\text{ }^{\circ}\text{C}$ to $29.7\text{ }^{\circ}\text{C}$ of SST), as well as from extremely oligotrophic to mesotrophic. Only 427 samples are from euphotic depth ($<30\text{ m}$), while most of the samples are from mesophotic conditions. Despite that, the average depth of the samples was $21.2\pm 31\text{ m}$ below present sea level. Light radiation flux (light availability) ranges between 252.7 W/m^2 and 0.0 W/m^2 ($\bar{x} = 99.63\pm 73.4\text{ W/m}^2$). The most abundant allochems in the data set (Figure 2.2) are molluscs ($\bar{x} = 26.6\pm 20.8\%$), followed by SBCC ($\bar{x} = 20.2\pm 20.9\%$). Molluscs occurred in nearly all samples (98% of samples), whereas SBCC were reported only between 29°S and 32°N (74% of samples). The least abundant were MA ($\bar{x} = 0.5\pm 1.7\%$) and echinoderms ($\bar{x} = 2.6\pm 5.0\%$). Foraminifera and RCA occur in 90% and 74% of samples, respectively, but usually in low abundance ($\bar{x}_{\text{For}} = 11.1\pm 13.3\%$; $\bar{x}_{\text{RCA}} = 11.7\pm 15.0\%$). Other carbonate producers were reported in 59% of samples and NSG only in 32%. It is unclear if the latter is due to the terminology used or their actual absence (the latter is assumed for our study).

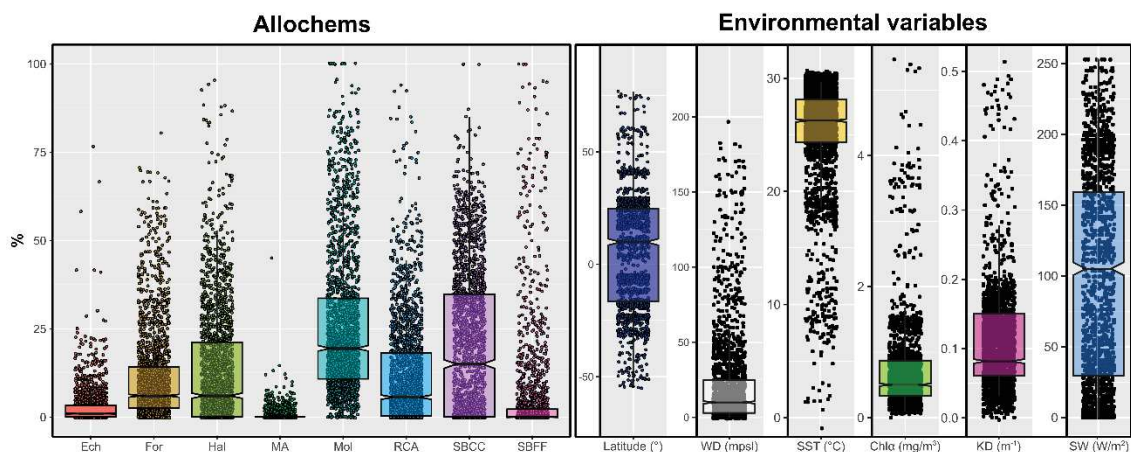


Figure 2.2 Box and whiskers plot showing the range of all the variables discussed in this study. See text from abbreviations.

Analysis of the correlations between different allochem categories shows little to no correlation between the different categories nor between the categories and abiotic parameters (Figure 2.3). Despite that, the size of the dataset allows the detection of statistically significant correlations ($p\text{-value} < 0.01$) even for relatively low correlation coefficients. The most robust correlation observed is between SBCC, water depth ($\rho = -0.58$), SST ($\rho = 0.58$), and light availability at depth ($\rho = 0.60$). This is well consistent with known limitations on SBCC habitat range. *Halimeda* is the only other group which exhibits a similar relationship with light availability and temperature but with a lower

coefficient. In contrast, SBFF exhibits the mirror image: positive correlation to water depth ($\rho=0.44$) and negative to SST ($\rho=-0.43$) and light availability ($\rho=-0.43$).

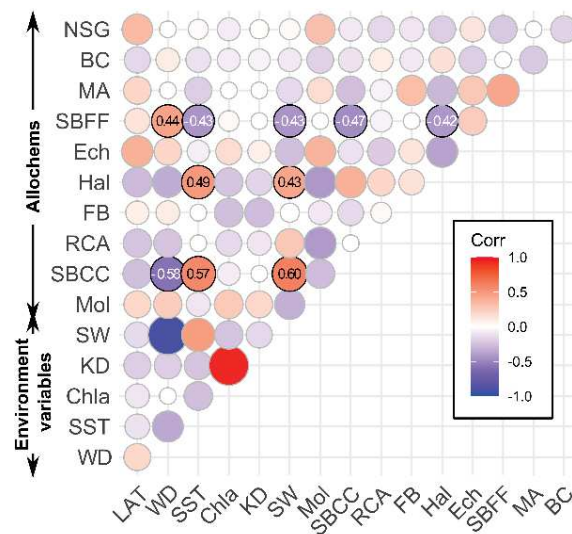


Figure 2.3 Correlation matrix with Spearman’s ρ for all the variables analysed in this study. Note that SW is a function of WD while KD is a function of Chl α , and as such, their correlation is expected. Red indicates a positive correlation, and Blue negative. Cells with no statistical significance were left uncoloured.

The absence of single-variable correlations here is taken as an indication of non-linear multi-variable dependence in the distribution of allochems. As such, to infer a relationship a multi-variant analysis is required. Multiple ordination methods have been applied to the dataset (including PCA, DCA, NMDS and CCA; see Supplement 1). In none of these methods, a clear differentiation between “T-Type” and “C-Type” carbonate factories (*sensu* Schlager, 2005) was observed. Rather, all analyses exhibited a continuous gradient. Most of the variance in this multi-variant gradient occurred on two main axes, the principal of which was loaded by SBCC, *Halimeda* and RCA (phototrophs) in one direction and by echinoderms, SBFF, MA and molluscs (heterotrophs) in the other direction (Figure 2.4). Foraminifera, bioclasts and NSG do not form major loads on that axis. This may be due to the possible biasing in reporting for bioclasts and NSG. For foraminifera, a different bias exists as most reports did not differentiate between larger benthic foraminifera (LBF) and smaller benthic foraminifera. Would a proper differentiation for foraminifera be available, based on their known distributions^{25,26}, LBF would likely group with the phototrophs. The environmental variables exhibit similar variability, with one main axis with SST and light in one direction (associated with the phototrophs), vs. KD, chlorophyll α , latitude (representing climate belts), and water depth in the other (associated with the heterotrophs) (Figure 2.4). Water depth and latitude mostly converge, with higher latitude assemblages overlapping with deeper water assemblages. These results, paired with prior observations challenging classical hydrodynamic zoning^{27,28}, require some reevaluation of

microfacies interpretation. The observations here suggest that depth, temperature and trophic state are essentially interchangeable to a certain extent, resulting in a level of non-uniqueness. That is to say, for example, that the loss of a phototrophic group in an assemblage (e.g., SBCC), may be due to cooling or sea level rise or turbidity. This does not mean that there is no environmental information inferable from the allochem assemblage, rather that multiple factors can cause the same change. The findings here point to the energy source being a key parameter in determining the allochem assemblage. Energy availability and utilisation dictate physiology²⁹. Organisms which can harness solar energy directly prevail in environments where its availability (either directly or in the form of temperature) is the highest. Organisms which obtain their energy from chemical sources (e.g., the breakdown of sugars sourced from other organisms) prevail where the availability of these is highest and do not compete with the former group in their optimal habitat. Therefore, allochem assemblage can inform directly on the trophic state of the environment, but caution must be applied when extrapolating this to relative sea-level changes if no geometrical, paleogeographical or paleontological information is available. It is also important to stress that the absence of differentiation between the “T-Type” and “C-Type” carbonate factories reported here refers to allochem assemblages, not to geometries. That said, extrapolating from the findings here and in light of detailed work done on geometries of carbonate deposits^{30,31}, the “T-Type” and “C-Type” geometries may similarly represent end-members along a gradient. A gradient that goes from prevailing solar energy to prevailing chemical energy.

2.5 Conclusions

Microfacies is a key tool in paleoenvironmental reconstruction. The inference of past environments based on the compositions of allochem assemblages and rock textures is a cornerstone of carbonate sedimentology. The results presented here suggest that these allochem assemblages exist on a multi-dimensional continuum that does not differentiate between “carbonate factories”. Similarly, there is a convergence between environmental variables such as depth and climate belts. These findings stress the need for more caution in water-depth reconstruction purely based on microfacies, as allochem assemblages appear to be most dependent on energy availability (either from solar or chemical/biological sources). This work is the first step towards a reevaluation of the microfacies paradigm relying on an evidence-based approach. This is still an incomplete endeavour as at this time there is limited information for parameters like terrigenous supply, carbonate mud abundance, as well as deconvolution of the distribution of the various types of non-skeletal grains and of foraminifera. This work has also limited itself only to direct measurements. It is likely that more dimensions (such as alkalinity and nutrients) from models and extrapolations would add further information. We

implore researchers, both those working on modern and ancient deposits, to embrace a more quantitative and standardised approach and to make their data available. Generally, more data and work on modern and ancient environments using a quantitative and consistent approach is required to improve our ability to reconstruct the past, understand the present, and forecast the future.

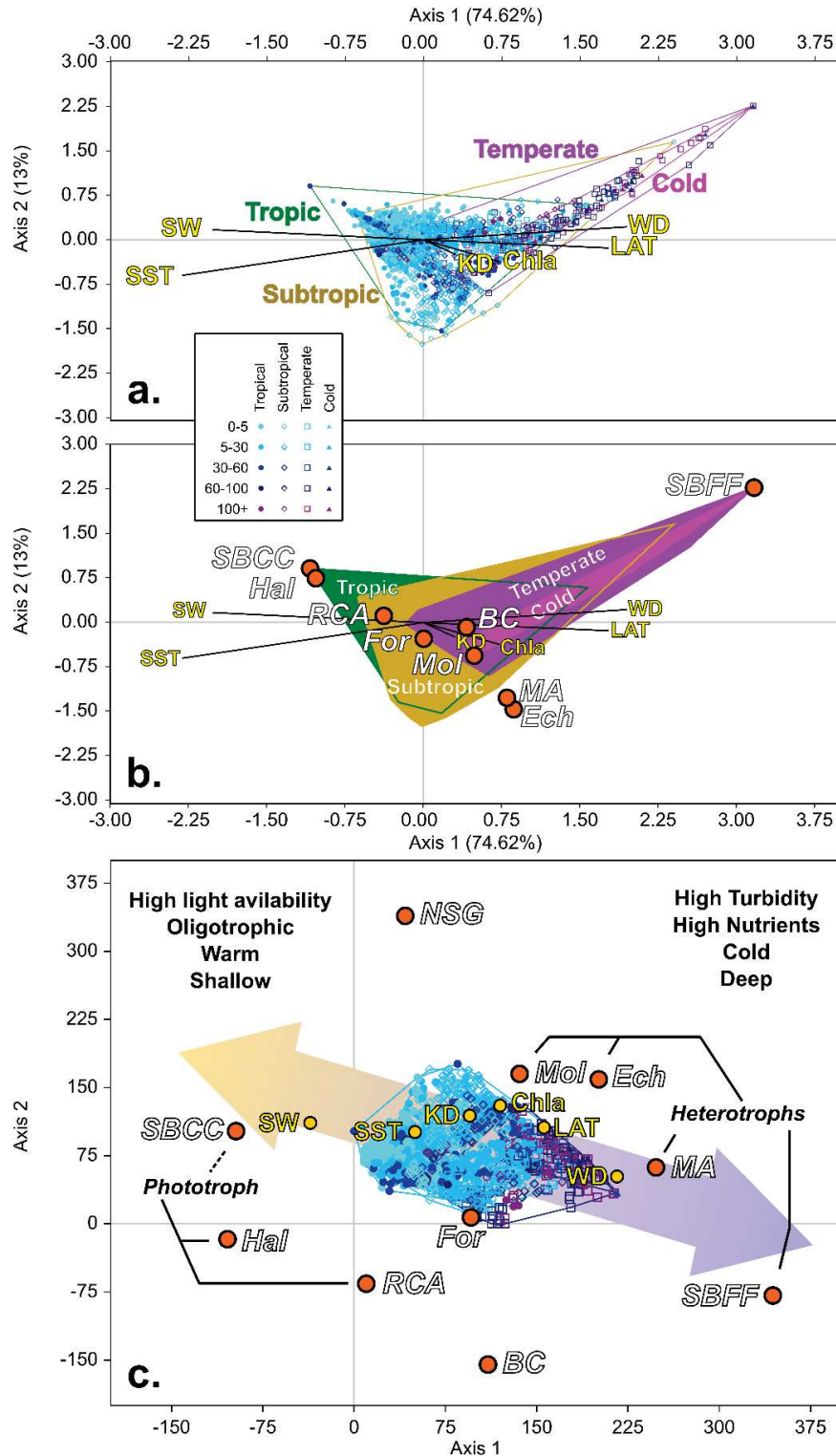


Figure 2.4 Ordination analysis. a. CCA analysis showing the data points with respect to environmental variables and climate belts grouping. b. As above but showing allochems vectors without data points. c. DCA analysis with all variables and data points, specific allochems groups are noted; arrow and additional text are for visualisation.

Acknowledgments

This work had not been supported directly by any external funding. OMB is partially supported by the German (GEOMAR) - Israeli (University of Haifa) Helmholtz International Laboratory EMS-FORE. The authors are also grateful to Andrea Giulia Varzi for her help in cross-checking the position of data points.

Data availability

All data will be made available online via repository upon acceptance. All data and additional information on the methods are available online through the FigShare repository at <https://figshare.com/s/9e41576427eb4d86350a>.

References

1. Silverman, J., Lazar, B., Cao, L., Caldeira, K. & Erez, J. Coral reefs may start dissolving when atmospheric CO₂ doubles. *Geophys. Res. Lett.* 36, L05606 (2009).
2. Reddin, C. J., Aberhan, M., Raja, N. B. & Kocsis, Á. T. Global warming generates predictable extinctions of warm- and cold-water marine benthic invertebrates via thermal habitat loss. *Global Change Biology* 28, 5793–5807 (2022).
3. Milliman, J. D., Müller, G. & Förstner, U. Recent Sedimentary Carbonates - Part 1: Marine Carbonates. (Springer Berlin Heidelberg, 1974). doi:10.1007/978-3-642-65528-9.
4. Wilson, J. L. Principles of Carbonate Sedimentation. in *Carbonate Facies in Geologic History* 1–19 (Springer New York, 1975). doi:10.1007/978-1-4612-6383-8_1.
5. Tucker, M. E. & Wright, V. P. *Carbonate Sedimentology*. (Blackwell Publishing Ltd., 1990). doi:10.1002/9781444314175.
6. Flügel, E. *Microfacies of Carbonate Rocks: Analysis, Interpretation and Application*. (Springer Berlin Heidelberg, 2010). doi:10.1007/978-3-642-03796-2.
7. Lees, A. & Buller, A. T. Modern temperate-water and warm-water shelf carbonate sediments contrasted. *Marine Geology* 13, M67–M73 (1972).
8. Carannante, G., Esteban, M., Milliman, J. D. & Simone, L. Carbonate lithofacies as paleolatitude indicators: problems and limitations. *Sedimentary Geology* 60, 333–346 (1988).
9. Hayton, S., Nelson, C. S. & Hood, S. D. A skeletal assemblage classification system for non-tropical carbonate deposits based on New Zealand Cenozoic limestones. *Sedimentary Geology* 100, 123–141 (1995).
10. *Cool-Water Carbonates*. (SEPM (Society for Sedimentary Geology), 1997). doi:10.2110/pec.97.56.
11. *Carbonate Sedimentology and Sequence Stratigraphy*. (SEPM (Society for Sedimentary Geology), 2005). doi:10.2110/csp.05.08.
12. Laugié, M., Michel, J., Pohl, A., Poli, E. & Borgomano, J. Global distribution of modern shallow-water marine carbonate factories: a spatial model based on environmental parameters. *Sci Rep* 9, 16432 (2019).
13. Reijmer, J. J. G. Marine carbonate factories: Review and update. *Sedimentology* 68, 1729–1796 (2021).
14. Halfar, J., Godinez-Orta, L., Mutti, M., Valdez-Holguín, J. E. & Borges, J. M. Nutrient and temperature controls on modern carbonate production: An example from the Gulf of California, Mexico. *Geol* 32, 213 (2004).
15. *Phanerozoic Reef Patterns*. (SEPM (Society for Sedimentary Geology), 2002). doi:10.2110/pec.02.72.
16. Pandolfi, J. M. & Kiessling, W. Gaining insights from past reefs to inform understanding of coral reef response to global climate change. *Current Opinion in Environmental Sustainability* 7, 52–58 (2014).
17. Pomar, L., Baceta, J. I., Hallock, P., Mateu-Vicens, G. & Basso, D. Reef building and carbonate production modes in the west-central Tethys during the Cenozoic. *Marine and Petroleum Geology* 83, 261–304 (2017).
18. Coletti, G. et al. Palaeocene to Miocene southern Tethyan carbonate factories: A meta-analysis of the successions of South-western and Western Central Asia. *The Depositional Record* 8, 1031–1054 (2022).

19. Hammer, Ø., Harper, D. A. T. & Ryan, P. D. PAST: paleontological statistics software package for education and data analysis. *Palaeontologia Electronica* 4, (2001).
20. R Core Team. R: A Language and Environment for Statistical Computing. <http://www.r-project.org/> (2020).
21. Bialik, O. M., Jarochowska, E. & Grossowicz, M. Ordination analysis in sedimentology, geochemistry and palaeoenvironment—Background, current trends and recommendations. *Depositional Rec* 7, 541–563 (2021).
22. Lokier, S. W., Wilson, M. E. J. & Burton, L. M. Marine biota response to clastic sediment influx: A quantitative approach. *Palaeogeography, Palaeoclimatology, Palaeoecology* 281, 25–42 (2009).
23. Bialik, O. M., Sisma-Ventura, G., Vogt-Vincent, N., Silverman, J. & Katz, T. Role of oceanic abiotic carbonate precipitation in future atmospheric CO₂ regulation. *Sci Rep* 12, 15970 (2022).
24. Geyman, E. C. et al. The origin of carbonate mud and implications for global climate. *Proc. Natl. Acad. Sci. U.S.A.* 119, e2210617119 (2022).
25. Beavington-penney, S. Ecology of extant nummulitids and other larger benthic foraminifera: applications in palaeoenvironmental analysis. *Earth-Science Reviews* 67, 219–265 (2004).
26. Murray, J. W. Ecology and applications of benthic foraminifera. (Cambridge University Press, 2006).
27. Peters, S. E. & Loss, D. P. Storm and fair-weather wave base: A relevant distinction? *Geology* 40, 511–514 (2012).
28. Betzler, C. et al. Carbonate platform drowning caught in the act: The sedimentology of Saya de Malha Bank (Indian Ocean). *Sedimentology* 70, 78–99 (2023).
29. Kooijman, B. Dynamic Energy Budget Theory for Metabolic Organisation. (Cambridge University Press, 2009). doi:10.1017/CBO9780511805400.
30. Pomar, L. & Kendall, C. G. St. C. Architecture of Carbonate Platforms: A Response to Hydrodynamics and Evolving Ecology. in *Controls on Carbonate Platform and Reef Development* (eds. Lukasik, J. & Simo, J. A. (Toni)) (SEPM (Society for Sedimentary Geology), 2008). doi:10.2110/pec.08.89.
31. Williams, H. D., Burgess, P. M., Wright, V. P., Della Porta, G. & Granjeon, D. Investigating Carbonate Platform Types: Multiple Controls and a Continuum of Geometries. *Journal of Sedimentary Research* 81, 18–37 (2011).

3. Cenozoic Shallow water carbonates. Palaeocene to Miocene southern Tethyan carbonate factories: a meta-analysis of the successions of South-western and Western Central Asia

This chapter is taken from the scientific paper:

Coletti, G., Commissario, L., Mariani, L., Bosio, G., Desbiolles, F., Soldi, M. & Bialik, O. M. (2022). Palaeocene to Miocene southern Tethyan carbonate factories: A meta-analysis of the successions of South-western and Western Central Asia. *The Depositional Record*, 8, 1031–1054. <https://doi.org/10.1002/dep2.204>

3.1 Abstract

One hundred and forty-four published successions of shallow-water carbonates, deposited between the Palaeocene and the Miocene, from the Levant to the Himalayas, have been re-analysed using a standardised approach to investigate the distribution of carbonate facies and carbonate-producing organisms. Large benthic foraminifera were found to be the volumetrically most important group of carbonate producers during the whole period, with a peak in abundance during the Eocene. Colonial corals are relatively abundant during the Palaeocene and Miocene, their abundance peaks during the Oligocene and has a minimum during the Eocene. Red calcareous algae have a similar pattern although their peak in abundance covers both the Oligocene and Miocene. Green calcareous algae decrease from the Palaeocene onward. Facies related to very shallow and/or restricted marine conditions peak during the Miocene and in particular during the Aquitanian. Both the pattern of large benthic foraminifera and of colonial corals seems to be related to temperature, with warm periods favouring the former group and cool periods the latter group. Red calcareous algae display a pattern similar to that of colonial corals suggesting that the periods favourable for one group are, on a large scale, also favourable for the other. The progressive decrease of green calcareous alga could be tentatively related to a preservation bias connected to the transition from Palaeogene assemblages that included presumably calcitic taxa of green algae to Neogene assemblages entirely constituted by aragonitic taxa with limited preservation potential. The Aquitanian peak in facies related to very shallow and/or restricted marine conditions is most likely connected to the progressive narrowing of the Tethys related to the collision between Arabia and Eurasia. These results denote an overall agreement between the abundance of the various types of shallow-water carbonate facies and large-scale environmental and geological processes, highlighting the potential for palaeoenvironmental reconstruction locked in the shallow-water record.

3.2 Introduction

Earth's biosphere is the result of a complex and ever-changing balance. Biomes can migrate geographically, expand, recede or disappear entirely with new ones arising to take their place. These environmental shifts have been recorded in the fossil record. While many biomes leave limited trace of their existence, others, like tropical carbonate factories, produce massive sedimentary successions that testify to their evolution through time. Carbonate factories represent both the space where biological carbonate sediments are produced and the associations of carbonate-producing organisms (Schlager, 2003; Tucker & Wright, 1990; Wright & Burchette, 1996). Since a sizable share of the benthic organisms inhabiting the biomes of the carbonate factories (e.g., corals, molluscs, calcareous algae, foraminifera) possess a mineralised skeleton, generally either calcite, aragonite or a combination of both, their remains have a high preservation potential and can accumulate in rock-forming quantities. Thanks to this massive and widespread fossil record, it is possible to use carbonate factories as a proxy for studying the changes in the climate of the planet through time (Bosellini & Perrin, 2008; Halfar & Mutti, 2005; Perrin & Bosellini, 2012; Perrin & Kiessling, 2012; Pomar et al., 2017; Wilson, 2008). The distribution of carbonate factories and their palaeoenvironmental implications have been extensively reviewed at both regional and global scale (Halfar & Mutti, 2005; Johnson et al., 2008; Kiessling et al., 1999, 2002; Nebelsick et al., 2005; Pomar et al., 2017). However, these studies often encounter two main limitations. The first is the lack of quantitative data, which significantly hinders any large-scale analysis and accurate comparison of sedimentary successions. The second limitation relates to the geographic distribution of case studies, with the overwhelming majority of well-studied carbonate successions being located in the European area for historical reasons. This study tries to overcome both of these limitations by compiling a database that summarises the distribution of Cenozoic carbonate facies of South-western and Western Central Asia. With this meta-analysis, the intent is to reconstruct the large-scale patterns of carbonate factories and discuss their palaeoenvironmental implications. This vast region of the world is characterised by extensive carbonate successions deposited during the Cenozoic in the shallow water of the Tethys. The presence of large hydrocarbon reservoirs in these successions (especially in Iran; Amirshahkarami et al., 2007a, 2007b; Coletti et al., 2017; Perry & Choquette, 1985) provides us with a trove of information scattered in individual publications which have not been considered in a larger framework. These papers provide a sizable and invaluable dataset for the investigation of the distribution of carbonate factories and carbonate producers, and to better grasp the global evolution of shelfal biomes during the Cenozoic.

3.3 Geological context

The regions referred to here as South-western and Western Central Asia consists of land masses mostly located south of the suture line between the African-Arabian and Indian plates and the Eurasian plate (Figure 3.1). During the Palaeocene to early Miocene, this area was occupied by part of the Tethys Ocean that separated the African, Arabian and Indian landmasses (Gondwanian derived fragments) in the south from the Eurasia in the north (Figure 3.1). During the entirety of the investigated period (Palaeocene–Miocene) the Tethys Ocean was mainly located at tropical latitudes (Dercourt et al., 2000; Rögl, 1999; Scotese, 2014a, 2014b). This, combined with an overall warm climate punctuated by extremely warm spikes during the early Palaeogene (Barnet et al., 2019; Miller et al., 2020; Zachos et al., 2001), favoured the deposition of shallow-water carbonates (and, at times, evaporites) along Tethys' shelves through most of the investigated time interval. These carbonates formed in a wide variety of environments, ranging from open shelves to restricted embayments and from nutrient-rich to oligotrophic settings, providing a comprehensive overview of the various types of carbonate factories of the Cenozoic. The northward movement of the African, Arabian and Indian landmasses caused the progressive closure of the Tethys Ocean (Garzanti et al., 2016; Hu et al., 2016; Robertson et al., 2012). The initial collision between the Indian and Eurasian plates took place around 60-61 Ma (An et al., 2021; Hu et al., 2016), leading to the end of marine sedimentation in Tibet and in the Indus Basin (i.e., the western part of the study area) during the Eocene (Afzal et al., 2009, 2011b; Ahmad et al., 2016; Blondeau et al., 1986) (Figure 3.1). The collision between the Arabian and Eurasian plates probably initiated during the latest Eocene-early Oligocene and was entirely completed before *ca* 14 Ma (middle Miocene) (Agard et al., 2011; Ballato et al., 2010; Bialik et al., 2019; Cornacchia et al., 2018; Gholami Zadeh et al., 2021), leading to the end of marine sedimentation in most of the Mesopotamian and Iranian regions (i.e. the central part of the study area) during the Miocene (Al-Juboury & McCann, 2008; Ameen-Lawa & Ghafur, 2015; Mohammadi et al., 2013; Mossadegh et al., 2009; Reuter et al., 2009; Sadooni & Alsharhan, 2019; Sissakian, 2013; Ziegler, 2001) (Figure 3.1). The Arabian and Levant regions (i.e., the eastern and central part of the study area), during the late Eocene–Oligocene, were also affected by a regional uplift testified by large hiatuses (Agard et al., 2011; Al-Juboury & McCann, 2008; Alsharhan & Nairn, 1995; Avni et al., 2012; Bernecker, 2014; Buchbinder et al., 2005; Coletti et al., 2019; Farouk et al., 2013; Sadooni & Alsharhan, 2019; Whittle et al., 1995). This event has been related to the development of the Afar Dome and the opening of the Red Sea (Avni et al., 2012; Bernecker, 2014; Ziegler, 2001). Both geodynamic processes progressively affected the Tethyan marine environments that are now exposed as outcrops in this vast area running from western Tibet to the south-eastern Mediterranean.

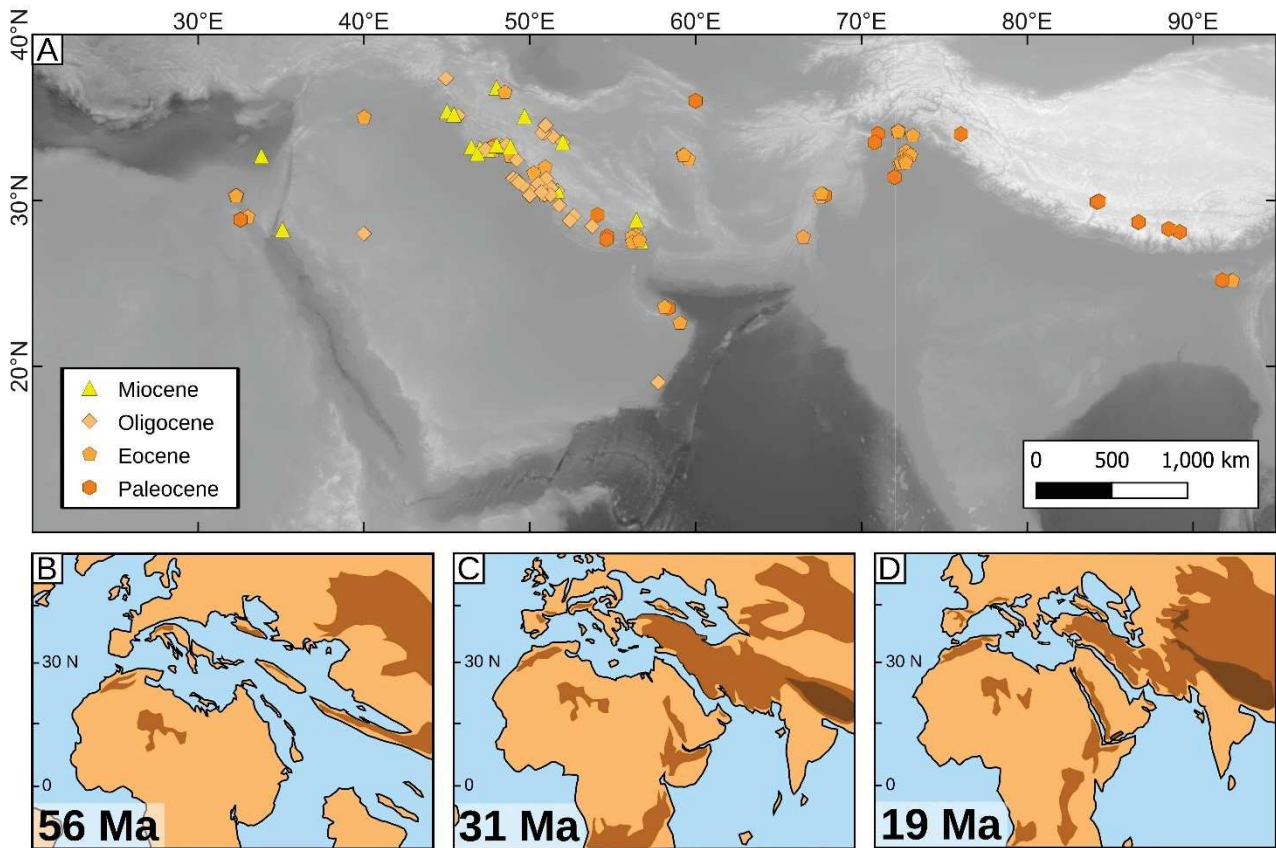


Figure 3.1 Geographic locations of the studied facies and palaeogeographical reconstructions. (A) Geographic location of the fossil Neogene facies investigated in this study. Note the different symbols and colours for different epochs. All the references are reported in Table S1. (B) Palaeogeographical reconstruction of South-western and Western Central Asia about 56 Ma (Palaeocene–Eocene), after Scotese (2014a, 2014b). (C) Palaeogeographical reconstruction of South-western and Western Central Asia about 31 Ma (early Oligocene), after Scotese (2014a, 2014b). (D) Palaeogeographical reconstruction of south-Western and western Central Asia about 19 Ma (early Miocene), after Scotese (2014a, 2014b).

3.4 Materials and methods

In order to prepare the database, the main online repositories (e.g., Google Scholar, Scopus) were searched for papers dealing with the Cenozoic carbonate successions of Egypt, Cyprus, Israel, Jordan, Saudi Arabia, United Arab Emirates (UAE), Yemen, Oman, Iraq, Iran, Pakistan, India, Nepal and China (Tibet). To be included into the database, a paper needed to fulfil the following requirements: (1) a lithostratigraphic description of a section completed with a lithostratigraphic column; (2) facies descriptions, including a qualitative or quantitative assessment of the main carbonate producers; (3) information on facies distribution within the investigated section; (4) microphotographs of the recognised facies suitable for double checking facies descriptions; (5) a biostratigraphic or chronostratigraphic framework; (6) a reasonably accurate location of the investigated section. The facies described in the selected papers were analysed based on the abundance of the following categories of carbonate grains: free-living larger benthic foraminifera (LBF), encrusting benthic foraminifera (EBF), smaller benthic foraminifera (SBF), red calcareous algae (RCA), green calcareous algae (GCA), colonial corals (CC), molluscs, echinoderms, bryozoans, ostracods,

microbial crusts, ooids, peloids and carbonate mud. Each facies was reclassified based on its dominant component (e.g., RCA dominated), or on its codominant components (e.g., RCA and LBF-dominated). Facies dominated by terrigenous grains, pelagic material or evaporites were excluded from the analysis. Each section included into the database was subdivided into fractions at epoch level (e.g., Eocene, Oligocene) and, wherever possible, at stage level (e.g., Ypresian, Lutetian). Within each fraction of a section, the abundance of each recognised facies was calculated based on how many metres of the fraction are characterised by the facies (e.g., a 40 m fraction of section, deposited during the Ypresian, consists of 20 m of LBF-dominated packstone and of 20 m of ooids-dominated grainstone, thus the fraction of the section consists of 50% of LBF-dominated facies and 50% of ooids-dominated facies). The raw data are available as Table S1. The data have been grouped based on two different approaches: section-average and formation-average. With the section-average approach, the averages are calculated as the average of each fraction belonging to the same time slice (e.g., the average of all Miocene-aged fractions of sections; the average of all Burdigalian-aged fractions of sections). With the formation-average approach, the averages of all the fractions of sections belonging to the same formation and the same time slice are calculated and then a general average is provided. Overall, this meta-analysis can be affected by two main biases: the first related to the reliability of the original information and the second related to the geographic distribution of the sections included into the database. The former bias has been partially countered by cross checking both facies descriptions and biostratigraphic information and focussing only on those elements of the facies that were (1) described as dominant and (2) appeared as dominant also in the microphotographs included in the source material. The geographic distribution of the sections is strongly related to the geological setting. While Palaeocene and Eocene sections are more or less evenly distributed into the study area, Oligocene and Miocene sections mainly occur in the Iraq–Iran area (Figure 3.1A). This is mainly related to the progressive closure of the Tethys Ocean due to the collision of the Indian and African–Arabian plates with Eurasia, which results in the lack of shallow-water carbonate successions in several regions during the Oligocene–Miocene (e.g., Tibet). This geographical bias has been partially countered by proposing both a section-average and a formation-average for each time interval. The section-average approach clearly indicates the average volume of a certain facies among the investigated carbonate successions. This approach provides quantitative data but can over-represent certain areas where there are more investigated outcrops per square kilometre (e.g., the Asmari and Qom Formations of Iran during the Oligo–Miocene interval). The formation-average approach partially solves this problem by averaging the data from each formation, thus reducing the overrepresentation of certain areas. Neither the geographic nor the reliability bias can be entirely solved and must be taken into account when approaching a palaeoenvironmental

interpretation of the results. In order to test whether or not the aforementioned averages are related to large-scale palaeoenvironmental patterns rather than the result of random processes, different statistical procedures were used. Bootstrap analysis was performed on the abundance of the most relevant carbonate facies (i.e., those that constitute the large majority of the analysed sections, i.e., LBF, RCA, CC and GCA dominated and codominated facies). The bootstrap can be used to estimate the precision of an estimated parameter of a population (Efron, 1979). A random sub-sample of the dataset is selected, and the parameter is calculated on the sub-sample. The procedure is repeated, and the confidence interval of the selected parameter is analysed. A random sub-sample size was selected corresponding to 2/3 (Sengupta et al., 2016) of the original sample (e.g., all the Miocene fractions of sections) and performed 10,000 iterations. A sensitivity analysis was also performed. Since each sub-sample consists of a randomly chosen part of the available fractions of sections of each epoch, the large number of iterations should clarify whether the observed trends in carbonate facies distribution are simply the results of the available group of analysed outcrops. If the distribution of the carbonate facies in the study area during the Cenozoic is not related to large-scale palaeoenvironmental patterns of the planet, one would expect the averages of the various sub-samples to be highly variable, resulting in large and overlapping confidence intervals. On the other hand, if the distribution is indeed the result of large-scale patterns, then the various sub-samples should be relatively homogeneous and the confidence interval on the averages relatively narrow. Multivariate statistics was also used to test the results. If during the Cenozoic, within the study area, the distribution of carbonate factories was random, one would expect the distribution of carbonate facies to be relatively similar during each epoch, with no statistically significant difference between the various time slices (e.g., no difference between Palaeocene and Miocene distribution of carbonate factories). The analysis was carried out following the recommendations in Bialik et al. (2021) and normal distribution of the variable was tested using Shapiro–Wilk, Anderson–Darlin, Lilliefors and Jarque–Bera tests. PERMANOVA analysis was then carried out to test the dissimilarity between the data of each epoch. Both bootstrap and multivariate statistics were performed on section-averages as formation-averages essentially stem from section-averages.

3.5 Results

Some 114 papers providing information on shallow-water carbonate facies from the Palaeocene to the Miocene were identified. Based on the aforementioned requirements, 66 papers and 144 sections, from Cyprus, Egypt, Saudi Arabia, Oman, Iraq, Iran, Pakistan, India and China were included into the database (Table 3.1; Table S1; the database is also accessible online, <https://doi.org/10.6084/m9.figshare.19323821.v1>). The remaining papers, although providing

qualitative data on the distribution of the main carbonate producers, lacked quantitative information on facies distribution throughout the described sections. The information from this latter group of papers was still included into the discussion. The sections included into the database range in age from the Palaeocene to the Miocene. The Palaeocene is represented (in order of abundance) by the Thanetian, Danian and Selandian. As the database largely consists of shallow-water carbonates, the stratigraphic framework is strongly reliant upon LBF biostratigraphy. Since LBF zonation is poorly constrained in the Danian–Selandian interval (Serra-Kiel et al., 1998), the pre-Thanetian stratigraphic framework is not well defined. The Eocene is largely represented by the Ypresian stage. Both stages of the Oligocene and both stages of the early Miocene are well represented within the database. On the other hand, the middle and late Miocene are poorly represented. Overall, the various epochs of the database have sample sizes in the same order of magnitude: 42 fractions of sections for the Palaeocene; 61 for the Eocene; 70 for the Oligocene; 85 for the Miocene.

3.5.1 Epochs

Photozoan facies (sensu James, 1997), that is those dominated by CC, GCA, LBF and RCA, dominate the carbonate successions of the study area, during the whole Palaeocene-Miocene interval (Table 3.2; Figure 3.2). Heterozoan facies (sensu James, 1997), that is those facies mainly dominated by heterotroph carbonate producers like molluscs, echinoderms, SBF and bryozoans, are less common; their combined abundance peaks during the Miocene (Table 3.2; Figure 3.2). The LBF-dominated facies are the most abundant element of the shallow-water carbonates of the study area (Table 3.2; Figure 3.3). Overall, taken together, the facies dominated by LBF and the facies codominated by LBF represent the majority of shallow-water carbonates of the Palaeocene, Eocene and Oligocene and Miocene epochs (Table 3.3; Figure 3.4). The abundance of LBF peaks during the Eocene and decreases hereafter. The LBF-dominated sections (>90% of the section) persist through all periods. Facies dominated solely by RCA are relatively rare; on the other hand, facies codominated by RCA are rather abundant, usually representing the second or third most abundant facies type (generally after LBF-dominated and LBF-codominated) (Table 3.2; Figure 3.3). The RCA codominated facies are relevant during the Palaeocene, Oligocene and Miocene and their abundance is the lowest during the Eocene (Table 3.2; Figure 3.3). Taken together CC dominated and CC codominated facies are usually the next most abundant facies type (Table 3.3; Figure 3.4). Their abundance peaks during the Oligocene and has a minimum during the Eocene. The GCA facies (either solely considering GCA dominated facies or both GCA dominated and GCA codominated facies) only occur in significant amounts during the Palaeocene and Eocene, being more common in the former (Tables 3.2 and 3.3; Figures 3.3 and 3.4). All other producers are uncommon for the entire time period (Palaeocene to

early Miocene). The EBF facies are very rare in all the epochs except in the Eocene where they account, on average, for 2.5% of section-average fractions (Tables 3.2 and 3.3). Microbial crust-dominated facies are extremely rare during every epoch (Tables 3.2 and 3.3). Facies characterised by the dominance of non-skeletal grains are relatively rare during the Palaeocene and Eocene and become more common during the Oligocene and Miocene (Tables 3.2 and 3.3; Figure 3.2). Intertidal mud dominated facies occur in every epoch and their abundance peaks during the Miocene where they are one of the most common non-skeletal facies types (Tables 3.2 and 3.3).

#	Reference	Country	Formation	Stratigraphic range	N. of sections
1	Rahmani et al., 2009	Iran	Asmari	Chattian - Burdigalian	1
2	Adabi et al., 2008	Iran	Taleh Zang	Lutetian - Bartonian	2
3	Roospeykar & Moghaddam, 2016	Iran	Asmari	Rupelian - Burdigalian	1
4	Nafarieh et al., 2012	Iran	Jahrum	Selandian - Ypresian	2
5	Mahyad et al., 2019	Iran	Qom	Aquitanian - Burdigalian	2
6	Moghaddam et al., 2002	Iran	Jahrum & Pabdeh	Ypresian	1
7	Heidari et al., 2014	Iran	Mishan (Guri Member)	Aquitanian - Langhian	2
8	Shabafrooz et al., 2015	Iran	Asmari	Rupelian - Burdigalian	9
9	Vaziri-Moghaddam et al., 2006	Iran	Asmari	Chattian - Burdigalian	1
10	Zohdi et al., 2013	Iran	Jahrum	Ypresian - Bartonian	4
11	Daraei et al., 2015	Iran	Asmari	early Miocene	3
12	Roospeykar et al., 2019	Iran	Asmari	Burdigalian	1
13	Avarjania et al., 2015	Iran	Asmari	Chattian - Burdigalian	4
14	Bagherpour & Vaziri, 2012	Iran	Taleh Zang	Thanetian - Ypresian	2
15	Amirshahkarami & Zebarjadi, 2018	Iran	Jahrum	Thanetian - Ypresian	1
16	Zoeram et al., 2015	Iran	Asmari	Rupelian - Burdigalian	1
17	Basso et al., 2019	Iran	Qom	Rupelian	1
18	Mohammadi et al., 2011	Iran	Qom	Chattian	1
19	Hadi et al., 2016	Iran	Ziarat	Ypresian - Bartonian	3
20	Sadeghi et al., 2011	Iran	Asmari	Rupelian - Chattian	3
21	Amirshahkarami, 2013	Iran	Asmari	Rupelian - Aquitanian	2
22	Vaziri-Moghaddam et al., 2010	Iran	Asmari	Chattian - Burdigalian	4
23	Amirshahkarami & Karavan, 2015	Iran	Qom	Rupelian - Burdigalian	1
24	Dill et al., 2018	Iran	Asmari	Rupelian - Burdigalian	5
25	Dill et al., 2012	Iran	Asmari	Chattian - Burdigalian	1
26	Noorian et al., 2021	Iran	Asmari	Rupelian - Burdigalian	3
27	Safari et al., 2020	Iran	Qom	Rupelian - Chattian	2
28	Amirshahkarami et al., 2007	Iran	Asmari	Rupelian - early Miocene	1
29	Babazadeh & Alavi, 2013	Iran	Lut platform	Ypresian	3
30	Taheri et al., 2008	Iran	Jahrum	Lutetian	1
31	Mossadegh et al., 2009	Iran	Asmari	Chattian - Burdigalian	2
32	Amirshahkarami et al., 2007	Iran	Asmari	Chattian - early Miocene	1
33	Adabi et al., 2016	Iran	Asmari	Rupelian - Burdigalian	1

34	Vaziri-Moghaddam et al., 2011	Iran	Asmari	Rupelian - Chattian	1
35	Mahboubi et al., 2001	Iran	Chehel- Kaman	Thanetian	2
36	Mohammadi, 2020	Iran	Qom	Rupelian - Burdigalian	2
37	Joudaki et al., 2020	Iran	Asmari	Rupelian - Burdigalian	2
38	Al-Qayim et al., 2016	Iraq	Bajwan, Anah, Euphrates, Jeribe	Rupelian - Burdigalian	1
39	Hussein et al., 2017	Iraq	Euphrates, Jeribe	Aquitanian - Burdigalian	5
40	Swati et al., 2013	Pakistan	Margalla Hill Limestone	Ypresian	1
41	Afzal et al., 2011	Pakistan	Lockhart, Patala, Dungan	Thanetian - Ypresian	5
42	Fahad et al., 2021	Pakistan	Chorgali	Ypresian	1
43	Ishaq et al., 2019	Pakistan	Sakesar Limestone	Ypresian	2
44	Ghazi et al., 2020	Pakistan	Nammal	Ypresian	6
45	Hanif et al., 2014	Pakistan	Lockhart	Thanetian	3
46	Ahmad et al., 2020	Pakistan	Dungan	Thanetian - Ypresian	1
47	Kamran et al., 2021	Pakistan	Patala	Thanetian - Ypresian	1
48	Kahsnitz, 2017	India	Spanboth, Zhepure Shan, Zongpu, Langzhu	Selandian - Ypresian	5
49	Sarkar, 2016	India	Umlatdoh (Umlatdoh Limestone)	Ypresian	1
50	Sarkar, 2017	India	Prang	Lutetian - Bartonian	1
51	Banerjee et al., 2018	India	Furla Limestone, Maniyara Fort	Lutetian - Bartonian, Chattian	2
52	Jahuri et al., 2006	India	Lakadong (Lakadong Limestone)	Thanetian	1
53	Jiang et al., 2021	China	Jialazi	Thanetian - Ypresian	2
54	Li et al., 2015	China	Zongpu	Danian - Ypresian	2
55	Li et al., 2020	China	Not reported (probably Zhepure Shan)	Thanetian - Ypresian	1
56	Willems et al., 1996	China	Zhepure Shan	Danian - Lutetian	1
57	Mattern & Bernecker, 2019	Oman	Jafnayn	Thanetian - Ypresian	1
58	Tomás et al., 2016	Oman	Jafnayn	Ypresian	1
59	Beavington-Penney et al., 2006	Oman	Seeb	Lutetian - Bartonian	1
60	Reuter et al., 2008	Oman	Shuwayr, Warak, Ghubbarah	Rupelian - Aquitanian	2
61	Al-Kahtany, 2017	Saudi Arabia	Jabal Kibrit (Wadi Waqb Member)	middle Miocene	1
62	Corlett et al., 2018	Egypt	Hammam Faraun fault block	Ypresian - Lutetian	1
63	Sallam et al., 2015	Egypt	Minia, Sannor, Maadi	Ypresian, Bartonian - Priabonian	5
64	Scheibner et al., 2000	Egypt	Southern Galala	Thanetian	6
65	Scheibner et al., 2003	Egypt	Southern Galala	Thanetian	4
66	Coletti et al., 2019	Cyprus	-	early Miocene -late Miocene	1

Table 3.1 Summary list of the papers considered in this work, reporting references, countries, formations, stratigraphic ranges and the number of sections analysed in the work. See Table S1 for the complete dataset.

3.5.2 Rupelian-Burdigalian detailed analysis

Since the Palaeocene is mainly represented by Thanetian deposits, the Eocene by Ypresian deposits, and the Miocene by early Miocene deposits, the analysis at stage level was performed only in the Rupelian–Burdigalian interval. As in the epoch analysis, the photozoan facies dominate the investigated carbonate successions (Tables 3.4 and 3.5). The heterozoan facies reach their maximum during the Burdigalian (Tables 3.4 and 3.5). Both type of calcifiers decrease through the time period as the non-skeletal grains dominated facies become more significant (Tables 3.4 and 3.5). The LBF-dominated facies display a clear peak during the Rupelian and reach their lowest abundance in the

Aquitanian (Table 3.4). By taking together both LBF-dominated and LBF-codominated facies, the Rupelian peak can no longer be observed in both the formation-average and section-average representations, while the minimum during the Aquitanian still occurs (Table 3.5). Similarly, the abundance of CC dominated facies (either solely considering CC dominated facies or considering both CC dominated and CC codominated facies) displays a minimum during the Aquitanian (Tables 3.4 and 3.5). Both the facies dominated by non-skeletal grains in general and those characterised by intertidal muds specifically peak during the Aquitanian, in both the section-average and in the formation-average representations (Tables 3.4 and 3.5).

3.5.3 Statistical analysis

The average abundances of the most relevant carbonate facies of the Palaeocene, Eocene, Oligocene and Miocene obtained from the various iterations of the bootstrap method show a normal distribution. Their confidence intervals (i.e., average \pm 2 SD; Table 3.6) display limited to no overlap, especially with regards to the most volumetrically important facies: LBF-dominated, LBF codominated, RCA codominated and CC codominated facies (Figure 3.4). Sensitivity analysis also indicates that the calculated averages and standard deviations display no sensitivity to the number of the iterations of the bootstrap and very limited sensitivity to the size of the sub-sample. PERMANOVA dissimilarity analysis of the time slices indicates that these groups are dissimilar at $p < 0.05$.

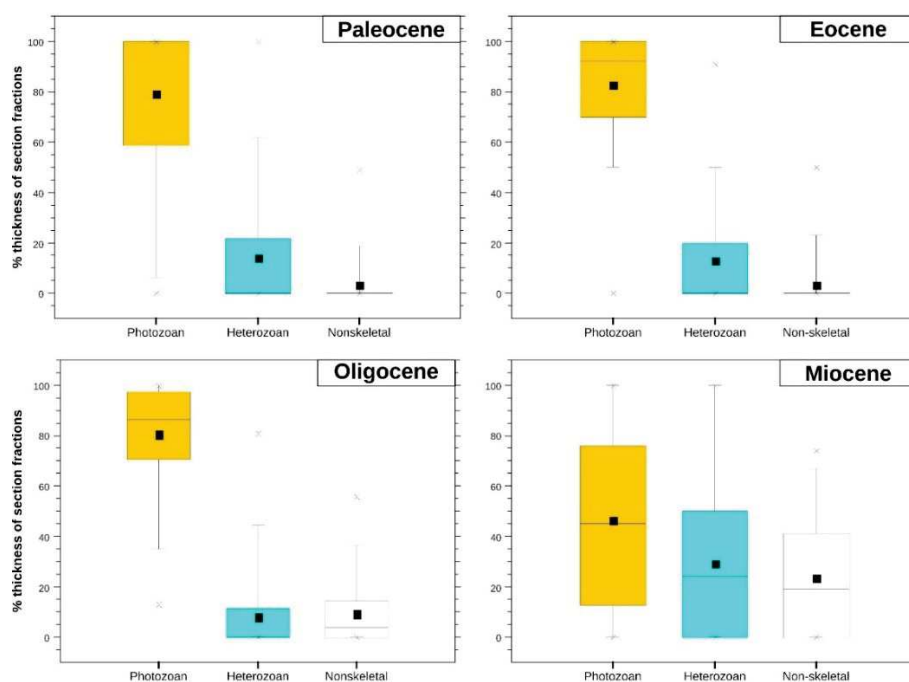


Figure 3.2 Box and whisker plots showing the Photozoan (yellow), Heterozoan (light blue) and non-skeletal dominated (white) facies distribution in the investigated fossil facies during the different epochs (Palaeocene, Eocene, Oligocene, Miocene).

Section Average																				
Dominant components	LBF	LBF & RCA	LBF & GCA	LBF & CC	CC	CC & RCA	CC & EBF	RCA	RCA & Peloids	GCA	GCA & SBF	EBF	SBF	SBF & Peloid	Micro-bial crusts	Ooids	Peloids	Intra-clasts	Mud	Hetero-zoan
Paleocene	35.21 %	19.40 %	9.29%	0.00%	3.38%	2.69%	0.00%	3.60%	0.00%	8.55%	0.67%	0.00%	7.69%	1.81%	0.24%	1.14%	0.36%	0.38%	1.33%	4.26%
Eocene	78.21 %	3.21%	0.28%	0.00%	0.61%	0.00%	0.00%	0.95%	0.03%	0.33%	0.11%	2.39%	4.97%	0.00%	0.38%	0.25%	0.07%	0.00%	2.95%	5.35%
Oligocene	47.93 %	17.91 %	0.00%	4.40%	1.80%	8.51%	0.00%	2.06%	0.00%	0.00%	0.00%	0.00%	2.86%	0.00%	0.00%	0.29%	1.51%	0.00%	7.81%	5.06%
Miocene	33.02 %	8.88%	0.00%	0.29%	1.88%	2.42%	0.05%	1.02%	0.00%	0.00%	0.00%	0.00%	13.65%	0.00%	0.13%	4.94%	2.64%	0.00%	15.72%	15.35%

Formation Average																				
Dominant components	LBF	LBF & RCA	LBF & GCA	LBF & CC	CC	CC & RCA	CC & EBF	RCA	RCA & Peloids	GCA	GCA & SBF	EBF	SBF	SBF & Peloid	Micro-bial crusts	Ooids	Peloids	Intra-clasts	Mud	Hetero-zoan
Paleocene	35.89%	18.36%	5.74%	0.00%	1.56%	0.81%	0.00%	6.86%	0.00%	11.68%	0.40%	0.00%	7.24%	0.54%	0.26%	1.59%	0.41%	0.57%	2.31%	5.77%
Eocene	77.26%	3.65%	0.71%	0.00%	0.51%	0.00%	0.00%	1.81%	0.08%	0.83%	0.29%	2.54%	6.53%	0.00%	0.13%	0.21%	0.02%	0.00%	2.04%	3.38%
Oligocene	41.34%	11.90%	0.00%	32.71%	0.99%	2.90%	0.00%	1.57%	0.00%	0.00%	0.00%	0.00%	2.82%	0.00%	0.00%	0.05%	0.29%	0.00%	3.19%	2.23%
Miocene	16.36%	9.79%	0.00%	3.13%	7.68%	10.61%	0.01%	0.83%	0.00%	0.00%	0.00%	0.00%	10.51%	0.00%	0.02%	6.74%	1.85%	0.00%	5.36%	27.11%

Table 3.2 Percent distribution of the dominant components during the Palaeocene, Eocene, Oligocene, Miocene, following the section-average and the formation-average approaches, respectively.

3.6 Discussion

3.6.1 Carbonate factories evolution

Large benthic foraminifera appear to be the most important carbonate producers within the investigated time interval in the southern Tethyan realm as they are very common in every region and in every epoch (Tables 3.2 and 3.3; Figures 3.3 and 3.5). They reach their maximum abundance during the Eocene (where they are overwhelmingly dominant) and their lowest during the Miocene (still remaining the most important carbonate producers). The results indicate that, from the late Palaeocene to the early Miocene, in the southern Tethyan realm, the majority share of the biogenic carbonates accumulated in shelfal carbonate factories, has been produced by benthic foraminifera. This now manifests with a large fraction of the shallow-water Carbonates of the study area being comprised of LBF-dominated facies. These results are also supported by the lithostratigraphic information reported by Höntzsch et al. (2011) and Hussein (2019) for Egypt, by Schaub et al. (1995), Buchbinder et al. (2005) and Rosenfeld and Hirsch (2005) for Israel, by Farouk et al. (2013) for Jordan, by Alsharhan and Nairn (1995) for the Arabian Peninsula, by Sadooni and Alsharhan (2019) for UAE, by Bernecker (2014) for Oman, by Sissakian (2013), Ameen-Lawa and Ghafur (2015), and Sadooni and Alsharhan (2019) for Iraq, by Reuter et al. (2009), Van Buchem et al. (2010), Yazdi-Moghadam et al. (2018a), Hadi et al. (2019), Dill et al. (2020) and Benedetti et al. (2021) for Iran, by Akhtar and Butt (1999), Naveed and Chaudhry (2008), Afzal et al. (2011b), Özcan et al. (2015), Ahmad et al. (2016), Khan et al. (2018) and Özcan et al. (2018) for Pakistan, by Gaetani et al. (1983), Less et al. (2018) and Sarkar (2018) for India, and by Zhang et al. (2013) for China. Other reviews of Cenozoic carbonate production in the Eurasian province also highlighted a remarkable abundance of LBF during the Palaeocene, Eocene (where they dominates), Oligocene and early Miocene (BouDagher-Fadel, 2018; Cornacchia et al., 2021; Geel, 2000; Nebelsick et al., 2005; Pomar et al., 2017; Scheibner & Speijer, 2008). A similar pattern can be also observed in the American province (Aguilera et al., 2020). In the modern oceans, LBF distribution is strongly controlled by temperature (Langer & Hottinger, 2000; Renema, 2018) and so is their diversity. Tropical assemblages display a much larger number of genera and species than sub-tropical ones (Beavington-Penney & Racey, 2004). During the early Eocene, following an extinction event at the Palaeocene–Eocene boundary, LBF became significantly more diverse with the rise of large nummulitids that would dominate LBF assemblages until the Bartonian (Benedetti & Papazzoni, 2022; BouDagher-Fadel, 2018). The high temperatures of the early Eocene as well as the temperature drop at the end of the Bartonian (Zachos et al., 2001) suggests, as already noted by other authors (Scheibner & Speijer, 2008), a strong relationship between temperature and LBF abundance. During the early Palaeogene their dominance started at low latitudes and progressed towards higher latitudes as temperatures rose, paralleled by a decrease of CC (Martín-Martín et al.,

2020; Scheibner & Speijer, 2008). Therefore, LBF success during the Palaeogene would have been favoured by the greenhouse conditions that prevailed for most of the period (except during the Oligocene, when the opening of the Tasmanian and Drake passages lead to the isolation and the progressive build-up of ice in Antarctica; Zachos et al., 2001). Meta-analysis clearly shows that LBF facies peak in the Eocene (which is mainly represented by the early Eocene in the database). However, taken together, LBF-dominated and codominated facies do not diminish much during the Oligocene. The review of Nebelsick et al. (2005), focussed on Eocene circum-Alpine carbonates, also indicates that LBF facies largely dominated during the middle Eocene, far after the Early Eocene Climatic Optimum. This suggests a more complex pattern. According to Pomar et al. (2017) and Hallock and Seddighi (2022), LBF are perfectly suited to deal with extreme oligotrophic conditions associated with periods of reduced thermohaline circulation. This might have played a role in fostering their abundance during the warm periods of the Palaeogene. The LBF also seem to be better adapted than CC to water turbidity related to nutrient abundance (Wilson & Vecsei, 2005), and to outperform both

Section Average									
Dominated + codominated facies	LBF	CC	RCA	GCA	EBF	Ooids & Peloids	Mud	Microbial crusts	Heterozoan
Paleocene	63.90%	6.07%	25.69%	18.50%	0.00%	3.31%	1.33%	0.24%	14.43%
Eocene	81.70%	0.61%	4.20%	0.72%	2.39%	0.34%	2.95%	0.38%	10.43%
Oligocene	70.24%	14.71%	28.49%	0.00%	0.00%	1.80%	7.81%	0.00%	7.91%
Miocene	42.20%	4.65%	12.33%	0.00%	0.05%	7.58%	15.72%	0.13%	29.00%

Formation Average									
Dominated + codominated facies	LBF	CC	RCA	GCA	EBF	Ooids & Peloids	Mud	Microbial crusts	Heterozoan
Paleocene	60.00%	2.36%	26.03%	17.82%	0.00%	2.54%	2.31%	0.26%	13.95%
Eocene	81.61%	0.51%	5.54%	1.83%	2.54%	0.31%	2.04%	0.13%	10.21%
Oligocene	85.95%	36.61%	16.37%	0.00%	0.00%	0.34%	3.19%	0.00%	5.05%
Miocene	29.27%	21.42%	21.22%	0.00%	0.01%	8.59%	5.36%	0.02%	37.63%

Table 3.3 Percent distribution of the main groups of carbonate grains (dominated plus codominated facies) during the Palaeocene, Eocene, Oligocene, Miocene, following the section-average and the formation-average approaches, respectively.

CC and RCA in environments characterised by high sedimentation rates (Coletti et al., 2021b; Lokier et al., 2009). It should be remembered that, although relatively complex, LBF are unicellular organisms, and thus, they are very flexible. Despite certain groups of LBF clearly evolving through geological time pursuing a K-strategy compared to other benthic foraminifera (see Hottinger, 1982), their life cycle is still significantly different from that of multicellular organism like RCA and CC. Furthermore, unlike CC and RCA, LBF are mobile and so they can relocate if they need to.

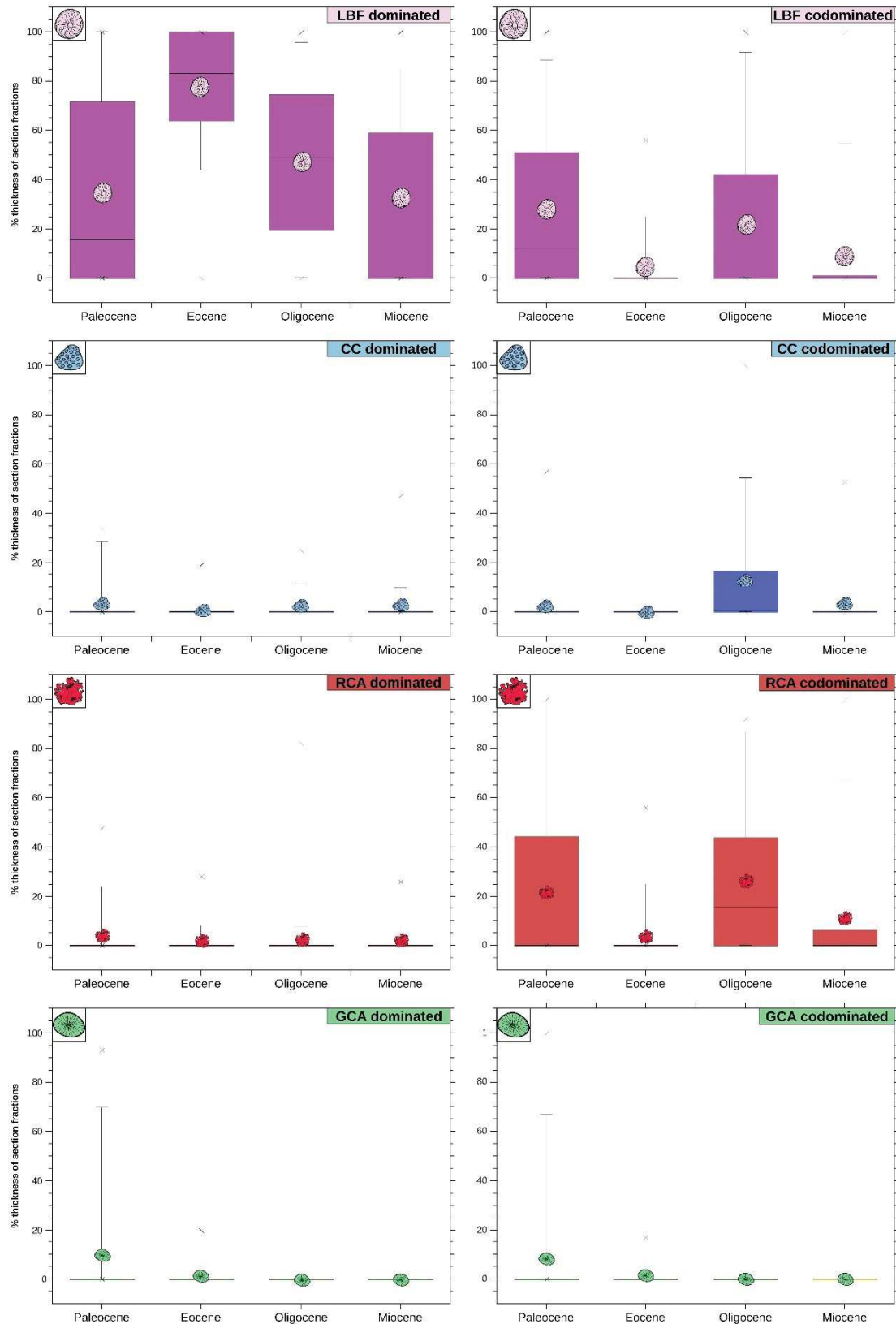


Figure 3.3 Box and whisker plots showing the distribution during time (Palaeocene, Eocene, Oligocene, Miocene) of the LBF-dominated and codominated facies (purple), CC dominated and codominated facies (blue), RCA dominated and codominated facies (red), and GCA dominated and codominated facies (green); the key for the statistical symbols of the box and whisker plot is as in Figure 3.2.

The LBF probably took advantage of the reduced competition in shelfal settings caused by the harsh conditions created by the Palaeocene Eocene Thermal Maximum and the other Palaeogene hyperthermals and, thanks to their adaptability, they thrived even after the end of the early Palaeogene greenhouse. The EBF, similarly to free-living LBF, reach peak abundance during the Eocene (Tables 3.3 and 3.4). Presently EBF are relatively rare and can produce centimetre-sized nodules (Bassi et al., 2012; Hottinger, 1983). However, during the early and middle Eocene LBF were a relevant group of reef-builders, creating extensive reefs in the Western Tethys (Perrin, 1992, 2009; Rasser, 1994). While modern EBF do not harbour symbionts (Leutenegger, 1984) and usually occur between water depths of 40 m and 105 m (Bassi et al., 2012; Rasser & Piller, 1997), Eocene EBF are often associated with shallow-water assemblages typical of the upper part of the photic zone (e.g. they are commonly associated with alveolinids) (Coletti et al., 2021b; Rasser, 1994; Tomás et al., 2016), indicating that Eocene EBF might have been relatively different from their modern counterparts. More detailed analysis might help clarify if Eocene EBF were symbiont bearing organisms or not, and thus suggest the environmental reasons for their abundance during the Eocene. Colonial corals are abundant in the Palaeocene and in the Miocene, while they reach a peak during the Oligocene (Tables 3.2 and 3.3; Figures 3.3 and 3.5). They are rare during the Eocene (Tables 3.2 and 3.3; Figures 3.3 and 3.5). This is also supported by the lithostratigraphic information provided by Coletti et al. (2021a) for Cyprus, by Kuss and Boukhary (2008) for Egypt, by Whittle et al. (1995) and Sadooni and Alsharhan (2019) for UAE, by Bernecker (2014) for Oman, by Sissakian (2013), Ameen-Lawa and Ghafur (2015), Ghafur (2015) and Sadooni and Alsharhan (2019) for Iraq, by Reuter et al. (2009), Van Buchem et al. (2010), Ghaedi et al. (2016), Yazdi-Moghadam et al. (2018a, 2018b, 2021) and Dill et al. (2020) for Iran, by Afzal et al. (2011b) for Pakistan, by Less et al. (2018) and Sarkar (2018) for India. The results of this study are overall consistent with other reviews of Cenozoic CC distribution in the Eurasian province (Perrin & Bosellini, 2012; Pomar et al., 2017; Scheibner & Speijer, 2008), East Pacific province (López-Pérez, 2005, 2017) and American province (Budd, 2000; Johnson et al., 2008), that indicate the Oligocene as a favourable period for both CC and CC dominated reefs. Similarly to LBF, this pattern seems to be strongly connected to global temperatures. In the Eurasian province, during the Palaeocene, CC are actually more abundant during the early to late Palaeocene interval (Martín-Martín et al., 2020; Scheibner & Speijer, 2008). This time interval is characterised by temperatures lower than those of the latest Palaeocene and of the early Eocene (Barnet et al., 2019). During the early to middle Eocene CC are relatively rare and only become relevant carbonate producers again during the late Eocene (Bernecker, 2014; Nebelsick et al., 2005; Scheibner & Speijer, 2008), which is the coldest stage of the epoch (Zachos et al., 2001). The Oligocene is the coldest period of the Palaeogene (Zachos et al., 2001), and it is recognised worldwide as a period of great

abundance of CC (Dishon et al., 2020). During the early Miocene CC are still very common, but during the middle Miocene, worldwide, RCA become significantly more abundant in shelfal tropical situations at the expenses of CC (Bialik et al., 2022; Cornacchia et al., 2021; Esteban, 1979, 1996; Halfar & Mutti, 2005; López-Pérez, 2005). The abundance of CC increased during the late Miocene in the Western Tethys (Cornacchia et al., 2021; Esteban, 1979, 1996; Pomar et al., 2017; Pomar & Hallock, 2007) and during the Plio-Pleistocene in the East Pacific and in the Caribbean (Johnson et al., 2008; López-Pérez, 2005). Thus, the distribution of CC during the Neogene can be also related to temperatures as CC are less abundant in the warm Middle Miocene Climatic Optimum and more abundant during cooler periods (Dishon et al., 2020; Herbert et al., 2016; Steinthorsdottir et al., 2020; Zachos et al., 2001). The CC presently thrive in a narrow temperature range and are severely damaged (i.e., the coral bleaching) whenever temperatures exceed this threshold (Crabbe, 2008; Marshall & Clode, 2004), it is conceivable that the warm peaks of the Cenozoic might have had a detrimental effect on CC abundance. Colder periods are also characterised by a stronger oceanic circulation than warmer periods, and this factor could also have favoured CC over other carbonate producers like LBF (Pomar et al., 2017). Furthermore, colder periods are favourable towards aragonite-producing organisms like CC (Hallock, 1997; Scheibner & Speijer, 2008), whereas the ocean chemistry of warm periods (like the Palaeocene-Eocene) is favourable for calcite generation (Stanley, 2006) and possibly detrimental to CC. However, the low pH (Boudreau et al., 2019), which characterised most of the Palaeocene and Eocene, likely had a significant negative impact also on the accumulation and preservation potential of CC - if they even calcified in shallow water at this time and had not shifted to a non-calcifying lifestyle (Fine & Tchernov, 2007). With the currently available data, disentangling the effects of these factors is probably impossible, although it is clear that temperature played an important role. The RCA abundance displays a pattern similar to the one of CC and characterised by a minimum during the Eocene (Tables 3.2 and 3.3; Figures 3.3 and 3.5). This is supported by the lithostratigraphic information provided by Coletti et al. (2021a) for Cyprus, by Kuss and Boukhary (2008) for Egypt, by Whittle et al. (1995) for UAE, by Afzal et al. (2011b) for Pakistan, by Bernecker (2014) for Oman, by Seyrafian and Toraby (2005), Reuter et al. (2009), Ghaedi et al. (2016) and Yazdi-Moghadam et al. (2021) for Iran. Within the various sections the abundance of CC and RCA codominant facies shows a positive correlation in the Palaeocene and in the Miocene, but not as clearly during the Eocene and the Oligocene (Figure 3.3).

Section Average																				
Dominant components	LBF	LBF & RCA	LBF & GCA	LBF & CC	CC	CC & RCA	CC & EBF	RCA	RCA & Peloids	GCA	GCA & SBF	EBF	SBF	SBF & Peloid	Microbial crusts	Ooids	Peloids	Intra-clasts	Mud	Hetero-zoan
Rupelian	51.3 5%	22.13 %	0.00%	4.35%	2.00%	8.74%	0.00%	1.43%	0.00%	0.00%	0.00%	0.00%	2.17%	0.00%	0.00%	0.00%	1.26%	0.00%	2.82%	3.96%
Chattian	45.5 0%	15.95 %	0.00%	4.73%	1.82%	8.98%	0.00%	2.52%	0.00%	0.00%	0.00%	0.00%	3.41%	0.00%	0.00%	0.45%	1.75%	0.00%	10.84 %	4.05%
Aquitanian	30.8 1%	9.89%	0.00%	0.69%	0.42%	0.47%	0.00%	1.08%	0.00%	0.00%	0.00%	0.00%	11.83%	0.00%	0.08%	11.19%	3.81%	0.00%	20.72 %	9.00%
Burdigalian	37.6 1%	6.95%	0.00%	0.00%	2.45%	1.03%	0.11%	0.87%	0.00%	0.00%	0.00%	0.00%	16.61%	0.00%	0.18%	0.45%	0.84%	0.00%	13.32 %	19.61%

Formation Average																				
Dominant components	LBF	LBF & RCA	LBF & GCA	LBF & CC	CC	CC & RCA	CC & EBF	RCA	RCA & Peloids	GCA	GCA & SBF	EBF	SBF	SBF & Peloid	Microbial crusts	Ooids	Peloids	Intra-clast	Mud	Hetero-zoan
Rupelian	40.20 %	15.90 %	0.00%	25.00%	1.57%	4.34%	0.00%	1.65%	0.00%	0.00%	0.00%	0.00%	4.53%	0.00%	0.00%	0.00%	0.45%	0.00%	1.90%	4.52%
Chattian	35.28 %	14.97 %	0.00%	34.67%	1.28%	4.02%	0.00%	2.42%	0.00%	0.00%	0.00%	0.00%	0.83%	0.00%	0.00%	0.10%	0.38%	0.00%	4.41%	1.65%
Aquitanian	15.47 %	11.65 %	0.00%	5.00%	0.12%	0.14%	0.00%	2.81%	0.00%	0.00%	0.00%	0.00%	7.46%	0.00%	0.02%	10.70%	2.67%	0.00%	11.80 %	32.17%
Burdigalian	24.83 %	14.41 %	0.00%	0.00%	7.56%	0.73%	0.04%	1.35%	0.00%	0.00%	0.00%	0.00%	14.31%	0.00%	0.06%	0.71%	1.11%	0.00%	7.71%	27.19%

Table 3.4 Percent distribution of the dominant components in the Oligocene (Rupelian, Chattian) and early Miocene (Aquitanian, Burdigalian), following the section-average and the formation-average approaches, respectively.

Modern RCA are extremely adaptable and can thrive in both warm and cold climates, in both oligotrophic and nutrient-rich water and from the shallow intertidal zone to the lowest limit of the photic zone (Pomar et al., 2017; Riosmena-Rodríguez, 2017). The CC require a hard substrate for their initial recruitment on the seafloor and RCA can generate hard substrates. Free-living nodules can progressively coalesce leading to the creation of a hard substrate suitable for the colonisation of other organisms or the expansion of RCA bioconstructions. In turn the complex framework of CC-reefs creates several niches that can be used by coralline algae. Therefore, to a certain extent, the two groups are mutually beneficial to one another, justifying why the periods favourable for the former can be also favourable for the latter. However, most of the analysed papers pay little attention to RCA in comparison to LBF (which are useful for biostratigraphy), and CC (that can be easily observed in the outcrops), therefore a bias in the database that could lead to an underestimation of RCA cannot be excluded. Within the study area, during the Palaeocene, GCA are rarely a dominant component of the skeletal assemblage (Tables 3.2 and 3.3; Figures 3.3 and 3.5). In the Eocene, they dominate very rarely, while in the Oligocene and in the Miocene they occur only as a minor component of the skeletal assemblage. These results are supported by the lithostratigraphic information provided by Höntzsch et al. (2011) for Egypt, by Nafarih et al. (2019) and Benedetti et al. (2021) for Iran, by Akhtar and Butt (1999), Afzal et al. (2011b), Khan et al. (2018) and Khitab et al. (2020) for Pakistan, by Gaetani et al. (1983) for India, and by Zhang et al. (2013) for China. Unlike the results given here, the review of Pomar et al. (2017) of Cenozoic carbonates of western-central Tethys indicates abundant GCA only in the Danian (mainly dasyclads) and in the Miocene (mainly Halimadales). Based on the fossil record, during the Cenozoic, GCA biodiversity peaks in the Palaeocene and decreases afterwards (Aguirre & Riding, 2005). This pattern is consistent with the abundance of GCA in the successions of the study area. However, while biodiversity may be related to abundance it is usually decoupled from carbonate production (Johnson et al., 2008). Modern GCA mostly precipitate aragonite and are thus easily susceptible to diagenetic dissolution, which can start even when the algae are still alive (Granier, 2012). Several fossil taxa of Dasycladales are thought to have precipitated calcite instead of aragonite (Granier, 2012). The last of these supposedly calcitic taxa occurred during the Eocene (Granier, 2012). Therefore, the observed pattern of GCA distribution might be, possibly similar to CC, related to a preservation bias as opposed to an environmental variable as in the case of LBF. The progressive decrease of GCA abundance throughout the Cenozoic in this region might have been connected to a transition from early Palaeogene assemblages rich in calcite-producing taxa to Neogene assemblages entirely constituted of aragonitic taxa.

Section Average									
Dominated + codominated facies	LBF	CC	RCA	GCA	EBF	Ooids & Peloids	Mud	Microbial crusts	Heterozoan
Rupelian	77.83%	15.09%	32.30%	0.00%	0.00%	1.26%	2.82%	0.00%	6.13%
Chattian	66.18%	15.52%	27.45%	0.00%	0.00%	2.20%	10.84%	0.00%	7.45%
Aquitanian	41.39%	1.58%	11.44%	0.00%	0.00%	15.00%	20.72%	0.08%	20.83%
Burdigalian	44.55%	3.58%	8.84%	0.00%	0.11%	1.29%	13.32%	0.18%	36.21%

Formation Average									
Dominated + Codominated facies	LBF	CC	RCA	GCA	EBF	Ooids & Peloids	Mud	Microbial crusts	Heterozoan
Rupelian	81.10%	30.91%	21.89%	0.00%	0.00%	0.45%	1.90%	0.00%	9.05%
Chattian	84.92%	39.97%	21.41%	0.00%	0.00%	0.48%	4.41%	0.00%	2.48%
Aquitanian	32.12%	5.26%	14.59%	0.00%	0.00%	13.36%	11.80%	0.02%	39.63%
Burdigalian	39.24%	8.33%	16.49%	0.00%	0.04%	1.81%	7.71%	0.06%	41.49%

Table 3.5 Percent distribution of the main groups of carbonate grains (dominated plus codominated facies) in the Oligocene (Rupelian, Chattian) and early Miocene (Aquitanian, Burdigalian), following the section-average and the formation-average approaches, respectively.

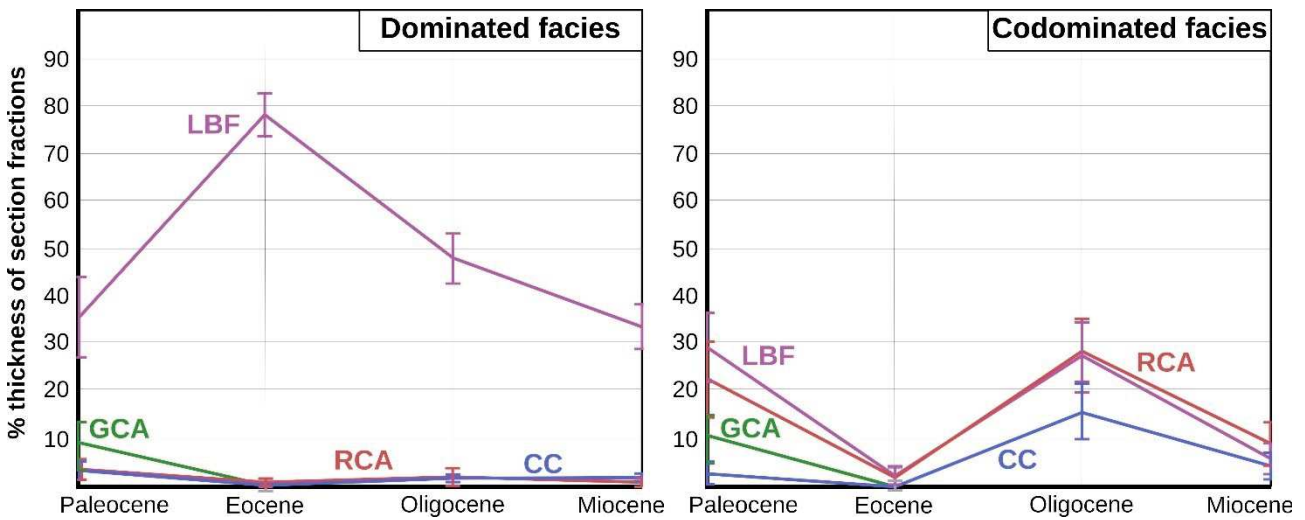


Figure 3.4 Bootstrap calculated averages (thick line) and confidence intervals (thin bars) of the most abundant and relevant carbonate factories in the study area during the Cenozoic; grey confidence intervals are related to less than zero minimum values of the confidence interval caused by the low average abundance of the facies during the epoch.

3.6.2 Regional and global implications

Several remarkable similarities can be observed by comparing these results for South-western and Western Central Asia with the other few available reviews of carbonate production: the peak in LBF abundance during the Eocene and the increase in coral abundance during the Oligocene (Aguilera et al., 2020; Johnson et al., 2008; Kiessling et al., 1999; Nebelsick et al., 2005; Pomar et al., 2017; Scheibner & Speijer, 2008). These changes are likely to have been strongly related to temperature, as the global increase in both CC diversity and importance as carbonate producers is paired with a

decrease in temperatures, while the Eocene widespread abundance of LBF is heralded by high global temperatures (Zachos et al., 2001). The CC achieve the highest calcification rates within a narrow temperature range (Crabbe, 2008; Marshall & Clode, 2004). This range is usually much larger for LBF (Titelboim et al., 2019), suggesting that LBF can take advantage of the detrimental effect that very high temperatures have on their competitors. These results are backed by quantitative data on facies abundance, and thus provide a strong argument in favour of the major rearrangements of shallow-water carbonate factories at the Palaeocene-Eocene and Eocene-Oligocene boundaries indicated by the other reviews. As these changes are witnessed at the global scale and are most likely temperature driven, they provide clear evidence on the long-term effect of temperatures on carbonate factories and shelfal biomes. Unlike the north-western Mediterranean Tethys area analysed by Pomar and Hallock (2007) and Pomar et al. (2004, 2012, 2017), LBF are always the dominant carbonate producers, even after the Eocene. The LBF, in north-western Mediterranean Tethys, are reported to diminish during the Oligocene and show a resurgence during the Miocene (Pomar et al., 2017). This is not observed in the study area. Such a difference could be still, at least partially, temperature related, as the study area was located south of the north-western Mediterranean Tethys and thus was probably more favourable for LBF. During the Oligocene and the early Miocene, thanks to global cooling and a progressive northward shift, southern Tethys became more favourable to CC, leading to their increase. This cooling is also evidenced by the progressive increase of Heterozoan carbonate facies (Figure 3.2). While in the north-western Mediterranean Tethys RCA abundance increases only in the Miocene, in the study area, RCA facies are already very common by the Oligocene following the increase in CC, suggesting a favourable relationship with the two groups. The abundance of non-skeletal facies related to restricted conditions (Flügel, 2004) peaks in the early Miocene and in particular in the Aquitanian. This is also supported by the lithostratigraphic information provided by Al-Juboury and McCann (2008) and Ameen-Lawa and Ghafur (2015) for Iraq, Reuter et al. (2009) and Mohammadi et al. (2013) for Iran. During the Miocene, the convergence between the African-Arabian and Eurasian plate lead to the progressive restriction and then to the closure of the Mediterranean-Indian Ocean Seaway (Robertson et al., 2012; Rögl, 1999). Sedimentation rates in the Eastern Mediterranean indicates that most of the deep-water restriction occurred in the 24-21 Ma interval (Torfstein & Steinberg, 2020), while Nd isotopes indicates that surface water exchange was reduced by *ca* 90% at *ca* 20 Ma (Bialik et al., 2019). Consequently, although a shallow connection between the two basins persisted for much longer (Buchbinder, 1996; Cornacchia et al., 2018; Sissakian, 2013), most of the restriction occurred during the Aquitanian, consistent with the observed peak of carbonate facies related to restricted marine conditions.

Dominated Facies	Paleocene	Eocene	Oligocene	Miocene	Codominated Facies	Paleocene	Eocene	Oligocene	Miocene
LBF mean	35.19%	78.20%	47.86%	33.03%	LBF mean	28.70%	2.27%	26.97%	5.82%
LBF standard deviation	4.36%	2.24%	2.66%	2.35%	LBF standard deviation	3.62%	1.00%	3.57%	1.60%
LBF lower confidence interval	26.47%	73.72%	42.54%	28.33%	LBF lower confidence interval	21.46%	0.27%	19.83%	2.62%
LBF upper confidence interval	43.91%	82.68%	53.18%	37.73%	LBF upper confidence interval	35.94%	4.27%	34.11%	9.02%
CC mean	3.39%	0.31%	1.78%	1.88%	CC mean	2.70%	0.00%	15.55%	4.31%
CC (standard deviation)	0.94%	0.60%	0.40%	0.52%	CC (standard deviation)	1.27%	0.00%	2.77%	1.39%
CC lower confidence interval	1.51%	-0.89%	0.98%	0.84%	CC lower confidence interval	0.16%	0.00%	10.01%	1.53%
CC upper confidence interval	5.27%	1.51%	2.58%	2.92%	CC upper confidence interval	5.24%	0.00%	21.09%	7.09%
RCA mean	3.61%	0.95%	2.05%	1.02%	RCA mean	22.17%	1.91%	27.87%	8.95%
RCA standard deviation	1.07%	0.39%	0.91%	0.33%	RCA standard deviation	3.83%	1.00%	3.35%	2.27%
RCA lower confidence interval	1.47%	0.17%	0.23%	0.36%	RCA lower confidence interval	14.51%	-0.09%	21.17%	4.41%
RCA upper confidence interval	5.75%	1.73%	3.87%	1.68%	RCA upper confidence interval	29.83%	3.91%	34.57%	13.49%
GCA mean	8.50%	0.33%	0.00%	0.00%	GCA mean	9.90%	0.57%	0.00%	0.00%
GCA standard deviation	2.53%	0.24%	0.00%	0.00%	GCA standard deviation	2.53%	0.31%	0.00%	0.00%
GCA lower confidence interval	3.44%	-0.15%	0.00%	0.00%	GCA lower confidence interval	4.84%	-0.05%	0.00%	0.00%
GCA upper confidence interval	13.56%	0.81%	0.00%	0.00%	GCA upper confidence interval	14.96%	1.19%	0.00%	0.00%

Table 3.6 Bootstrap analysis of the averages of the most abundant and relevant Cenozoic carbonate factories of the study area; the analysis was performed using a 2/3 sub-sample size and 10,000 iterations.

Bootstrap analysis and the comparison of formation-averages and section-averages indicate that the observed trends displayed by the most relevant carbonate facies, that account for most of the thickness of the analysed carbonate successions and for most of the variability of the system, cannot be simply considered a result of the noise of the dataset. Whether different sub-samples are considered, (i.e., the carbonate successions analysed), whether or not the results are grouped based on their geological provenance, the same general trends pop out (Figures 3.4 and 3.5). The remarkable differences between the different time slices, highlighted by dissimilarity analysis, also testifies in favour of the robustness of the results as a randomised development process of the various carbonate factories would have ended up with similar abundances of the various carbonate facies in each epoch. While the formation-average/section-average approach and the bootstrap suggest that the bias related to the geographical position of the studied sections has only a limited effect, the accuracy and the reliability of the source material, which most times consists of qualitative descriptions, prevents more detailed analysis. To test the effects of the relative position of the various sections within the study area, which in turn affects temperature and nutrient availability, a proper quantification of the various components of the skeletal assemblages would be necessary. Such an analysis would also require further subdivision of the database, leading to unequal distribution of sections in the various time slices and their uneven geographical distribution, reducing the robustness of the results as the new sub-sets would be probably characterised by widely different sample-sizes.

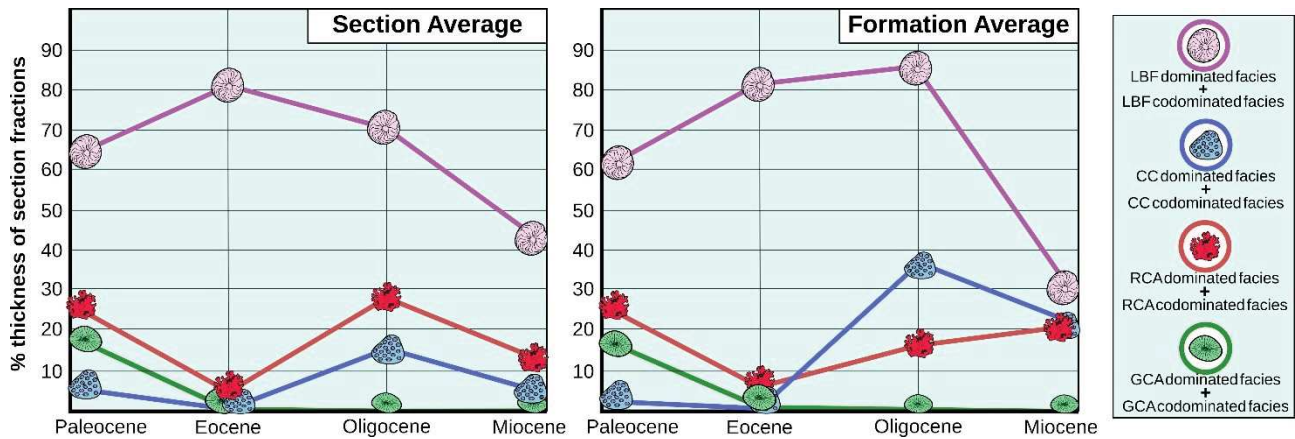


Figure 3.5 Summary diagrams showing the distribution of the main recognised facies (LBF, CC, RCA, GCA) during the Palaeocene, the Eocene, the Oligocene, and the Miocene, using the two different approaches (see Methods): The section-average and the formation-average approaches. Note the preponderance of LBF-dominated and codominated facies in all the epochs; the key to the symbols of the various carbonate producers is as in Figure 3.3; colour coding is as in Figure 3.4; as certain facies can be codominated by, for example LBF and CC (and thus be included in both the CC dominated + CC codominated facies and in the LBF-dominated + LBF codominated facies), in this graph the total can exceed 100%.

3.7 Conclusions

This meta-analysis of Palaeocene to Miocene outcrops of shallow carbonates of the South-western and Western Central Asian regions highlighted several trends in the composition of carbonate factories and in the abundance of carbonate-producing organisms. Large benthic foraminifera are the most quantitatively relevant group of carbonate producers during the whole investigated period, with their abundance peaking during the Eocene and dwindling only during the Miocene. The abundance of CC is highest during the Oligocene and lowest during the Eocene (which in the database is mainly represented by the lower Eocene). Both patterns seem to be related to global temperatures which (within the investigated time period) reach their maximum during the early Eocene and their lowest in the Oligocene. Colonial corals achieve the highest calcification rate in a very narrow temperature range compared to large benthic foraminifera. The very high temperatures of the early Palaeogene of the tropical southern Tethys, might, thus, have favoured LBF-dominated carbonate factories. Thanks to their adaptability LBF would have kept their position as dominant carbonate producers for the whole period, even after the end of the early Palaeogene greenhouse. Red calcareous algae display a pattern much like the one of CC. Since RCA and CC are currently the main framework builder of shallow-water tropical reefs it is possible that, on the large scale, the two groups are probably mutually beneficial to one another in terms of carbonate production. Green calcareous algae decreased from the Palaeocene onward. As the last taxa of presumably calcitic GCA went extinct during the Eocene, it is possible that their overall decrease as carbonate producers might be related to a preservation bias connected to the transition towards modern assemblages that are entirely constituted by fragile, aragonite-producing, taxa. Nutrient abundance and seawater chemistry most likely also played a role in shaping these large-scale patterns of carbonate production. However, any attempt at disentangling

the weight of the various variables not backed by more accurate and standardised data on the skeletal assemblages, would be only speculative. The Aquitanian peak in the abundance of carbonate facies related to very shallow and/or restricted marine conditions is most likely connected to the progressive narrowing of the Tethys Ocean related to the ongoing collision with the Arabian plate. Overall, this meta-analysis displays a clear agreement between large-scale patterns in shallow-water carbonate sedimentation and both environmental and geological processes, indicating the trove of information locked within the shallow-water sedimentary record. However, to unlock this potential, a standardised, quantitative and reproducible approach is absolutely necessary.

Acknowledgements

The authors are grateful to Professor Sam Purkis for his revisions and his wise suggestions that have significantly improved the manuscript, and to the editorial board and editorial office of The Depositional Record for their help and their courtesy. G.C., L.M. and G.B. would like to thank Milano Bicocca University for funding their doctoral and post-doctoral grants. O.M.B. is supported by the Marie Skłodowska Curie fellowship (101003394-RhodoMalta). The first and last authors would also like to thank the IAS for supporting their research activities and for creating an environment conducive to the development of this study. This research represents a scientific contribution of Project MIUR-Dipartimenti di Eccellenza 2018-2022.

Data availability statement

The data that support the findings of this study are openly available at <https://doi.org/10.6084/m9.figshare.19323821.v1>

References

- Adabi, M.H., Kakemem, U. & Sadeghi, A. (2016) Sedimentary facies, depositional environment, and sequence stratigraphy of Oligocene–Miocene shallow water carbonate from the Rig Mountain, Zagros basin (SW Iran). *Carbonates and Evaporites*, 31(1), 69–85.
- Adabi, M.H., Zohdi, A., Ghabeishavi, A. & Amiri-Bakhtiyar, H. (2008) Applications of nummulitids and other larger benthic foraminifera in depositional environment and sequence stratigraphy: an example from the Eocene deposits in Zagros Basin, SW Iran. *Facies*, 54(4), 499–512.
- Afzal, J., Williams, M. & Aldridge, R.J. (2009) Revised stratigraphy of the lower Cenozoic succession of the greater Indus Basin in Pakistan. *Journal of Micropalaeontology*, 28(1), 7–23.
- Afzal, J., Williams, M., Leng, M.J. & Aldridge, R.J. (2011a) Dynamic response of the shallow marine benthic ecosystem to regional and pan-Tethyan environmental change at the Paleocene–Eocene boundary. *Palaeogeography, Palaeoclimatology, Palaeoecology*, 309(3–4), 141–160.
- Afzal, J., Williams, M., Leng, M.J., Aldridge, R.J. & Stephenson, M.H. (2011b) Evolution of Paleocene to early Eocene larger benthic foraminifer assemblages of the Indus Basin, Pakistan. *Lethaia*, 44(3), 299–320.
- Agard, P., Omrani, J., Jolivet, L., Whitechurch, H., Vrielynck, B., Spakman, W., Monié, P., Meyer, B. & Wortel, R. (2011) Zagros orogeny: a subduction-dominated process. *Geological Magazine*, 148(5–6), 692–725.
- Aguilera, O., Bencomo, K., de Araújo, O.M.O., Dias, B.B., Coletti, G., Lima, D., Silane, A.F., Polk, M., Alves-Martin, M.V., Jaramillo, C., Kutter, V.T. & Lopes, R.T. (2020) Miocene heterozoan carbonate systems from the western Atlantic equatorial margin in South America: the Pirabas formation. *Sedimentary Geology*, 407, 1–28. <https://doi.org/10.1016/j.sedgeo.2020.105739>
- Aguirre, J. & Riding, R. (2005) Dasycladalean algal biodiversity compared with global variations in temperature and sea level over the past 350 Myr. *Palaios*, 20(6), 581–588.

- Ahmad, S., Kroon, D., Rigby, S. & Khan, S. (2016) Paleogene Nummulitid biostratigraphy of the Kohat and Potwar basins in North-Western Pakistan with implications for the timing of the closure of eastern Tethys and uplift of the western Himalayas. *Stratigraphy*, 13, 277–301.
- Ahmad, S., Wadood, B., Khan, S., Ullah, A., Mustafa, G., Hanif, M. & Ullah, H. (2020) The sedimentological and stratigraphical analysis of the Paleocene to early Eocene Dungan formation, Kirthar fold and Thrust Belt, Pakistan: implications for reservoir potential. *Journal of Sedimentary Environments*, 5(4), 473–492.
- Akhtar, M. & Butt, A.A. (1999) Microfacies and foraminiferal assemblages from the early tertiary rocks of the kala Chitta range (northern Pakistan). *Géologie Méditerranéenne*, 26(3), 185–201.
- Al-Juboury, A.I. & McCann, T. (2008) The middle Miocene Fatha (lower Fars) formation, Iraq. *GeoArabia*, 13(3), 141–174.
- Al-Kahtany, K.M. (2017) Facies development of the Middle Miocene reefal limestone in Northwest Saudi Arabia. *Journal of African Earth Sciences*, 130, 134–140.
- Al-Qayim, B., Ibrahim, A. & Kharajiany, S. (2016) Microfacies and sequence stratigraphy of the Oligocene–Miocene sequence at Golan Mountain, Kurdistan, Iraq. *Carbonates and Evaporites*, 31(3), 259–276.
- Alsharhan, A.S. & Nairn, A.E.M. (1995) Tertiary of the Arabian Gulf: sedimentology and hydrocarbon potential. *Palaeogeography, Palaeoclimatology, Palaeoecology*, 114(2–4), 369–384.
- Ameen-Lawa, F.A. & Ghafur, A.A. (2015) Sequence stratigraphy and biostratigraphy of the prolific late Eocene, Oligocene and early Miocene carbonates from Zagros fold-thrust belt in Kurdistan region. *Arabian Journal of Geosciences*, 8(10), 8143–8174.
- Amirshahkarami, M. (2013) Microfacies correlation analysis of the Oligocene–Miocene Asmari Formation, in the central part of the Rag-e-Safid anticlinal oil field, Zagros Basin, south-West Iran. *Turkish Journal of Earth Sciences*, 22(2), 204–219.
- Amirshahkarami, M. & Karavan, M. (2015) Microfacies models and sequence stratigraphic architecture of the Oligocene–Miocene Qom Formation, south of Qom City, Iran. *Geoscience Frontiers*, 6(4), 593–604.
- Amirshahkarami, M., Vaziri-Moghaddam, H. & Taheri, A. (2007a) Paleoenvironmental model and sequence stratigraphy of the Asmari Formation in Southwest Iran. *Historical Biology*, 19(2), 173–183.
- Amirshahkarami, M., Vaziri-Moghaddam, H. & Taheri, A. (2007b) Sedimentary facies and sequence stratigraphy of the Asmari formation at chaman-Bolbol, Zagros Basin, Iran. *Journal of Asian Earth Sciences*, 29(5–6), 947–959.
- Amirshahkarami, M. & Zebarjadi, E. (2018) Late Paleocene to early Eocene larger benthic foraminifera biozones and microfacies in Estahbanate area, southwest of Iran with Thetyan biozones correlation. *Carbonates and Evaporites*, 33(4), 869–884.
- An, W., Hu, X., Garzanti, E., Wang, J.G. & Liu, Q. (2021) New precise dating of the India-Asia collision in the Tibetan Himalaya at 61 Ma. *Geophysical Research Letters*, 48(3), e2020GL090641.
- Avarjani, S., Mahboubi, A., Moussavi-Harami, R., Amiri-Bakhtiar, H. & Brenner, R.L. (2015) Facies, depositional sequences, and biostratigraphy of the oligo-Miocene Asmari Formation in Marun oilfield, North Dezful embayment, Zagros Basin, SW Iran. *Palaeoworld*, 24(3), 336–358.
- Avni, Y., Segev, A. & Ginat, H. (2012) Oligocene regional denudation of the northern Afar dome: pre-and syn-breakup stages of the Afro-Arabian plate. *Bulletin*, 124(11–12), 1871–1897.
- Babazadeh, S.A. & Alavi, M. (2013) Paleoenvironmental model for early Eocene larger benthic foraminiferal deposits from South Birjand region, East Iran. *Revue de Paléobiologie, Genève*, 32(1), 223–233.
- Bagherpour, B. & Vaziri, M.R. (2012) Facies, paleoenvironment, carbonate platform and facies changes across Paleocene Eocene of the Taleh Zang formation in the Zagros Basin, SW-Iran. *Historical Biology*, 24(2), 121–142.
- Ballato, P., Mulch, A., Landgraf, A., Strecker, M.R., Dalconi, M.C., Friedrich, A. & Tabatabaei, S.H. (2010) Middle to late Miocene Middle Eastern climate from stable oxygen and carbon isotope data, southern Alborz mountains, N Iran. *Earth and Planetary Science Letters*, 300(1–2), 125–138.
- Banerjee, S., Khanolkar, S. & Saraswati, P.K. (2018) Facies and depositional settings of the middle Eocene–Oligocene carbonates in Kutch. *Geodinamica Acta*, 30(1), 119–136.
- Barnet, J.S., Littler, K., Westerhold, T., Kroon, D., Leng, M.J., Bailey, I., Röhl, U. & Zachos, J.C. (2019) A high-Fidelity benthic stable isotope record of late cretaceous–early Eocene climate change and carbon-cycling. *Paleoceanography and Paleoclimatology*, 34(4), 672–691.
- Bassi, D., Iryu, Y., Humblet, M., Matsuda, H., Machiyama, H., Sasaki, K., Matsuda, S., Arai, K. & Inoue, T. (2012) Recent macrofossils on the Kikai jima shelf, Central Ryukyu Islands, Japan. *Sedimentology*, 59, 2024–2041.
- Basso, D., Coletti, G., Bracchi, V.A. & Yazdi-Moghaddam, M. (2019) Lower oligocene coralline algae of the Uromieh section (Qom formation, NW Iran) and the oldest record of *Titanoderma pustulatum* (Corallinophycidae, Rhodophyta). *Rivista Italiana di Paleontologia e Stratigrafia*, 125(1), 197–218.
- Beavington-Penney, S.J. & Racey, A. (2004) Ecology of extant nummulitids and other larger benthic foraminifera: applications in palaeoenvironmental analysis. *Earth-Science Reviews*, 67(3–4), 219–265.
- Beavington-Penney, S.J., Wright, V.P. & Racey, A. (2006) The middle Eocene Seeb formation of Oman: an investigation of acyclicity, stratigraphic completeness, and accumulation rates in shallow marine carbonate settings. *Journal of Sedimentary Research*, 76(10), 1137–1161.

- Benedetti, A., Consorti, L., Schlagintweit, F. & Rashidi, K. (2021) *Ornatorotalia* pila n. sp. from the late Palaeocene of Iran: ecological, evolutionary and paleobiogeographic inferences. *Historical Biology*, 33(9), 1796–1803.
- Benedetti, A. & Papazzoni, A. (2022) Rise and fall of rotaliid foraminifera across the Paleocene and Eocene times. *Micropaleontology*, 68, 185–196.
- Bernecker, M. (2014) Palaeogene carbonates of Oman: lithofacies and stratigraphy. In: Rocha, R., Pais, J., Kullberg, J. & Finney, S., (Eds.) *STRATI 2013*. Cham: Springer, pp. 71–74.
- Bialik, O.M., Frank, M., Betzler, C., Zammit, R. & Waldmann, N.D. (2019) Two-step closure of the Miocene Indian Ocean gateway to the Mediterranean. *Scientific Reports*, 9(1), 1–10.
- Bialik, O.M., Jarochowska, E. & Grossowicz, M. (2021) Ordination analysis in sedimentology, geochemistry and palaeoenvironment—background, current trends and recommendations. *The Depositional Record*, 7, 541–563.
- Bialik, O.M., Reolid, J., Kulhanek, D.K., Hincke, C., Waldmann, N.D. & Betzler, C. (2022) Sedimentary response to current and nutrient regime rearrangement in the Eastern Mediterranean during the early to middle Miocene (Southwestern Cyprus). *Palaeogeography, Palaeoclimatology, Palaeoecology*, 588, 110819.
- Blondeau, A., Bassoulet, J.P., Colchen, M., Han, T.L., Marcoux, J., Mascle, G. & Van Haver, T. (1986) Disparition des formations marines à l'Éocène inférieur en Hymalaïa. *Sciences de la Terre, Mémoire*, 47, 103–111.
- Bosellini, F. & Perrin, C. (2008) Estimating Mediterranean Oligocene-Miocene Sea surface temperatures: an approach based on coral taxonomic richness. *Palaeogeography Palaeoclimatology Palaeoecology*, 258, 71–88.
- BouDagher-Fadel, M.K. (2018) *Evolution and geological significance of larger benthic foraminifera*. London: University College London Press, p. 693.
- Boudreau, B.P., Middelburg, J.J., Sluijs, A. & van der Ploeg, R. (2019) Secular variations in the carbonate chemistry of the oceans over the Cenozoic. *Earth and Planetary Science Letters*, 512, 194–206.
- Buchbinder, B. (1996) Miocene carbonates of the eastern Mediterranean, the Red Sea and the Mesopotamian Basin: geodynamic and eustatic controls. In: Franseen, E.K., Esteban, M., Ward, W.C., & Rouchy, J.M. (Eds.) *Models for carbonate stratigraphy, from Miocene reef complex of the Mediterranean area*. Concepts in Sedimentology and Paleontology 5. Tulsa, OK: Society for Sedimentary Geology, pp. 89–96.
- Buchbinder, B., Calvo, R. & Siman-Tov, R. (2005) The Oligocene in Israel: a marine realm with intermittent denudation accompanied by mass-flow deposition. *Israel Journal of Earth Sciences*, 54(2), 63–85.
- Budd, A.F. (2000) Diversity and extinction in the Cenozoic history of Caribbean reefs. *Coral Reefs*, 19(1), 25–35.
- Coletti, G., Balmer, E.M., Bialik, O.M., Cannings, T., Kroon, D., Robertson, A.H.F. & Basso, D. (2021a) Microfacies evidence for the evolution of Miocene coral-reef environments in Cyprus. *Palaeogeography Palaeoclimatology Palaeoecology*, 584, 11067.
- Coletti, G., Basso, D., Betzler, C., Robertson, A.H., Bosio, G., El Kateb, A., Foubert, A., Meilijson, A. & Spezzaferri, S. (2019) Environmental evolution and geological significance of the Miocene carbonates of the Eratosthenes Seamount (ODP Leg 160). *Palaeogeography, Palaeoclimatology, Palaeoecology*, 530, 217–235.
- Coletti, G., Basso, D. & Frixa, A. (2017) Economic importance of coralline carbonates. In: *Rhodolith/Maërl beds: a global perspective*. Cham: Springer, pp. 87–101.
- Coletti, G., Mariani, L., Garzanti, E., Consani, S., Bosio, G., Vezzoli, G., Xiumian, H. & Basso, D. (2021b) Skeletal assemblages and terrigenous input in the Eocene carbonate systems of the Nummulitic limestone (NW Europe). *Sedimentary Geology*, 425, 106005.
- Corlett, H.J., Bastesen, E., Gawthorpe, R.L., Hirani, J., Hodgetts, D., Hollis, C. & Rotevatn, A. (2018) Origin, dimensions, and distribution of remobilized carbonate deposits in a tectonically active zone, Eocene Thebes Formation, Sinai, Egypt. *Sedimentary Geology*, 372, 44–63.
- Cornacchia, I., Agostini, S. & Brandano, M. (2018) Miocene oceanographic evolution based on the Sr and Nd isotope record of the Central Mediterranean. *Paleoceanography and Paleoclimatology*, 33(1), 31–47.
- Cornacchia, I., Brandano, M. & Agostini, S. (2021) Miocene paleoceanographic evolution of the Mediterranean area and carbonate production changes: a review. *Earth-Science Reviews*, 221, 103785.
- Crabbe, M.J.C. (2008) Climate change, global warming and coral reefs: modelling the effects of temperature. *Computational Biology and Chemistry*, 32(5), 311–314.
- Daraei, M., Amini, A. & Ansari, M. (2015) Facies analysis and depositional environment study of the mixed carbonate–evaporite Asmari Formation (Oligo-Miocene) in the sequence stratigraphic framework, NW Zagros, Iran. *Carbonates and evaporites*, 30(3), 253–272.
- Dercourt, J., Gaetani, M., Vrielynck, B., Barrier, E., Biju-Duval, B., Brunet, M.F., Cadet, J.P., Crasquin, S. & Sandulescu, M. (2000) Atlas peri-Tethys, Palaeogeographical maps.
- Dill, M.A., Seyrafian, A. & Vaziri-Moghaddam, H. (2012) Palaeoecology of the Oligocene-Miocene Asmari formation in the Dill anticline (Zagros Basin, Iran). *Neues Jahrbuch für Geologie und Paläontologie-Abhandlungen*, 263, 167–184.
- Dill, M.A., Vaziri-Moghaddam, H., Seyrafian, A. & Behdad, A. (2018) Oligo-Miocene carbonate platform evolution in the northern margin of the Asmari intra-shelf basin, SW Iran. *Marine and Petroleum Geology*, 92, 437–461.

- Dill, M.A., Vaziri-Moghaddam, H., Seyrafian, A., Behdad, A. & Shabafrooz, R. (2020) A review of the oligo–Miocene larger benthic foraminifera in the Zagros basin, Iran: new insights into biozonation and palaeogeographical maps. *Revue de Micropaleontologie*, 66, 100408.
- Dishon, G., Grossowicz, M., Krom, M., Guy, G., Gruber, D.F. & Tchernov, D. (2020) Evolutionary traits that enable scleractinian corals to survive mass extinction events. *Scientific Reports*, 10(1), 1–10.
- Efron, B. (1979) Bootstrap methods: another look at the jackknife. *The Annals of Statistics*, 7, 1–26.
- Esteban, M. (1979) Significance of the upper Miocene coral reefs of the western Mediterranean. *Palaeogeography, Palaeoclimatology, Palaeoecology*, 29, 169–188.
- Esteban, M. (1996) An overview of of Miocene reefs from Mediterranean areas: general trends and facies models. In: Franseen, E.K., Esteban, M., Ward, W.C. & Rouchy, J.M. (Eds.) *Models for carbonate stratigraphy, from Miocene reef complex of the Mediterranean area. Concepts in sedimentology and paleontology 5*. Tulsa, OK: Society for Sedimentary Geology, pp. 3–53.
- Fahad, M., Khan, M.A., Hussain, J., Ahmed, A. & Yar, M. (2021) Microfacies analysis, depositional settings and reservoir investigation of Early Eocene Chorgali Formation exposed at Eastern Salt Range, Upper Indus Basin, Pakistan. *Carbonates and Evaporites*, 36(3), 1–18.
- Farouk, S., Ahmad, F. & Smadi, A.A. (2013) Stratigraphy of the Middle Eocene–Lower Oligocene successions in northwestern and eastern Jordan. *Journal of Asian Earth Sciences*, 73, 396–408.
- Fine, M. & Tchernov, D. (2007) Scleractinian coral species survive and recover from decalcification. *Science*, 315(5820), 1811.
- Flügel, E. (2004) *Microfacies of carbonate rocks*. Berlin, Heidelberg: Springer.
- Gaetani, M., Nicora, A., Premoli-Silva, I., Fois, E., Garzanti, E. & Tintori, A. (1983) Upper cretaceous and Paleocene in Zanskar range (NW Himalaya). *Rivista Italiana di Paleontologia e Stratigrafia*, 89, 81–118.
- Garzanti, E., Al-Juboury, A.I., Zoleikhaei, Y., Vermeesch, P., Jotheri, J., Akkoca, D.B., Allen, M., Ando, S., Limonta, M., Padoan, M., Resentini, A., Rittner, M. & Vezzoli, G. (2016) The Euphrates-Tigris-Karun river system: provenance, recycling and dispersal of quartz-poor foreland-basin sediments in arid climate. *Earth-Science Reviews*, 162, 107–128.
- Geel, T. (2000) Recognition of stratigraphic sequences in carbonate platform and slope deposits: empirical models based on microfacies analysis of Palaeogene deposits in southeastern Spain. *Palaeogeography, Palaeoclimatology, Palaeoecology*, 155(3–4), 211–238.
- Ghaedi, M., Johnson, K. & Yazdi, M. (2016) Paleoenvironmental conditions of Early Miocene corals, western Makran, Iran. *Arabian Journal of Geosciences*, 9(17), 1–20.
- Ghafur, A.A. (2015) Integrated depositional model of the carbonate Kirkuk group of southern Kurdistan-Iraq. *Journal of Natural Science Research*, 5, 79–106.
- Ghazi, S., Sharif, S., Zafar, T., Riaz, M., Haider, R. & Hanif, T. (2020) Sedimentology and stratigraphic evolution of the Early Eocene Nammal Formation, Salt Range, Pakistan. *Stratigraphy and Geological Correlation*, 28(7), 745–764.
- GholamiZadeh, P., Hu, X., Garzanti, E. & Adabi, M.H. (2021) Constraining the timing of Arabia-Eurasia collision in the Zagros orogen by sandstone provenance (Neyriz, Iran). *GSA Bulletin*, 134, 1793–1810. <https://doi.org/10.1130/B35950>
- Granier, B. (2012) The contribution of calcareous green algae to the production of limestones: a review. *Geodiversitas*, 34(1), 35–60.
- Hadi, M., Less, G. & Vahidinia, M. (2019) Eocene larger benthic foraminifera (alveolinids, nummulitids, and orthophragmines) from the eastern Alborz region (NE Iran): taxonomy and biostratigraphy implications. *Revue de Micropaleontologie*, 63, 65–84.
- Hadi, M., Mosaddegh, H. & Abbassi, N. (2016) Microfacies and biofabric of nummulite accumulations (Bank) from the Eocene deposits of Western Alborz (NW Iran). *Journal of African Earth Sciences*, 124, 216–233.
- Halfar, J. & Mutti, M. (2005) Global dominance of coralline red-algal facies: a response to Miocene oceanographic events. *Geology*, 33, 481–484.
- Hallock, P. (1997) Reefs and reef limestones in earth history. In: Birkeland, C. (Ed.) *Life and death of coral reefs*. New York: Chapman and Hall, pp. 13–42.
- Hallock, P. & Seddighi, M. (2022) Why did some larger benthic foraminifera become so large and flat? *Sedimentology*, 69(1), 74–87.
- Hanif, M., Imraz, M., Ali, F., Haneef, M., Saboor, A., Iqbal, S. & Ahmad, S. (2014) The inner ramp facies of the Thanetian Lockhart formation, western salt range, Indus Basin, Pakistan. *Arabian Journal of Geosciences*, 7(11), 4911–4926.
- Heidari, A., Mahboubi, A., Moussavi-Harami, R., Gonzalez, L. & Moalemi, S.A. (2014) Biostratigraphy, sequence stratigraphy, and paleoecology of the lower–middle Miocene of northern Bandar Abbas, southeast Zagros basin in south of Iran. *Arabian Journal of Geosciences*, 7(5), 1829–1855.
- Herbert, T.D., Lawrence, K.T., Tzanova, A., Peterson, L.C., Caballero-Gill, R. & Kelly, C.S. (2016) Late Miocene global cooling and the rise of modern ecosystems. *Nature Geoscience*, 9, 843–847.
- Höntzsch, S., Scheibner, C., Guasti, E., Kuss, J., Marzouk, A.M. & Rasser, M.W. (2011) Increasing restriction of the Egyptian shelf during the Early Eocene? —new insights from a southern Tethyan carbonate platform. *Palaeogeography, Palaeoclimatology, Palaeoecology*, 302(3–4), 349–366.
- Hottinger, L. (1982) Larger foraminifera, giant cells with a historical background. *Naturwissenschaften*, 69(8), 361–371.
- Hottinger, L.K. (1983) Neritic macroid genesis: an ecological approach. In: Peryt, T.M. (Ed.) *Coated grains*. Berlin: Springer-Verlag, pp. 38–55.

- Hu, X., Garzanti, E., Wang, J., Huang, W., An, W. & Webb, A. (2016) The timing of India-Asia collision onset—facts, theories, controversies. *Earth-Science Reviews*, 160, 264–299.
- Hussein, A.W. (2019) Cyclic hierarchy and depositional sequences of the middle-upper Eocene ramp facies: An example from Beni Suef area, East Nile Valley, Egypt. *Journal of African Earth Sciences*, 149, 307–333.
- Hussein, D., Collier, R., Lawrence, J.A., Rashid, F., Glover, P.W.J., Lorinczi, P. & Baban, D.H. (2017) Stratigraphic correlation and paleoenvironmental analysis of the hydrocarbon-bearing Early Miocene Euphrates and Jeribe formations in the Zagros folded-thrust belt. *Arabian Journal of Geosciences*, 10(24), 1–15.
- Ishaq, M., Jan, I.U., Hanif, M. & Awais, M. (2019) Microfacies and diagenetic studies of the early Eocene Sakesar Limestone, Potwar Plateau, Pakistan: approach of reservoir evaluation using outcrop analogue. *Carbonates and Evaporites*, 34(3), 623–656.
- James, N.P. (1997) The cool-water carbonate depositional realm. In: James, N.P. & Clarke, J.A.D. (Eds.), *Cool-water carbonates*, vol. 56. SEPM Special Publication, Tulsa, OK: SEPM Society for Sedimentary Geology, pp. 1–22.
- Jauhri, A.K., Misra, P.K., Kishore, S. & Singh, S.K. (2006) Larger foraminiferal and calcareous algal facies in the Lakadong Formation of the South Shillong Plateau, NE India. *Journal of the Palaeontological Society of India*, 51(2), 51–61.
- Jiang, J., Hu, X., Li, J., BouDagher-Fadel, M. & Garzanti, E. (2021) Discovery of the Paleocene-Eocene thermal maximum in shallow-marine sediments of the Xigaze forearc basin, Tibet: a record of enhanced extreme precipitation and siliciclastic sediment flux. *Palaeogeography, Palaeoclimatology, Palaeoecology*, 562, 110095.
- Johnson, K.G., Jackson, J.B. & Budd, A.F. (2008) Caribbean reef development was independent of coral diversity over 28 million years. *Science*, 319(5869), 1521–1523.
- Joudaki, M., Asnavandi, H., Panah, F.M. & Baghbani, D. (2020) The regional facies analysis and depositional environments of the Oligocene and lower Miocene deposits; Zagros Basin, SW of Iran. *Carbonates and Evaporites*, 35(2), 1–18.
- Kahsnitz, M. (2017) Paleocene to lower Eocene sediments of the eastern Neo-Tethyan Ocean: sedimentary and geodynamic evolution as well as biostratigraphy of the larger benthic foraminifera Lockhartia and the genesis of nodular limestones. Doctoral dissertation, Universität Bremen.
- Kamran, M., Frontalini, F., Xi, D., Papazzoni, C.A., Jafarian, A., Latif, K., Jiang, T., Mirza, K., Song, H. & Wan, X. (2021) Larger benthic foraminiferal response to the PETM in the Potwar Basin (eastern Neotethys, Pakistan). *Palaeogeography, Palaeoclimatology, Palaeoecology*, 575, 110450.
- Khan, M., Khan, M.A., Shami, B.A. & Awais, M. (2018) Microfacies analysis and diagenetic fabric of the Lockhart Limestone exposed near Taxila, Margalla Hill range, Punjab, Pakistan. *Arabian Journal of Geosciences*, 11(2), 1–15.
- Khitab, U., Umar, M. & Jamil, M. (2020) Microfacies, diagenesis and hydrocarbon potential of Eocene carbonate strata in Pakistan. *Carbonates and Evaporites*, 35(3), 1–15.
- Kiessling, W., Flügel, E. & Golonka, J. (1999) Paleo reef maps: evaluation of a comprehensive database on Phanerozoic reefs. *American Association of Petroleum Geologists Bulletin*, 83, 1552–1587.
- Kiessling, W., Flügel, E., Golonka, J. 2002. *Phanerozoic reef patterns*. SEPM Special Publication, Tulsa, OK: Society for Sedimentary Geology (SEPM), 775 pp.
- Kuss, J. & Boukhary, M.A. (2008) A new upper Oligocene marine record from northern Sinai (Egypt) and its paleogeographic context. *GeoArabia*, 13(1), 59–84.
- Langer, M.R. & Hottinger, L. (2000) Biogeography of selected "larger" foraminifera. *Micropaleontology*, 46, 105–126.
- Less, G., Frijia, G., Özcan, E., Saraswati, P.K., Parente, M. & Kumar, P. (2018) Nummulitids, lepidocyclinids and Sr-isotope data from the Oligocene of Kutch (western India) with chronostratigraphic and paleobiogeographic evaluations. *Geodinamica Acta*, 30(1), 183–211.
- Leutenegger, S. (1984) Symbiosis in benthic foraminifera; specificity and host adaptations. *The Journal of Foraminiferal Research*, 14, 16–35.
- Li, J., Hu, X., Garzanti, E., An, W. & Wang, J. (2015) Paleogene carbonate microfacies and sandstone provenance (Gamba area, South Tibet): stratigraphic response to initial India–Asia continental collision. *Journal of Asian Earth Sciences*, 104, 39–54.
- Li, J., Hu, X., Zachos, J.C., Garzanti, E. & BouDagher-Fadel, M. (2020) Sea level, biotic and carbon-isotope response to the Paleocene–Eocene thermal maximum in Tibetan Himalayan platform carbonates. *Global and Planetary Change*, 194, 103316.
- Lokier, S.W., Wilson, M.E. & Burton, L.M. (2009) Marine biota response to clastic sediment influx: a quantitative approach. *Palaeogeography, Palaeoclimatology, Palaeoecology*, 281(1–2), 25–42.
- López-Pérez, A. (2017) Revisiting the Cenozoic history and the origin of the eastern Pacific coral fauna. In: Glynn, P., Manzello, D. & Enochs, I. (Eds.) *Coral reefs of the eastern tropical Pacific*. Dordrecht: Springer, pp. 39–57.
- López-Pérez, R.A. (2005) The Cenozoic hermatypic corals in the eastern Pacific: history of research. *Earth-Science Reviews*, 72(1–2), 67–87.
- Mahboubi, A., Moussavi-Harami, R., Lasemi, Y. & Brenner, R.L. (2001) Sequence stratigraphy and sea level history of the upper Paleocene strata in the Kopet-Dagh basin, northeastern Iran. *AAPG Bulletin*, 85(5), 839–859.
- Mahyad, M., Safari, A., Vaziri-Moghaddam, H. & Seyrafian, A. (2019) Biofacies, taphofacies, and depositional environments in the north of Neotethys seaway (Qom Formation, Miocene, Central Iran). *Russian Geology and Geophysics*, 60(12), 1368–1384.

- Marshall, A.T. & Clode, P. (2004) Calcification rate and the effect of temperature in a zooxanthellate and an azooxanthellate scleractinian reef coral. *Coral Reefs*, 23(2), 218–224.
- Martín-Martín, M., Guerrero, F., Tosquella, J. & Tramontana, M. (2020) Paleocene-lower Eocene carbonate platforms of westernmost Tethys. *Sedimentary Geology*, 404, 105674.
- Mattern, F. & Bernecker, M. (2019) A shallow marine clinoform system in limestones (Paleocene/Eocene Jafnayn Formation, Oman): geometry, microfacies, environment and processes. *Carbonates and Evaporites*, 34(1), 101–113.
- Miller, K.G., Browning, J.V., Schmelz, W.J., Kopp, R.E., Mountain, G.S. & Wright, J.D. (2020) Cenozoic sea-level and cryospheric evolution from deep-sea geochemical and continental margin records. *Science Advances*, 6(20), eaaz1346.
- Moghaddam, H.V., Seyrafian, A. & Taraneh, P. (2002) Biofacies and sequence stratigraphy of the Eocene succession, at Hamzeh-Ali area, north-central Zagros, Iran. *Carbonates and Evaporites*, 17(1), 60–67.
- Mohammadi, E. (2020) Sedimentary facies and depositional environments of the Oligocene–early Miocene marine Qom formation, Central Iran Back-Arc Basin, Iran (northeastern margin of the Tethyan seaway). *Carbonates and Evaporites*, 35(1), 1–29.
- Mohammadi, E., Hasanazadeh-Dastgerdi, M., Ghaedi, M., Dehghan, R., Safari, A., Vaziri-Moghaddam, H., Baizidi, C., Vaziri, M. & Sfidari, E. (2013) The Tethyan Seaway Iranian Plate Oligo-Miocene deposits (the Qom Formation): distribution of Rupelian (Early Oligocene) and evaporate deposits as evidence for timing and trending of opening and closure of the Tethyan Seaway. *Carbonate Evaporite*, 28, 321–345.
- Mohammadi, E., Safari, A., Vaziri-Moghaddam, H., Vaziri, M.R. & Ghaedi, M. (2011) Microfacies analysis and paleoenvironmental interpretation of the Qom formation, south of the Kashan, Central Iran. *Carbonates and Evaporites*, 26(3), 255–271.
- Mossadegh, Z.K., Haig, D.W., Allan, T., Adabi, M.H. & Sadeghi, A. (2009) Salinity changes during late Oligocene to early Miocene Asmari formation deposition, Zagros mountains, Iran. *Palaeogeography, Palaeoclimatology, Palaeoecology*, 272(1–2), 17–36.
- Nafarieh, E., Boix, C., Cruz-Abad, E., Ghasemi-Nejad, E., Tahmasbi, A. & Caus, E. (2019) Imperforate larger benthic foraminifera from shallow-water carbonate facies (middle and late Eocene), Zagros Mountains, Iran. *Journal of Foraminiferal Research*, 49(3), 275–302.
- Nafarieh, E., Vaziri-Moghaddam, H., Taheri, A. & Ghabeshavi, A. (2012) Biofacies and palaeoecology of the Jahrum Formation in Lar area, Zagros Basin, (SW Iran). *Iranian Journal of Science and Technology*, 36(A1), 51.
- Naveed, A. & Chaudhry, M.N. (2008) Geology of Hettangian to middle Eocene rocks of Hazara and Kashmir basins, northwest lesser Himalayas, Pakistan. *Geological Bulletin of Panjab University*, 43, 131–152.
- Nebelsick, J.H., Rasser, M.W. & Bassi, D. (2005) Facies dynamics in Eocene to Oligocene circumalpine carbonates. *Facies*, 51(1), 197–217.
- Noorian, Y., Moussavi-Harami, R., Reijmer, J.J., Mahboubi, A., Kadkhodaie, A. & Omidpour, A. (2021) Paleo-facies distribution and sequence stratigraphic architecture of the Oligo-Miocene Asmari carbonate platform (Southeast Dezful Embayment, Zagros Basin, SW Iran). *Marine and Petroleum Geology*, 128, 105016.
- Özcan, E., Hanif, M., Ali, N. & Yücel, A.O. (2015) Early Eocene orthophragminids (foraminifera) from the type-locality of *Discocyclina ranikotensis* Davies, 1927, Thal, NW Himalayas, Pakistan: insights into the orthophragminid palaeobiogeography. *Geodinamica Acta*, 27(4), 267–299.
- Özcan, E., Saraswati, P.K., Yücel, A.O., Ali, N. & Hanif, M. (2018) Bartonian orthophragminids from the Fulra limestone (Kutch, W India) and coeval units in Sulaiman range, Pakistan: a synthesis of shallow benthic zone (SBZ) 17 for the Indian subcontinent. *Geodinamica Acta*, 30(1), 137–162.
- Perrin, C. (1992) Signification écologique des foraminifères acervulinidés et leur rôle dans la formation de facies récifaux et organogènes depuis le Paléocène. *Geobios*, 25(6), 725–751.
- Perrin, C. (2009) Solenomeris: from biomineralization patterns to diagenesis. *Facies*, 55(4), 501–522.
- Perrin, C. & Bosellini, F.R. (2012) Paleobiogeography of scleractinian reef corals: changing patterns during the Oligocene–Miocene climatic transition in the Mediterranean. *Earth-Science Reviews*, 111(1–2), 1–24.
- Perrin, C. and Kiessling, W. (2012) Latitudinal trends in Cenozoic reef patterns and their relationship to climate. In: Mutti, M., Piller, W., Betzler, C. (Eds.), *Carbonate systems during the Oligocene-Miocene climatic transition*, vol. 42. Oxford, UK: Wiley-Blackwell. International Association of Sedimentologists Special Publications, pp. 17–34.
- Perry, O.R. & Choquette, P.W. (1985) *Carbonate petroleum reservoirs*. New York: Springer.
- Pomar, L., Baceta, J.I., Hallock, P., Mateu-Vicens, G. & Basso, D. (2017) Reef building and carbonate production modes in the west-central Tethys during the Cenozoic. *Marine and Petroleum Geology*, 83, 261–304.
- Pomar, L., Bassant, P., Brandano, M., Ruchonnet, C. & Janson, X. (2012) Impact of carbonate producing biota on platform architecture: insights from Miocene examples of the Mediterranean region. *Earth-Science Reviews*, 113(3–4), 186–211.
- Pomar, L., Brandano, M. & Westphal, H. (2004) Environmental factors influencing skeletal grain sediment associations: a critical review of Miocene examples from the western Mediterranean. *Sedimentology*, 51(3), 627–651.
- Pomar, L. & Hallock, P. (2007) Changes in coral-reef structure through the Miocene in the Mediterranean province: adaptive versus environmental influence. *Geology*, 35(10), 899–902.

- Rahmani, A., Vaziri-Moghaddam, H., Taheri, A. & Ghabeshavi, A. (2009) A model for the paleoenvironmental distribution of larger foraminifera of Oligocene–Miocene carbonate rocks at Khaviz Anticline, Zagros Basin, SW Iran. *Historical Biology*, 21(3–4), 215–227.
- Rasser, M.W. and Piller, W.E. (1997) Depth distribution of calcareous encrusting associations in the northern Red Sea (Safaga, Egypt) and their geological implications. Proceedings of the 8th international Coral Reef Symposium, 743–748.
- Rasser, W.M. (1994) Facies and palaeoecology of rhodoliths and acervulinid macroids in the Eocene of the Krappfeld (Austria). *Beiträge zur Paläontologie*, 19, 191–217.
- Renema, W. (2018) Terrestrial influence as a key driver of spatial variability in large benthic foraminiferal assemblage composition in the central Indo-Pacific. *Earth-Science Reviews*, 177, 514–544.
- Reuter, M., Piller, W.E., Harzhauser, M., Kroh, A. & Bassi, D. (2008) Termination of the Arabian shelf sea: stacked cyclic sedimentary patterns and timing (Oligocene/Miocene, Oman). *Sedimentary Geology*, 212(1–4), 12–24.
- Reuter, M., Piller, W.E., Harzhauser, M., Mandic, O., Berning, B., Rogl, F., Kroh, A., Aubry, M.P., Wielandt-Schuster, U. & Hamedani, A. (2009) The oligo–Miocene Qom Formation (Iran): evidence for an early Burdigalian restriction of the Tethyan Seaway and closure of its Iranian gateways. *International Journal of Earth Sciences*, 98(3), 627–650. <https://doi.org/10.1007/s00531-007-0269-9>
- Riosmena-Rodríguez, R. (2017) Natural history of Rhodolith/Maërl beds: their role in near-shore biodiversity and management. In: Riosmena-Rodríguez R., Nelson W. & Aguirre J. (Eds), *Rhodolith/Maërl beds: a global perspective*. Coastal research library, vol. 15, 3–27. Cham, Switzerland: Springer.
- Robertson, A.H.F., Parlak, O. & Ustaömer, T. (2012) Overview of the Palaeozoic–Neogene evolution of Neotethys in the Eastern Mediterranean region (Southern Turkey, Cyprus, Syria). *Petroleum Geoscience*, 18, 381–404.
- Rögl, F. (1999) Mediterranean and Paratethys facts and hypotheses of an Oligocene to Miocene paleogeography (short overview). *Geologica Carpathica*, 50, 339–349.
- Rooypeykar, A., Maghfouri-Moghaddam, I., Yazdi, M. & Yousefi-Yegane, B. (2019) Facies and paleoenvironmental reconstruction of Early-Middle Miocene deposits in the north-west of the Zagros Basin. *Iran Geologica Carpathica*, 70(1), 75–87.
- Rooypeykar, A. & Moghaddam, I.M. (2016) Benthic foraminifera as biostratigraphical and paleoecological indicators: an example from oligo-Miocene deposits in the SW of Zagros basin, Iran. *Geoscience Frontiers*, 7(1), 125–140.
- Rosenfeld, A. & Hirsch, F. (2005) The Paleocene–Eocene of Israel. In: Hall, J.K., Krasheninnikov, V.A., Hirsch, F., Benjamini, C. & Flexer, A. (Eds.) *Geological framework of the levant –Volume II: The Levantine Basin and Israel*. Jerusalem: Historical Productions-Hall, pp. 437–458.
- Sadeghi, R., Vaziri-Moghaddam, H. & Taheri, A. (2011) Microfacies and sedimentary environment of the Oligocene sequence (Asmari Formation) in Fars sub-basin, Zagros Mountains, Southwest Iran. *Facies*, 57(3), 431–446.
- Sadooni, F.N. & Alsharhan, A.S. (2019) Regional stratigraphy, facies distribution, and hydrocarbons potential of the Oligocene strata across the Arabian plate and Western Iran. *Carbonates and Evaporites*, 34(4), 1757–1770.
- Safari, A., Ghanbarloo, H., Mansoury, P. & Esfahani, M.M. (2020) Reconstruction of the depositional sedimentary environment of Oligocene deposits (Qom formation) in the Qom Basin (northern Tethyan Seaway), Iran. *Geologos*, 26(2), 93–111.
- Sallam, E., Wanas, H.A. & Osman, R. (2015) Stratigraphy, facies analysis and sequence stratigraphy of the Eocene succession in the Shabrawet area (north Eastern Desert, Egypt): an example for a tectonically influenced inner ramp carbonate platform. *Arabian Journal of Geosciences*, 8(12), 10433–10458.
- Sarkar, S. (2016) Early Eocene calcareous algae and benthic foraminifera from Meghalaya, NE India: a new record of microfacies and palaeoenvironment. *Journal of the Geological Society of India*, 88(3), 281–294.
- Sarkar, S. (2017) Microfacies analysis of larger benthic foraminifera-dominated middle Eocene carbonates: a palaeoenvironmental case study from Meghalaya, NE India (eastern Tethys). *Arabian Journal of Geosciences*, 10(5), 1–13.
- Sarkar, S. (2018) The enigmatic Palaeocene-Eocene coralline *Distichoplax*: approaching the structural complexities, ecological affinities and extinction hypotheses. *Marine Micropaleontology*, 139, 72–83.
- Schaub, H., Benjamini, C. and Moshkovitz, S. (1995) The biostratigraphy of the Eocene of Israel: nummulites Planktic Foraminifera and Calcareous Nannofossils. *Kommission der Schweizerischen Paläontologischen Abhandlungen*, 58 p.
- Scheibner, C., Kuss, J. & Marzouk, A.M. (2000) Slope sediments of a Paleocene ramp-to-basin transition in NE Egypt. *International Journal of Earth Sciences: Geologische Rundschau*, 88(4), 708–724.
- Scheibner, C., Reijmer, J.J.G., Marzouk, A.M., Speijer, R.P. & Kuss, J. (2003) From platform to basin: the evolution of a Paleocene carbonate margin (Eastern Desert, Egypt). *International Journal of Earth Sciences*, 92(4), 624–640.
- Scheibner, C. & Speijer, R.P. (2008) Late Paleocene–early Eocene Tethyan carbonate platform evolution –a response to long-and short-term paleoclimatic change. *Earth-Science Reviews*, 90(3–4), 71–102.
- Schlager, W. (2003) Benthic carbonate factories of the Phanerozoic. *International Journal of Earth Sciences*, 92, 445–464.
- Scotese, C.R. (2014a) Atlas of Paleogene paleogeographic maps (Mollweide projection), maps 8–15, Volume 1. The Cenozoic, PALEOMAP Atlas for ArcGIS, PALEOMAP Project, Evanston, IL.

- Scotese, C.R. (2014b) Atlas of Neogene paleogeographic maps (Mollweide projection), maps 1–7, volumes 1. The Cenozoic, PALEOMAP Atlas for ArcGIS, PALEOMAP Project, Evanston, IL.
- Sengupta, S., Volgushev, S. & Shao, X. (2016) A subsampled double bootstrap for massive data. *Journal of the American Statistical Association*, 111(515), 1222–1232.
- Serra-Kiel, J., Hottinger, L., Caus, E., Drobne, K., Ferrandez, C., Jauhri, A.K., Less, G., Pavlovec, R., Pignatti, J., Samsó, J.M., Schaub, H., Sirel, E., Strougo, A., Tambareau, Y., Tosquella, J. & Zakrevskaya, E. (1998) Larger foraminiferal biostratigraphy of the Tethyan. *Bulletin de la Société géologique de France*, 169, 281–299.
- Seyrafian, A. & Toraby, H. (2005) Petrofacies and sequence stratigraphy of the Qom Formation (Late Oligocene-Early Miocene?), north of Nain, southern trend of central Iranian Basin. *Carbonates and Evaporites*, 20(1), 82–90.
- Shabafrooz, R., Mahboubi, A., Vaziri-Moghaddam, H., Ghabeishavi, A. & Moussavi-Harami, R. (2015) Depositional architecture and sequence stratigraphy of the oligo–miocene Asmari platform; southeastern Izeh zone, Zagros Basin, Iran. *Facies*, 61(1), 1–32.
- Sissakian, V.K. (2013) Geological evolution of the Iraqi Mesopotamia foredeep, inner platform and near surroundings of the Arabian plate. *Journal of Asian Earth Sciences*, 72, 152–163.
- Stanley, S.M. (2006) Influence of seawater chemistry on biomineralization throughout phanerozoic time: paleontological and experimental evidence. *Palaeogeography, Palaeoclimatology, Palaeoecology*, 232(2–4), 214–236.
- Steinthorsdottir, M., Coxall, H.K., de Boer, A.M., Huber, M., Barbolini, N., Bradshaw, C.D., Burls, N.J., Feakins, S.J., Gasson, E., Henderiks, J., Holbourn, A., Kiel, S., Kohn, M.J., Knorr, G., Kürschner, W.M., Lear, C., Liebrand, D., Lunt, D.J., Mörs, T., Pearson, P.N., Pound, M.J., Stoll, H. and Strömberg, C.A.E. (2020) The Miocene: the future of the past. *Paleoceanography and Paleoclimatology*, 36, 1–71.
- Swati, M.A.F., Haneef, M., Ahmad, S., Naveed, Y., Zeb, W., Akhtar, N. & Owais, M. (2013) Biostratigraphy and depositional environments of the early Eocene Margalla Hill limestone, Kohala-Bala area, Haripur, Hazara fold-Thrust Belt, Pakistan. *Journal of Himalayan Earth Sciences*, 46(2), 65.
- Taheri, A., Vaziri-Moghaddam, H. & Seyrafian, A. (2008) Relationships between foraminiferal assemblages and depositional sequences in Jahrum formation, Ardal area (Zagros Basin, SW Iran). *Historical Biology*, 20(3), 191–201.
- Titelboim, D., Almogi-Labin, A., Herut, B., Kucera, M., Askenazi-Polivoda, S. & Abramovich, S. (2019) Thermal tolerance and range expansion of invasive foraminifera under climate changes. *Scientific Reports*, 9(1), 1–5.
- Tomás, S., Frijia, G., Bömelburg, E., Zamagni, J., Perrin, C. & Mutti, M. (2016) Evidence for seagrass meadows and their response to paleoenvironmental changes in the early Eocene (Jafnayn formation, Wadi Bani Khalid, N Oman). *Sedimentary Geology*, 341, 189–202.
- Torfstein, A. & Steinberg, J. (2020) The oligo–Miocene closure of the Tethys Ocean and evolution of the proto-Mediterranean Sea. *Scientific Reports*, 10(1), 1–10.
- Tucker, M.E. & Wright, V.P. (1990) *Carbonate sedimentology*. Oxford: Blackwell, pp. 1–496.
- Van Buchem, F.S.P., Allan, T.L., Laursen, G.V., Lotfpour, M., Moallemi, A., Monibi, S., Motiei, H., Pickard, N.A.H., Tahmasbi, A.R., Vedrenne, V. and Vincent, B. (2010) Regional stratigraphic architecture and reservoir types of the oligo–Miocene deposits in the Dezful embayment (Asmari and Pabdeh Formations) SW Iran. In: Van Buchem, F.S.P., Gerdes, K.D., & Esteban, M. (Eds.), *Mesozoic and Cenozoic carbonate systems of the Mediterranean and the Middle East: stratigraphic and diagenetic reference models*. Geological Society of London, Special Publications, London: Geological Society, 329, 219–263.
- Vaziri-Moghaddam, H., Kalanat, B. & Taheri, A. (2011) Sequence stratigraphy and depositional environment of the Oligocene deposits at Firozabad section, southwest of Iran based on microfacies analysis. *Geopersia*, 1(1), 71–152.
- Vaziri-Moghaddam, H., Kimiagari, M. & Taheri, A. (2006) Depositional environment and sequence stratigraphy of the Oligo–Miocene Asmari Formation in SW Iran. *Facies*, 52(1), 41–51.
- Vaziri-Moghaddam, H., Seyrafian, A., Taheri, A. & Motiei, H. (2010) Oligocene–Miocene ramp system (Asmari Formation) in the NW of the Zagros basin, Iran: microfacies, paleoenvironment and depositional sequence. *Revista mexicana de ciencias geológicas*, 27(1), 56–71.
- Whittle, G.L., Alsharhan, A.S. & El Deeb, W.M.Z. (1995) Bio-lithofacies and diagenesis in the early-middle oligocene of Abu Dhabi, United Arab Emirates. *Carbonates and Evaporites*, 10(1), 54–64.
- Willems, H., Zhou, Z., Zhang, B.G. & Gräfe, K.U. (1996) Stratigraphy of the upper cretaceous and lower tertiary strata in the Tethyan Himalayas of Tibet (Tingri area, China). *Geologische Rundschau*, 85(4), 723–754.
- Wilson, M.E.J. (2008) Global and regional influences on equatorial shallow-marine carbonates during the Cenozoic. *Palaeogeography Palaeoclimatology Palaeoecology*, 265, 262–274.
- Wilson, M.E.J. & Vecsei, A. (2005) The apparent paradox of abundant foramol facies in low latitudes: their environmental significance and effect on platform development. *Earth-Science Reviews*, 69(1–2), 133–168.
- Wright, V.P. & Burchette, T.P. (1996) Shallow-water carbonate environments. In: Reading, H.G. (Ed.) *Sedimentary environments*. Oxford: Blackwell, pp. 325–394.
- Yazdi-Moghadam, M., Sadeghi, A., Adabi, M.H. & Tahmasbi, A. (2018a) Foraminiferal biostratigraphy of the lower Miocene Hamzian and Arashtanab sections (NW Iran), northern margin of the Tethyan Seaway. *Geobios*, 51(3), 231–246.

- Yazdi-Moghadam, M., Sadeghi, A., Adabi, M.H. & Tahmasbi, A. (2018b) Stratigraphy of the lower Oligocene nummulitic limestones, north of Sonqor (Nw Iran). *Rivista Italiana di Paleontologia e Stratigrafia*, 124(2), 407–416.
- Yazdi-Moghadam, M., Sarfi, M., Ghasemi-Nejad, E., Sadeghi, A. & Sharifi, M. (2021) Early Miocene larger benthic foraminifera from the northwestern Tethyan seaway (NW Iran): new findings on shallow benthic zone 25. *International Journal of Earth Sciences*, 110(2), 719–740.
- Zachos, J., Pagani, M., Sloan, L., Thomas, E. & Billups, K. (2001) Trends, rhythms, and aberrations in global climate 65 ma to present. *Science*, 292(5517), 686–693.
- Zhang, Q., Willems, H. & Ding, L. (2013) Evolution of the Paleocene-early Eocene larger benthic foraminifera in the Tethyan Himalaya of Tibet, China. *International Journal of Earth Sciences*, 102(5), 1427–1445.
- Ziegler, A.M. (2001) Late Permian to Holocene paleofacies evolution of the Arabian plate and its hydrocarbon occurrences. *GeoArabia*, 6(3), 445–504.
- Zoeram, F.Z., Vahidinia, M., Sadeghi, A., Mahboubi, A. & Bakhtiar, H.A. (2015) Larger benthic foraminifera: a tool for biostratigraphy, facies analysis and paleoenvironmental interpretations of the oligo-Miocene carbonates, NW central Zagros Basin, Iran. *Arabian Journal of Geosciences*, 2(8), 931–949.
- Zohdi, A., Mousavi-Harami, R., Ali Moallemi, S., Mahboubi, A. & Immenhauser, A. (2013) Evolution, paleoecology and sequence architecture of an Eocene carbonate ramp, southeast Zagros Basin, Iran. *GeoArabia*, 18(4), 49–80.

4. Foraminifera

4.1 Introduction

After discussing the distribution of carbonate-producing organism relative to modern and fossil shallow-water environments, it has been possible to understand the response of carbonate producers to different ecological parameters and to provide a global, quantitative and standardised overview of this. Moreover, large benthic foraminifera were found to be the most quantitatively and volumetrically important group of carbonate producers, at least until the Miocene, with a peak in abundance during the Eocene. Thus, benthic foraminifera will be introduced, with a discussion about their biology, ecology and their significance in palaeontology.

Foraminifera are an important order of unicellular protozoa that live in both benthic conditions on the seafloor and planktonic conditions within the water column. These organisms are characterized by a cytoplasm enclosed within a shell or skeleton, called test. The solid skeleton can be composed of various materials, including organic secretions like tectin, mineral secretions, or agglutinated particles (the latter two are of greater paleontological interest; Brasier, 2005). This group of organisms derives its name from certain characteristic elements of the skeleton, known as *foramina*, which are openings present on the walls of the foraminifer's shell. Regarding the structure of the shell, foraminifera are classified as either multilocular, with many chambers inside the shell, or unilocular, where the entire skeleton consists of a single chamber.

Foraminifera are highly significant in geology as they serve as excellent biostratigraphic and paleoecological indicators, particularly in the Cenozoic era when they reached their zenith, but also in the Mesozoic and Late Paleozoic (Brasier, 2005). They inhabit a wide range of environments on Earth, from marine to continental, from tropical to polar latitudes (Murray, 2006). The study of these organisms is essential for paleoclimatic analyses, as isotopic analyses conducted within their carbonate shells can provide information about ocean temperature and composition. Additionally, their fossil assemblages can contribute significantly to the study of deep-sea currents. From an ecological perspective, three main groups of foraminifera can be distinguished: i) planktonic foraminifera, characterized by wide geographical distribution and rapid evolutionary lines; ii) small benthic foraminifera, the most common category in stratigraphic records; and iii) large benthic foraminifera, equipped with photosymbionts and serving as valuable biostratigraphic and paleoecological indicators in tropical carbonate rocks and within the Tethys Ocean context, which is the primary focus of this thesis work.

4.2 Foraminiferal biology

The cell of foraminifera (Figure 4.1) is divided into an inner part called endoplasm and an outer part called ectoplasm, connected to the inside of the cell through an opening. The endoplasm is protected by the shell and contains a nucleus (or multiple nuclei in the case of multinucleate cells), numerous small organelles including mitochondria, the Golgi apparatus, and ribosomes, as well as food vacuoles that make up the cell's "digestive system" (Brasier, 2005). Endoplasm often contains cells of photosymbiotic organisms (including diatoms and dinoflagellates) that perform chlorophyll-based photosynthesis, releasing oxygen and receiving phosphorus, nitrogen, and carbon dioxide from the foraminifera itself. *Pseudopodia*, branched filamentous structures used by the organism to capture organic particles for food, develop from the ectoplasm. In benthic forms, *pseudopodia* are also used for motility and anchoring (Brasier, 2005).

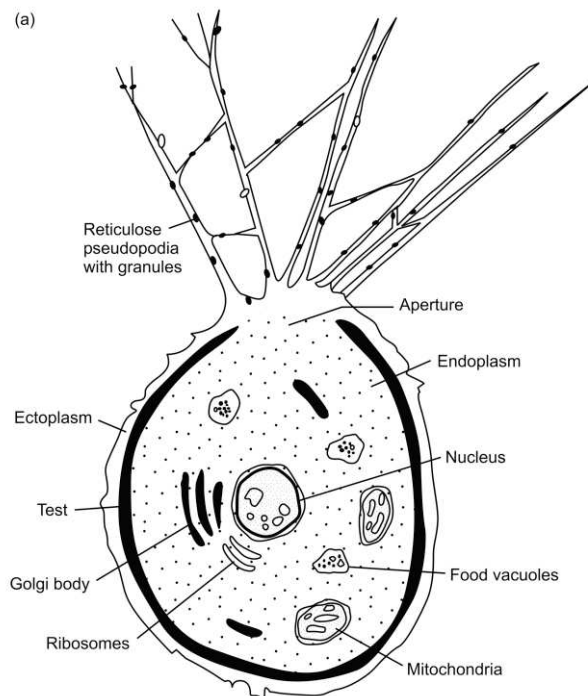


Figure 4.1 A living, single-chambered benthic foraminifer, as seen in cross-section with transmitted light. Is it possible to appreciate the different structures and organelles. From Brasier, 2005.

The life cycle of foraminifera (Figure 4.2) is rather complex. Its duration varies from the tropics (where it is shorter) to the poles (where it is longer), and it is characterized by the alternation between two generations: a gamont that reproduces sexually and an agamont that reproduces asexually. The asexual reproduction of an agamont occurs through multiple divisions of the cytoplasm, resulting in numerous small haploid cells that contain only half of the chromosomal set. This gives rise to a generation of gamonts which, after gametogenesis through mitosis, form gametes containing the same number of chromosomes as the haploid parent cells. At this point, two gametes can fuse through sexual reproduction to form a zygote, which gives rise to a new generation of agamonts. The agamont

generation, whose cell is diploid, contains a complete chromosomal set. The cycle can then repeat. Additionally, there are cases where the life cycle of foraminifera includes another type of generation called schizonts: these are diploid cells produced by multiple divisions without meiosis, starting from an agamont cell.

An important observation, also from a paleontological perspective, is related to the shells of different life stages of foraminifera: they exhibit significant differences, especially in large benthic foraminifera. Gamont cells have a large initial chamber called protoconch or *proloculus*, with a small-sized shell. This type of shell is called megalosphere (also referred to as "form A"). Agamont cells, on the other hand, have a small protoconch with a larger-sized shell, known as microsphere (also referred to as "form B"). This phenomenon is referred to as a form of dimorphism related to the foraminifera's life cycle and can also be observed in the fossil record.

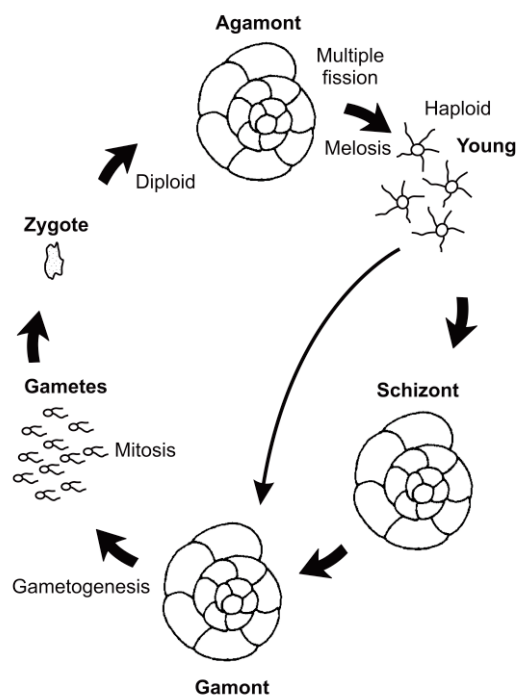


Figure 4.2 The classical foraminiferid life cycle with a regular alternation of generations between gamont and agamont. From Brasier, 2005, after Goldstein, in Sen Gupta, 1999.

Regarding the shell, it serves as a protective element for the cell against various stress factors, including biological stress such as predation, physical stress like solar radiation, turbulence, mechanical abrasion, and chemical stress related to salinity, CO₂ and O₂ content, and pH. In benthic foraminifera, the presence of a shell promotes a benthic lifestyle by weighing down the cell and limiting its buoyancy (Brasier, 2005).

As mentioned earlier, the composition of foraminifera shells can vary depending on the type of organism. Some foraminifera have an organic shell composed of tectin, a substance similar to a protein, pseudo-chitinous in nature. Other foraminifera, like the Textulariida, have an agglutinated type of shell, made up of organic and mineral particles collected by the cell on the seafloor and cemented together by calcareous or iron oxide substances. However, the majority of shells are composed of carbonate minerals. The minerals that form the test are secreted directly by the cell within the cytoplasm and then transported outward through vesicles. In other cases, calcium carbonate precipitates above a tectin membrane that encloses the shell. Carbonate shells can come in three types: imperforate porcelaneous, microgranular, or hyaline. Imperforate porcelaneous shells are typical of the Miliolina suborder and are made of calcite with a high magnesium content, with crystals randomly distributed in the central portion and surrounded by two layers with horizontally oriented crystals. Hyaline shells, found in Rotaliida, are typically perforated and have a glassy, transparent appearance. They are composed of either low to high magnesium calcite or aragonite and can be mono or polycrystalline. In many groups, rhomboidal crystals of calcite or aragonite are oriented with the principal axis *c* perpendicular to the shell surface and exhibit characteristic patterns when observed under an optical microscope with two polarizers. Microgranular shells, on the other hand, consist of microgranules assembled with random orientations or arranged parallel or perpendicular to the shell edges. Shells of this type appear black under transmitted light in an optical microscope and exhibit a fibrous structure. The shells of the earliest foraminifera were mostly unilocular, consisting of a single chamber. Only later did multilocular forms develop, consisting of several chambers added at regular intervals during the organism's growth (Brasier, 2005). Each chamber has an opening called *foramen*, which is protected by a septum and connects each chamber to the next. In more complex forms, individual chambers can be subdivided into small chambers with multiple openings, a typical structure of large benthic foraminifera with symbionts. The growth of multilocular shells is related to the interaction of three different variables: the translation rate, which is the ratio of movement along the growth axis to movement opposite to this axis, the chamber expansion rate, and the shape of the chamber. Different translation rates produce different types of shell coiling: planispiral, trochospiral, biserial, and uniserial. A planispiral shell has a translation rate of zero, and the chambers are symmetrically arranged along the growth axis on a plane of coiling. The spiral can be evolute if the chambers do not cover the previous ones or involute if the opposite is true. When the shell takes on the form of a helical spiral, it is called trochospiral; when no spiral is present, the shell can be uniserial or biserial (Figure 4.3). Foraminifera shells exhibit various external structures that are used to distinguish different genera and species.

4.3 Ecology of small benthic foraminifera

Approximately 5,000 species of small benthic foraminifera are known. Small benthic foraminifera are of particular significance as environmental indicators because they have adapted to marine habitats ranging from the most extreme tidal marshes to the deepest ocean trenches (Murray, 2006). Their ability to exploit resources across this wide range of habitats is reflected in the adaptations of their test morphology (Murray, 2006).

The ecology of small benthic foraminifera is controlled by different ecological parameters. The first abiotic factor to be considered is the presence of light. The photic zone, i.e., the depth of the zone of light penetration in the oceans, is influenced by various factors, such as water clarity and the angle at which the Sun's rays strike the surface. Consequently, the photic zone is deeper in tropical waters and becomes shallower towards the poles, where it also experiences pronounced seasonality (Brasier, 2005).

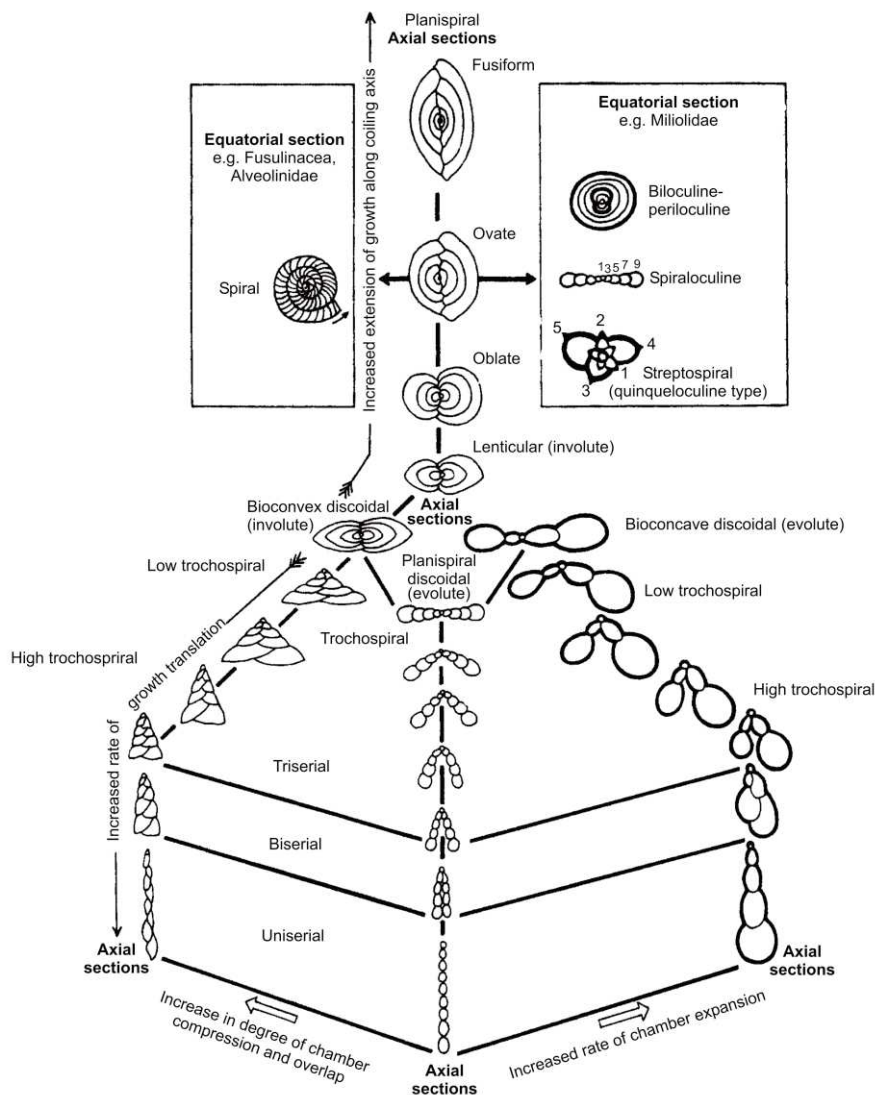


Figure 4.3 Growth forms in multilocular tests of foraminifera. Axial sections are those cut parallel to and including the main axis of symmetry and growth. Equatorial sections are cut at right angles to this axis, at the widest point on the test. From Brasier, 2005.

Foraminifera are attracted to this zone due to primary production by planktonic and benthic protozoa, as well as the presence of algae and seagrasses that provide protection and substrates (e.g., Brasier, 2005; Murray, 2006). Furthermore, the tests of some foraminifera, such as the porcelaneous wall of miliolids, is believed to protect their cytoplasm from damage in shallow waters by scattering short-wavelength ultraviolet light. Another factor that controls small benthic foraminifera distribution is food. Indeed, foraminifera play a prominent role in marine ecosystems as micro-omnivores, feeding on small bacteria, protozoa, and invertebrates (Brasier, 2005). Some smaller benthic forms are known to host photosymbionts (e.g., *Elphidium*); others are strictly infaunal, and live within the sediment, even below the photic zone, feeding on dead organic particles or grazing on bacteria (Brasier, 2005). The tests of active foraminifera tend to be lenticular or elongate, whereas foraminifera living on abyssal plains often have erect, tubular, and branched tests fixed to the substrate. Foraminifera that prefer hard substrates, such as rocks, shells, sea grasses, and algae, are typically attached, either temporarily or permanently, using a flat or concave lower surface. Their growth forms are hydrodynamically stable and include discoidal, plano-convex, concavo-convex, dendritic, and irregular shapes. Adherent forms often develop relatively thin tests and tend to exhibit greater morphological variability than sediment-dwelling and planktonic forms. While some foraminifera have been found to live up to 200 mm below the sediment surface, the majority are within the top 10 mm (Brasier, 2005). Those found in higher-energy sands and gravel on the inner shelf tend to be either adherent or free-living with thick-shelled, heavily ornamented forms of lenticular or globular shape. Low-energy habitats with silty and muddy substrates, typical of lagoons and the mid-shelf to bathyal slope, tend to encourage bacterial blooms and are attractive to free-living foraminifera. Most foraminifera are adapted to normal marine salinities (around 35‰), and the highest diversity assemblages are found in these conditions. Brackish lagoons and marshes, with lower salinities, favour low-diversity assemblages of agglutinated foraminifera and certain hyaline forms. Hypersaline waters, with salinities exceeding 40‰, seem to favour porcelaneous foraminifera (Figure 4.4).

The availability of nutrients like phosphate and nitrate significantly influences primary productivity rates in oceans. In areas with low food supply rates, such as the deep sea, foraminiferal densities tend to be low, but diversity can be high. In upwelling zones, where nutrients are brought to the surface, foraminifera populations can be relatively dense. When nutrient supply rates to the surface are high, it often leads to a reduction in foraminiferal diversities for several reasons. The increased nutrient flux tends to discourage photosymbiosis, which impacts planktonic and larger benthic foraminifera that rely on symbionts. Additionally, high rates of primary production at the surface can result in anaerobic bacterial blooms in the oxygen minimum zone of mid-waters and on the seafloor. In anaerobic conditions, foraminifera populations may become scarce, but in dysaerobic conditions,

eutrophic benthic foraminifera can dominate the biota. These assemblages are characterized by small, thin-shelled, unornamented calcareous foraminifera, such as *Bulimina*, *Bolivina*, *Uvigerina*, or primitive agglutinated forms.

Temperature adaptation varies among foraminiferal species, and the most critical factor consists of the temperature range for successful reproduction. Generally, species adapted to stable tropical climates have a narrower temperature range. However, ocean stratification leads to progressively cooler conditions in the lower water layers, even in tropical regions where surface temperatures may average 28°C, but abyssal plain depths may average less than 4°C. These cooler, deeper waters support cool-water benthic assemblages typically found at shallower depths nearer the poles.

Water mass history is another critical aspect, as certain hyaline, benthic foraminiferal species are closely tied to specific water masses rather than just water depth. This connection allows the ancient distribution of certain species to be used in reconstructing the history of specific water masses, in response to changes in global climate or basin geometry.

Diversity, referring to the number of taxa in an assemblage, can be measured using techniques that are not dependent on sample size, such as the alpha index. In living assemblages, one species is often more abundant than any other and is considered dominant. Dominance is usually expressed as a percentage of the population, and lower dominance tends to be associated with higher diversity. Modern benthic foraminiferal assemblages in marginal marine habitats typically exhibit lower diversity compared to normal marine and deep-sea habitats. Higher diversity in the latter suggests greater resource partitioning among species, especially in stable habitats with scarce food resources. In contrast, environments with oscillating environmental stability, like marshes and lagoons, often see foraminiferal blooms with high abundance but lower diversity. These opportunistic species need to reach maturity quickly and tend to be relatively small in size.

4.4 Ecology of large benthic foraminifera

Large benthic foraminifera (LBF hereinafter) are characterised by complex internal morphology and a volume of at least 3 mm³, although some species reach volumes of more than 500 mm³ (Ross, 1974). Currently living species mainly inhabit shallow-water carbonate tropical environments, and the majority of them host symbiotic algae inside their shells (Cowen, 1983). Studying the ecology of living species is an essential prerequisite for the study of fossil forms. However, the relationship between LBF distribution and various environmental factors is very complex and is challenging to establish a direct correlation between the characteristics of LBF and a specific external influence (Beavington-Penney & Racey, 2004). The knowledge of the zonation and the depth of life of modern species is an excellent paleoenvironmental indicator to be used as a tool for reconstructing the

depositional history of Nummulitic limestones or other rock types containing LBF (Beavington-Penney & Racey, 2004). Hallock (1985) reports that LBF are biostratigraphically important, as their evolutionary history is characterized by rapid diversifications and sudden extinctions. Their development, however, is linked to periods of global warming, characterized by marine transgression events and the expansion of tropical systems, with reduced ocean circulation (Hallock & Glenn, 1986). These factors lead to oligotrophic conditions, which are very advantageous for LBF, especially when they host symbionts (Beavington-Penney & Racey, 2004). Such conditions were present in the early Tertiary, where large benthic foraminifera belonging to the families Nummulitidae (e.g., *Nummulites*, *Operculina*, *Assilina*), Orthophragminidae (e.g., *Discocyclina*, *Asterocyclina*), and Alveolinidae (*Alveolina*) thrived in carbonate ramp environments within the Tethys, playing a role as major sediment producers (Buxton & Pedley, 1989). The study of LBF is also important from an economic perspective, especially concerning the nummulitids, which belong to the sub-order Rotaliina. Reservoirs consisting of *Nummulites* deposits from the Eocene, for instance, can possibly contain significant volumes of hydrocarbons (Racey, 2001).

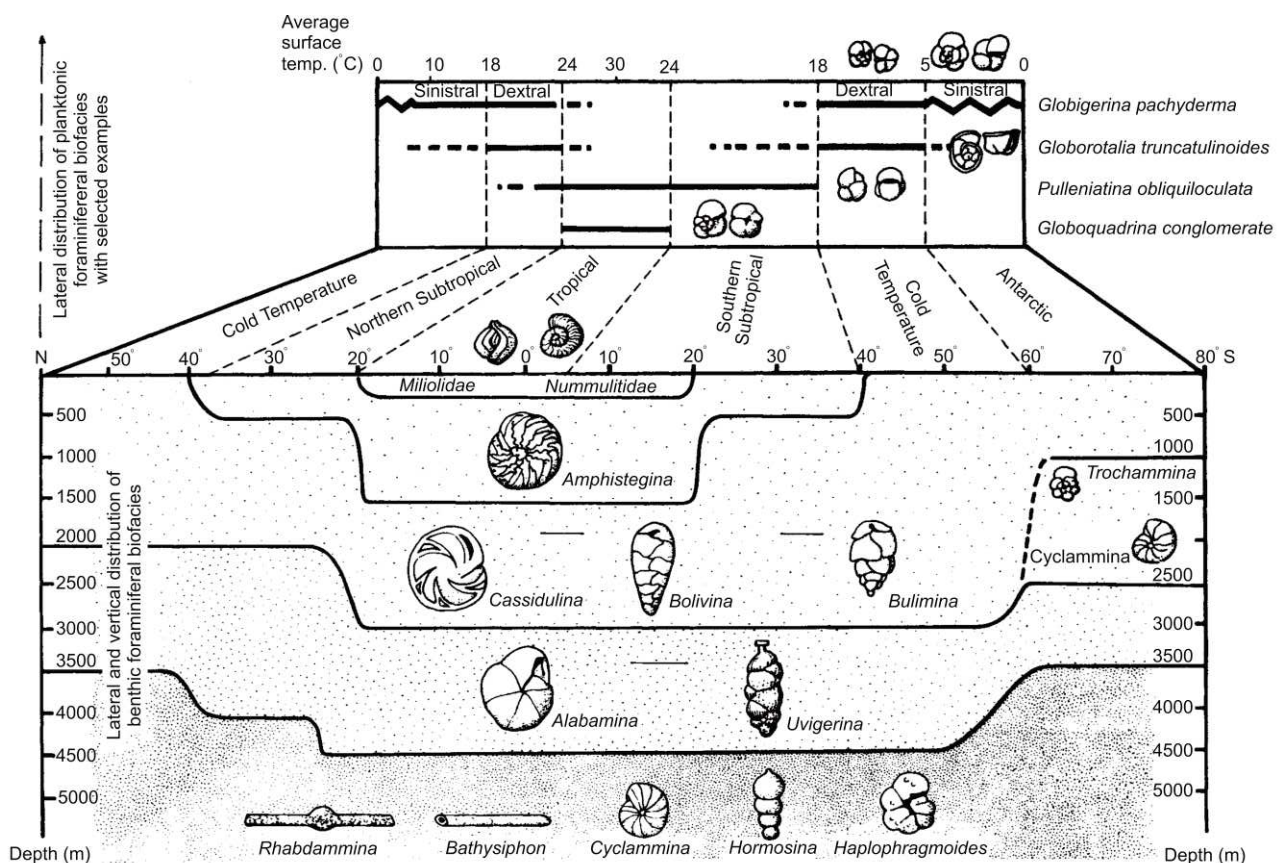


Fig. 4.4 Benthic and planktonic foraminiferid abundance and general composition change with depth and salinity. From Brasier, 2005.

In favourable environmental conditions, LBF adopt an "r-selected" growth strategy, characterized by rapid development and reproduction at relatively small sizes (Hallock & Glenn, 1986). Under stress conditions associated with low temperatures, insufficient food and light, and other factors, individuals grow slowly, and reproductive maturity is achieved at larger sizes, following a "k-selected" growth strategy (Bradshaw, 1957). When environmental conditions fall outside the tolerance limits for reproduction, LBF do not reproduce, and the size of their shells increases significantly. Often, shell size increases with depth but decreases in the deepest part of their habitat (Hallock, 1985; Drooger, 1993). This observation indicates that the number of microspheric forms increases with depth, reaching an optimum within a specific depth range, while their number drastically decreases in surface waters (Beavington-Penney & Racey, 2004). The primary ecological factor that changes with increasing depth is light intensity, which is linked to plant growth. Along with light, other factors that significantly influence reproduction, especially sexual reproduction, in large benthic foraminifera are nutritional factors and substrate and water column composition (Beavington-Penney & Racey, 2004). Some authors hypothesize that the high number of microspheric forms at greater depths is due to the passive transport of gametes downward, whereas gamonts of macrospheric forms (also called "A forms") can be found at all depths (Beavington-Penney & Racey, 2004). In any case, despite the complex distribution of sexual and asexual forms along the water column, the ratio between macrospheres and microspheres can be used to distinguish the depth range (Hottinger, 1997), taking into account taphonomic processes as well. Regarding *Nummulites*, Bombita (1973) observed that microspheric forms are rare within the Eocene strata in the Carpathians, and other authors have noted the same phenomenon in other locations during the Eocene epoch. Brasier & Green (1993) proposed a ratio of 49:1 between macrospheric and microspheric forms, although different ratios have been reported in other studies. The challenge in calculating this type of data also lies in the distinction between A and B forms, which is determined solely by measuring shell dimensions. Without the observation of the protoconch, the calculated ratio can be incorrect due to intraspecific variability, leading to inaccurate conclusions (Racey, 2001). In any case, it is impossible to define a normal or correct ratio, as this can vary depending on the surrounding environmental conditions or, in the case of fossil assemblages, post-mortem processes (Beavington-Penney & Racey, 2004).

Regarding lifespan, many publications have reported that Eocene *Nummulites* had a variable lifespan ranging from several months to a few years, similar to present-day benthic forms. However, the absence of modern counterparts of similar size to early Tertiary large foraminifera makes it difficult to draw convincing conclusions about their lifespan, which is estimated to be only 1 to 5 years based on currently available data (Beavington-Penney & Racey, 2004).

Many species of LBF are characterized by the presence of symbiotic algae located within their shells (Haynes, 1965). This symbiotic interaction suggests that most LBF, during their lifetime, inhabited shallow, well-illuminated marine environments. The fossil presence of LBF, in the absence of transport, indicates a depth limit of less than 130 meters, within the photic zone (Hallock, 1984). Growth and calcification processes in various LBF species are dependent on the activity of symbiotic algae (Leutenegger, 1984). Jones (1999) demonstrated that for rotaliids, typically found in oligotrophic environments, the presence of nutrient-providing symbionts is more critical than for miliolids, which are typical of mesotrophic to eutrophic environments. The presence of symbionts leads to modifications within the calcareous shells of foraminifera, including small holes in the chamber walls where the algae reside or the formation of small additional chambers (Beavington-Penney & Racey, 2004). The pillars present on the shells of LBF act as lenses that collect and channel light to favour the symbionts (Reiss & Hottinger, 1984). In the Nummulitidae family, the reproduction of symbiotic algae takes place inside the foraminifera itself, within the canal system, which simultaneously provides protection to the algae from the external environment (Beavington-Penney & Racey, 2004) (Figure 4.5). The symbiotic relationship between algae and LBF facilitates calcification, allowing the foraminifera to produce thicker shell walls, and reducing the risk of predation (Beavington-Penney & Racey, 2004). The ability to produce calcium carbonate in the presence of light is directly proportional to photosynthesis and occurs at a rate 2-3 times greater than in darkness.

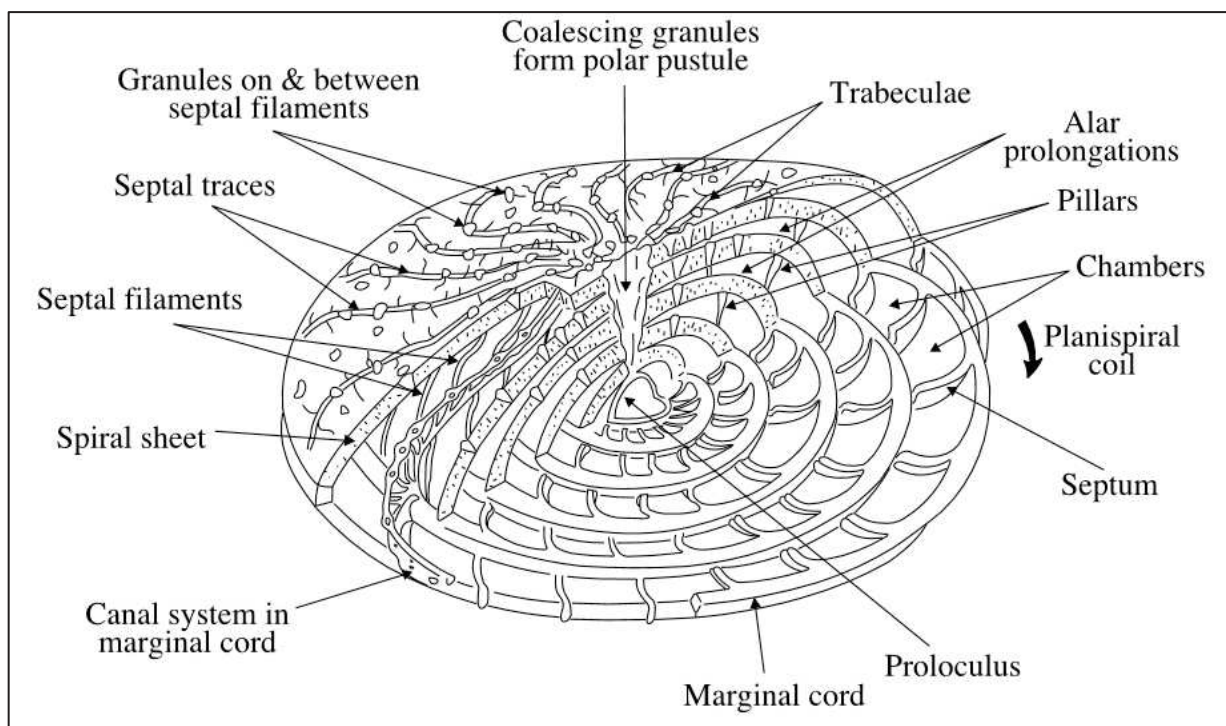


Figure 4.5 Structure of a megalospheric *Nummulites* test. From Beavington-Penney and Racey, 2004.

The shell morphology of a foraminifera is influenced by light, in addition to metabolism and hydrodynamic factors (Haynes, 1965). Within the same genus, test's shape can vary based on the amount of received light (Hallock & Hansen, 1979). Oblate morphologies and thicker tests are typical of shallow environments. Larsen (1976) demonstrated that the diameter-to-thickness (D/T) ratio is directly proportional to depth and is linked to light availability.

At the group level, the zonation of foraminifera is closely influenced by light availability. Generally, porcelain-like forms dominate in the top 50 meters of the water column, while rotaliids are more common at greater depths. Symbiont-bearing rotaliids extend to the base of the photic zone, where illumination corresponds to 0.5% of that at the surface (Hottinger, 1983), while below this depth, small benthic foraminifera devoid of symbionts dominate. LBF are adapted to live in oligotrophic, stable environments with low nutrient levels and are not competitive in areas characterized by abundant nutrient inputs (Hallock, 1985). An excessive nutrient input (nitrates and phosphates) can stimulate phytoplankton growth, reducing water transparency and, consequently, carbonate production, thus limiting the depth range of foraminifera (Beavington-Penney & Racey, 2004). A high nutrient availability can also encourage symbionts to adopt a planktonic lifestyle. In eutrophic contexts, marine sediments often exhibit anoxic to suboxic conditions, which are unsuitable for the life of LBF. Moreover, the presence of phosphates can pose problems for calcification processes. Nutrient input is often linked to temperature and salinity: upwelling phenomena add nutrients and reduce temperature, continental runoff increases nutrient concentration and reduces salinity, while evaporation concentrates nutrients and increases salinity (Hallock & Schlager, 1986). Another effect of a high nutrient load is the increased occurrence of bioerosion on shells caused by algae and endolithic fungi (note that Brasier, 1995, advises caution when using bioerosion as an indicator of nutrient abundance, as it is necessary to consider effects related to low sedimentation rates, lack of oxygen, depth, and light intensity). The amount of nutrients present is also often influenced by substrate type (Gerlach, 1972). The substrate can exert a significant influence on the distribution of large benthic foraminifera. It includes organic and inorganic particles, along with interstitial water and air. Sandy and gravelly substrates have good porosity and generally contain a small amount of nutrients, hosting small populations of LBF, typically characterized by thick shells and biconvex morphologies. Conversely, muddy and silty substrates are often rich in organic matter and support larger populations (Beavington-Penney & Racey, 2004).

Hydrodynamics is a factor that strongly influences the morphology of LBF tests (Hallock & Hansen, 1979). Greater hydrodynamic activity is associated with thicker shells because it forces the shells to be more robust, albeit at the expense of reducing the overall growth rate (Beavington-Penney & Racey, 2004). Salinity variations are of considerable importance mainly in coastal settings, where

they control the distribution of LBF (Phleger, 1960). Generally, rotaliids are stenohaline organisms, with tolerance limits between 30-45 ‰ (Hallock & Glenn, 1986). Temperature influences many chemical, physical, and biological processes that occur within the marine environment. Foraminifera are poikilothermic organisms, so their body temperature closely matches that of the external environment (Beavington-Penney & Racey, 2004). Their small mass responds very quickly to temperature changes, although these changes are related to simultaneous alterations in other environmental properties such as light, salinity, pressure, and dissolved gases (Kinne, 1970). The large-scale distribution of LBF is associated with specific temperature ranges, particularly seasonal ranges, which influence reproduction (Beavington-Penney & Racey, 2004). LBF are distributed within a range between the maximum summer isotherm of 25°C and the minimum winter isotherm of 15°C (Beavington-Penney & Racey, 2004). The presence of warm ocean currents can influence the distribution of LBF. Temperature also controls the type of LBF associations: tropical and subtropical associations are characterized by a greater number of species compared to temperate associations (Beavington-Penney & Racey, 2004).

Taphonomic processes encompass various phenomena that mostly occur after the death of the organism. The transport of foraminiferal shells, both living and fossil, by currents has a significant impact on the distribution of many LBF (Beavington-Penney & Racey, 2004). Susceptibility to transport is more effective in surface conditions than in deep environments. Abrasion and fracturing phenomena are common in LBF fossils. A significant phenomenon is the dissolution of calcareous shells, which is linked to calcium carbonate undersaturation within the water column and can lead to the complete destruction of the shell. Bioerosion is a phenomenon caused by both microorganisms and predators and can lead to the destruction or weakening of the shell, making it more susceptible to dissolution and abrasion (Beavington-Penney & Racey, 2004). Peebles & Lewis (1988) have demonstrated that rotaliids are less susceptible to bioerosion compared to miliolids. Rapid burial can favour the protection of the shell from bioerosion by microorganisms (Beavington-Penney & Racey, 2004). Additionally, fossil records can be modified due to the selective action on shells by bioturbating organisms (Schafer & Pelletier, 1976).

Additional factors that influence the distribution of LBF include oxygen deficiency, which reduces the number of species in associations but increases the number of individuals, and pH, as acidic conditions cause significant stress in calcium carbonate production (Beavington-Penney & Racey, 2004).

4.4.1 Distribution of large benthic foraminifera

Hallock & Glenn (1986) presented a model for the ideal distribution of modern foraminifera in reef contexts (Figure 4.6), which can also be applied to the analysis of fossil distributions. Racey (2001) summarized the complex relationships among LBF that inhabited carbonate platforms in the early Tertiary, concluding that *Nummulites* occupied a wide range of marine environments, both on ramps and platforms, while being absent in restricted water environments. *Nummulites* with wide and flat shapes are associated with *Assilina* and *Discoyclina*, which exhibit similar morphologies. They are typical of deeper water environments. On the other hand, smaller and lenticular *Nummulites* are characteristic of shallow-waters in inner platform contexts, often associated with *Alveolina* (Beavington-Penney & Racey, 2004). Banks of medium/large-sized *Nummulites* with globular/lenticular shapes are associated with intermediate environments (Beavington-Penney & Racey, 2004). The distribution of Eocene LBF is illustrated within the model shown in Figure 4.7. However, it is essential to consider that the distribution of LBF is also influenced by local factors that vary between different basins. This observation indicates that the foraminiferal associations present in the fossil record can only be used as a relative paleobathymetric indicator and not as an absolute indicator of the depth of deposition (Beavington-Penney & Racey, 2004).

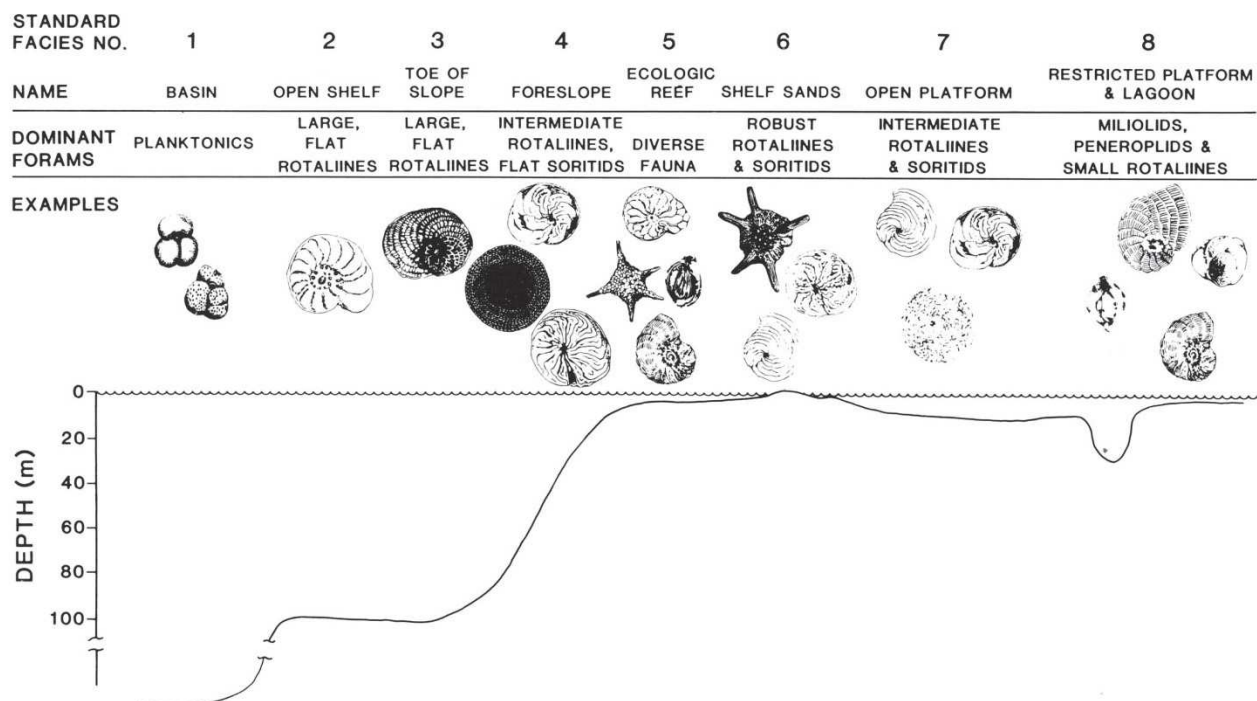


Figure 4.6 Idealised distribution of major foraminiferal groups in reef-associated environments, from Hallock & Glenn (1986). Key to modern examples (listed top to bottom): 1- *Globigerinoides ruber*, *G. sacculifer*. 2- *Operculina ammonoides*. 3- *Heterostegina depressa*. 4- *Amphistegina lessonii*, *Sorites marginalis*, *A. radiata*. 5- *H. depressa*, *Baculogypsina sphaerulata*, *Triloculina trigonula*, *Peneroplis pertusus*. 6- *Calcarina spengleri*, *Amphistegina lobifera*, *Peneroplis proteus*. 7- *P. proteus*, *A. lessonii*, *Amphisorus hemprichii*. 8- *Peneroplis planatus*, *Quinqueloculina candelana*, *Rosalina* sp., *P. pertusus*.

An important observation is that the ratio of planktonic to benthic foraminifera decreases when moving from open ocean environments to platform contexts (Beavington-Penney & Racey, 2004). This trend shows a positive correlation with decreasing depth and distance from the ocean (Murray, 1976).

Finally, in this last paragraph the main uses of analyses on large benthic foraminifera for paleoenvironmental reconstructions are described, with a particular focus on *Nummulites* and orthophragminids. Associations of foraminifera dominated by "A" type forms are linked to shallow environments or, for some species, extremely deep environments within tolerance limits. "B" type forms are more common in intermediate-depth contexts. The A:B ratio can provide indications of paleobathymetry, with the caveat that distinguishing between these two different forms must be done through the observation of the internal shell structures in thin section. However, this ratio cannot be used to distinguish autochthonous and allochthonous populations of *Nummulites* (Beavington-Penney & Racey, 2004). Another useful parameter for paleoenvironmental analysis is the D/T ratio, which is the ratio of shell diameter to thickness. An increase in the D/T value indicates flat and thin shells associated with greater depths. Conversely, a decrease in the D/T value indicates lenticular and thick shells typical of shallower environments (Beavington-Penney & Racey, 2004). This parameter can be applied to both nummulitids and orthophragminids. Regarding the latter, Čosović et al. (2004) describe how orthophragminids are associated with a greater number of nummulitids, characterized by thick and lenticular shells, when they have a T/D ratio (in this case, the reciprocal ratio is calculated) greater than 0.45; conversely, orthophragminids associated with planktonic foraminifera have a T/D ratio ranging from 0.2 to 0.3. This information indicates that differences in shell morphology are linked to depth variations, confirmed by the study of fossil associations and sedimentological characteristics: orthophragminids from shallower waters have a higher T/D ratio compared to those associated with environments considered to be of greater depth (Čosović et al., 2004). Another parameter used is the ratio between orthophragminids and nummulitids (O/N), which has a paleobathymetric significance: an increase in this ratio corresponds to deepening of the basin.

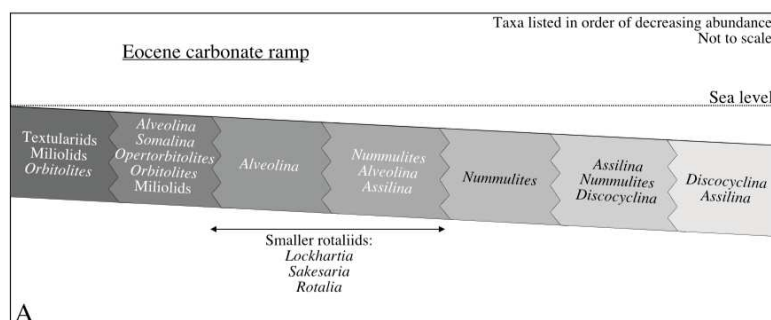


Figure 4.7 Idealized model of an Eocene carbonate ramp and the relative foraminiferal association. From Beavington-Penney & Racey, 2004.

References

- Beavington-Penney, S. J. & Racey, A. 2004: Ecology of extant nummulitids and other larger benthic foraminifera: applications in paleoenvironmental analysis, *Earth-Science Reviews* 67, 219–265.
- Bombita, P.G., 1973: Macroforaminifères des Carpates Orientales: leur position et leur signification stratigraphique. *Eclogae Geologicae Helveticae* 66, 447–477 (in French).
- Bradshaw, J.S. 1957: Laboratory studies of the rate of growth of the foraminifera *Stebulus beccarii* (Linne'), var. *tepida* Cushman. *Journal of Paleontology* 31, 1138–1147.
- Brasier, M.D., Green, O.R. 1993: Winners and losers: stable isotopes and microhabitats of living Archaiadae and Eocene Nummulites (larger foraminifera). *Marine Micropaleontology* 20, 267–276.
- Brasier, M.D. 1995: Fossil indicators of nutrient levels: 2. Evolution and extinction in relation to oligotrophy. In: Bosence, D.W.J., Allison, P.A. (Eds.), *Marine Palaeoenvironmental Analysis from Fossils*. Geological Society of London Special Publication, vol. 83, pp. 133–150.
- Brasier, M.D. 2005: *Microfossils*, Second edition, Chapter 15, Foraminifera, 142–188.
- Buxton, M.W.N., Pedley, H.M. 1989: Short paper: a standardised model for Tethyan Tertiary carbonate ramps. *Journal of the Geological Society (London)* 146, 746–748.
- Cosovic, V., Drobne, K. & Moro, A. 2004: Paleoenvironmental model for Eocene foraminiferal limestones of the Adriatic carbonate platform (Istrian Peninsula), *Facies*, 50, 61–75.
- Cowen, R., 1983: Algal symbiosis and its recognition in the fossil record. In: Tevesz, M.J.S., McCall, P.L. (Eds.), *Biotic Interactions in Recent and Fossil Benthic Communities*. Plenum, New York.
- Drooger, C.W., 1993: Radial foraminifera: morphometrics and evolution. *Verhandelingen, Afdeling Natuurkunde, Koninklijke Nederlandse Akademie van Wetenschappen*, 1e Reeks, 41.
- Gerlach, S.A. 1972: Substratum: general introduction. In: Kinne, O. (Ed.), *Marine Ecology*. Wiley, New York, pp. 1245–1250.
- Hallock, P., Hansen, H.J. 1979: Depth adaptation in *Amphistegina*: change in lamellar thickness. *Bulletin of the Geological Society of Denmark* 27, 99–104.
- Hallock, P. 1984: Distribution of larger foraminiferal assemblages on two Pacific coral reefs. *Journal of Foraminiferal Research* 14, 250–261.
- Hallock, P. 1985: Why are larger foraminifera large? *Paleobiology* 11, 195–208.
- Hallock, P., Glenn, E.C. 1986: Larger foraminifera: a tool for paleoenvironmental analysis of Cenozoic depositional facies. *Palaaios* 1, 55–64.
- Hallock, P., Schlager, W. 1986: Nutrient excess and the demise of coral reefs and carbonate platforms. *Palaaios* 1, 389–398.
- Haynes, J.R. 1965: Symbiosis, wall structure and habitat in foraminifera. *Special Publication-Cushman Foundation for Foraminiferal Research* 16, 40–43.
- Hottinger, L. 1983: Processes determining the distribution of larger foraminifera in space and time. *Utrecht Micropaleontological Bulletins* 30, 239–253.
- Hottinger, L. 1997: Shallow benthic foraminiferal assemblages as signals for depth of their deposition and their limitations. *Bulletin de la Societe Geologique de France* 168, 491–505.
- Jones, R.W. 1999: Marine invertebrate (chiefly foraminiferal) evidence for the palaeogeography of the Oligocene–Miocene of western Eurasia, and consequences for terrestrial vertebrate migration. In: Agusti, J., Andrews, P., Rook, L. (Eds.), *Hominoid Evolution and Climatic Change in Europe. The Evolution of Neogene Terrestrial Systems in Europe*, vol. 1. Cambridge Univ. Press, UK, pp. 274–308.
- Kinne, O. 1970: Temperature: general introduction. In: Kinne, O. (Ed.), *Marine Ecology*, vol. 1 (1). Wiley, New York, pp. 321–346.
- Larsen, A.R. 1976: Studies of recent *Amphistegina*: taxonomy and some ecological aspects. *Israel Journal of Earth-Sciences* 25, 1–26.
- Leutenegger, S. 1984: Symbiosis in benthic foraminifera: specificity and host adaptations. *Journal of Foraminiferal Research* 14, 16–35. Lipps, J.H., 1982.
- Murray, J.W. 1976: A method of determining proximity of marginal seas to an ocean. *Marine Geology* 22, 103–119. Murray, J.W., 1987.
- Murray, J.W., 2006. *Ecology and Applications of Benthic Foraminifera*. Cambridge University Press, Cambridge, p. 426.

- Peebles, M.W., Lewis, R.D. 1988: Differential infestation of shallow-water benthic foraminifera by microboring organisms: possible biases in preservation potential.
- Phleger, F.B. 1960: Ecology and Distribution of Recent Foraminifera. John Hopkins Univ. Press, Baltimore.
- Racey, A. 2001: A review of Eocene nummulite accumulations: structure, formation and reservoir potential. *Journal of Petroleum Geology* 24, 79–100.
- Reiss, Z., Hottinger, L. 1984: The Gulf of Aqaba. *Ecological Micropaleontology*. Springer-Verlag, New York.
- Ross, C.A. 1974: Evolutionary and ecological significance of large, calcareous Foraminiferida (Protozoa), Great Barrier Reef. *Proceedings of the 2nd International Coral Reef Symposium, Brisbane, Australia, vol. 1, pp. 327–333.*
- Schafer, C.T., Pelletier, B.R. 1976: Benthonics '75: first international symposium on benthonic foraminifera of continental margins: Part A. *Ecology and Biology. Atlantic Geology* 1.

5. Epiphytic foraminifera. Testing an indirect palaeo-seagrass indicator: Benthic foraminifera from the Lower Pleistocene *Posidonia* meadow of Fauglia (Tuscany, Italy)

After introducing and discussing the importance of benthic foraminifera, the focus will shift on epiphytic foraminifera, stressing their significance as palaeo-seagrass proxies. It will be emphasised the importance of the analysis of seagrass-related environments, even in palaeontology, with the aim of understanding how these environments might evolve in the future in response to changes in climate conditions.

This chapter is taken from the scientific paper:

Mariani, L., Coletti, G., Mateu Vicens, G., Bosio, G., Collareta, A., Khokhlova, A., Di Cencio, A., Casati, S. and Malinverno, E. (2021a). Testing an indirect palaeo-seagrass indicator: Benthic foraminifera from the Lower Pleistocene *Posidonia* meadow of Fauglia (Tuscany, Italy), *Marine Micropaleontology*, v. 173. <https://doi.org/10.1016/j.marmicro.2022.102126>

5.1 Abstract

Well-preserved remains of a *Posidonia oceanica* meadow have been found in a Lower Pleistocene (Calabrian) succession cropping out near Fauglia (Tuscany, Italy). This paper analyses and describes the benthic foraminiferal community associated with this well-preserved Pleistocene *P. oceanica* meadow, with the purpose of testing the usefulness of foraminifera as an Indirect Palaeo-Seagrass Indicator (IPSI), providing both qualitative and quantitative parameters to recognize other meadow-related environments where fossil remains of seagrasses are not preserved. Despite being influenced by some diagenetic processes that might have affected the foraminiferal assemblage, the Fauglia succession represents a suitable setting for testing benthic foraminifera as IPSI in a temperate environment. Considering this limitation, together with other ecological constraints such as seawater temperature, this study provides evidence of the high potential of benthic foraminifera as IPSI. Several parameters such as the modified Foraminifera Index (FI'), the "long vs. short life-span index" (I_{LS}), and the presence of permanently attached, encrusting foraminifera were tested. New indexes were also developed, namely the K/R ratio, consisting of the ratio between keeled *Elphidium* and the sum of rounded elphidiids (e.g., *Elphidium translucens*, *Criboelphidium*, *Porosonion*) and *Haynesina*, and the K/R_{EXT} ratio, consisting of the ratio between keeled *Elphidium* and the sum of rounded elphidiids, *Haynesina* and other related genera that display a rounded periphery (i.e., *Astrononion*, *Melonis*, *Nonion*, *Nonionella*, *Valvulineria*). All these indexes were examined, suggesting their potential use for recognizing seagrass-related palaeoenvironments. The K/R_{EXT} ratio (and K/R) in association with the presence of permanently attached foraminifera revealed to be the

most reliable palaeo-seagrass indicators, suggesting that this combination could be very useful also in other case studies where diagenesis altered the foraminiferal association.

5.2 Introduction

Posidonia oceanica is a seagrass species endemic of the Mediterranean Sea. It dominates infralittoral soft bottoms, developing one of the most biologically diverse and ecologically relevant marine ecosystems of the Mediterranean Sea (Duarte and Chiscano, 1999; Short et al., 2007). Within the benthic zonation of the Mediterranean Sea (Pérès and Picard, 1964), *P. oceanica* meadows constitute the climax stage of the soft-bottom ecosystem succession of the infralittoral zone. *Posidonia oceanica* is an ecosystem engineer that stabilizes the seafloor with its dense rhizome-meshwork, while the leaves favour local sedimentation by baffling floating particles (Boudouresque and Grissac, 1983; Moriarty and Boon, 1989; De Falco et al., 2000; Gacia and Duarte, 2001; Sanchez-Vidal et al., 2021). By creating a complex three-dimensional structure with separate foliar and rhizomatic strata, it provides the microhabitat for a wide variety of organisms, many of them with epiphytic living modes, such as encrusting red algae, bryozoans, molluscs, hydrozoans, and foraminifera (Chimenz et al., 1989; Langer, 1993; Murray, 2006; Pardi et al., 2006; Frezza et al., 2011; Mateu-Vicens et al., 2014). Many of these epiphytes are characterized by a mineralized skeleton, contributing to carbonate production within the meadow (Mazzella and Russo, 1989; Langer, 1993; De Falco et al., 2008; Mateu-Vicens et al., 2014; Brandano et al., 2016). In addition to the epiphytic taxa, *P. oceanica* meadows also host abundant infaunal foraminifera that can proliferate in the sediment trapped among the rhizomes (Den Hartog, 1979; Langer, 1993). Indeed, the main carbonate-producing biota associated with the meadow are calcareous algae and foraminifera, which allows to name the carbonate factories typical of seagrass meadows as GA-Foralgal (characterized by green calcareous algae) and RA-Foralgal (characterized by red calcareous algae) (Brandano et al., 2019). Whereas the epiphytic foraminiferal communities, meadow-related carbonate factories, and other indirect evidence of fossil meadows, have been widely reported from the geological record (e.g., Beavington-Penney et al., 2004; Reich, 2014; V'elez-Juarbe, 2014; Reich et al., 2015; Forsey, 2016), the preservation of fossil seagrasses is an exceedingly rare event. Seagrass leaves, roots and pollens decompose easily, making their preservation into the geological record very rare, though not impossible (e.g., Brasier, 1975; Ivany et al., 1990; Hesse et al., 1999; Moissette et al., 2007). Fossils of marine plants have been reported by different authors, the oldest of which is a stem of *Thalassocharis muelleri* from the lower Campanian of the Netherlands (Debey, 1848, 1851; Pomel, 1849). Other Upper Cretaceous well-preserved seagrass remains were described from the Izumi Stone, in Japan (Koriba and Miki, 1931; Oishi, 1931); from Westphalia, in Germany (Hosius and Von

der Marck, 1880); from the Coon Creek Formation of Tennessee, USA (Dilcher, 2016); and from the Netherlands (Voigt and Domke, 1955; Voigt, 1981). An upper Paleocene fossil seagrass was reported from Belgium (De Saporta and Marion, 1878), while *Posidonia* and *Cymodocea* remains are described from the lower Eocene of France (Den Hartog, 1970) and the middle and upper Eocene of Southern England (Selsey Formation; Chandler, 1961; Curry, 1965; Wright and Murray, 1972; Collinson, 1996). Other Eocene seagrasses are known from the London Clay Formation (Herne Bay, England; Chandler, 1961; Collinson, 1983); from the Brussels Sands Formation (Belgium; Stockmans, 1936); from the Avon Park Formation (Florida, USA; Lumbert et al., 1984; Brack-Hanes and Greco, 1988; Ivany et al., 1990; Benzecry and Brack-Hanes, 2008); and from the Birket Qarum and Qasr El Sagha formations (Egypt; Zalmout and Gingerich, 2012). Additional Eocene fossil seagrasses were found in France (Phillips and Meñez, 1988), northern Italy (Gregor, 1991) and southern Germany (Gregor, 2003). Oligocene fossil seagrasses were described from the Isle of Wight (UK; Chesters et al., 1967) and from the Guayanilla Formation of southwestern Puerto Rico (V'elez-Juarbe and Santos, 2008). Several *Cymodocea* remains have been reported from the Miocene of Sulawesi, Indonesia (Laurent and Laurent, 1926) and from the Messinian of Guadalquivir Basin, in southern Spain (Braga et al., 2021). The most recent examples of fossilized seagrass-meadows have been described by 1) Moissette et al. (2007), who reported *Posidonia* leaves and rhizomes in the Lower Pleistocene deposits of the Kritika Member of the Rhodes Formation in Greece; 2) Brunetti and Vecchi (2005, 2012), who reported well-preserved *P. oceanica* specimens from the Pleistocene of the Arda River (Emilia-Romagna, Italy); and 3) Raffi and Serpagli (2003), who reported examples of seagrass rhizomes from the Pleistocene of the Stirone River (Parma, Italy). In addition to these examples, the lower Pleistocene seagrass of *P. oceanica* exposed at the Fauglia Quarry has been recently reported by Bosio et al. (2021). Therefore, excluding the aforementioned examples, the recognition of paleo-seagrass meadows generally relies on indirect lines of evidence (Brasier, 1975; Eva, 1980; Domning, 2001; Beavington-Penney et al., 2004; Leonard-Pingel, 2005; Reuter et al., 2010; V'elez-Juarbe, 2014; Reich, 2014; Reich et al., 2015; Forsey, 2016). These indirect palaeo-seagrass indicators (or IPSIs) have been recently reviewed by Reich et al. (2015), who summarized different criteria for recognizing ancient seagrass occurrences: 1) the fossil assemblages including benthic foraminiferal associations, coralline red algae, hydroids, corals, bryozoans, molluscs (e.g., different bivalve taxa such as Pinnidae and chemosymbiotic species, gastropods), ostracods, echinoderms, fish otoliths, dugongid remains; 2) textural features such as the occurrence of unsorted sediments and fining-upward sequences; 3) the abundance of “constructive” micrite envelopes and taphonomic signature of skeletal remains (e.g., root etchings on shells and root casts); 4) the carbon isotopic signal of mollusc shells; and 5) seagrass biomarkers. While several potential IPSIs have been

investigated in the literature and several works analysed the foraminiferal associations related to vegetated substrates (Colom, 1942; Blanc-Vernet, 1969; Mateu, 1970; Blanc-Vernet et al., 1979; Langer, 1993; Ribes et al., 2000; Mateu-Vicens et al., 2010, 2012, 2014; Frezza et al., 2011), only a few of these indicators have been tested directly. With the purpose of evaluating the usefulness of foraminifera as IPSI, this paper analyses and describes the benthic foraminiferal community associated with a well-preserved Pleistocene *P. oceanica* meadow. This fossil meadow is recorded within a succession dated to the Calabrian that crops out in a sand quarry near the Fauglia village, Tuscany, central Italy (Bosio et al., 2021). The sedimentary succession exposed herein consists of silts and sands that also host a *Cladocora caespitosa* bank and an oyster reef at the top. The aim of this paper is, thus, to provide a qualitative and quantitative description of the foraminiferal assemblages associated with the fossil meadow through indices that might prove useful for recognizing other meadow-related palaeoenvironments where seagrass remains are not preserved. Furthermore, these indices can be compared with those calculated for modern case studies, in order to create models that have the capability of providing us with more reliable and detailed palaeoenvironmental reconstructions.

5.3 Geological setting

The study site consists of an active quarry located at Podere Montalto, ca. 1.3 km ESE of Fauglia (Pisa Province, Tuscany, Italy), along the Eastern side of the Isola stream (geographic coordinates: 43°33'52" N, 10°31'53" E) (Fig. 5.1). Near the study site, Pleistocene strata occur atop of Pliocene marine deposits (Marroni et al., 1990; Bossio et al., 1999) and include, from bottom to top, the Morrone Formation (ART), the Sabbie di Nugola Vecchia Fm (NUG) and the Casa Poggio ai Lecci Fm (QPL) (Mazzanti, 2016). The ART consists of lower Calabrian (i.e., Santernian according to the ‘Italian Marine Stages’ regional scheme; Gibbard and Cohen, 2008) sands and clays. ART strata are usually rich in macroscopic remains of marine molluscs (mostly bivalves and gastropods), brachiopods, echinoids, corals, crustaceans and annelids. Boreal faunal elements (e.g., *Arctica islandica*) typically occurs in the ART, representing the geologically oldest occurrence of such taxa in this area. These records appear to be chronostratigraphically consistent with observations of the “Northern guest” *A. islandica* in other coeval deposits of Italy (e.g., Crippa et al., 2019). The ART reaches a maximum thickness of about 50 m (Mazzanti, 2016). The NUG consists of fine, yellowish sands interbedded with lenses of conglomerates and calcarenites that have been assigned by Mazzanti (2016) to the Emilian (i.e., mid-Calabrian; Gibbard and Cohen, 2008). The NUG strata contain few remains of marine macro-invertebrates, which are mainly represented by bivalves (mostly oysters and pectinids). The maximum thickness of the NUG exceeds 100 m (Mazzanti, 2016). The QPL consists

of conglomerates with subordinate sands and silts, deposited in a transitional environment (including riverine, deltaic and lagoonal settings; Barsotti et al., 1974) during the Chibanian (Middle Pleistocene). The strata of the QPL typically contain very scarce remains of macro-invertebrates, including rare bivalves and gastropods. The thickness of the QPL ranges between 1 and ca. 30 m (Mazzanti, 2016). There is no consensus regarding the sequence stratigraphic interpretation of the ART and NUG. Some authors (Bossio et al., 1993; Tani and Gazzero, 1999; Mazzanti, 2016) consider these formations to represent the transgressive and regressive tracts of a single depositional cycle; other authors, in turn, regard them as corresponding to two distinct depositional cycles (Sarti et al., 2007, 2008). Recent geological mapping of the Fauglia area at the national (Mazzanti, 2016), regional (Regione Toscana, 2006–2009), and local (Marroni et al., 1990) scales, concur in indicating that deposits belonging to the NUG crop out at the study site. That said, the abundant fossil content of these deposits does not match the palaeontological traits of the NUG as observed elsewhere (Mazzanti, 2016), resembling instead some ART outcrops some tens of kilometres farther south. So far, published works on the palaeontology of the Fauglia pit have attributed the stratigraphic succession revealed by the quarrying surfaces to unnamed Lower Pleistocene deposits (Brunetti et al., 2008; Chirli and Forli, 2017; Cresti and Forli, 2020) or to the NUG (Berta et al., 2015; Bosio et al., 2021), the latter view being embraced herein.

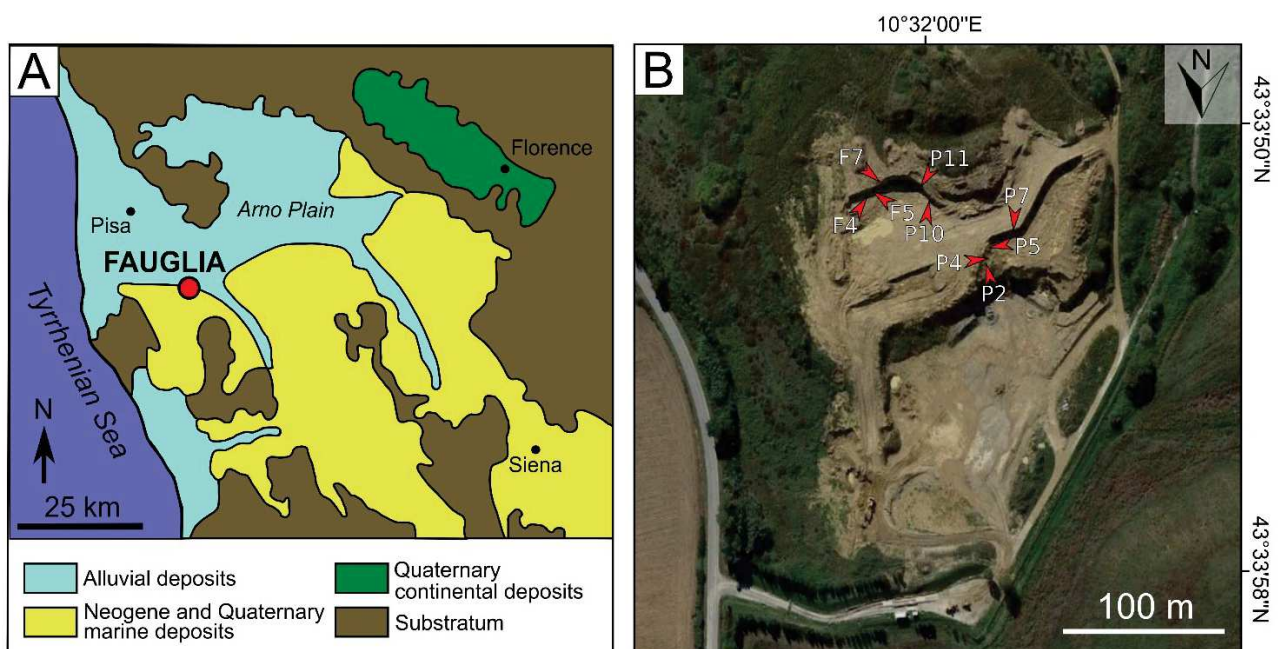


Figure 5.1 A. Simplified geological map of Tuscany, showing the areas of Mio-Pleistocene outcrops, and the location of the study area (modified from Carnevale et al., 2008). Azure: alluvial deposits; yellow: Neogene and Quaternary marine deposits; green: Quaternary continental deposits; brown: substratum. B. Satellite image of the Fauglia quarry (Google Earth), with the location of the sampling sites.

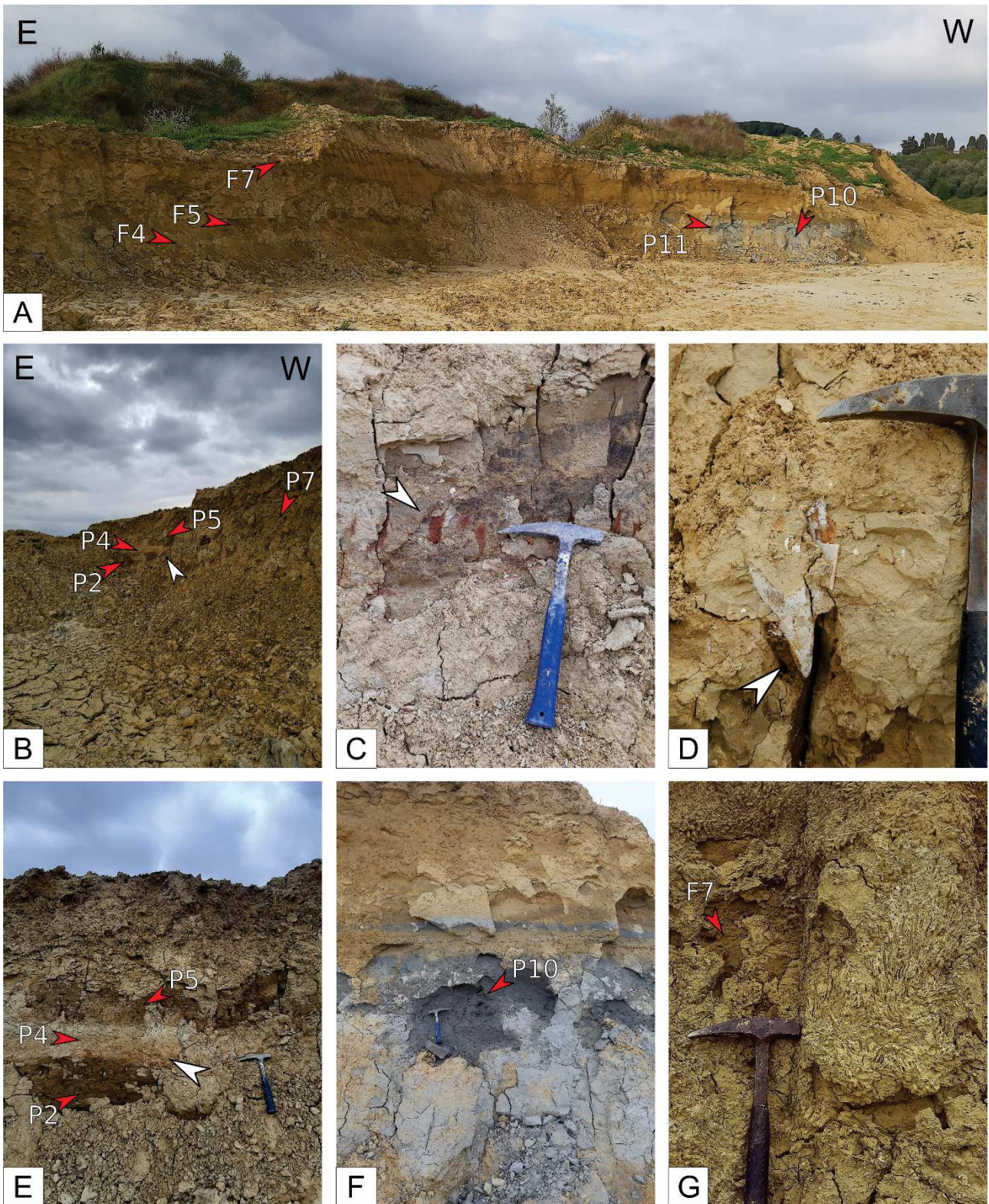


Figure 5.2 Field views and photos of the lower Pleistocene deposits cropping out at the Fauglia quarry, with location of the collected samples. A, B. Overview of the outcrop. The base of the section corresponds to picture B (lower interval), whereas the top is shown in A (upper interval). C. *Posidonia*-bearing layer. The arrow indicates in situ *Posidonia* rhizomes; D. *Pinna nobilis* specimen (arrow), in-life position, within *Posidonia* bearing layer; E. Lower section of the Fauglia succession. The arrow indicates the sandy layer interbedded between two *Posidonia*-bearing layers (lower interval); F. Dark coloured sediments within the upper *Posidonia*-bearing layer (upper interval); G. Detail of the *Cladocora caespitosa* bank.

5.4 Materials and methods

The Pleistocene deposits cropping out at the Podere Montalto quarry (Fig. 5.2 A, B) were investigated in detail by describing the lithology, sedimentary structures, and microfossil distribution. A stratigraphic log was built integrating that of Bosio et al. (2021) with a description of the lower portion of the outcrop (Fig. 5.3; Table 5.1). A total of 9 samples were collected at different stratigraphic heights, focusing mainly on the two *Posidonia*-bearing strata - namely, the lower interval (samples P2, P4, P5, P7) and the upper interval (samples F4, F5, P10, P11) (Figs. 5.2 and 5.3) - to investigate both vertical and lateral variations. All samples were obtained by collecting at least 20 g of sediment, after slightly digging inside the deposits in order to remove the weathered surface. Four samples (P2, P5, P7, F5) were collected from different, very-fine-sandy to fine-silty layers featuring in situ *Posidonia oceanica* rhizomes (Fig. 5.2 C) and *Pinna nobilis* shells (Fig. 5.2 D); two samples (P4, F4) from two very-fine-sandy to very-coarse-silty layers occurring within the two *Posidonia*-bearing strata (Fig. 5.2 E); two samples (P10, P11) from lenses of dark-coloured sediments within the *Posidonia*-bearing layer in the upper interval (Fig. 5.2 F; P11 was collected at the boundary of the dark-coloured sediment lens, whereas P10 was collected from the core of the lens); one sample (F7) from the *Cladocora caespitosa* bank, which lies above the meadow and does not display remains of seagrass (Fig. 5.2 G). Grain size analyses were performed on each sample with a Malvern Mastersizer 2000E™ Laser Granulometer at the Università degli Studi di Milano-Bicocca (Table 5.1). Subsequently, the software GRADISTAT Version 4.0 (Blott and Pye, 2001) was employed to analyse the grain size distribution and to perform statistics. For the analysis of microfossils, a small amount of each sample (see Table 2 for the detailed quantities) was weighted, treated with 30% hydrogen peroxide to remove organic matter (Dimiza et al., 2016) and wet-sieved through a 125- μm -sized mesh, to separate the fraction for the benthic foraminifera picking ($> 125 \mu\text{m}$). Samples F4 and F5 were wet-sieved through 63- μm -sized mesh, in order to check for grain-size-based differences in the composition of the foraminiferal assemblages (analysing the fraction $>63 \mu\text{m}$). After sieving, the samples were oven-dried and divided into equal fractions using a microsplitter, thus obtaining subsets containing at least 300 specimens each (Murray, 2006). The picking and the identification of the foraminifera were performed under a ZEISS Olympus SZ61 stereo microscope equipped with a high-resolution camera. The taxonomic determination of the foraminifera was based on Cimerman and Langer (1991), Langer and Schmidt- Sinns (2006), Milker and Schmiedl (2012), the Foraminifera.eu-Project (Hesemann, 2020), and World Register of Marine Species (WoRMS Editorial Board, 2021). SEM imaging of epiphytic foraminifera and *P. oceanica* leaves and rhizomes was also performed using a FEG (SEM-FEG) Gemini 500 Zeiss scanning electron microscope at the Università degli Studi di Milano-Bicocca. The total amount of benthic foraminifera, the standardized quantity of

benthic foraminifera within 100 g of sediment, the species richness (i. e., number of species) and the relative frequency of each species, were calculated. To analyse the taxonomic structure of the fossil assemblage, biodiversity was measured using the Shannon-Weaver index H' (Shannon and Weaver, 1963; Mateu-Vicens et al., 2014):

$$H' = - \sum_{i=0}^R p_i \ln(p_i)$$

where p_i is the relative abundance of each species (i) and R is the species richness (i.e., number of species). Since miliolid foraminifera can be easily altered, or even dissolved, due to their porcelaneous test of high-Mg calcite (Budd and Hiatt, 1993), several parameters were also calculated excluding miliolids to highlight the signal of the meadow while avoiding the bias from miliolids dissolution. The relative abundance of epiphytic foraminifera was calculated using the Index_{EP} i.e., the ratio between epiphytic foraminifera and the total of benthic foraminifera (Mateu-Vicens et al., 2014). $\text{Index}_{\text{EP-M}}$, a variant of Index_{EP} that excludes miliolids, was also calculated. According to Langer (1993) and Mateu-Vicens et al. (2014), epiphytic foraminifera can be divided into five different groups based on their type of motility, life span, feeding mode, and test morphology and structure. The recognized ecomorphological groups are: A*) long-living (> 10 months), sessile species, permanently attached to the substrate (e.g., *Nubecularia lucifuga*, *Planorbulina mediterraneensis*); SB) long-living (> 10 months), symbiont-bearing taxa (e.g., *Sorites*, *Peneroplis*, *Amphistegina*); B) short-living (3–5 months), generally motile species that temporarily attach to the substrate using organic materials (e.g., *Rosalina* spp., *Cibicides* spp., *Ammonia* spp.); C) short-living, motile, suspension-feeding foraminifera (e.g., keeled elphidiids, *Astrononion*, *Criboelphidium*); and D*) short-living, permanently motile, grazing foraminifera (e.g., opportunistic species living within rhizomes and sediment particles). Thus, epiphytic foraminifera specimens were assigned to the different morphotypes (A* to D*). Another classification was developed without including miliolids. Here, we refer to the traditional classification (i.e., that from Langer, 1993 and Mateu-Vicens et al., 2014) as “Mode-1”, and to the classification without miliolids as “Mode-2”. Pie-plots showing the percentage of the different morphotypes were compiled for both classifications and for each sample. The modified FORAM Index (FI') developed by Mateu-Vicens et al. (2014) based on Hallock et al. (2003) FORAM Index (FI), and the “long vs. short life-span” index (I_{LS} ; Mateu-Vicens et al., 2014) were also tested. FI' is expressed as:

$$\text{FI}' = 10 \times (P_{A^*} + P_{SB}) \times P_{D^*} + 2 \times (P_B + P_C)$$

Values of $\text{FI}' > 4$ indicate optimal environmental conditions, whereas values of $\text{FI}' < 2$ are indicative of stressed conditions (Mateu-Vicens et al., 2014). I_{LS} , which consists of the ratio between longer-

living and short-living forms, was built to highlight the differences between well-preserved and stressed *P. oceanica* meadows (Mateu-Vicens et al., 2014) and is expressed as:

$$I_{LS} = (3.5 \times (P_{A^*} + P_{SB}) + 0.01) / (P_{D^*} + 0.01)$$

I_{LS} values range between 0 and 36. If D^* is the dominant morphotype, the index is close to 0; if the dominant morphotypes are A^* and SB , the index points towards 36. A new index based on the ratio between keeled *Elphidium* and the sum of rounded elphidiids (e.g., *Elphidium translucens*, *Criboelphidium*, *Porosonion*) and *Haynesina* was elaborated and defined as K/R index. An additional index, K/REXT, consisting of the ratio between keeled *Elphidium* and the sum of rounded elphidiids (e.g., *E. translucens*, *Criboelphidium*, *Porosonion*), and other related genera that display a rounded periphery, such as *Haynesina*, *Astrononion*, *Melonis*, *Nonion*, *Nonionella* and *Valvulineria*, was also tested. Finally, a Q-mode cluster analysis, based on the similarity of species abundances across the samples, was performed with the software Primer v.6. The Log (x + 1) transformation was applied to both indexes. Dendrograms were plotted using the Bray-Curtis similarity index.

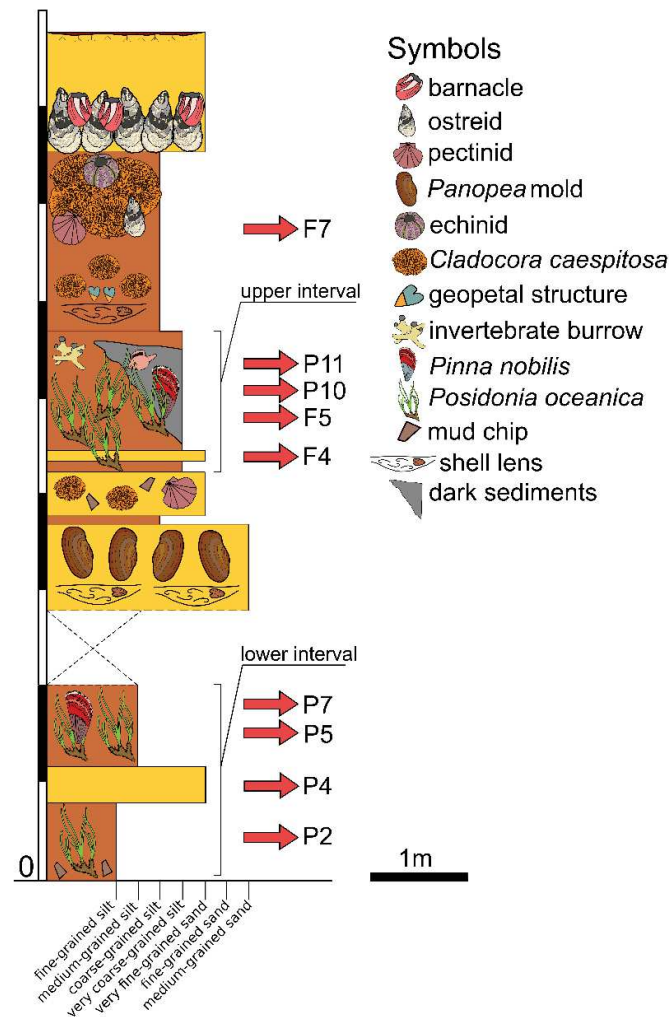


Figure 5.3 Stratigraphic log of the Fauglia quarry outcrop with information on the fossil content and average grain-size based on laser granulometer analyses. The stratigraphic position of the collected samples is also indicated.

Sample	Stratigraphic height (cm)	Sample type	Sorting	Sediment name	Textural group	Gravel %	Sand %	Mud %
F7	620	Bimodal	Very poorly sorted	Very Fine Sandy Coarse Silt	Sandy Mud	0	14.8	85.2
P11	490	Bimodal	Poorly sorted	Medium Silt	Mud	0	6.9	93.1
P10	460	Bimodal	Poorly sorted	Very Fine Sandy Very Coarse Silt	Sandy Mud	0	15.7	84.3
F5	450	Trimodal	Very poorly sorted	Very Fine Sandy Very Coarse Silt	Sandy Mud	0	25.0	75.0
F4	420	Trimodal	Very poorly sorted	Very Fine Sandy Very Coarse Silt	Sandy Mud	0	36.6	63.4
P7	170	Bimodal	Poorly sorted	Fine Silt	Mud	0	2.1	97.9
P5	140	Trimodal	Poorly sorted	Medium Silt	Mud	0	8.3	91.7
P4	95	Trimodal	Very poorly sorted	Very Fine Sandy Very Coarse Silt	Sandy Mud	0	33.9	66.1
P2	50	Bimodal	Poorly sorted	Fine Silt	Mud	0	0.2	99.8

Table 5.1 Grain-size analysis of the collected sample. The analysis and the results were obtained with software GRADISTAT version 4.0 (Blott and Pye, 2001)

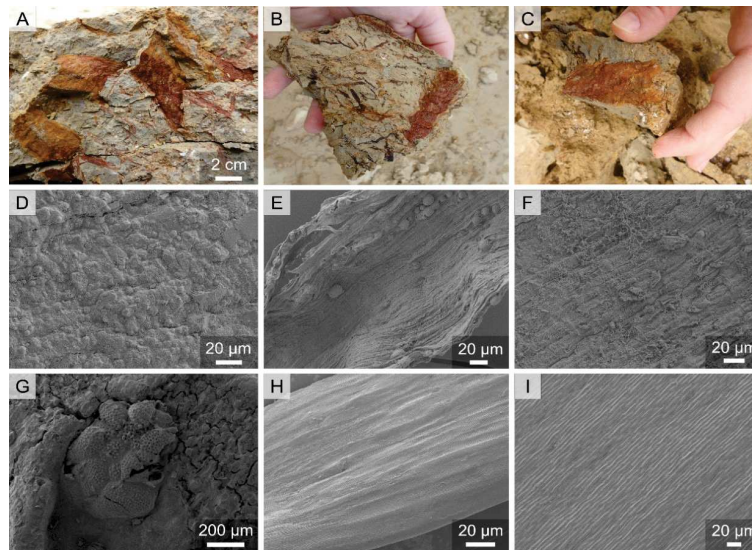


Figure 5.4 A, B, C. Detail of the well-preserved *Posidonia oceanica* rhizomes collected within the Fauglia outcrop. D. Fossil *P. oceanica* rhizome surface; E. Fossil *P. oceanica* leaf; F. Fossil *P. oceanica* leaf, surface detail. Even if the single plant cells are not preserved, it is possible to appreciate the preferential orientation of the fibres that constitute the leaf. G. Recent *P. oceanica* rhizome surface, with a *Planorbulina mediterraneensis* specimen attached to the surface. H. Recent *P. oceanica* leaf. It is possible to appreciate the single cells that constitute the leaf. I. Recent *P. oceanica* leaf, surface detail. Images D, E, F, G, H, I were obtained with a scanning electron microscope (SEM).

5.5 Results

5.5.1 Field observations and stratigraphic section

The measured stratigraphic section is an 8.5-m-thick mixed carbonate-siliciclastic succession (Figs. 5.2 A, B and 5.3) whose upper portion has been recently described by Bosio et al. (2021). The base of the succession is characterized by the presence of two brownish, fine- to medium-grained, silty layers, about 1 m thick each, displaying well-preserved, reddish-to-brown coloured, in-situ rhizomes of *Posidonia oceanica* (lower interval; Figs. 5.2 C, 5.3, and 5.4) associated with *Pinna nobilis* specimens preserved in life position (Fig. 5.2 D). These *Posidonia*-bearing layers are separated by a 50-cm-thick very fine-grained sandy to coarse silty horizon (Fig. 5.2 E), lacking macrofossils. Upwards, a quarry road hides about 1 m of the succession. The overlying first interval consists of an 80-cm-thick layer characterized by a fine- to medium-grained sand with silt intercalations, shell lenses and internal molds of the bivalve *Panopea*. This layer is followed by a 10-cm-thick silty layer and by a 30-cm-thick fine-grained sandy layer with scattered specimens of the zooxanthellate coral *Cladocora caespitosa*, pectinid shells and clay chips. Just above, a 150-cm-thick, brownish, coarse-grained silty layer, including a very fine-grained sandy to coarse-grained silty interval, occurs (upper interval; Fig. 5.3). Inside this layer, in situ rhizomes of *P. oceanica*, molluscs and invertebrate burrows occur. Laterally, these deposits pass into a large lens of dark-coloured material (Fig. 5.2 F), with leaves of *P. oceanica* preserved as peaty remains (Fig. 5.4) and aragonitic macrofossils, such as gastropods and *P. nobilis* specimens. The uppermost part of the section includes a 250-cm-thick coarse-grained silt layer. At the base, the horizon displays fragments and scattered colonies of *C. caespitosa* (Fig. 5.2 G), together with bivalves featuring geopetal structures. At the top of this layer *C. caespitosa* colonies coalesce to form a decametric to metric *Cladocora* bank. The bank is abruptly overlain by an oyster reef, rich in barnacles and included in a massive sandy deposit.

5.5.2 Foraminiferal analysis

Micropalaeontological analyses reveal that the Fauglia skeletal assemblages is constituted by a large variety of carbonate producers, including benthic foraminifera, planktic foraminifera, ostracods, bryozoans (for the most part belonging to “erect” forms), molluscs and echinoids. Among these, benthic foraminifera are the most abundant group. A total of 97 benthic foraminiferal species were identified (see Table 5.2; Figs. 5.5–5.10; Appendix 5.1). Foraminiferal density (i.e., the abundance of benthic foraminifera per 100 g of material) varies between 26,992 and 84,479 individuals throughout the samples, with the exception of samples P4 and F4 in which this value is almost one order of magnitude higher, between 200,810 and 258,535 individuals (Table 5.2; Fig. 5.3). The percentage of broken tests displays no significant difference across the samples, exhibiting an average value of 4%

(Table 5.2). Only in sample F7 (the *Cladocora*-bearing layer; Fig. 5.3) broken foraminiferal tests are one order of magnitude higher, displaying a value of 11.7% (Table 5.2). Species richness is relatively variable, showing the highest value in sample F4 (74) and the lowest value in sample F7 (47) (Table 5.2). In contrast, diversity is more homogeneous in all samples, as indicated by the Shannon-Weaver Index (H'), whose values are high and range from 3.10 in P11 to 3.63 in P10 (Table 5.2). The relative abundances of the identified benthic foraminifera species are presented in Appendix 5.1. The most common taxa (i.e., those with abundance higher than 5%) (Table 5.3) are: *Ammonia* group (except for F7); *Aubignyna perlucida* (F7); *Bolivina* spp. (P5, F4, F7); *Lobatula lobatula* (except for F5 and F7); *Cibicides refulgens* (all samples); *Criboelphidium* cf. *magellanicum* (F7); keeled elphidiids group (except for F7); *Elphidium translucens* (P4, P5, F5); *Fissurina* spp. (P2, P5, P11, F7); *Fursenkoina subacuta* (P10); *Haynesina* spp. (F7); *Reussella spinulosa* (except for P2); *Neoconorbina terquemi* (P4, P5, F4); *Rosalina bradyi* (P2, P7, P11, F5); *Rosalina globularis* (P2, P7); miliolids (P10). Well-preserved miliolid tests actually occur only in samples P10 and P11, corresponding to a dark-grey lens within the upper *Posidonia*-bearing layer. In the remaining samples, miliolids are rare and usually display altered and corroded tests. The largest differences in the associations of common benthic foraminifera can be observed between the samples from the *Posidonia*-bearing layers (P2, P4, P5, P7, P10, P11, F4, F5) and the sample from the *Cladocora* bank (F7) (Table 5.3). In particular, the *Ammonia* group is less abundant in F7, whereas *Aubignyna perlucida* and *Astrononion stelligerum* are more common. *Bolivina* spp. show higher abundances in F7, but also in P5 and F4 (i.e., samples that were sieved with 63 μm mesh size). On the contrary, *Bulimina* spp. remain approximately constant among all the samples. Cibicididae (e.g., *Lobatula lobatula*, *Cibicides refulgens*, *Cibicidoides pachyderma* and *Cibicidoides pseudoungerianus*) display the lowest values in F7. Within this group, the species that contributes more to the variation is *L. lobatula*, whose abundance is considerably lower in F7 with respect to the samples from *Posidonia*-bearing layers. *C. refulgens*, instead, is abundant also in F7. *Criboelphidium* cf. *magellanicum* and *Haynesina* spp. have the highest abundance in the *Cladocora* bank (F7). Keeled *Elphidium* represent one of the most abundant group within all the samples from the *Posidonia*-bearing layers. Among them, the most common species are *Elphidium aculeatum*, *Elphidium advenum*, *Elphidium crispum*, and *Elphidium fichtelianum*; these species are almost absent in F7. *Fissurina* spp. are abundant in every sample. *Fursenkoina subacuta* displays large frequency variations, but no significant trends. *Planorbulina mediterraneensis* exhibits almost constant values in all the samples, except for F7, where it is absent. *Elphidium translucens* and *Reussella spinulosa* do not show particular trends, being common in every sample. Rosalinidae (i.e., *Gavelinopsis praegeri*, *Neoconorbina terquemi*, *Neoconorbina* sp., *Rosalina bradyi*, *Rosalina globularis* and *Rosalina williamsoni*) display the lowest

abundance in F7, whereas in the other samples they constitute one of the most populated groups. Agglutinated foraminifera (the only species identified is *Sahulia conica*) are generally scarce, except for P10. Miliolids occur in P10 and, to a lesser extent, in P11. In all the other samples they are rare and poorly preserved. The well-preserved miliolids of P10 include the encrusting species *Nubecularia lucifuga*. Index_{EP} displays its lowest value of 0.4 in correspondence of F7, while in the other samples its average value is 0.6 (Table 5.2). Index_{EP-M}, calculated without considering miliolids, shows a similar trend (Table 5.2). No remarkable differences in the abundances were observed between samples sieved through 63- μ m and 125- μ m-sized meshes. The only difference is the slightly higher abundance of some opportunistic species (e.g., *Bolivina* spp.) in the finer fraction. The division of the epiphytic species into the different morphotypes is visible in Table 5.4. No specimens belonging to the SB group was recognized. Morphotype percentages for both study modes are shown in Table 5.5 and Fig. 5.11.

5.5.2.1 Mode-1: Classification with miliolids

In this classification, morphotype A* includes *P. mediterraneensis* and *N. lucifuga*. The relative frequency of this morphotype is low in all the samples, and no members of this group were observed in F7. The highest value, 1.5%, was recorded in sample P10, which was collected from the dark-coloured sediment within a *Posidonia*-bearing layer (Table 5.5). Morphotype B includes members of *Ammonia* (i.e., *A. beccarii*, *A. parkinsoniana*, *A. tepida*); Cibicididae (i.e., *L. lobatula*, *C. refulgens*, *C. pachyderma*, *C. pseudoumgerianus*), Rosalinidae (i.e., *G. praegeri*, *N. terquemi*, *Neoconorbina* sp., *R. bradyi*, *R. globularis*), *Asterigerinata mamilla*, *Eponides repandus*, *Discorbinella bertheloti*, *Discorbis vilardeboanus*, *Planulina ariminensis*, *Planulina* sp., *Hanzawaia boueana* and *Buccella* aff. *frigida*. Morphotype B is predominant in all samples (44.1% on average) with the lowest value in sample F7 (19.5%) (Table 5.5). Morphotype C includes keeled *Elphidium* taxa (*E. aculeatum*, *E. advenum*, *E. complanatum*, *E. crispum*, *E. fichtelianum*, *E. macellum*, *E. maioricense*, *E.* aff. *aculeatum*, *Elphidium* sp., *Elphidium* sp.1, *Elphidium* sp. 5; Cimerman and Langer, 1991), *C.* cf. *magellanicum* and *A. stelligerum*. The frequency of morphotype C does not show any particular trend and its values range between 18.6% (F7) to 5.6% (P10) (Table 5.5). However, even if in F7 morphotype C displays its higher values, keeled *Elphidium* are almost absent, whereas in the other samples they constitute the largest portion of this morphotype. Indeed, in F7 the high frequency of morphotype C is related to the high abundance of *C.* cf. *magellanicum* and *A. stelligerum*, which are much less abundant in the other samples. Morphotype D* comprises *S. conica* and small miliolids. It displays the highest abundance in P10 (18.5%), i.e., the sample collected inside the dark-grey lens, whereas in the other samples its contribution is always lower than 2.5% (Table 5.5). FI' values remain

almost constant in all the samples from the *Posidonia*-bearing layers, with an average value of 1.24 (Table 5.2). Its lowest value (0.78) was observed in the *Cladocora* bank sample F7 (Table 5.2). I_{LS} is rather constant, with the lowest value (0.31) in sample P10. However, on average, *Posidonia*-bearing samples display higher (0.88) values than F7 (0.36), the sample from the *Cladocora* bank (Table 5.2).

5.5.2.2 Mode-2: Classification without miliolids

In this case, Morphotype A* does not include *N. lucifuga*. Thus, the frequency of morphotype A* is equal to the frequency of *P. mediterraneensis*. Morphotypes B and C are as in Mode-1. Morphotype D* is constituted just by agglutinated foraminifera. Therefore, the frequency of morphotype D* is equal to that of *S. conica* and the highest value (3.5%) is still found in sample P10 (Table 5.5). FI'_{-M} displays the lowest value in F7 (0.78). In the other samples FI'_{-M} remains almost constant, with an average value of 1.20 (Table 5.2). I_{LS-M} shows almost constant values within the different samples from the *Posidonia*-bearing layers, with an average value of 1.47. The lowest value occurs within the *Cladocora* bank sample, F7, and corresponds to 0.40 (Table 5.2).

5.5.2.3 Keeled/Rounded ratio

The keeled/rounded ratio (K/R) exhibits the lowest value in F7 (0.11), whereas in the other samples it is higher, with an average value of 1.45 (Table 5.2). The K/R_{EXT} ratio shows the same pattern as K/R, displaying the lowest values in F7 (0.08), whereas in all the other samples it is at least one order of magnitude higher, with an average value of 0.99 (Table 5.2).

Sample	P2	P4	P5	P7	P10	P11	F4	F5	F7
Fraction	>125 µm	>125 µm	>125 µm	>125 µm	>125 µm	>125 µm	> 63 µm	> 63 µm	>125 µm
Total weight [g]	1.96	2.17	1.93	2.02	1.99	2.07	5.48	5.55	5.30
Tot.BF	556	4364	520	746	680	1752	14168	2916	1588
BF/100g	28330	200810	26992	36934	34143	84479	258535	52530	29961
SR	50	65	65	50	64	59	74	61	47
Index _{BR}	0.025	0.034	0.021	0.024	0.044	0.045	0.062	0.077	0.117
H'	3.326	3.290	3.481	3.149	3.634	3.110	3.561	3.231	3.326
Index _{EP}	0.701	0.637	0.552	0.635	0.540	0.694	0.589	0.604	0.398
Index _{EP-M}	0.699	0.630	0.543	0.638	0.475	0.687	0.587	0.604	0.395
FI'	1.41	1.29	1.09	1.27	1.03	1.41	1.20	1.22	0.78
I _{LS}	0.72	1.39	0.95	0.67	0.31	0.92	1.29	0.86	0.36
FI' _{-M}	1.39	1.29	1.09	1.27	0.79	1.39	1.19	1.21	0.78
I _{LS-M}	1.66	2.09	1.40	0.83	0.67	1.93	1.96	1.16	0.40
K/R	1.26	0.96	0.90	1	0.47	4.58	1.80	0.63	0.11
K/R _{EXT}	0.83	0.67	0.59	0.63	0.25	3.60	0.89	0.44	0.08

Table 5.2 Foraminifera data and parameters calculated from all the samples. Fraction: grain-size fraction considered within the analysis; Total weight: total amount of dry sediment before sieving; Tot. BF: number of benthic foraminifera within each sample; BF/100g: number of benthic foraminifera normalized within 100g of sediment; SR: Species Richness; Index_{BR}: proportion of broken tests (BR) within a sample, BR/(Tot.BF+BR); H': Shannon-Weaver index; Index_{EP}: number of epiphytic specimens/total foraminifera (Mateu-Vicens et al., 2014); Index_{EP-M}: number of epiphytic specimens/total foraminifera without miliolids; FI': modified FORAM Index (Mateu-Vicens et al., 2014); I_{LS}: long vs. short life-span index (Mateu-Vicens et al., 2014); FI'_{-M}: FORAM Index modified without miliolids; I_{LS-M}: long vs. short life-span index without miliolids; K/R: ratio between keeled *Elphidium* and the sum of rounded elphidiids (e.g., *Elphidium translucens*, *Criboelphidium*, *Porosonion*) and *Haynesina*; K/R_{EXT}: ratio between keeled *Elphidium* and the sum of rounded elphidiids (e.g., *Elphidium translucens*, *Criboelphidium*, *Porosonion*) and associated taxa that display a rounded periphery (i.e., *Astrononion*, *Haynesina*, *Melonis*, *Nonion*, *Nonionella*, *Valvulineria*).

Ammonia group	8.27	10.27	5.58	7.51	5.59	11.87	5.08	14.13	3.27
<i>Ammonia beccarii</i>	5.40	6.97	3.46	5.63	4.12	7.99	2.03	8.09	1.51
<i>Ammonia parkinsoniana</i>	1.44	2.02	1.15	1.07	0.59	2.97	1.69	4.46	0.50
<i>Ammonia tepida</i>	1.44	1.28	0.96	0.80	0.88	0.91	1.36	1.58	1.26
<i>Asterigerinata mamilla</i>	0.00	0.64	0.38	0.27	0.15	0.00	1.24	0.21	0.50
<i>Astrononion stelligerum</i>	0.36	0.00	0.38	0.00	0.44	0.34	0.45	0.00	2.01
<i>Aubignyna per lucida</i>	0.00	0.18	0.19	0.54	3.24	0.11	0.00	0.00	7.55

<i>Bolivina</i> spp.	1.44	1.65	6.15	1.34	1.32	1.14	9.26	1.17	7.56
Cibicididae	23.02	28.77	21.73	19.57	11.32	21.69	24.28	12.48	8.56
<i>Cibicides refulgens</i>	13.67	13.57	14.23	11.53	6.32	14.04	16.60	7.20	7.05
<i>Cibicoides pachyderma</i>	0.00	1.28	0.77	0.80	0.44	0.00	2.77	0.82	0.25
<i>Cibicoides pseudoungerianus</i>	1.08	2.29	0.58	2.68	0.29	1.26	0.11	1.10	0.00
<i>Lobatula lobatula</i>	8.27	11.64	6.15	4.56	4.26	6.39	4.80	3.36	1.26
<i>Criboelphidium</i> cf. <i>magellanicum</i>	3.96	0.00	0.00	0.80	0.44	0.57	0.00	0.00	13.35
Keeled Elphidium group	10.43	10.08	8.85	7.24	4.71	16.21	11.29	6.31	3.27
<i>Elphidium aculeatum</i>	0.72	1.47	2.12	1.07	0.74	1.26	1.98	0.96	0.25
<i>Elphidium advenum</i>	0.72	1.74	1.73	0.54	0.59	0.80	1.02	1.51	0.25
<i>Elphidium complanatum</i>	1.80	0.27	0.38	0.54	0.00	0.68	0.00	0.07	0.00
<i>Elphidium crispum</i>	1.08	1.01	0.77	1.34	0.74	2.28	0.56	1.99	0.00
<i>Elphidium fichtelianum</i>	3.24	0.82	0.77	0.54	0.59	1.48	1.24	0.41	0.00
<i>Elphidium macellum</i>	1.08	0.92	1.15	0.80	0.44	0.57	0.79	0.41	0.50
<i>Elphidium maiorcense</i>	0.00	0.64	0.00	0.00	0.00	0.00	0.11	0.00	0.00
<i>Elphidium</i> sp.	0.00	0.00	0.00	0.00	0.00	5.48	0.00	0.00	0.00
<i>Elphidium</i> sp. 1	0.00	0.18	0.58	0.00	0.00	0.23	0.17	0.00	0.00
<i>Elphidium</i> sp. 5; C. & L. 1991	0.00	0.55	0.19	1.07	0.00	0.11	0.56	0.48	0.00
<i>Elphidium</i> spp.	1.80	2.47	1.15	1.34	1.62	3.20	4.86	0.48	2.27
<i>Elphidium translucens</i>	1.44	8.16	5.77	4.02	4.26	1.37	2.94	6.45	3.78
<i>Fissurina</i> spp.	9.35	2.38	6.35	3.75	3.38	8.22	3.39	3.77	6.04
<i>Fursenkoina subacuta</i>	0.36	0.00	0.38	2.14	7.94	0.23	0.28	2.26	2.01
<i>Haynesina germanica</i>	0.36	0.64	0.96	0.27	1.91	0.57	0.85	1.99	5.54
<i>Haynesina depressula</i>	0.36	0.55	0.96	0.54	0.88	0.00	0.45	0.14	1.01
<i>Haynesina</i> spp.	2.16	0.27	1.15	0.27	0.74	0.57	1.02	0.89	3.53
<i>Melonis affinis</i>	0.00	1.47	1.35	0.27	0.00	0.00	2.15	0.14	0.25
<i>Nonion boueanum</i>	1.08	1.10	1.54	2.68	2.35	0.00	1.86	1.85	1.51
<i>Nonion commune</i>	0.72	0.46	0.96	0.27	0.88	0.34	0.73	0.41	2.52
<i>Planorbulina mediterraneensis</i>	0.36	0.37	0.19	0.27	0.59	0.46	0.62	0.55	0.00
<i>Porosonion granosum</i>	0.00	0.92	0.96	1.34	1.76	0.46	1.02	0.62	3.02
<i>Reussella spinulosa</i>	3.96	10.17	9.23	15.26	7.94	13.01	6.49	14.20	7.05

Rosalinidae	19.42	9.99	13.85	23.59	10.88	15.87	12.08	19.34	6.05
<i>Gavelinopsis praegeri</i>	1.44	0.64	1.15	0.27	0.74	0.34	0.34	0.14	0.50
<i>Neoconorbina terquemi</i>	2.88	6.60	5.58	2.95	0.88	0.11	7.17	1.71	1.26
<i>Rosalina bradyi</i>	7.19	2.38	3.65	12.58	4.12	9.02	1.75	12.55	0.50
<i>Rosalina globularis</i>	5.04	0.37	2.12	6.69	2.79	3.08	1.24	4.53	2.77
<i>Rosalina williamsoni</i>	0.36	0.00	0.00	0.00	0.00	1.26	0.00	0.00	0.00
<i>Neoconorbina</i> sp.	2.52	0.00	1.35	1.07	2.35	2.05	1.58	0.41	1.01
<i>Sahulia conica</i>	0.36	0.09	0.19	1.34	3.53	0.34	0.62	1.51	1.51
Miliolids	1.80	0.55	0.58	0.54	15.00	1.48	0.85	0.89	0.25

Table 5.3 Relative frequency (%) of the most common species within all the samples. Raw data of all species are in Appendix 5.1.

Epiphytes Morphotype	Species
A*	<i>Planorbulina mediterranensis</i> ; <i>Nubecularia lucifuga</i>
B	<i>Ammonia beccarii</i> ; <i>Ammonia parkinsoniana</i> ; <i>Ammonia tepida</i> ; <i>Cibicides refulgens</i> ; <i>Cibicidoides pachyderma</i> ; <i>Cibicidoides pseudoungerianus</i> ; <i>Lobatula lobatula</i> ; <i>Neoconorbina terquemi</i> ; <i>Neoconorbina</i> sp.; <i>Rosalina bradyi</i> ; <i>Rosalina globularis</i> ; <i>Rosalina williamsoni</i> ; <i>Asterigerinata mamilla</i> ; <i>Eponides repandus</i> ; <i>Discorbinella bertheloti</i> ; <i>Discorbis vilardeboanus</i> ; <i>Gavelinopsis praegeri</i> ; <i>Planulina ariminensis</i> ; <i>Planulina</i> sp.; <i>Hanzawaia boueana</i> ; <i>Buccella</i> aff. <i>B. frigida</i> .
C	Keeled <i>Elphidium</i> (<i>Elphidium aculeatum</i> ; <i>Elphidium advenum</i> ; <i>Elphidium complanatum</i> ; <i>Elphidium crispum</i> ; <i>Elphidium fichtelianum</i> ; <i>Elphidium macellum</i> ; <i>Elphidium maioricense</i> ; <i>Elphidium</i> sp.; <i>Elphidium</i> sp.1; <i>Elphidium</i> sp. 5 Cimerman & Langer 1991). <i>Criboelphidium</i> cf. <i>magellanicum</i> ; <i>Astrononion stelligerum</i> .
D*	<i>Sahulia conica</i> ; Miliolids

Table 5.4 Morphotype classification used in this study. Species were assigned to a specific morphotype as in literature (Langer, 1993; Mateu-Vicens et al., 2010; Mateu-Vicens et al., 2014).

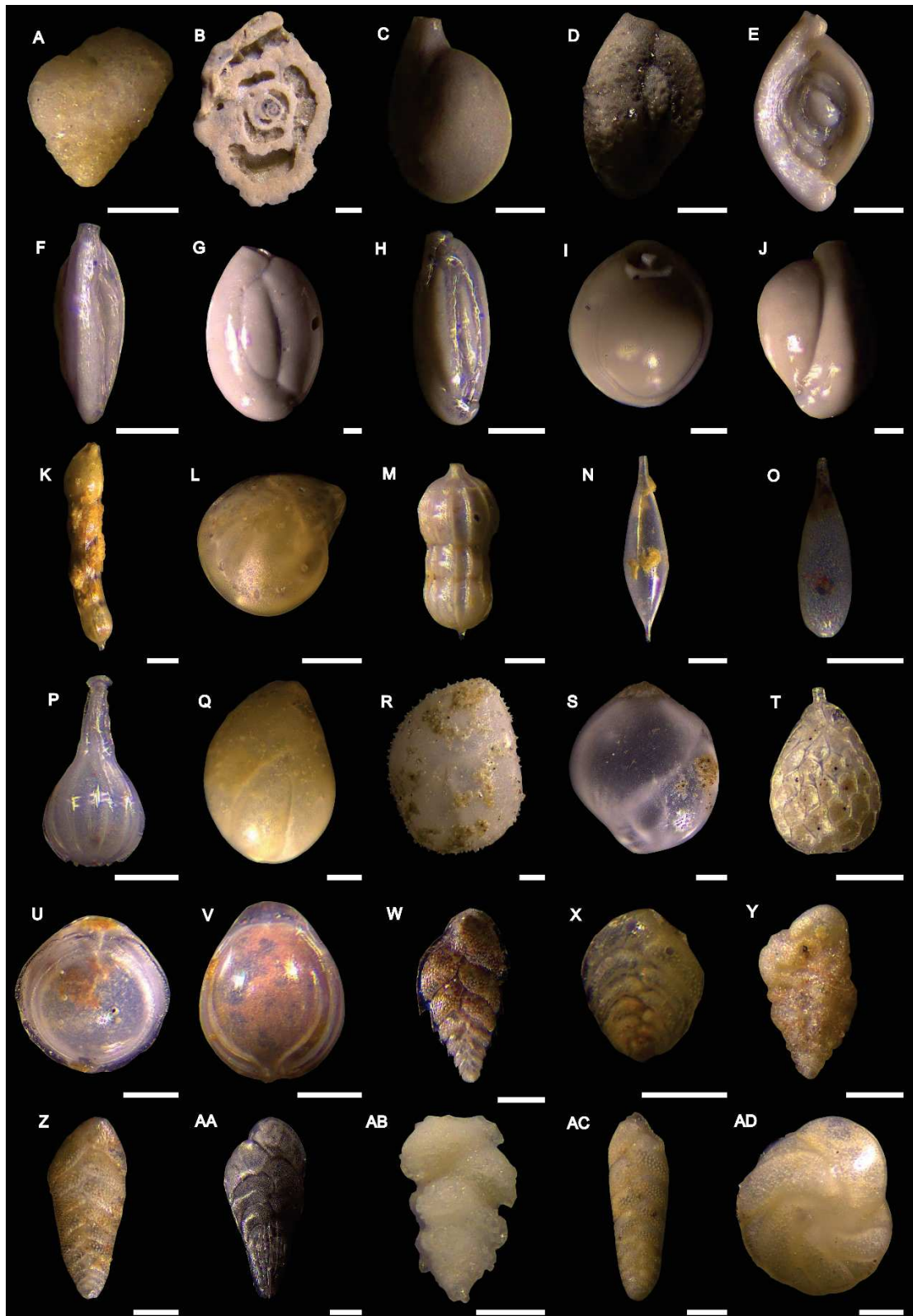


Figure 5.5 LM images of selected foraminifera species. A. *Sahulica conica*; B. *Nubecularia lucifuga*; C. *Adelosina* sp. (juvenile specimens); D. *Quinqueloculina irregularis*; E. *Spiroloculina excavata*; F. *Cycloforina* sp.; G. *Quinqueloculina seminulum*; H. *Quinqueloculina schlumbergeri*; I. *Pyrgo subsphaerica*; J. *Triloculina* sp.; K. *Dentalina albatrossi*; L. *Lenticulina orbicularis*; M. *Amphicoryna scalaris*; N. *Hyalinonetrion gracillimum*; O. *Lagena doveyensis*; P. *Lagena striata*; Q. *Globulina gibba*; R. *Globulina punctata*; S. *Guttulina communis*; T. *Favulina hexagona*; U. *Fissurina orbignyana*; V. *Fissurina pseudoorbignyana*; W. *Bolivina alata*; X. *Bolivina dilatata*; Y. *Bolivina pseudoplicata*; Z. *Bolivina spatulata*; AA. *Bolivina striatula*; AB. *Bolivina subspinescens*; AC. *Bolivina variabilis*; AD. *Cassidulina carinata*. The white bars correspond to 100 μm .

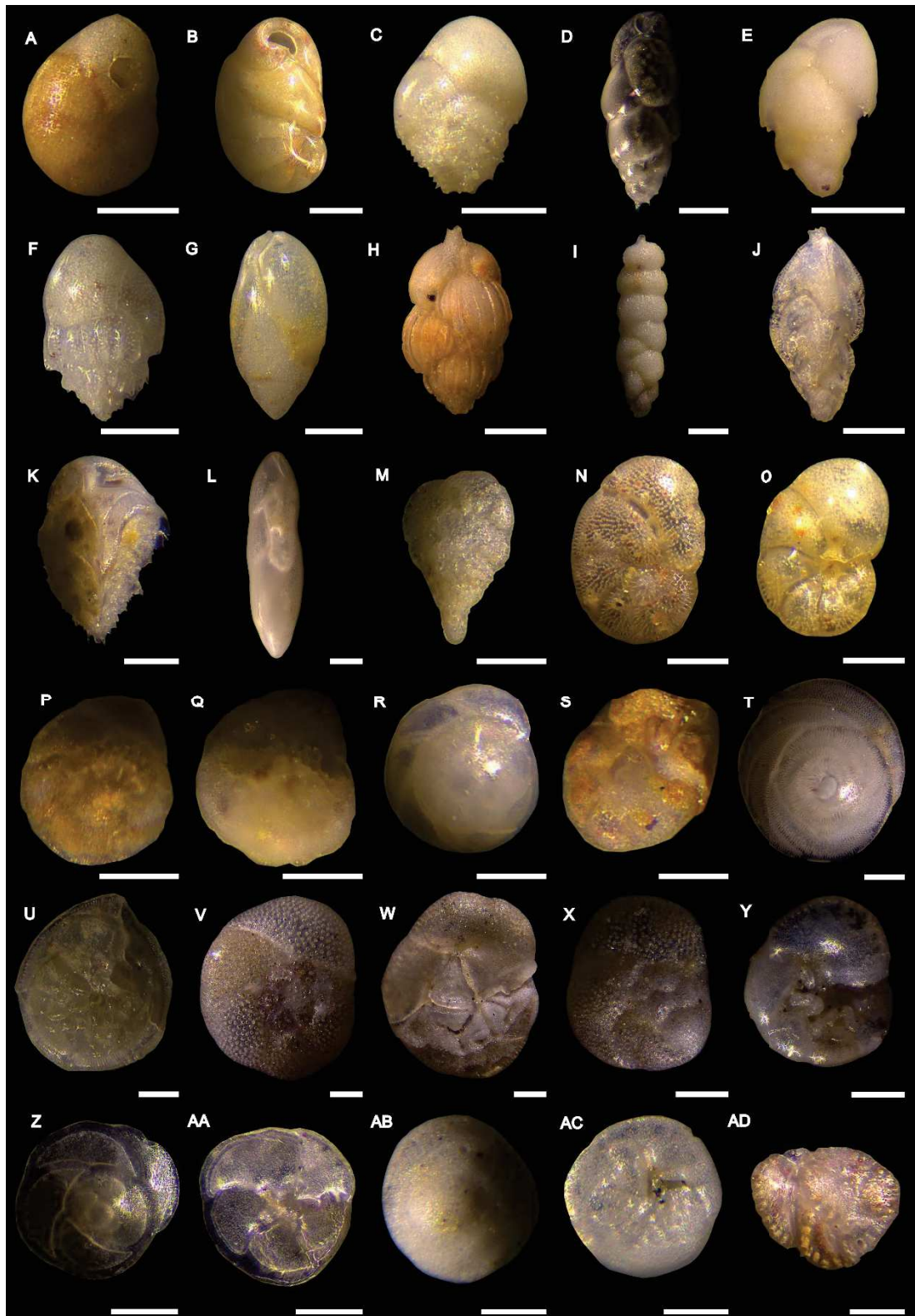


Figure 5.6 LM images of selected foraminifera species. A. *Globocassidulina subglobosa*; B. *Evolocassidulina bradyi*; C. *Bulimina aculeata*; D. *Bulimina elongata*; E. *Bulimina marginata*; F. *Bulimina striata*; G. *Globobulimina affinis*; H. *Uvigerina mediterranea*; I. *Rectuvigerina siphogenerinoides*; J. *Trifarina angulosa*; K. *Reussella spinulosa*; L. *Fursenkoina subacuta*; M. *Sigmavirgulina tortuosa*; N. *Valvulineria bradyana*, spiral side; O. *V. bradyana*, umbilical side; P. *Eponides repandus*, spiral side; Q. *E. repandus*, umbilical side; R. *Gavelinopsis praegeri*, spiral side; S. *G. praegeri*, umbilical side; T. *Neoconorbina terquemi*, spiral side; U. *N. terquemi*, umbilical side; V. *Rosalina bradyi*, spiral side; W. *R. globularis*, spiral side; X. *Rosalina globularis*, spiral side; Y. *R. globularis*, umbilical side; Z. *Rosalina williamsoni*, spiral side; AA. *R. williamsoni*, umbilical side; AB. *Neoconorbina* sp., spiral side; AC. *Neoconorbina* sp., umbilical side; AD. *Siphonina reticulata*. The white bars correspond to 100 μm .

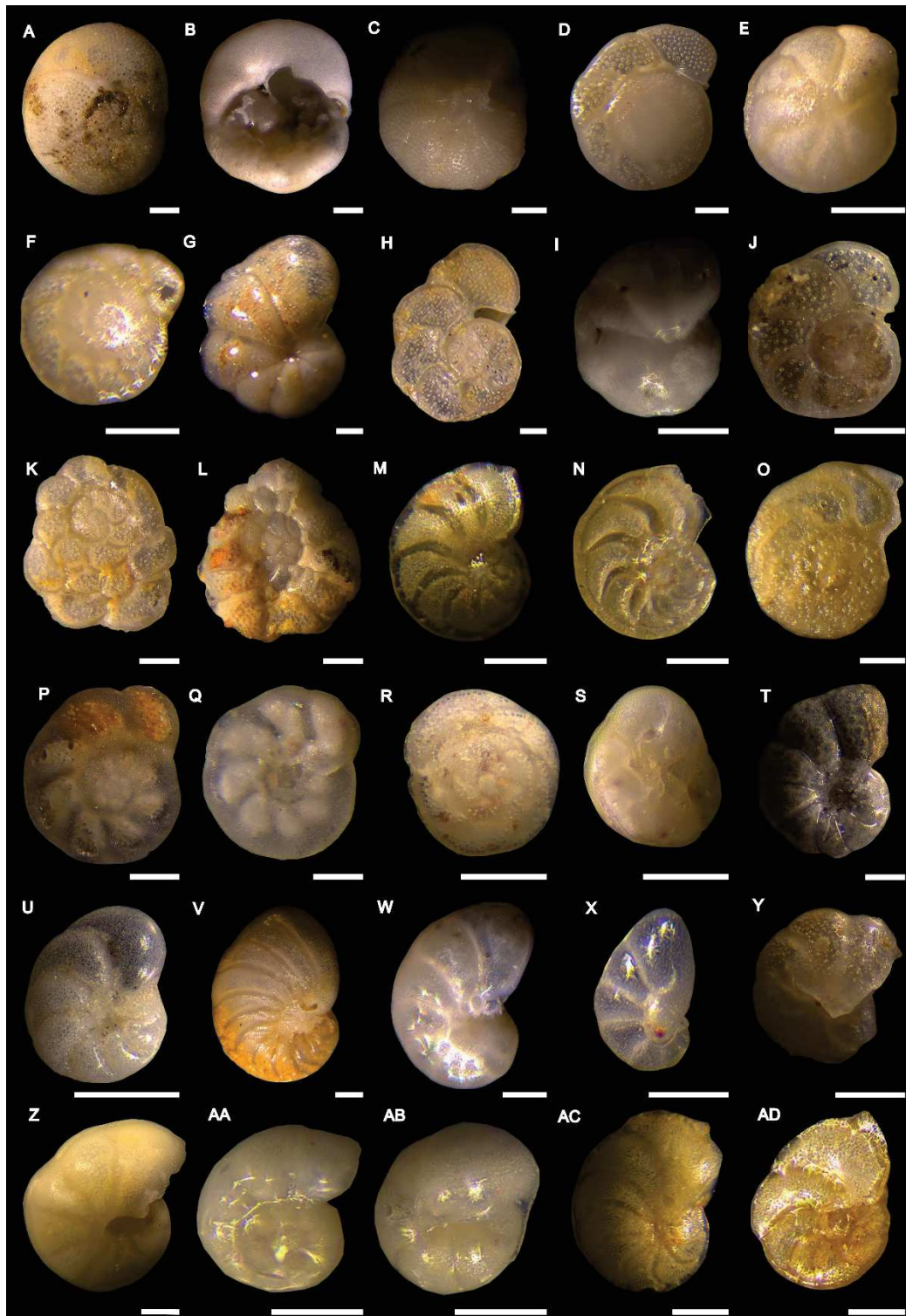


Figure 5.7 LM images of selected foraminifera species. A. *Discorbis vilardeboanus*, spiral side; B. *D. vilardeboanus*, umbilical side; C. *Cibicidoides pseudoungerianus*, spiral side; D. *C. pseudoungerianus*, umbilical side; E. *Cibicidoides pachyderma*, spiral side; F. *C. pachyderma*, umbilical side; G. *Lobatula lobatula*, spiral side; H. *L. lobatula*, umbilical side; I. *Cibicides refulgens*, spiral side; J. *C. refulgens*, umbilical side; K. *Planorbulina mediterranensis*, umbilical side; L. *P. mediterranensis*, spiral side; M. *Hanzawaia boueana*, spiral side; N. *H. boueana*, umbilical side; O. *Planulina ariminensis*; P. *Planulina* sp., spiral side; Q. *Planulina* sp., umbilical side; R. *Asterigerinata mamilla*, spiral side; S. *A. mamilla*, umbilical side; T. *Haynesina depressula*; U. *Haynesina germanica*; V. *Nonion boueanum*; W. *Nonion commune*; X. *Nonionella turgida*; Y. *Astrononion stelligerum*; Z. *Melonis affinis*; AA. *Gyroidina soldanii*, spiral side; AB. *G. soldanii*, umbilical side; AC. *Discorbinella bertheloti*, spiral side; AD. *D. bertheloti*, umbilical side. The white bars correspond to 100 μm .

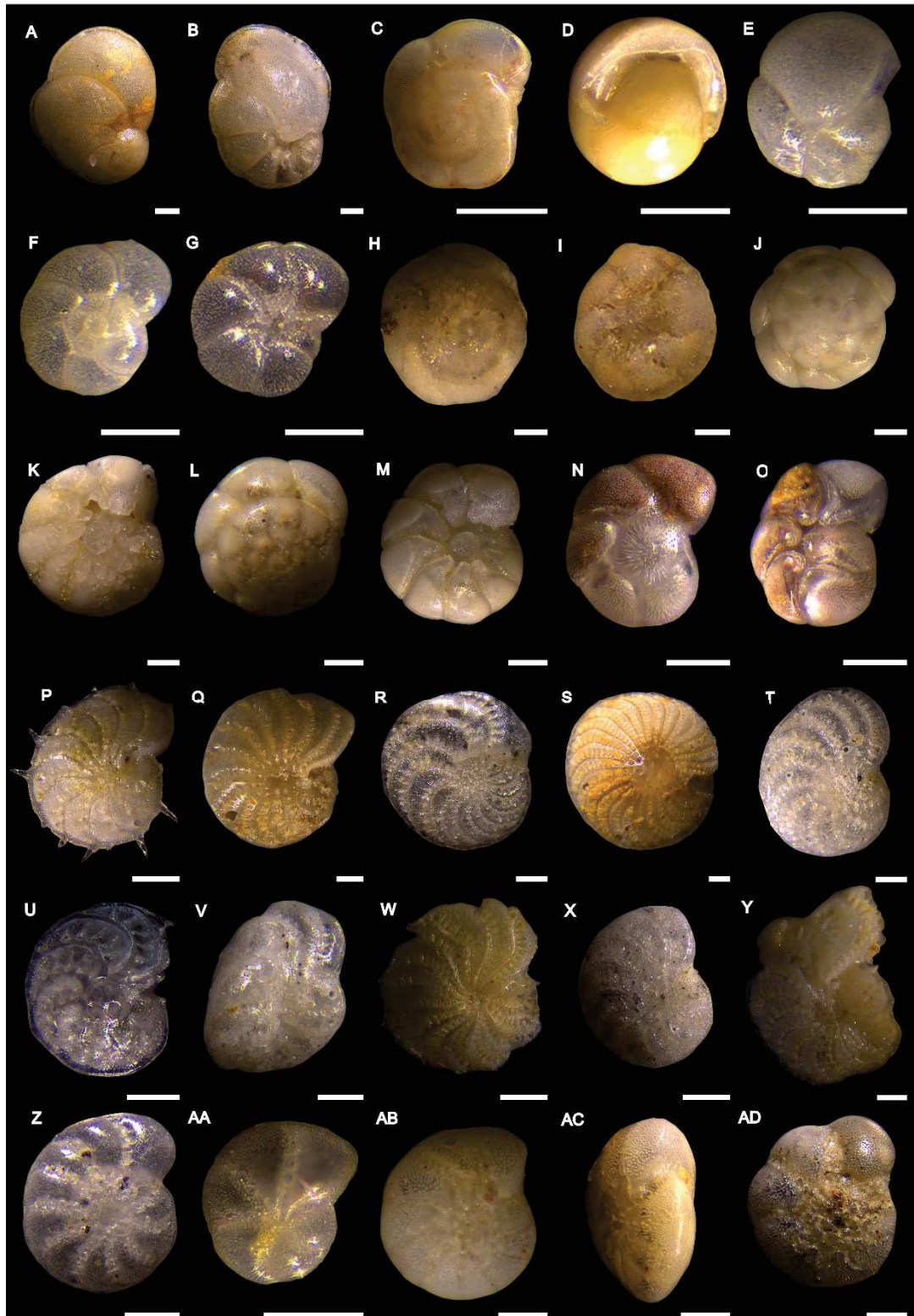


Figure 5.8 LM images of selected foraminifera species. A. *Cancris auricola*, spiral side; B. *C. auricola*, umbilical side; C. *Oridorsalis umbonatus*; D. *Pullenia bulloides*; E. *Pullenia quadriloba*; F. *Aubignyna perlucida*, spiral side; G. *A. perlucida*, umbilical side; H. *Buccella* aff. *frigida*, spiral side; I. *Buccella* aff. *frigida*, umbilical side; J. *Ammonia beccarii*, spiral side; K. *A. beccarii*, umbilical side; L. *Ammonia parkinsoniana*, spiral side; M. *A. parkinsoniana*, umbilical side; N. *Ammonia tepida*, spiral side; O. *A. tepida*, umbilical side; P. *Elphidium aculeatum*; Q. *Elphidium advenum*; R. *Elphidium complanatum*; S. *Elphidium crispum*; T. *Elphidium fichtelianum*; U. *Elphidium* sp.; V. *Elphidium incertum*; W. *Elphidium macellum*; X. *Elphidium* sp.1; Y. *Elphidium* aff. *aculeatum*; Z. *Elphidium* sp.5 Cimerman and Langer, 1991; AA. *Cribroelphidium* cf. *magellanicum*; AB. *Elphidium translucens*.; AC. *E. translucens*, lateral; AD. *Porosonion granosum*. The white bars correspond to 100 μm .

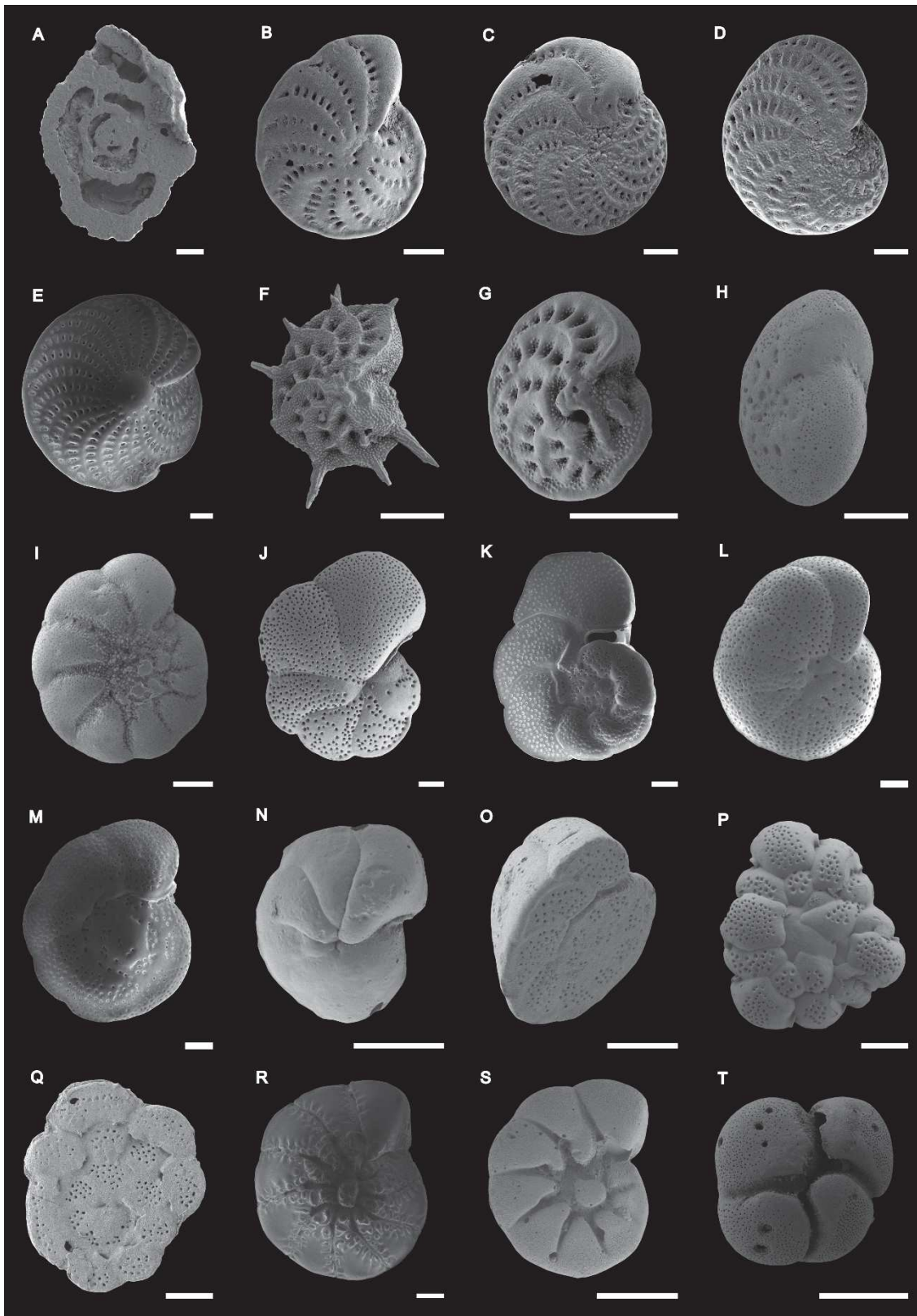


Figure 5.9 SEM images of selected foraminifera species. A. *Nubecularia lucifuga*; B. *Elphidium advenum*; C. *Elphidium complanatum*; D. *Elphidium fichtelianum*; E. *Elphidium crispum*; F. *Elphidium aculeatum*; G. *Elphidium* sp.; H. *Elphidium translucens*; I. *Porosonion granosum*; J. *Lobatula lobatula*, spiral side; K. *L. lobatula*, umbilical side; L. *Cibicidoides pseudoungerianus*, spiral side; M. *C. pseudoungerianus*, umbilical side; N. *Cibicides refulgens*, spiral side; O. *C. refulgens*, umbilical side; P. *Planorbulina mediterraneensis*, spiral side; Q. *P. mediterraneensis*, umbilical side; R. *Ammonia beccarii*, umbilical side; S. *Ammonia parkinsoniana*, umbilical side; T. *Ammonia tepida*, umbilical side. The white bars correspond to 100 μm .

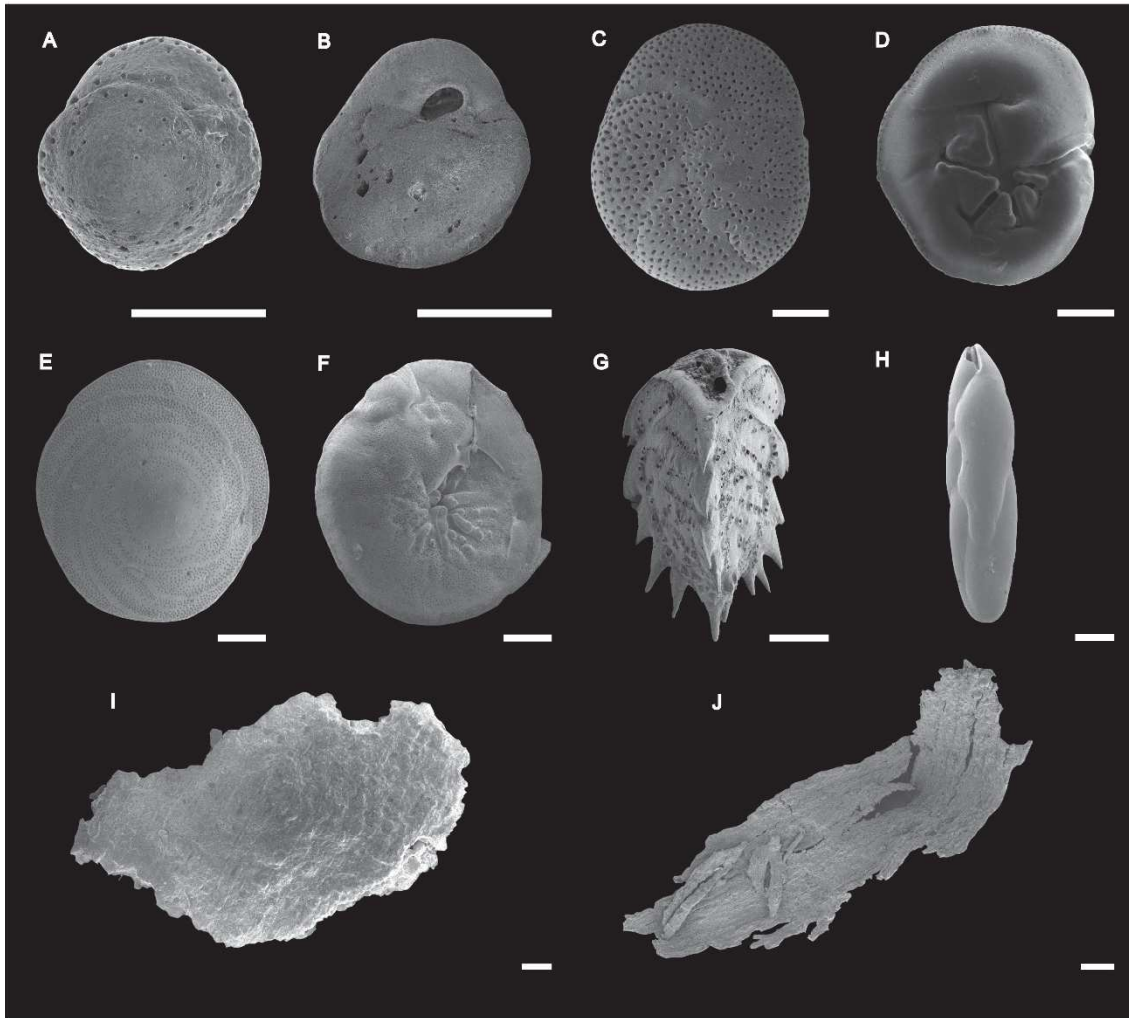


Figure 5.10 SEM images of selected foraminifera species and fossil *Posidonia*. A. *Asterigerinata mamilla*, spiral side; B. *A. mamilla*, umbilical side; C. *Rosalina bradyi*, spiral side; D. *R. bradyi*, umbilical side; E. *Neoconorbina terquemi*, spiral side; F. *N. terquemi*, umbilical side; G. *Reussella spinulosa*; H. *Fursenkoina subacuta*; I. Fossil *Posidonia* rhizome fragment; J. Fossil *Posidonia* leaf fragment. The white bars correspond to 100 μm .

5.6 Discussion

5.6.1 The exceptional preservation of *Posidonia oceanica* and the diagenetic imprint on the foraminiferal association

Seagrass preservation within the fossil record is an exceedingly rare event (e.g., Ivany et al., 1990; Moissette et al., 2007; Van der Ham et al., 2007; Reich et al., 2015; Dilcher, 2016; Van der Ham et al., 2017). Indeed, most of the unequivocal fossils of seagrasses are clearly linked to cases of exceptional preservation (e.g., Ivany et al., 1990; Moissette et al., 2007; Van der Ham et al., 2017). For instance, Maastrichtian seagrass from Belgium and the Netherlands occur as silicified material or embedded in flint (Van der Ham et al., 2017). The intact in situ rhizomes from the Eocene of Florida (Avon Park Formation) have been related to the sudden burial by fine-grained sediments caused by a storm (Ivany et al., 1990). The spectacularly preserved lower Pleistocene seagrass of Rhodes also underwent these particular conditions, having experienced a limited post-mortem transport before a

quick burial (Moissette et al., 2007). Consistently with this peculiar mode of preservation, elements of the seagrass meadow and seagrass-associated communities are often finely preserved (e.g., they display cell-level structures of the plant leaves, as well as epiphytes in life position), and, in the Pleistocene example, carbonate shells highly susceptible to diagenesis (e.g., gastropods) were also preserved (Moissette et al., 2007). The palaeoenvironmental reconstruction of the Fauglia succession indicates a shallow-water, low- to moderate-energy marine environment. This is supported by the presence of *Posidonia oceanica*, that usually extend from 0 to 40 m water depth, with the upper and lower limits being controlled by hydrodynamic energy and light penetration, (Duarte, 1991; Piazzzi et al., 2000; Infantes et al., 2009; Vacchi et al., 2017) and by the presence of a *Cladocora* bank above (close to the top of the section). This type of bioconstruction generally occurs between 5 and 35 m water depth (Kružić and Požar-Domac, 2003; Kružić and Benković, 2008; Kersting and Linares, 2012; El Kateb et al., 2016; Kersting et al., 2017; Macić et al., 2019) in sheltered areas (Kružić and Benković, 2008; Kersting and Linares, 2012; Chefaoui et al., 2017; Coletti et al., 2018). The presence of an oyster reef at the top of the succession also points towards a shallow (less than 10 m), low- to moderate-energy setting as these bioconstructions usually develop along gently sloping complex coastlines with hydrodynamic conditions favouring larval pooling (and thus clustering of various generations of individuals) (Puffer and Emerson, 1953; Haven and Whitcomb, 1983; Luckenbach et al., 1999; Boudreaux et al., 2006; La Peyre et al., 2014; Gain et al., 2017; Toscano et al., 2018; Kregting et al., 2020). The common presence of *Ammonia* is also supportive of a coastal, shallow-water environment, possibly influenced by river discharge (and thus high sedimentation rates) and significant salinity variations (Murray, 2006). The foraminifera of the *Ammonia* group are tolerant to brackish conditions and dwell in organic-matter-rich and oxygen-depleted sediments (Murray, 2006). Similar conditions, where seagrass meadows coexist with cladocorian corals in riverine-influenced environments, have been reported from the shallow-water deposits of the middle Eocene of the Western Pyrenees (Baceta and Mateu-Vicens, 2022). In the inferred coastal setting, *Posidonia* leaves and rhizomes were exceptionally preserved thanks to the low-to-moderate hydrodynamic energy and to sedimentation rates sufficiently high to cover the organic remains and inhibiting their decomposition. In the Fauglia succession, *P. oceanica* specimens consist of in-situ rhizomes (Fig. 5.4) that are either reddish, possibly fossilized through permineralization within brownish sediments, or blackish, with a peaty consistence as typical of coalified compressions in dark-grey sediments (Bosio et al., 2021), and finely preserved leaves (Fig. 5.4). The reddish colour is most likely the result of iron oxides formation occurred during diagenesis, whereas the dark grey colour of the sediments in which blackish rhizomes are preserved is probably related to local enrichment in organic material, which in turn is likely linked to oxygen deficiency at or just below the seafloor (Bosio et al., 2021).

The *Posidonia*-associated foraminiferal assemblage is also affected by diagenetic processes, which have the potential to skew fossil associations by preferentially dissolving aragonitic shells and subsequently high-Mg calcite shells like those of miliolids (Budd and Hiatt, 1993; Cherns and Wright, 2000; Cherns et al., 2011). Well-preserved miliolids tests were in fact recognized only within the dark-coloured sediments (P10, P11), where both organic matter and aragonitic fossils are well preserved (Bosio et al., 2021). The destructive effect of dissolution must thus be considered when calculating morphotype frequencies and related parameters (i.e., FI', I_{LS}) in fossil assemblages, differently from recent environments, where diagenesis does not play a role (e.g., El Kateb et al., 2020). Differing from what proposed by Reich et al. (2015), the fossilization potential of miliolids, although not low, is lower than that of rotaliids. This means that, when performing paleoenvironmental reconstructions, IPSIs and quantitative parameters based on porcelaneous foraminifera could be biased by diagenetic processes, and as such, diagenesis should be considered for reliable interpretations.

5.6.2 Epiphytic foraminifera analysis

The composition and diversity of the epiphytic communities are influenced by ecological parameters, structural features of the meadow and temporal persistence of the phytal substrates (Langer, 1993; Mateu- Vicens et al., 2014). Symbiont-bearing taxa are typically reported as a major component of the epiphytic foraminifera community (e.g., Murray, 2006; Langer, 1993; Mateu-Vicens et al., 2014). The lack of symbiont-bearing foraminifera (morphotype SB) in the Fauglia succession is most likely related to climatic constraints (Hollaus and Hottinger, 1997; Beavington-Penney and Racey, 2004; Murray, 2006; Langer, 2008; El Kateb et al., 2018). Common Mediterranean symbiont-bearing taxa like *Amphistegina*, *Sorites* and *Peneroplis* are in fact limited by temperature, being abundant in the eastern Mediterranean and displaying a restricted distribution in the western part of the basin (Mateu-Vicens et al., 2014). *Amphistegina* only occurs in the eastern Mediterranean and is limited by the 14 °C winter isotherm (Langer et al., 2012; El Kateb et al., 2018). It is common along the eastern and southern parts of the Mediterranean (Langer et al., 2012) and its current distribution reaches the south of Sicily (Caruso and Cosentino, 2014), the Maltese Islands (Yokes et al., 2007) and Crete (Hollaus and Hottinger, 1997). *Sorites* and *Peneroplis* are constrained by the 18 °C isotherm (Beavington-Penney and Racey, 2004; Murray, 2006). Currently, peneroplids and soritids are widely distributed over all the *P. oceanica* meadows in the Mediterranean (Blanc-Vernet, 1969; Colom, 1974; Murray, 2006). Peneroplids, in particular, are common in the *Posidonia* meadows of northern Sardinia (Benedetti and Frezza, 2016), which is located south of the study area. Soritids and peneroplids are also known from Elba Island, which is located at about the same latitude as the study area (Langer

and Schmidt-Sinns, 2006). Although in most of the samples these symbiont-bearing miliolids would have not been preserved due to diagenesis, their absence from the miliolid-bearing samples P10 and P11 suggests that Early Pleistocene temperatures in northern-central Italy were probably lower than today. The high terrigenous content of the Fauglia deposits is also consistent with low-light penetration that hampers the occurrence of SB foraminifera, as also observed in modern *P. oceanica* meadows located close to river mouths, and thus influenced by sediment discharge (e.g., the Santa Marinella *P. oceanica* meadow, central Italy; Frezza et al., 2011). In general, the number of individuals and the species richness decrease with increasing mesh size, but this is especially true for deep-sea environments (Schröder et al., 1987; Rathburn and Corliss, 1994; Wollenburg and Mackensen, 1998a, 1998b; Alve, 2003), in which sieving through meshes larger than 63 µm could provide misleading results (Murray, 2006). No remarkable differences in the benthic foraminiferal associations were found between the analysed >125 µm and > 63 µm sediment fractions. This quite homogeneous distribution of the foraminiferal assemblages, regardless of the mesh size, is related to the shallow-water character of the Fauglia succession. The only detectable trend is the slightly higher abundance of some opportunistic genera (i.e., *Bolivina* and *Bulimina*) in the samples sieved through the 63-µm-sized mesh. $Index_{EP}$ and $Index_{EP-M}$ display a significant difference between the samples from the *Posidonia*-bearing layers and the *Cladocora* bank, revealing a good potential in indicating ancient seagrass meadows. FI' and FI'_{-M} also display differences between the *Posidonia*-bearing layers and the *Cladocora* bank, suggesting their potential usefulness as IPSIs. However, a straightforward application of the FI might induce some interpretative mistakes, for example when symbiont-bearing taxa are not present due to thermal constraints (Mateu-Vicens et al., 2014) or when the fossil association has been altered through diagenetic and/or transport processes (as in the case for the Fauglia outcrop). The same applies for I_{LS} , which consists in the ratio between long and short life-span forms, and whose values must be calibrated with observations on other independent variables (i.e., plant canopy, oxygen concentration, etc.; Mateu-Vicens et al., 2014). The morphotype analysis considering miliolids (Mode-1) shows that the morphotype distribution is similar for all the samples except P10 (in which miliolids are abundantly present) and F7 (the sample collected from the *Cladocora* bank), thus highlighting the significant difference between the foraminiferal association of the *P. oceanica* meadow and the *Cladocora* bank (Fig. 5.11). The morphotype analysis excluding miliolids (Mode-2) allowed to remove the bias produced by diagenesis. In Mode-2, sample P10 is more similar, although not identical, to all the others from the *Posidonia*-bearing layers, whereas sample F7 is still remarkably different (Fig. 5.11). Sample P10 displays a higher frequency of morphotype D* in comparison to the other samples, due to the larger abundance of agglutinated foraminifera. This is probably related to dissolution processes having occurred at a lesser extent

within the dark-coloured sediments, in which organic matter is still preserved, thus permitting a better preservation of agglutinated tests formed by particles bound together by an organic or calcareous cement (Armstrong and Brasier, 2013). The presence of permanently attached, encrusting foraminifera such as *Planorbulina mediterranensis* and *Nubecularia lucifuga* (morphotype A*) confirms as one of the most decisive tools to detect ancient *Posidonia* expanses and to distinguish them from other phytal substrates (e.g., macroalgae; Mateu-Vicens et al., 2010). Indeed, the foraminiferal assemblage typical of these seagrass meadows, the *Planorbulinatum mediterranensae*, was formally described (Colom, 1942) based upon the abundance of this species. In the studied outcrop, *P. mediterranensis* is present in all the samples from the *Posidonia*-bearing layers and is absent from the *Cladocora* bank sample. The same applies for *N. lucifuga*, whose occurrence as a fossil is however strongly controlled by diagenetic processes (which explains why it only occurs in sample P10). However, since these taxa can be rare (as in the Fauglia case), their use as a tool for detecting ancient *Posidonia* meadows requires a detailed quantitative micropalaeontological analysis. Furthermore, the low abundance of these taxa within the Fauglia meadow could be related to the environmental stress that possibly influenced this site. Indeed, the stress produced by riverine discharge (testified also by the high terrigenous content and the abundance of organic matter) could deeply influence the development of seagrass leaves, which are the preferred surface onto which morphotype A* taxa live. The presence of other foraminifera with a curved basal surface such as Cibicididae (Fig. 5.13) indicates that these foraminifera lived attached onto a firm substrate, which in this case likely consists of *Posidonia* leaves and/or rhizomes (Fig. 5.4). However, this observation is not necessarily diagnostic of a vegetated substrate. While hooked morphologies in relatively large carbonate producers, such as coralline algae and acervulinids, have been used to infer the occurrence of seagrasses in the fossil record (Beavington-Penney et al., 2004; Tomás et al., 2016; Baceta and Mateu-Vicens, 2022), small benthic foraminifera like Cibicididae could develop a curved attachment surface even when attached onto a non-phytal substrate. Morphotype B epiphytic foraminifera, such as Rosalinidae, *Asterigerinata mamilla* and *Lobatula lobatula*, are present within the *Cladocora caespitosa* bank sediments, although scarcer than in the *Posidonia*-bearing layers. That can be explained by the occurrence of a phytal substrate, with life-span shorter than 1 year, associated to this coral-dominated environment. Indeed, morphotype B taxa are not exclusively related to seagrass meadows, being indeed commonly reported attached to a broad diversity of macroalgae (Langer, 1993). Within the context of the Fauglia succession the most reliable proxies for inferring the presence of ancient seagrass meadows seem to be K/R and K/R_{EXT} indexes, whose variations range across at least one order of magnitude between the *Posidonia* meadow samples and the *Cladocora* bank sample. This suggests that, differing from what has been proposed by Reich et al. (2015), the

abundance of keeled elphidiids and in particular the ratio between keeled *Elphidium* and rounded elphidiids (e. g., *Elphidium translucens*, *Cribrorhynchium*, *Porosonion*), combined with other related genera that display rounded periphery (i.e., *Astronion*, *Haynesina*, *Melonis*, *Nonion*, *Nonionella* and *Valvulineria*) represent a useful IPSI. Keeled elphidiids are known as typically epiphytes (Langer, 1993; Murray, 2006; Mateu-Vicens et al., 2014) whereas rounded ones are more commonly infaunal organisms. Although elphidiids are not strictly related to seagrass, keeled *Elphidium* spp. are more common in vegetated environments; thus, thanks also to their high fossilization potential, they could be used as a proxy of a seagrass-related palaeobiotope. The K/R ratio, being mostly based on morphology, could be calculated also in more ancient successions, where species-level identification can be difficult and often needs to rely on thin sections, thus providing a useful tool for palaeoenvironmental reconstructions. All the calculated indices were compared to those from a modern case study, the present-day Santa Marinella *Posidonia* meadow, along the Tyrrhenian coast of Italy near Rome (Frezza et al., 2011; Mateu-Vicens et al., 2014). This site is heavily affected by anthropogenic activity and, most importantly, by river discharge. Furthermore, the Santa Marinella *P. oceanica* meadow is reportedly shallower than 15 m water depth. In both meadows, stress-tolerant taxa, such as *Ammonia* and *Haynesina*, are abundant and they are accompanied by the presence of taxa that tolerate high organic content within the sediments of the seafloor (e.g., *Bolivina* and *Bulimina*). The values of the calculated indices in both seagrass meadows are similar (see Mateu-Vicens et al., 2014 for the detailed values of Santa Marinella). The Shannon-Weaver index (H') exhibits similar values at both sites (3.12 and 3.3 on average at Santa Marinella and Fauglia, respectively). FI' presents an average value of 1.88 and 1.24 at Santa Marinella and Fauglia, respectively, thus evoking stressed environmental conditions. I_{LS} displays an average value of 0.24 and 0.89 at Santa Marinella and Fauglia, respectively, confirming the presence of environmental stress that drove the development of the meadows, as highlighted also by the abundance of low-oxygen tolerant, opportunistic forms, which are associated with decaying seagrass in the sediment (Mateu-Vicens et al., 2014). K/R_{EXT} index was also tested, including the data obtained by Frezza et al. (2011) for Santa Marinella site. Both *Posidonia* meadows show similar values: 0.74 and 0.99 on average at Santa Marinella and Fauglia, respectively, strengthening the similarities between the two meadows as well as the potential of the K/R_{EXT} index as IPSI. Thus, excluding the anthropogenic influence, the environmental characteristics of these meadows are comparable: both meadows are located in shallow water and in both the influence of riverine discharge most likely implicates their growth under stressed condition. Furthermore, the morphotype analysis performed at the two different meadows led to very similar results (see Mateu-Vicens et al., 2014 for details). In particular, the presence of morphotype A*, which is regarded by the authors among the most reliable

IPSI, is very scarce in the *Posidonia* meadows, with values $\leq 1\%$ in both. This witnesses that the presence, rather than the abundance, of morphotype A* foraminifera is the most characteristic feature of the foraminiferal assemblage of a seagrass meadow (especially if the meadows grew under stressed condition). Finally, the cluster analysis (Fig. 5.12) clearly highlights the differences between the two analysed palaeoenvironments preserved at Fauglia (i.e., the *Posidonia* meadow and the *Cladocora* bank). Indeed, such a clustering is mainly related to the different abundance of specific taxa within the two deposits: Cibicididae, Rosalinidae and keeled *Elphidium* species are more abundant within the *Posidonia*-bearing layers (Table 5.3; Appendix 5.1), whereas the abundance of *Criboelphidium* and *Haynesina* (and generally that of infaunal taxa that display rounded peripheries) is higher within the sample from the *Cladocora* layer (Table 5.3; Appendix 5.1).

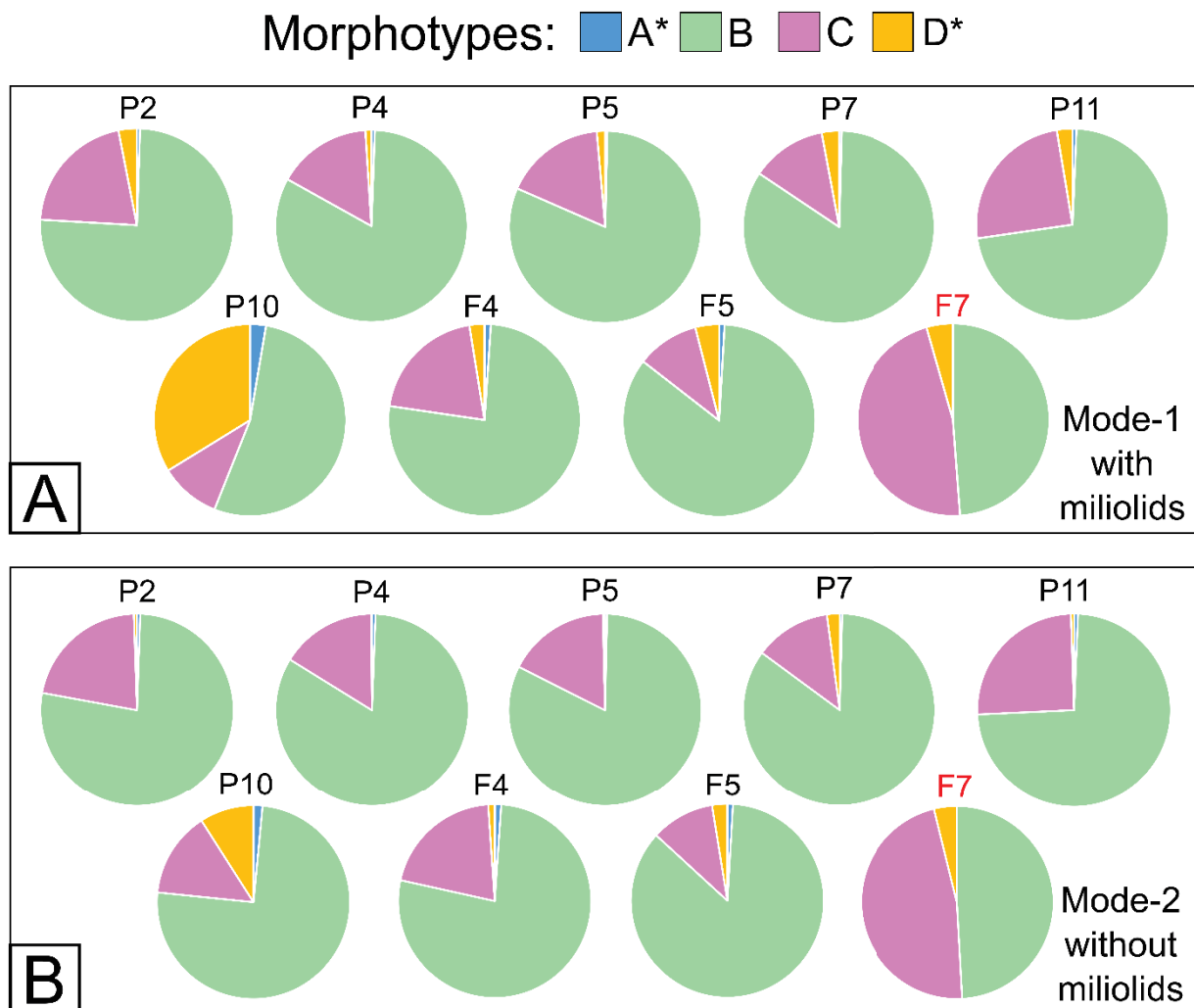


Figure 5.11 Pie-plots representing morphotypes frequencies in the collected samples. A. Mode-1 analysis, with miliolids. B. Mode-2 analysis, without miliolids.

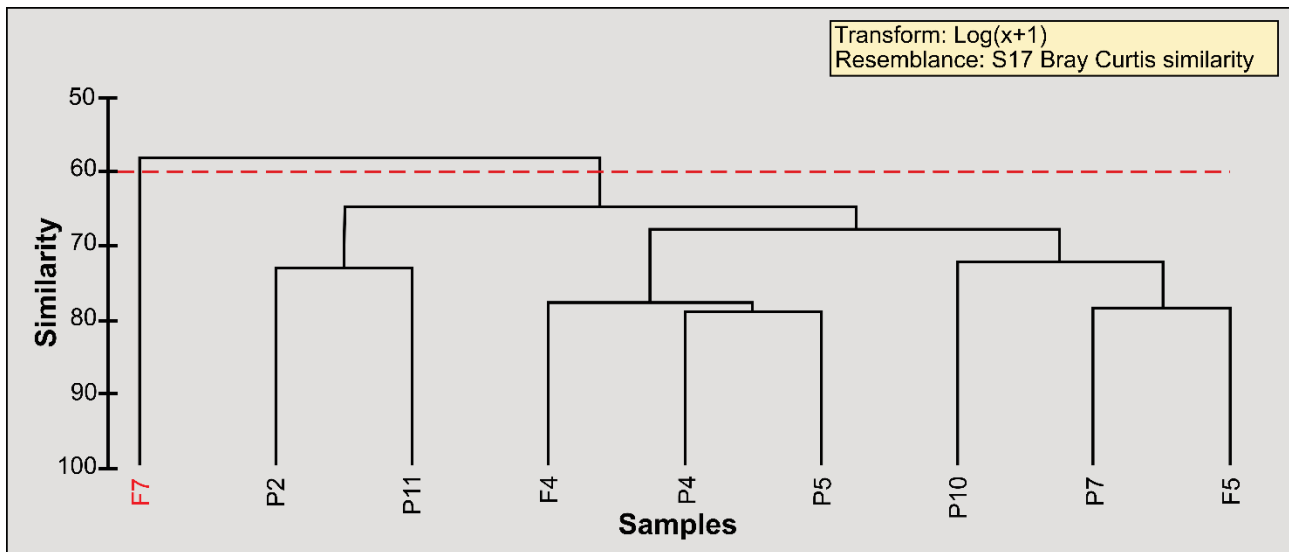


Figure 5.12 Q-mode cluster analysis.

5.7 Conclusions

At the Fauglia quarry, two stratigraphic intervals are characterized by the occurrence of remarkably well-preserved fossil remains of marine plants (leaves and in-situ rhizomes of *Posidonia oceanica*). Within this setting, we tested the potential of foraminiferal-based Indirect Palaeo- Seagrass Indicators (IPSIs). The Fauglia succession formed in a shallow, low- to moderate-energy, marginal-marine environment, as indicated by the presence of in situ *P. oceanica* rhizomes, a *Cladocora caespitosa* bank, an oyster reef and abundant foraminifera of the *Ammonia* group. Even if the *Posidonia* remains at Fauglia represent a case of exceptional seagrass preservation, diagenetic processes such as dissolution have modified the original composition of the seagrass-related communities. Such effect is reflected by the reported foraminiferal assemblage that displays differences related to diagenesis, e.g., the preferential loss of miliolids whose tests consist of high-Mg calcite. The fossil assemblage is also influenced by environmental parameters, such as the seawater temperature. The lack of symbiont-bearing foraminifera (e.g., *Amphistegina*, *Sorites*, *Peneroplis*), which are common in seagrass-related environments, indicates that Early Pleistocene temperatures in northern Tuscany were probably too low for their development. Considering these constraints, we discussed the potential of benthic foraminifera and foraminifera-based indices as indirect paleo-seagrass indicators. Although highly reliable for the analysis of recent seagrass environments, FI' and I_{LS} display only slight differences between the *Posidonia*-bearing strata and the *Cladocora* bank. However, these indexes confirmed to be reliable for the environmental analysis of seagrass meadows: at Fauglia, their values point to stressed environmental condition, similar to what has been observed at a modern case study (e.g., the Santa Marinella *Posidonia* meadow). Based on our data, the presence of permanently

attached, encrusting foraminifera (e.g., *Planorbulina mediterraneensis*, *Nubecularia lucifuga*) is considered a highly reliable IPSI. The ratio between keeled *Elphidium* and rounded elphidiids (e.g., *Elphidium translucens*, *Criboelphidium*, *Porosononion*) combined with other related genera that display rounded periphery (i.e., *Astrononion*, *Haynesina*, *Melonis*, *Nonion*, *Nonionella*, *Valvulineria*), also displays a significant role as IPSI. Since this latter index is based on rotaliids, which are resistant to diagenetic dissolution, and on the general morphology rather than on species identification, when combined with the presence of permanently attached encrusting taxa, it could represent a precious tool in the analysis of sedimentary successions, where seagrass remains have not been preserved. Further studies, based on both fossil and recent seagrass-related environments, could allow to improve those indexes and estimate threshold values useful for recognizing the presence of seagrasses in the fossil record.

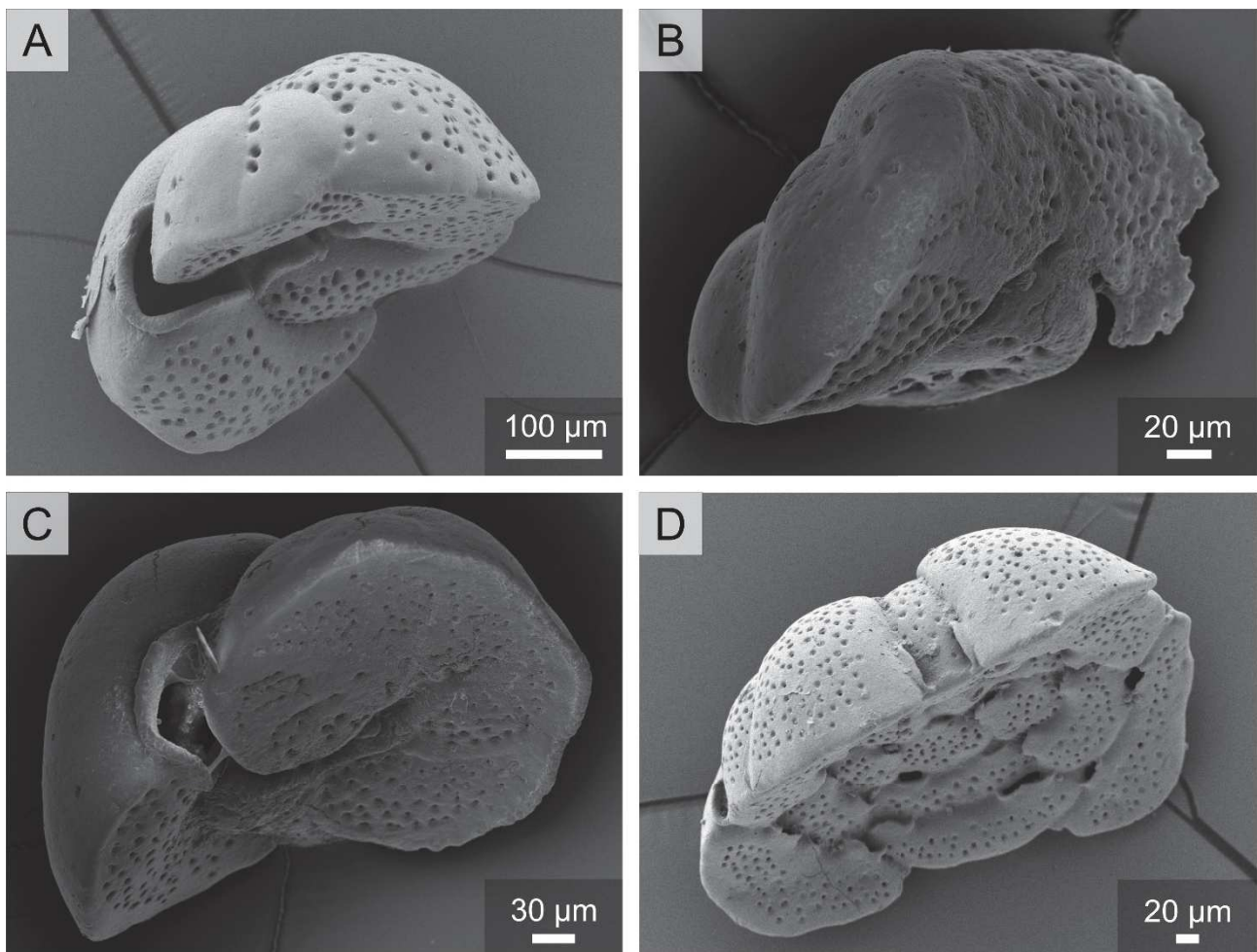


Figure 5.13 Benthic foraminifera specimens with curved attaching surface, typical of epiphytic forms. A. *Lobatula lobatula*; B, C. *Cibicides refulgens*. D. *Planorbulina mediterraneensis*.

Analysis	Morphotypes	P2	P4	P5	P7	P10	P11	F4	F5	F7
Mode 1	A*	0.36	0.37	0.19	0.27	1.47	0.46	0.62	0.55	0
	B	52.88	52.31	44.04	53.28	29.26	50.00	44.44	50.89	19.45
	C	14.75	10.08	9.23	8.03	5.59	17.12	11.74	6.31	18.63
	D	2.16	0.64	0.77	1.87	18.53	1.83	1.47	2.40	1.76
Mode 2	A*	0.36	0.37	0.19	0.27	0.59	0.46	0.62	0.55	0
	B	52.88	52.31	44.04	53.28	29.26	50.00	44.44	50.89	19.45
	C	14.75	10.08	9.23	8.03	5.59	17.12	11.74	6.31	18.63
	D*	0.36	0.09	0.19	1.34	3.53	0.34	0.62	1.51	1.51

Table 5.5 Morphotypes abundances within the different samples. Mode-1 indicates the study considering miliolids. Mode-2 indicates the study without considering miliolids. For graphical representation see Fig. 5.11.

Acknowledgments

The authors wish to warmly thank Nicoletta Fusi for her help with grain-size analyses and Valentina Beccari, for her help with benthic foraminifera identification. The authors would like to thank two anonymous reviewers and the handling editor Professor Valeria Luciani for their useful suggestions. This research did not receive any specific grant from funding agencies in the public, commercial, or not-for-profit sectors. This article is also an outcome of Project MIUR-Dipartimenti di Eccellenza 2018-2022.

Appendix 5.1. Supplementary data

Supplementary data to this article can be found online at <https://doi.org/10.1016/j.marmicro.2022.102126>.

References

- Alve, E., 2003. A common opportunistic foraminiferal species as an indicator of rapidly changing conditions in a range of environments. *Estuarine, Coastal and Shelf Science*, v. 57, p. 501–14.
- Armstrong, H. and Brasier, M., 2013. *Microfossils*, Second Edition. 10.1002/9781118685440.ch15.
- Baceta, J.I. and Mateu-Vicens, G., 2022. Seagrass development in terrigenous-influenced inner ramp settings during the middle Eocene (Urbasa-Andia Plateau, Western Pyrenees, North Spain). *Sedimentology*. In press.
- Barsotti, G., Federici, P.R., Granelli, L., Mazzanti, R. and Salvatorini, G., 1974. Studio del Quaternario livornese, con particolare riferimento alla stratigrafia ed alle faune delle formazioni del bacino di carenaggio della Torre del Fanale. *Memorie della Società Geologica Italiana*, v. 13, p. 425–495.
- Beavington-Penney, S. J. and Racey, A., 2004. Ecology of extant nummulitids and other larger benthic foraminifera; applications in palaeoenvironmental analysis. *Earth Science Reviews*, v. 67 p.219-265.
- Beavington-Penney, S.J., Wright, V.P. and Woelkerling, W.J., 2004. Recognising macrophytevegetated environments in the rock record: a new criterion using 'hooked' forms of crustose coralline red algae. *Geol.* 166, 1–9.
- Benedetti, A., and Frezza, V., 2016. Benthic foraminiferal assemblages from shallow-water environments of northeastern Sardinia (Italy, Mediterranean Sea). *Facies*, v. 62(2), p. 14.
- Benzecry, A. and Brack-Hanes, S.D., 2008. A new hydrocharitacean seagrass from the Eocene of Florida. *Bot. J. Linn. Soc.* v. 157, p. 19–30.
- Berta, A., Kienle, S., Bianucci and G., Sorbi, S. 2015. A reevaluation of *Pliophoca etrusca* (Pinnipedia, Phocidae) from the Pliocene of Italy: phylogenetic and biogeographic implications. *Journal of Vertebrate Paleontology*, v. 35(1), e889144.
- Blanc-Vernet, L., 1969. Contribution a l'étude des foraminifères de Méditerranée. *Recueil des travaux de la Station Marine d'Endoume*, v. 64, p. 1–279.

- Blanc-Vernet, L., Clairefond, P. and Orsolini, P., 1979. La Mer pelagienne: les foraminifères. *Géologie Méditerranéenne*, v. 61, p. 171–209.
- Blott, S.J. and Pye, K., 2001. GRADISTAT: a grain size distribution and statistics package for the analysis of unconsolidated sediments. *Earth surface processes and Landforms*, v. 26(11), p. 1237-1248.
- Bosio, G., Di Cencio, A., Coletti, G., Casati, S. and Collareta, A., 2021. Exceptionally preserved coral bank and seagrass meadow from the lower Pleistocene of Fauglia (Tuscany, Italy). *Alpine and Mediterranean Quaternary*, v. 34(2), pp. 237-256.
- Bossio A., Costantini A., Lazzarotto A., Liotta D. and Mazzanti, R., 1993. Rassegna delle conoscenze sulla stratigrafia del Neoaotoceno toscano. *Memorie della Società Geologica Italiana*, v. 49, p. 17-98.
- Bossio, A., Foresi, L.M., Liotta, D., Mazzanti, R., Mazzei, R., Salvatorini, G. and Squarci, P., 1999. Riordino delle conoscenze sul Bacino neogenico del Tora-Fine (Toscana-Italia). *Atti della Società Toscana di Scienze Naturali, Memorie, Serie A*, v. 106, p. 1-16.
- Boudouresque, Charles and Grissac, A., 1983. L'herbier à *Posidonia oceanica* en Méditerranée: Les interactions entre la plante et le sediment. *Journal de Recherche Océanographique*, v. 8, p. 99-122.
- Boudreaux, M.L., Stiner, J.L. and Walters, L.J. 2006. Biodiversity of sessile and motile macrofauna on intertidal oyster reefs in Mosquito Lagoon, Florida. *Journal of Shellfish Research*, v. 25(3), p. 1079-1089.
- Brack-Hanes, S. and Greco, A., 1988. Biomineralization in *Thalassia testudinum* (Liliopsida: Hydrocharitaceae) and an Eocene Seagrass. *Transactions of the American Microscopical Society*, v. 107(3), p. 286-292.
- Braga, J. C., Bajo-Campos, I., and Cárdenas-Carretero, J., 2021. Late Miocene *Cymodocea* seagrass in the Guadalquivir Basin (southern Spain). *Review of Palaeobotany and Palynology*, 104485.
- Brandano, M., Cuffaro, M., Gaglianone, G., Petricca, P., Stagno, V. and Mateu-Vicens, G., 2016. Evaluating the Role of Seagrass in Cenozoic CO2 Variations. *Frontiers in Environmental Science*, v. 4, p. 72.
- Brandano, M., Tomassetti, L., Mateu-Vicens, G. and Gaglianone, G., 2019. The seagrass skeletal assemblage from modern to fossil and from tropical to temperate: insight from Maldivian and Mediterranean examples. *Sedimentology*, v. 66, p. 2268 - 2296.
- Brasier M.D., 1975. An outline history of seagrass communities. *Palaeontology*, 18, 681-702.
- Brunetti, M.M., Forli, M. and Vecchi, G., 2008. Una nuova specie di *Gibbula* per il Pleistocene italiano: *Gibbula (Forskalea) sirigui* n. sp. (Mollusca: Gastropoda). *Bollettino Malacologico*, v. 44(7-11), p. 1-4.
- Brunetti, M.M. and Vecchi, G., 2005. *Rissoa quarantelli*, una nuova specie del Pleistocene inferiore italiano. *Bollettino Malacologico*, v. 41, p. 60-65.
- Brunetti, M.M. and Vecchi, G., 2012. Nuove specie del genere *Alvania* (Caenogastropoda: Rissoidae) nel Pleistocene dell'Emilia occidentale (Nord Italia). *Bollettino Malacologico*, v. 48(1), p. 42-50.
- Budd, D. and Hiatt, E., 1993. Mineralogical Stabilization of High-magnesium Calcite: Geochemical Evidence for Intracrystal Recrystallization Within Holocene Porcellaneous Foraminifera. *Journal of sedimentary petrology*, v. 63, p. 261-274.
- Carnevale, G., Longinelli, A., Caputo, D., Barbieri, M. and Landini, W., 2008. Did the Mediterranean marine reflooding precede the Mio-Pliocene boundary? Paleontological and geochemical evidence from upper Messinian sequences of Tuscany, Italy. *Palaeogeography, Palaeoclimatology, Palaeoecology*, v. 257(1-2), pp. 81-105.
- Caruso, A. and Cosentino, C., 2014. The first colonization of the Genus *Amphistegina* and other exotic benthic foraminifera of the Pelagian Islands and south-eastern Sicily (central Mediterranean Sea). *Marine Micropaleontology*, v. 111, p. 38–52, <https://doi.org/10.1016/j.marmicro.2014.05.002>
- Chandler, M.E.J., 1961. The Lower Tertiary Floras of Southern England. I. Palaeocene Floras, London Clay Flora (Supplement). British Museum of Natural History, London.
- Chefaoui, R. M., Casado-Amezúa, P., and Templado, J., 2017. Environmental drivers of distribution and reef development of the Mediterranean coral *Cladocora caespitosa*. *Coral Reefs*, v. 36(4), p. 1195-1209.
- Cherns, L. and Wright, V. P., 2000. Missing molluscs as evidence of large-scale, early skeletal aragonite dissolution in a Silurian sea. *Geology*, v. 28(9), p. 791-794.
- Cherns, L., Wheelley, J.R. and Wright, V.P., 2011. Taphonomic Bias in Shelly Faunas Through Time: Early Aragonitic Dissolution and Its Implications for the Fossil Record. In: Allison, P.A. and Bottjer, D.J. (eds) *Taphonomy. Aims & Scope Topics in Geobiology Book Series*, vol 32. Springer, Dordrecht. Doi: 10.1007/978-90-481-8643-3_3
- Chesters, K.I.M., Gnauck, F.R. and Hughes, N.F., 1967. Angiospermae. In: Harland, W.B., Holland, C.H., House, M.R., et al. (Eds.), *The Fossil Record—A Symposium with Documentation*. Geol Soc Lond, pp. 269–389.
- Chimenz C., Taramelli, E., Cironi, R., Contessini, A., Gravina, F., Maggiore, F. R., Maj R. L. C., Motta M. G. and Somaschini, A., 1989. Studies on animal populations of leaves and rhizomes of *Posidonia oceanica* (L.) Delile on the rocky bottom of Torvaldaliga, in Boudouresque, C. F., Meinesz, A., Fresi, E. and Gravez, V. (eds) *International workshop on Posidonia beds*. Marseilles. GIS Posidonie, p. 145–155.
- Chirli, C. and Forli, M., 2017. Il Calabrianesimo della Toscana. *Gasteropodi vol. I. L'Informatore Piceno*, Ancona, pp. 90.
- Cimerman, F. and Langer, M. R., 1991, *Mediterranean Foraminifera: Slovenska Akademija Znanosti, Ljubljana*, pp. 118.

- Coletti, G., Bracchi, V., Corselli, C., Marchese, F., Basso, D., Savini, A., and Vertino, A., 2018b. Quaternary build-ups and rhodalgal carbonates along the Adriatic and Ionian coasts of the Italian Peninsula: a review. *Rivista Italiana di Paleontologia e Stratigrafia*, v. 124(2), p. 387-406.
- Collinson, M.E., 1983. Fossil Plants of the London Clay. Palaeontological Association Field Guides No 1. Palaeontological Association, London.
- Collinson, M.E., 1996. Plant macrofossils from the Bracklesham Group (Early & Middle Eocene), Bracklesham Bay, West Sussex, England: review and significance in the context of coeval British Tertiary faunas. *Tertiary Res.*, v. 16, p. 175-202.
- Colom, G., 1942. Una contribució al conocimiento de los foraminíferos de la bahía de Palma de Mallorca. *Notas y Resúmenes Ser. II, Instituto Español de Oceanografía*, v. 108, p. 1-53.
- Colom, G. 1974. Foraminíferos Ibéricos. Introducción al estudio de las especies bentónicas recientes. *Investigación Pesquera*, t. 38, p. 1-245.
- Cresti M. and Forli M., 2020. New specimens of *Tectura rubroradiata* Chirli & Forli, 2017 (Gastropoda: Lottiidae), little known species from tuscan lower Pleistocene. *Bollettino Malacologico*, v. 56, p. 107-110.
- Crippa, G., Azzarone, M., Bottini, C., Crespi, S., Felletti, F., Marini, M., Petrizzo, M.R., Scarponi, D., Raffi, S. and Raineri, G., 2019. Bio-and lithostratigraphy of lower Pleistocene marine successions in western Emilia (Italy) and their implications for the first occurrence of *Arctica islandica* in the Mediterranean Sea. *Quaternary Research*, v. 92(2), p. 549-569.
- Curry, D., 1965. Palaeogene beds of south-east England. *Proc. Geol. Assoc.* v. 76, p. 151-173.
- De Saporta, G. and Marion, A.F., 1878. Révision de la flore Heersienne de Gelinden d'après une collection appartenant au comte G. de Looz. *Mém Acad R Belg, Cour Sav Étrang.* v.41, p. 1-112.
- Debey, M.H., 1848. Übersicht der urweltlichen Pflanzen des Kreidegebirges überhaupt und der Aachener Kreideschichten insbesondere. *Verh. Nat. Hist. Ver. Preuss. Rheinl.* v. 5, p. 113-125.
- Debey, M.H., 1851. Beitrag zur fossilen Fauna der holländischen Kreide (Vaels bei Aachen, Kunraed, Maastricht). *Verh. Nat. Hist. Ver. Preuss. Rheinl.* v. 8, p. 568-569.
- De Falco, G., Ferrari, S., Cancemi, G. and Baroli, M., 2000. Relationship between sediment distribution and *Posidonia oceanica* seagrass. *Geo-Marine Letters*, v. 20, p. 50-57.
- De Falco, G., Simeone, S. and Baroli, M., 2008. Management of Beach-Cast *Posidonia oceanica* Seagrass on the Island of Sardinia (Italy, Western Mediterranean). *Journal of coastal research*, v. 24, p. 69-75.
- Den Hartog, C., 1970. The seagrasses of the world. North Holland Publishing Co., Amsterdams.
- Den Hartog, C., 1979. Seagrasses and seagrass ecosystems, an appraisal of the research approach. *Aquatic Botany*, v. 7, p. 105-107.
- Dilcher, D., 2016. Fossil plants from the Coon Creek Formation of Tennessee. In: *Paleontology of Cretaceous Coon Creek Formation* (eds Ehret D, Jr, TLH, Ebersole S). The Alabama Museum of Natural History, Tuscaloosa, Alabama, p. 118-121.
- Dimiza, M. D., Koukousioura, O., Triantaphyllou, M. V. and Dermitzakis, M. D., 2016. Live and dead benthic foraminiferal assemblages from coastal environments of the Aegean Sea (Greece): Distribution and diversity, *Revue de Micropaléontologie*, v. 59, p. 19-32.
- Domning, D.P., 2001. Sirenians, seagrasses, and Cenozoic ecological change in the Caribbean. *Palaeogeogr. Palaeoclimatol. Palaeoecol.*, v. 166, p. 27-50.
- Duarte, C.M., 1991. Seagrass depth limits. *Aquatic botany*, 40(4), 363-377.
- Duarte, C. M., and Chiscano, C. L., 1999. Seagrass biomass and production: a reassessment. *Aquatic Botany*, v. 65, p. 159-174.
- El Kateb, A., Stalder, C., Neururer, C., Pisapia, C. and Spezzaferri, S., 2016. Correlation between pollution and decline of Scleractinian *Cladocora caespitosa* (Linnaeus, 1758) in the Gulf of Gabes. *Heliyon*, v. 2(11), e00195.
- El Kateb, A., Stalder, C., Stainbank, S., Fentimen, R. and Spezzaferri, S., 2018. The genus *Amphistegina* (Benthic foraminifera): Distribution along the southern Tunisian coast. *BioInvasions Records*, v. 7. 10.3391/bir.2018.7.4.06.
- El Kateb, A., Stalder, C., Martínez-Colón, M., Mateu-Vicens, G., Francescangeli, F., Coletti, G., Stainbank S. and Spezzaferri, S., 2020. Foraminiferal-based biotic indices to assess the ecological quality status of the Gulf of Gabes (Tunisia): Present limitations and future perspectives. *Ecological Indicators*, v. 111, 105962.
- Eva, A.N., 1980. Pre-Miocene seagrass communities in the Caribbean. *Palaeontology*, v. 23, p. 231-236.
- Forsy, G.F., 2016. Ostracods as proxies for past seagrass: A review. *Palaeogeography, Palaeoclimatology, Palaeoecology*, v. 447, p. 22-28.
- Frezza, V., Mateu-Vicens, G., Gaglianone, G., Baldassarre, A. and Brandano, M., 2011. Mixed carbonate-siliciclastic sediments and benthic foraminiferal assemblages from *Posidonia oceanica* seagrass meadows of the central Tyrrhenian continental shelf (Latium, Italy). *Italian Journal of Geosciences*, v. 130, p. 352-369.
- Gacia, E. and Duarte, C. M., 2001. Sediment retention by a Mediterranean *Posidonia oceanica* meadow: the balance between deposition and resuspension. *Estuarine, Coastal and Shelf Science*, v. 52, p. 505-514.

- Gain, I.E., Brewton, R.A., Robillard, M.M.R., Johnson, K.D., Smee, D.L. and Stunz, G.W., 2017. Macrofauna using intertidal oyster reef varies in relation to position within the estuarine habitat mosaic. *Marine Biology*, v. 164(1), p. 1-16.
- Gibbard, P. and Cohen, K.M., 2008. Global chronostratigraphical correlation table for the last 2.7 million years. *Episodes*, 31, 243-247.
- Gregor, H. J., 1991. Ein neues fossiles Seegras—*Posidocea frickhingeri* nov. gen. et spec. Im Paläogen Oberitaliens (Verona). *Doc. Nat.*, v. 65, p. 1–11.
- Gregor, H. J., 2003. Erstnachweis von Seegras-Resten (*Posidonia*) im Oberen Eozän der nördlichen Kalkalpen bei Hallthurm. *Doc. Nat.*, v. 148, p. 1–19.
- Hallock, P., Lidz, B. H., Cockey-Burkhard, E. M., and Donnelly, K. B., 2003. Foraminifera as bioindicators in coral reef assessment and monitoring: the FORAM Index: Environmental Monitoring and Assessment, v. 81, p. 221–238.
- Haven, D.S. and Whitcomb, J.P., 1983. The origin and extent of oyster reefs in the James River, Virginia. *Journal of Shellfish Research*, v. 3(2), p. 141.
- Hesemann, M., 2020. www.foraminifera.eu. 10.13140/RG.2.2.22727.11680/1.
- Hesse, M., Weber, M. and Halbritter, H.M., 1999. Pollen walls of Araceae, with special reference to their fossilization potential. *Grana* 38, 203–209.
- Hollaus, S.S. and Hottinger, L., 1997. Temperature dependance of endosymbiotic relationships? Evidence from the depth range of mediterranean *Amphistegina lessonii* (Foraminiferida) truncated by the thermocline. *Eclogae Geologicae Helvetiae*, v. 90(3), p. 591–598
- Hosius, A. and Von der Marck, W., 1880. Die Flora der Westfälischen Kreideformation. *Palaeontographica* 26, 125–236.
- Infantes, E., Terrados, J., Orfila, A., Canellas, B. and Alvarez-Ellacuria, A., 2009. Wave energy and the upper depth limit distribution of *Posidonia oceanica*. *Botanica Marina*, v. 52, p. 419-427.
- Ivany, L.C., Portell, R.W. and Jones, D.S., 1990. Animal–plant relationships and paleobiogeography of an Eocene seagrass community from Florida. *Palaio*, v. 5, p. 244–258.
- Kersting, D. K. and Linares, C., 2012. *Cladocora caespitosa* bioconstructions in the Columbretes Islands Marine Reserve (Spain, NW Mediterranean): distribution, size structure and growth. *Marine Ecology*, v. 33(4), p. 427-436.
- Kersting, D., Cebrian, E., Verdura, J. and Ballesteros, E., 2017. A new *Cladocora caespitosa* population with unique ecological traits. *Mediterranean Marine Science*, v. 18(1), p. 38-42
- Koriba, K. and Miki, S., 1931. On *Archeozostera* from the Izumi Sandstone. *Chikyū (The Globe)*, v. 15, p. 165–201 (in Japanese).
- Kregting, L. T., Hayden-Hughes, M., Millar, R. V., Joyce, P. W., and Smyth, D. M., 2020. A first record of intertidal *Ostrea edulis* 3D structural matrices in Strangford Lough Northern Ireland-An emergent reef?., *Journal of Sea Research*, v. 163, 101927.
- Kružić, P. and Benković, L., 2008. Bioconstructional features of the coral *Cladocora caespitosa* (Anthozoa, Scleractinia) in the Adriatic Sea (Croatia). *Marine Ecology*, v. 29(1), p. 125-139.
- Kružić, P. and Požar-Domac, A., 2003. Banks of the coral *Cladocora caespitosa* (Anthozoa, 666 Scleractinia) in the Adriatic Sea. *Coral reefs*, v. 22(4), p. 536-536.
- La Peyre, M., Furlong, J., Brown, L.A., Piazza, B.P. and Brown, K., 2014. Oyster reef restoration in the northern Gulf of Mexico: extent, methods and outcomes. *Ocean & Coastal Management*, v. 89, p. 20-28.
- Langer, M. R., 1993. Epiphytic foraminifera. *Marine Micropaleontology*, v. 20, p. 235–265.
- Langer, M. and Schmidt-Sinns, J., 2006. The 100 most common Foraminifera from the Bay of Fetovaia, Elba Island (Mediterranean Sea). *Monographie im Selbstverlag, Universität Bonn*, v. 1, p. 1-37.
- Langer, M.R., 2008a. Assessing the contribution of foraminiferan protists to global ocean carbonate production. *Journal of Eukaryotic Microbiology*, v. 55, p. 163–169, <https://doi.org/10.1111/j.15507408.2008.00321.x>
- Langer, M. R., Weinmann, A. E., Lötters, S., and Rödder, D., 2012. “Strangers” in paradise: modeling the biogeographic range expansion of the foraminifera *Amphistegina* in the Mediterranean Sea. *The Journal of Foraminiferal Research*, v. 42(3), p. 234-244.
- Laurent, L. and Laurent, J., 1926. Étude sur une plante fossile des dépôts du Tertiaire marin du sud de Célèbes. *Jaarb. Mijnwez. Ned. Oost-Indië*, v. 54, p. 169–190.
- Leonard-Pingel, J.S., 2005. Molluscan Taphonomy as a Proxy for Recognizing Fossil Seagrass Beds. M.S. Thesis. Louisiana State University, Baton Rouge.
- Luckenbach, M., Mann, R.L. and Wesson, J.A., 1999. Oyster Reef Habitat Restoration: a synopsis and synthesis of approaches; proceedings from the symposium, Williamsburg, Virginia, April 1995. Virginia Institute of Marine Science, College of William and Mary, Williamsburg, Virginia, U.S.A., v. 673, pp. 373.
- Lumbert, S.H., den Hartog, C., Phillips, R.C. and Olsen, F.S., 1984. The occurrence of fossil seagrasses in the Avon Park Formation (late Middle Eocene), Levy County, Florida (U.S.A.). *Aquat. Bot.*, v. 20, p. 121–129.

- Mačić, V., Dordević, N. and Petović, S., 2019. First monitoring of *Cladocora caespitosa* (Anthozoa, Scleractinia) in the Boka Kotorska Bay (Montenegro). *Studia Marina*, v. 32(1), p. 26-32.
- Marroni, M., Mazzanti, R. and Nencini, C., 1990. Nuovi elementi negli studi di scienze della terra nelle Colline Pisane. Quaderni del Museo di storia Naturale di Livorno, v. 11(Supplement 1), p. 1-40.
- Mateu, G., 1970. Estudio sistemático y bioecológico de los foraminíferos vivientes de los litorales de Cataluña y Baleares. *Trabajos del Instituto Español de Oceanografía*, v. 38, p. 1–84.
- Mateu-Vicens, G., Box, A., Deudero, S. and Rodriguez, B., 2010. Comparative analysis of epiphytic foraminifera in sediments colonized by seagrass *Posidonia oceanica* and invasive macroalgae *Caulerpa* spp. *Journal of Foraminiferal Research*, v. 40, p. 134–147.
- Mateu-Vicens, G., Brandano, M., Gaglianone, G. and Baldassarre, A., 2012. Seagrass-meadow sedimentary facies in a mixed siliciclastic-carbonate temperate system in the Tyrrhenian Sea (Pontinian Islands, western Mediterranean). *Journal of Sedimentary Research*, v. 82, p. 451–463.
- Mateu-Vicens, G., Khokhlova, A. and Sebastián-Pastor, T., 2014. Epiphytic foraminiferal indices as bioindicators in Mediterranean seagrass meadows. *The Journal of Foraminiferal Research*, v. 44, p. 325-339.
- Mazzanti R., 2016. Note illustrative della carta geologica d'Italia alla scala 1:50.000, Foglio 284, Rosignano Marittimo. Servizio Geologico d'Italia, ISPRA, Roma, pp. 189.
- Mazzella, L. and Russo, G. F., 1989. Grazing effect of two *Gibbula* species (Mollusca, Archaeogastropoda) on the epiphytic community of *Posidonia oceanica* leaves. *Aquatic Botany*, v. 35, p. 357-373.
- Milker, Y. and Schmiedl, G., 2012. A taxonomic guide to modern benthic shelf foraminifera of the western Mediterranean Sea. *Palaeontologia Electronica*, v. 15, p. 1-134.
- Moissette, P., Koskeridou, E., Corneé, J.J., Guillocheau, F. and Lécuyer, C., 2007. Spectacular preservation of seagrasses and seagrass-associated communities from the Pliocene of Rhodes, Greece. *Palaios* 22, 200–211.
- Moriarty, D. J. W., and Boon, P. I., 1989. Interactions of seagrass with sediment and water, in Larkum, A. W. D. and Sheppard, S. A. (eds.), *Biology of Seagrasses*. Elsevier, Amsterdam, p. 500–535.
- Murray, J. W., 2006. *Ecology and Applications of Benthic Foraminifera*. Cambridge University Press, Cambridge, 426 p.
- Oishi, S., 1931. Discovery of *Archeozostera* and *Sigillaria*-like impressions in Hokkaido. *J. Geog. Tokyo*, v. 43, p. 717-719 (in Japanese).
- Pardi, G., Piazzzi, L., Balata, D., Papi, I., Cinelli, F. and Benedetti-Cecchi, L., 2006. Spatial variability of *Posidonia oceanica* (L.) Delile epiphytes around the mainland and the islands of Sicily (Mediterranean Sea). *Marine Ecology*, v. 27, p. 397–403.
- Pérès, J. M. and Picard, J. 1964. Nouveau manuel de bionomie benthique. *Recueil des Travaux de la Station marine d'Endoume*, 31 (47), p. 5-137.
- Phillips, R.C. and Meñez, E.G., 1988. Seagrasses. *Smithson. Contrib. Mar. Sci.*, v. 34.
- Piazzzi, L., Acunto, S. and Cinelli, F., 2000. Mapping of *Posidonia oceanica* beds around Elba Island (western Mediterranean) with integration of direct and indirect methods. *Oceanologica acta*, v. 23(3), p. 339-346.
- Pomel, A., 1849. Matériaux pour servir à la flore fossile des terrains jurassiques de la France. *Amt Ber 25ste Versamm Deutsch Naturf Ärzte, Aachen* pp. 331–354.
- Puffer, E.L. and Emerson, W.K., 1953. The molluscan community of the oyster-reef biotope on the central Texas coast. *Journal of Paleontology*, v. 27, p. 537-544.
- Raffi, S. and Serpagli, E. 2003. *Introduzione alla Paleontologia*. Ed. UTET
- Rathburn, A. E. and Corliss, B. H., 1994. The ecology of living (stained) deep-sea benthic foraminifera from the Sulu Sea. *Paleoceanography*, v. 9, p. 87–150.
- Regione Toscana (2006-2009). Carta geologica regionale in scala 1:10.000. Available from: 738 <http://www502.regione.toscana.it/geoscopio/cartoteca.html>.
- Reich, S., 2014. Gastropod associations as a proxy for seagrass vegetation in a tropical, carbonate setting (San Salvador, Bahamas). *Palaios* 29, 467–482.
- Reich S., Di Martino E., Todd J.A., Wesselingh F.P. and Renema, W., 2015. Indirect paleo-seagrass indicators (IPSIs): a review. *Earth-Science Reviews*, 143, 161-186.
- Reuter, M., Piller, W.E., Harzhauser, M., Kroh, A., Roegl, F. and Coric, S., 2010. The Quilon Limestone, Kerala Basin, India: an archive for Miocene Indo-Pacific seagrass beds. *Lethaia*, v. 44, p. 76–86.
- Ribes, T., Salvadó, H., Romero, J. and Gracia, M. P., 2000. Foraminiferal colonization on artificial seagrass leaves. *Journal of Foraminiferal Research*, v. 30, p. 192–201.
- Sanchez-Vidal, A., Canals, M., de Haan, W.P., Romero, J. and Veny, M., 2021. Seagrasses provide a novel ecosystem service by trapping marine plastics. *Sci Rep* 11, 254. <https://doi.org/10.1038/s41598-020-79370-3>

- Sarti, G., Ciampalini, A., Consoloni, I. and Cerrina Feroni, A. 2007. I depositi del Pleistocene inferiore della bassa Val di Cecina (Toscana Italia): ricostruzione stratigrafico-deposizionale e proposta di suddivisione in unità allostratigrafiche. *Il Quaternario*, v. 20, p. 151-162.
- Sarti, G., Testa, G. and Zanchetta, G., 2008. A new stratigraphic insight of the Upper Pliocene-Lower Pleistocene succession of Lower Valdarno (Tuscany, Italy). *GeoActa*, v. 7, p. 27-41.
- Schröder, C. J., Scott, D. B. and Medioli, F. S., 1987. Can smaller foraminifera be ignored in paleoenvironmental analyses? *Journal of Foraminiferal Research*, 17: 101-5.
- Shannon, C. E. and Weaver, W., 1963. *The Mathematical Theory of Communication*. University of Illinois Press, Urbana, p. 144.
- Short, F. T., Carruthers, T. J. B., Dennison, W. C., and Waycott, M., 2007. Global seagrass distribution and diversity: a bioregional model. *Journal of Experimental Marine Biology and Ecology*, v. 350, p. 3-20.
- Stockmans, F., 1936. Végétaux éocènes des environs de Bruxelles. *Bull. Mus. R. Hist. Nat. Belg.*, p. 76, v. 1-56.
- Tani, F. and Gazzero, M. 1999. Nuove osservazioni sui depositi plio-pleistocenici nel bacino del Torrente Cascina. *Bollettino della Società Geologica Italiana*, v. 118(2), p. 237-241.
- Tomás, S., Frijia, G., Bömelburg, E., Zamagni, J., Perrin, C. and Mutti, M., 2016. Evidence for seagrass meadows and their response to paleoenvironmental changes in the early Eocene (Jafnayn Formation, Wadi Bani Khalid, N Oman). *Sed. Geol.*, v. 341, p. 189 - 202.
- Toscano, A.G., Lazo, D.G. and Luci, L., 2018. Taphonomy and paleoecology of lower cretaceous oyster mass occurrences from west-central Argentina and evolutionary paleoecology of gregariousness in oysters. *Palaios*, v. 33(6), p. 237-255.
- Vacchi, M., De Falco, G., Simeone, S., Montefalcone, M., Morri, C., Ferrari, M. and Bianchi C.N., 2017. Biogeomorphology of the Mediterranean *Posidonia oceanica* seagrass meadows. *Earth Surface Processes and Landforms*, v. 42(1), p. 42-54.
- Van der Ham, R.W.J.M., van Konijnenburg-van Cittert, J.H.A. and Indeherberge, L., 2007. Seagrass foliage from the Maastrichtian type areas (Maastrichtian, Danian, NE Belgium, SE Netherlands). *Rev. Palaeobot. Palynol.* 144, 301-321.
- Van der Ham, R.W.J.M., van Konijnenburg-van Cittert, J.H.A., Jagt, J.W.M., Indeherberge, L., Meuris, R., Deckers, M.J.M., Renkens, S. and Laffineur, J., 2017. Seagrass stems with attached roots from the type area of the Maastrichtian Stage (NE Belgium, SE Netherlands): Morphology, anatomy, and ecological aspects. *Review of Palaeobotany and Palynology*, v. 241, p. 49-69.
- Vélez-Juarbe, J. and Santos, H., 2008. Fossil Echinodermata from Puerto Rico. In: Ausich, W.I., Webster, G.D. (Eds.), *Echinoderm Paleobiology*. Indiana University Press, Bloomington, pp. 369-395.
- Vélez-Juarbe, J., 2014. Ghost of seagrasses past: using sirenians as a proxy for historical distribution of seagrasses. *Palaeogeogr. Palaeoclimatol. Palaeoecol.* 400, 41-49.
- Voigt, E., 1981. Upper Cretaceous bryozoan-seagrass association in the Maastrichtian of the Netherlands. In: Larwood, G.P., Nielsen, C. (Eds.), *Recent and Fossil Bryozoa*. Olsen & Olsen, Fredensborg, pp. 281-298.
- Voigt, E. and Domke, W., 1955. *Thalassocharis bosqueti* Debey ex Miquel, ein strukturell erhaltenes Seegrass aus der holländischen Kreide. *Mitt. Geol. Staatsinst. Hambg.* 24, 87-102.
- Wollenburg, J. E. and Mackensen, A., 1998a. On the vertical distribution of the living (rose Bengal stained) benthic foraminifers in the Arctic Ocean. *Journal of Foraminiferal Research*, v. 28, p. 268-85.
- Wollenburg, J. E. and Mackensen, A., 1998b. Living benthic foraminifers from the central Arctic Ocean: faunal composition, standing stock and diversity. *Marine Micropaleontology*, v. 34, p. 153-85.
- WoRMS Editorial Board, 2021. World Register of Marine Species. Available from <https://www.marinespecies.org> at VLIZ. Accessed 2021-07-09. doi:10.14284/170
- Wright, C.A. and Murray, J.W., 1972. Comparisons of modern and Palaeogene foraminiferid distributions and their environmental implications: Colloque sur la Géologie de la Manche, *Mémoires BRGM*, v. 79, p. 87-95.
- Yokes, M.B., Meric, E. and Avsar, N., 2007. On the presence of alien foraminifera *Amphistegina lobifera* Larsen on the coasts of the Maltese Islands. *Aquatic Invasions*, v. 2, p. 439-441, <https://doi.org/10.3391/ai.2007.2.4.15>
- Zalmout, I.S. and Gingerich, P.D., 2012. Late Eocene sea cows (mammalia, sirenia) from Wadi al Hitan in the western desert of Fayum, Egypt. *Papers on Paleontology*, v. 37. University of Michigan 156

6. Epiphytic foraminifera. Benthic foraminifera as proxy for fossil seagrass from the Lower Pleistocene deposits of the Stirone River (Emilia-Romagna, Italy)

This chapter is taken from the scientific paper:

Mariani, L., Coletti, G., Bosio, G., Tentorio, C., Mateu Vicens, G., Bracchi, V. A., Basso, D., and Malinverno, E. (2022b). Benthic foraminifera as proxy for fossil seagrass from the Lower Pleistocene deposits of the Stirone River (Emilia-Romagna, Italy), *Quaternary International*, v. 640, pp. 73-87, <https://doi.org/10.1016/j.quaint.2022.10.005>.

6.1 Abstract

This paper analyses and describes the benthic foraminiferal associations within the Pleistocene deposits of the Stirone River (Emilia-Romagna, Italy), with the purpose of testing foraminifera as Indirect Palaeo-Seagrass Indicators (IPSIs). Our analyses focused on two different biofacies: a *Thalassinoides* biofacies, characterised by an oligotypic biotic assemblage and a *Pinna* biofacies representing an infralittoral soft bottom colonised by marine phanerogams and characterized by high biodiversity. To strengthen the analyses, we have compared the Stirone foraminiferal association with the one of Fauglia (Tuscany, Italy), in which a well-preserved, early Pleistocene, fossil *Posidonia* meadow, is present. The aim of this work is to provide qualitative and quantitative parameters that can be used to recognize past vegetated environments, where fossil seagrass are no longer present. Considering the influence of ecological constraints and diagenetic processes on the foraminiferal assemblages, several indexes such as the $Index_{EP}$, the modified FORAM index (FI'), the “long vs. short life-span index” (I_{LS}), and the K/R_{EXT} (keeled/rounded morphotypes) have been calculated and a morphotype-based analysis has been provided. Among the tested indexes, the latter proved to be the most reliable IPSI, in association with the presence of morphotype A*, permanently attached, encrusting foraminifera and the abundance of Rosalinidae.

6.2 Introduction

The ecological significance and environmental importance of seagrass-related habitats is widely known. Seagrass meadows generally present a higher biodiversity than the surrounding unvegetated marine areas (e.g., Brasier, 1975; Hirst and Attrill, 2008; Barnes and Barnes, 2012). They provide indisputable ecosystem benefits and services (Sanchez-Vidal et al., 2021), including water quality improvement (de los Santos et al., 2020), carbon dioxide sequestration (Deyanova et al., 2017), stabilization of the seafloor, coastal protection and sediment production (Gacia et al., 2003; Ondiviela et al., 2014), and climate change mitigation (Duarte et al., 2013). With the term “seagrass meadows”, we identify large stretches of shelf environment (up to 100s m²) dominated by marine angiosperms (e.g., *Posidonia* spp., *Cymodocea* spp.) (Reich et al., 2015b). Patchy seagrass meadows are also

common. They are widespread worldwide in shallow coastal waters, at all latitudes, from Greenland to New Zealand (Cullen-Unsworth and Unsworth, 2013; Reich et al., 2015b). Nowadays the effects of climate change highlighted the importance of the relationship between environmental dynamics, such as sea-level fluctuations and temperature variations, and marine biodiversity. This is especially relevant in sensitive environments such as seagrass meadows (Alvarez et al., 2000; Mateu-Vicens et al., 2014; Unsworth et al., 2014; Arias-Ortiz et al., 2018). In this respect, the recognition of seagrass-related palaeoenvironments in the fossil record could help us in investigating habitat dynamics in response to environmental changes (Reich et al., 2015b). Although several studies of modern seagrass habitats and associated communities have been carried out (e.g., Heck et al., 1989; Langer, 1993; Boström and Bonsdorff, 1997; Barnes and Barnes, 2012; Mateu-Vicens et al., 2014; Benedetti and Frezza, 2016; Sanchez-Vidal et al., 2021), only few detailed studies on fossil seagrass meadows and related palaeocommunities exist (e.g., Brasier, 1975; Eva, 1980; Dominici, 2001; Domning, 2001; Vélez-Juarbe and Voigt, 2014; Baceta and Mateu-Vicens, 2021; Bosio et al., 2021; Pavia et al., 2022). The most significant reason for this numerical disparity is that seagrass roots, leaves and pollens decompose easily. Thus, even if finding well-preserved fossil seagrasses is not impossible, these occurrences are rare (e.g., Brasier, 1975; Ivany et al., 1990; Hesse et al., 1999; Moissette et al., 2007; Bosio et al., 2021). Furthermore, the recognition of patchy seagrass meadow environments in the fossil record is even more limited (Zuschin and Hohenegger, 1998; Kusworo et al., 2015). The most ancient examples of well-preserved fossil marine plants are reported from the Upper Cretaceous of the Netherlands (Debey, 1848, 1851; Pomel, 1849; Voigt and Domke, 1955; Voigt, 1981), Japan (Koriba & Miki, 1931; Oishi, 1931), Germany (Hosius and Von der Marck, 1880), and USA (Dilcher, 2016). Few other examples are reported from the Cenozoic (e.g., Ivany et al., 1990; Van der Ham et al., 2007; Van der Ham et al., 2017). The most recent fossil seagrasses are reported from the Pleistocene of 1) the Kritika Member of the Rhodes Formation in Greece (Moissette et al., 2007), 2) the Arda River outcrops of Emilia-Romagna (Italy; Brunetti and Vecchi, 2005; 2012), 3) the Fauglia sand quarry of Tuscany (Italy; Bosio et al., 2021) and 4) the Stirone River outcrops near Parma and Piacenza (Italy; Raffi and Serpagli, 2003), which is the study site described in this paper. Due to their scarce preservation potential, the recognition of paleo-seagrass meadows commonly relies on indirect evidence (Brasier, 1975; Eva, 1980; Langer, 1993; Domning, 2001; Beavington-Penney et al., 2004; Leonard-Pingel, 2005; Reuter et al., 2010; Vélez-Juarbe and Voigt, 2014; Reich, 2014; Reich et al., 2015b; Forsey, 2016; Mariani et al., 2022a). Generally, these proxies are either based on the presence and morphology of fossil organisms that are usually associated with seagrasses (Brasier, 1975; Eva, 1980; Reuter et al., 2010) or on taphonomic and sedimentological indicators considered as typical of seagrass-dominated environments. Reich et al. (2015b) defined all these indicators as IPSIs (Indirect

Palaeo-Seagrass Indicators) and critically reviewed them, exploring their usefulness in detecting fossil seagrass-related environments, where plant remains are no longer present. These IPSIs have been summarized in different categories, based on the different criteria used to infer the presence of a palaeo-seagrass meadow: i) taxonomic groups, including benthic foraminiferal assemblages (e.g., Betzler et al., 2000; Puga-Bernabéu et al., 2007; Mariani et al., 2022a), coralline red algae (e.g., Beavington-Penney et al., 2004), hydroids (e.g., Hughes et al., 1991), corals (e.g., Budd et al., 1996), bryozoans (e.g., Di Martino and Taylor, 2014), molluscs (bivalve taxa such as Pinnidae and chemosymbiotic species, gastropods; e.g., Pérès and Picard, 1964; Reich, 2014; Basso et al., 2015; Koskeridou et al., 2019; Bracchi et al., 2014, 2016, 2020; Pavia et al., 2022), ostracods (e. g., Forsey, 2016), echinoderms (Ivany et al., 1990), fish otoliths (Green, 2002), dugongid remains (e.g., Vélez-Juarbe and Voigt, 2014); ii) sedimentological features, such as grain size and sorting, since in modern seagrass meadows sediments are poorly sorted and display an abundant fine fraction (Fornos and Ahr, 1997), the presence of fining-upward sequences (Wanless, 1981), and the abundance of “constructive” micrite envelopes (Perry, 1999); iii) taphonomic features, including the taphonomic signature of skeletal remains (Leonard-Pingel, 2005; Reich et al., 2014), the presence of root casts (Cramer and Hawkins, 2009) and root etchings on shells (Parsons and Brett, 1991); iv) geochemical features, such as the carbon isotopic signal of mollusc shells (Reich et al., 2015a), and molecular seagrass biomarkers (e.g., De Leeuw et al., 1995). Regarding the IPSIs based on taxonomic groups, many of them are related to epiphytic carbonate producers, i.e., those organisms that present a mineralized skeleton and grow on a phytal substrate (Mazzella and Russo, 1989; Langer, 1993; De Falco et al., 2008; Mateu-Vicens et al., 2014; Brandano et al., 2016). The main carbonate-producing biota associated with seagrass meadows are foraminifera and calcareous algae, thus allowing to name “GA-Foralgal” or “RA-Foralgal” (depending on the abundance of green or red calcareous algae) the typical seagrass-related carbonate factories, also including other skeletal components such as molluscs and bryozoans (Brandano et al., 2019). Foraminiferal abundance within seagrass meadows has been widely studied by different authors (e.g., Den Hartog, 1979; Langer, 1993; Mateu-Vicens et al., 2014). Foraminifera have the advantage of being globally distributed and are usually abundant also in small samples (e.g., Murray, 2006). Furthermore, foraminifera have short reproductive cycles (Murray, 1991) making them useful to track environmental changes over short periods of time (Hallock et al., 2003; Pergent-Martini et al., 2005). Although foraminifera represent only a part of the trophic niches and guilds of an environment (Barras et al., 2014), their ecological diversification is large enough to obtain reliable reconstructions (e.g., Murray, 2006; Jorissen et al., 2007). Thus, benthic foraminifera present an extraordinary potential as (palaeo)ecological proxies (e.g., Murray, 2006; Benedetti and Frezza, 2016). According to Langer (1993) and Mateu-Vicens et al. (2014), the

analysis of epiphytic benthic foraminifera for palaeoecological purposes can be based on ecomorphological characteristics, overcoming problems related to the taxonomic identification at species level. Epiphytic foraminifera have been divided into five different groups based on: i) type of motility; ii) life span; iii) feeding mode; and iv) test morphology and structure. More recently, following the classification provided by Langer (1993), Mateu-Vicens et al. (2014) established five ecomorphological groups (morphotypes) to analyse epiphytic benthic foraminifera (Fig. 6.1): A*) long-lived (>10 months) sessile species, permanently attached to the substrate (e.g., *Planorbulina mediterraneensis*, *Nubecularia lucifuga*); SB) symbiont-bearing long-lived (>10 months) taxa (e.g., *Amphistegina*, *Peneroplis*, *Sorites*); B) short-lived (3–5 months), generally motile, taxa that temporarily attach their tests to the substrate using organic materials (e.g., *Ammonia*, Cibicididae, Rosalinidae); C) motile, short-lived, suspension-feeding foraminifera (e.g., keeled elphidiids, *Astrononion*, *Criboelphidium*); D*) short-lived (<4 months), permanently motile, grazing foraminifera, such as opportunistic species with porcelaneous or agglutinated test that live within rhizomes and sediment particles (e.g., small miliolids, textulariids). Based on this, several authors used foraminiferal associations as indirect indicators of palaeo-seagrass meadows in the geological record (e.g., Colom, 1942; Blanc-Vernet, 1969; Mateu, 1970; Brasier, 1975; Blanc-Vernet et al., 1979; Langer, 1993; Ribes et al., 2000; Beavington-Penney et al., 2004; Mateu-Vicens et al., 2010, 2012, 2014; Frezza et al., 2011; Tomassetti et al., 2016; Coletti et al., 2021; Baceta and Mateu-Vicens, 2021; Mariani et al., 2022a). This paper analyses the benthic foraminiferal associations of a Pleistocene succession exposed along the Stirone River, in the province of Parma (Northern Italy). As reported in literature, these deposits host rare but well-preserved seagrass rhizomes (Raffi and Serpagli, 2003) and common seagrass remains (Bracchi et al., 2020). Furthermore, the occurrence of several specimens of the bivalve *Pinna nobilis* in life position further supports the presence of a palaeo-seagrass meadow, or at least of a vegetated substrate (Bracchi et al., 2020). The aim of this paper is thus to describe quantitatively and qualitatively the foraminiferal assemblages of these deposits and to test them as valuable IPSI, with indices that can be applied in settings where seagrass remains are no longer preserved.








Morphotypes		Motility	Description	Life span
	A*	Encrusting	Mostly flat forms, permanently attached to the substrate e.g., <i>Planorbulina</i> , <i>Nubecularia</i>	1 year
	SB	Temporary motile	Symbiont-bearing taxa e.g., <i>Peneroplis</i> , <i>Sorites</i> , <i>Amphistegina</i>	1 year
	B	Temporary motile	Wide apertures faces e.g., Rosalinidae, Cibicididae	2-5 months
	C	Motile	Extrusion of pseudopodes from multiple apertural openings e.g., <i>Elphidium</i> , <i>Astrononion</i>	3-4 months
	D*	Permanently motile	Single aperture in upright position e.g., small miliolids, <i>Textularia</i>	short
for K/R analysis				
	R	Motile	Rounded periphery, planispiral or trochospiral, infaunal taxa e.g., <i>Haynesina</i> , <i>Porosononion</i>	3-4 months
	K	Motile	Keeled periphery, planispiral tests, related to ephypitic life-mode e.g., keeled <i>Elphidium</i>	3-4 months

Figure 6.1 Epiphytic benthic foraminifera morphotype categories, modified from Langer (1993) and Mateu-Vicens et al. (2014). Morphotype categories for the K/R analysis (Mariani et al., 2022a) are also present.

6.3 Geological setting

The studied outcrop is located along the Stirone River, near the village of San Nicomede, between the provinces of Piacenza and Parma (44°50'38.53" N, 9°59' 2.52" E) (Fig. 6.2). The Stirone River carves its way through a continuous upper Miocene (Messinian) to Pleistocene succession (Papani and Pelosio, 1962; Pelosio and Raffi, 1974; Mary et al., 1993; Channell et al., 1994; Pervesler et al., 2011; Gunderson et al., 2012). In the studied locality, easily accessible and well-exposed deposits crop out for about 100 m along the riverbanks. These deposits belong to the Castell'Arquato Basin (CAB), a small wedge-top basin developed since the upper Miocene (Messinian) above the Northern Apennines orogenic wedge (Roveri and Taviani, 2003; Pervesler et al., 2011; Ghielmi et al., 2013; Cau et al., 2015). After the Messinian salinity crisis, the newly restored marine conditions resulted in the deposition of deep marine sediments in the CAB (Ceregato et al., 2007; Calabrese and Di Dio, 2009). These deposits constitute the basal part of the succession. During the Pliocene and the Pleistocene, the depositional environment experienced a general regressive trend, from epibathyal to shelfal conditions (Gunderson et al., 2012; Coletti et al., 2018). Before the end of the early

Pleistocene, this shallowing upward trend culminated in the deposition of continental deposits (Cigala Fulgosi, 1976; Pelosio and Raffi, 1977; Ciangherotti et al., 1997; Esu, 2008; Esu and Girotti, 2015). Several authors interpreted the general late Cenozoic depositional environment of the Stirone River as a fluviodeltaic system within a tectonically active basin, dominated by fluvial floods and related hyperpycnal flows (Mutti et al., 1996; Martini et al., 2002), as it is typical for structurally confined basins characterised by phases of advancement and retreats of fan-delta systems (Einsele, 2000). The deposits analysed in this paper belong to two of the lithozones identified by Crippa et al. (2019) along the Stirone River succession (Figs. 6.2 and 6.3): i) the upper part of Lithozone 2, which consists of silty sands organized in metre-thick beds and heavily bioturbated sand-infilled and cemented *Thalassinoides* burrows, and ii) Lithozone 3, which consists of grey sandy to muddy sediments with Pinnidae specimens in life position (Dominici, 2001), corresponding to the *Pinna* biofacies described by Bracchi et al. (2020). More precisely, the section investigated in this paper corresponds to the 56–77 m interval of Crippa et al. (2019). This interval has been dated to the Calabrian (Early Pleistocene) (Crippa et al., 2019), based on nannofossils (zone CNPL7; Backman et al., 2012), foraminifera (*Globigerina cariacensis* zone; Cita et al., 2012 and references therein), and magnetostratigraphy (Gunderson et al., 2012; Monesi et al., 2016).

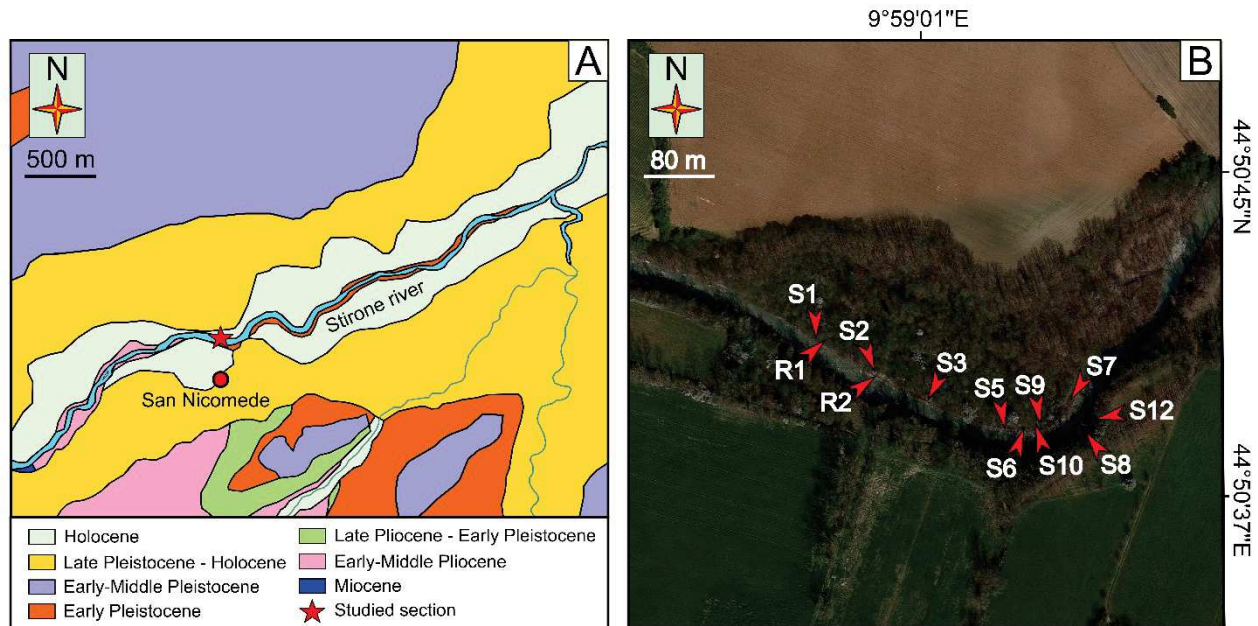


Figure 6.2 A. Simplified geological map of the analysed area. It is possible to appreciate the Stirone River section. Modified from Crippa et al. (2019). B. Satellite image of the analysed Stirone River section (Google Earth), with the location of the sampling sites.

6.4 Materials and methods

6.4.1 Field work

The Stirone deposits were investigated by describing lithology, macrofossils distribution, and sedimentary structures. A stratigraphic section was measured at centimetre-scale with a Jacob's staff, characterizing bed thickness, dip and dip-direction (Fig. 6.4). A total of 12 samples were collected at different stratigraphic heights along the two Lithozones (Figs. 6.2–6.4), together with the samples collected for the analysis of molluscs carried out by Bracchi et al. (2020). Samples R1 and R2 were collected within the upper section of Lithozone 2 in the sediments surrounding *Thalassinoides* ichnofossils. Samples S1, S2, S3, S5, S6, S7, S8, S9, S10 and S12 were collected in Lithozone 3 in correspondence of Pinnidae specimens in life position (S3, S5, S6, S9, S12), alongside Pinnidae specimens not in life position (S2) and randomly within the sediments of the Pinnidae biofacies (S1, S7, S8, S10). All samples were obtained by collecting at least 20 g of sediment, after slightly digging inside the deposits to remove the weathered material on the surface.

6.4.2 Sediments and foraminiferal analysis

6.4.2.1 Granulometry and foraminiferal assemblages

Grain-size analyses were performed on each sample with a Malvern Mastersizer 2000E™ Laser granulometer at the Università degli Studi di Milano-Bicocca. Grain-size distribution and sedimentological parameters were analysed through the software GRADISTAT Version 4.0 (Blott and Pye, 2001) (Table 6.1). For micropaleontological analyses, a small amount of each sample (Table 6.2) was weighted and treated with 30% hydrogen peroxide to remove organic matter (Dimiza et al., 2016). Each sample was then wet-sieved through a 125- μm -sized mesh, in order to separate the fraction for the picking of benthic foraminifera. We decided to identify benthic foraminifera in the $>125\ \mu\text{m}$ fraction to avoid counting juvenile forms, which are often abundant and difficult to identify (Malek et al., 2014). Before proceeding with the picking, the sieved fractions were oven-dried at 40°, weighted and divided into equal fractions using a microsplitter, to obtain sub-samples containing at least 300 specimens (Buzas, 1990; Murray, 1991; Murray, 2006; López-Belzunce et al., 2014). Handpicking was performed under a ZEISS Olympus SZ61 stereo microscope equipped with a high-resolution camera. We relied on Foraminiferi Padani (Agip S.p.A., 1982), Loeblich and Tappan (1988), Cimerman and Langer (1991), Langer and Schmidt-Sinns (2006), Milker and Schmiiedl (2012), the Foraminifera. eu-Project (Hesemann, 2020), and the World Register of Marine Species (WoRMS Editorial Board, 2021) for the taxonomic identification of foraminifera. SEM imaging of epiphytic foraminifera was performed using a FEG (SEM-FEG) Gemini 500 Zeiss scanning electron microscope at the Università degli Studi di Milano-Bicocca. For each sample, all foraminifera

identified, and relative counts are provided in the supplementary materials (Appendix 6.1; Mariani et al., 2022b), and the following parameters were calculated: i) the standardized abundance of benthic foraminifera (n/100 g of sediment), ii) the relative abundance (%) of each species, and iii) the ratio between broken and total number of tests. A Q-mode cluster analysis of species abundances across the samples, based on the Bray-Curtis similarity index, was performed with the software Primer v.6. No data transformation was applied.

6.4.2.2 Environmental indices

Epiphytic foraminiferal species were assigned to the different morphotypes (A* to D*) proposed by Langer (1993) and Mateu-Vicens et al. (2014). The abundance of each morphotype was calculated for each sample through the $Index_{EP}$ i.e., the ratio between the number of epiphytic and total benthic foraminifera (Mateu-Vicens et al., 2014). Two indices, created for the analysis of modern environments, were tested on the foraminiferal fossil assemblage: i) the modified FORAM Index (FI') developed by Mateu-Vicens et al. (2014) based on Hallock et al. (2003) FORAM Index. FI' is expressed as:

$$FI' = 10 \times (P_{A^*} + P_{SB}) \times P_{D^*} + 2 \times (P_B + P_C)$$

where P_{A^*} , P_{SB} , P_B , P_C , and P_{D^*} indicate the relative abundance of the foraminifera morphotypes. Values of $FI' > 4$ indicate optimal environmental conditions, whereas values of $FI' < 2$ are indicative of stressed conditions (Mateu-Vicens et al., 2014); ii) the “long vs. short life-span” index (I_{LS}) developed by Mateu-Vicens et al. (2014). I_{LS} , which consists of the ratio between longer-living and short-living forms, was built to highlight the differences between well-preserved and stressed *Posidonia oceanica* meadows (Mateu-Vicens et al., 2014) and is expressed as:

$$I_{LS} = (3.5 \times (P_{A^*} + P_{SB}) + 0.01) / (P_{D^*} + 0.01)$$

I_{LS} values range between 0 and 36. If D^* is the dominant morphotype, the index is close to 0; if the dominant morphotypes are A^* and SB, the index points towards 36. The K/R_{EXT} index from Mariani et al. (2022a) was also calculated in each sample. It consists of the ratio between keeled *Elphidium* and the sum of rounded elphidiids (e.g., *Criboelphidium*, *Porosonion*), and other related genera that display a rounded periphery (i.e., *Astrononion*, *Haynesina*, *Melonis*, *Nonion*, *Nonionella*, *Pullenia*, *Valvulineria*). Values of $K/R_{EXT} > 0.4$ point to the presence of vegetated substrate nearby. In this work, to facilitate the definition of this index, we introduce two new morphotypes, namely K and R, useful for the K/R analysis (Fig. 6.1). Morphotype K is constituted by epiphytic keeled *Elphidium*, whereas morphotype R includes the group of generally infaunal foraminifera that display a rounded periphery. This classification does not overlap with the epiphytic morphotypes from Langer (1993) and Mateu-Vicens et al. (2014). Thus, specimens belonging to morphotype C can be either

placed into morphotype K or R. Statistical analyses were performed with the software RStudio (RStudio Team, 2020). In particular, a bivariate statistical analysis was performed considering the relationship between K/R_{EXT} and morphotype A* abundance, taking into account all the samples from Stirone and the samples from the Fauglia site, described by Mariani et al. (2022a). The correlation between the two variables has been tested and a correlation coefficient was calculated. Only one sample from the latter site (P11) was excluded from the analysis, as an outlier.

Sample	Stratigraphic height (m)	Sample type	Sorting	Sediment name	Textural group	Gravel %	Sand %	Mud %
S12	16.00	Bimodal	Very poorly sorted	Very fine sandy very coarse silt	Sandy mud	0	34.1	65.9
S10	7.30	Unimodal	Poorly sorted	Very fine sandy very coarse silt	Sandy mud	0	31.5	68.5
S9	7.10	Bimodal	Very poorly sorted	Very fine sandy very coarse silt	Sandy mud	0	49.0	51.0
S8	12.50	Bimodal	Very poorly sorted	Very fine sandy very coarse silt	Sandy mud	0	28.9	71.1
S7	8.90	Bimodal	Very poorly sorted	Very fine sandy very coarse silt	Sandy mud	0	20.9	79.1
S6	8.20	Bimodal	Very poorly sorted	Very fine sandy very coarse silt	Sandy mud	0	25.2	74.8
S5	6.60	Unimodal	Very poorly sorted	Very fine sandy very coarse silt	Sandy mud	0	30.0	70.0
S3	5.80	Bimodal	Poorly sorted	Very fine sandy coarse silt	Sandy mud	0	10.6	89.4
S2	3.30	Trimodal	Very poorly sorted	Very fine sandy coarse silt	Sandy mud	0	20.2	79.8
S1	2.80	Bimodal	Very poorly sorted	Very fine sandy very coarse silt	Sandy mud	0	21.4	78.6
R2	1.30	Trimodal	Very poorly sorted	Fine sandy very coarse silt	Sandy mud	0	31.9	68.1
R1	0.80	Trimodal	Very poorly sorted	Very fine sandy coarse silt	Sandy mud	0	27.0	73.0

Table 6.1 Grain-size analysis of the collected sample. The analysis and the results were obtained with software GRADISTAT version 4.0 (Blott and Pye, 2001).

Sample	R1	R2	S1	S2	S3	S5	S6	S7	S8	S9	S10	S12
Total weight [g]	1.51	1.50	1.65	1.58	2.08	1.51	1.47	1.54	1.63	6.06	5.17	1.45
Tot. BF	248	259	1197	2480	688	1112	2800	3056	1464	5063	5840	4848
BF/100g	16439	17277	72537	156734	33026	73560	190606	198493	89629	83522	112922	333632
Index_{BR}	6.06	4.78	12.05	19.69	5.49	6.71	5.91	11.57	2.14	/	/	8.87
Index_{EP}	0.56	0.49	0.61	0.57	0.64	0.73	0.63	0.70	0.71	0.67	0.63	0.65
Index_{EP} average	0.53		0.65									
Index_{EP} - Ammonia	0.42	0.37	0.57	0.54	0.54	0.70	0.62	0.69	0.68	0.64	0.62	0.62
Index_{EP} - Ammonia average	0.39		0.62									
FI'	1.10	0.95	1.20	1.11	1.29	1.30	1.25	1.40	1.42	1.27	1.17	1.28
ILS	0.003	0.003	0.001	0.002	0.002	0.001	0.001	0.002	0.001	0.001	0.001	0.001
K/R_{EXT}	0.30	0.24	1.02	0.50	1.60	1.16	0.49	1.04	1.00	0.55	0.81	0.98
K/R_{EXT} average	0.27		0.91									

Table 6.2 Foraminifera data and parameters calculated from all the samples. Total weight: total weight of sediment before sieving; Tot. BF: Total number of benthic foraminifera counted and considered for the analysis for each sample, after the splitting; BF/100 g: standardized number of benthic foraminifera within 100 g of sediment; Index_{BR}: proportion of broken tests (BR) within a sample, BR/(Tot. BF + BR); Index_{EP}: number of epiphytic specimens/total foraminifera; Index_{EP}-*Ammonia*: Index_{EP} without considering *Ammonia* (and related genera such as *Aubignyna* and *Buccella*) as epiphytic specimens; FI': modified foraminifera index (Mateu-Vicens et al., 2014); ILS: long vs. short life-span index (Mateu-Vicens et al., 2014); K/R_{EXT}: ratio between morphotype K (keeled *Elphidium*) and morphotype R foraminifera (e.g., rounded elphidiids, *Astronion*, *Haynesina*, *Nontion*, *Pullenia*, *Valvulineria*) (Mariani et al., 2022a).

Group	R1	R2	S1	S2	S3	S5	S6	S7	S8	S9	S10	S12	R _{average}	S _{average}
<i>Ammonia</i> group	8.87	8.49	3.68	2.58	7.27	2.34	1.14	0.79	1.64	2.53	0.82	2.31	8.68	2.51
<i>Bolivina</i> group	8.87	8.49	7.44	3.87	6.98	3.60	7.43	4.45	1.09	3.79	6.85	4.95	8.68	5.05
<i>Bulimina</i> group	2.42	2.32	1.50	3.87	5.81	1.26	1.43	1.57	1.09	1.58	0.82	2.48	2.37	2.14
Cassidulinidae	7.26	8.49	8.19	7.10	12.79	6.47	7.71	4.19	7.10	8.53	13.70	8.09	7.88	8.39
Cibicididae	24.19	14.67	10.86	15.48	16.28	17.81	16.00	24.61	14.21	19.28	15.07	19.80	19.43	16.95
<i>Elphidium</i> group (keeled)	6.45	5.41	8.86	6.45	9.30	7.73	5.14	7.59	8.74	6.64	6.85	6.44	5.93	7.38
Rosalinidae	5.65	10.81	16.54	13.55	13.95	17.99	17.43	24.87	19.13	20.54	22.19	20.13	8.23	18.64
Rounded periphery group	21.77	22.39	8.69	12.90	5.81	6.65	10.57	7.33	8.74	12.01	8.49	6.60	22.08	8.78
Uvigerinidae	0.81	3.09	3.51	2.58	1.16	3.42	4.86	4.97	3.83	1.58	3.84	4.29	1.95	3.41
Miliolids	1.61	0.00	10.86	1.94	1.16	16.04	10.03	1.57	14.75	13.27	13.15	7.76	0.81	9.05
Agglutinated	1.61	3.47	3.34	5.81	6.98	4.14	4.58	3.40	2.73	0.14	1.92	3.96	2.54	3.70
Common taxa (>5%)														
<i>Ammonia beccarii</i>	5.65	6.95	2.01	1.94	6.10	1.08	0.86	0.79	1.64	0.95	0.00	1.65	6.30	1.70
<i>Bolivina spathulata</i>	6.45	5.41	2.17	1.94	4.65	1.08	1.43	1.83	1.09	1.26	3.01	1.65	5.93	2.01
<i>Cassidulina carinata</i>	5.65	6.95	7.85	4.52	6.98	5.77	6.88	3.93	7.10	7.58	12.05	7.26	6.30	6.99
<i>Cibicides refulgens</i>	14.52	6.18	5.85	8.39	8.14	11.53	10.03	15.97	9.29	14.85	11.51	10.89	10.35	10.64
<i>Cibicoides pachyderma</i>	7.26	3.86	2.51	5.81	5.81	3.24	2.29	3.66	1.64	1.58	1.10	2.15	5.56	2.98
<i>Neoconorbina terquemi</i>	4.03	7.72	11.19	9.68	10.47	10.27	7.45	14.92	8.74	13.27	18.36	12.54	5.88	11.69
<i>Elphidium translucens</i>	10.48	6.95	1.17	1.29	0.00	1.44	2.01	2.36	1.09	2.21	1.10	2.31	8.72	1.50

Table 6.3 Relative percentage frequency of the analysed foraminiferal groups and of the common taxa (i.e., those with an abundance higher than 5%).

6.5 Results

6.5.1 Field observations and stratigraphic section

The measured stratigraphic section consists of a 20-m-thick mixed carbonate-siliciclastic succession (Fig. 6.4). The base of the succession consists of 2 m of slightly NE dipping (with an average attitude of 042/18), fine sandy to coarse silty deposits. These deposits, which belong to Lithozone 2 of Crippa et al. (2019), can be divided into a 1.5-m-thick poorly consolidated layer, followed upward by a 0.5-m-thick cemented layer. The different cementation of the two layers is deeply enhanced by erosion (Fig. 6.4). Both layers are intensely bioturbated by *Thalassinoides*. Within this lithozone, macrofossils are scarce and consist solely of shells of the mollusc *Aequipecten opercularis*. In the present work, we will refer to these deposits as the *Thalassinoides* biofacies. Upwards, the stratigraphic section continues with a 19-m-thick, slightly N to NNE dipping (with an average attitude of 005/20), massive to laminated, very fine sandy to coarse silty deposits. These layers, which belong to the Lithozone 3 of Crippa et al. (2019), are mostly characterized by poorly cemented sediments, except for a 1-m-thick interval located at about 7.5 m from the base of this facies (approximately 9.5 m from the base of the entire section), which consists of two well cemented layers separated by a very thin and poorly cemented interval. The different cementation of the strata is once again enhanced by the erosion. Within Lithozone 3 macrofossils are common, easily recognizable, and mainly consist of molluscs (Dominici, 2001; Bracchi et al., 2020), solitary scleractinians, bryozoans, echinoids and fragments of red calcareous algae. *Pinna nobilis* specimens in life position were recorded (Figs. 6.3 and 6.4; *Pinna* biofacies). The measured section ends with a well-cemented biocalcarenite layer.

6.5.2 Foraminiferal analysis and skeletal assemblage

The associate sediments display noticeable differences between the samples from the two facies. In the *Thalassinoides* biofacies, the bioclastic fraction is scarce, mainly constituted by planktic foraminifera, while terrigenous grains (e.g., quartz) dominate the deposit. In the *Pinna* biofacies the bioclastic fraction (mainly consisting of benthic foraminifera, molluscs, ostracods and echinoderms associated with rare erect bryozoans' fragments and planktic foraminifera) is more relevant. Plant remains are also common in this biofacies. In the analysed samples, we identified i) 83 species of hyaline benthic foraminifera, ii) 4 genera of agglutinated foraminifera and iii) 7 genera of miliolids (Figs. 6.5 and 6.6). Hyaline benthic foraminifera were identified at species level and selected species were clustered in different groups to perform statistical analyses (Tables 6.3 and 6.4).

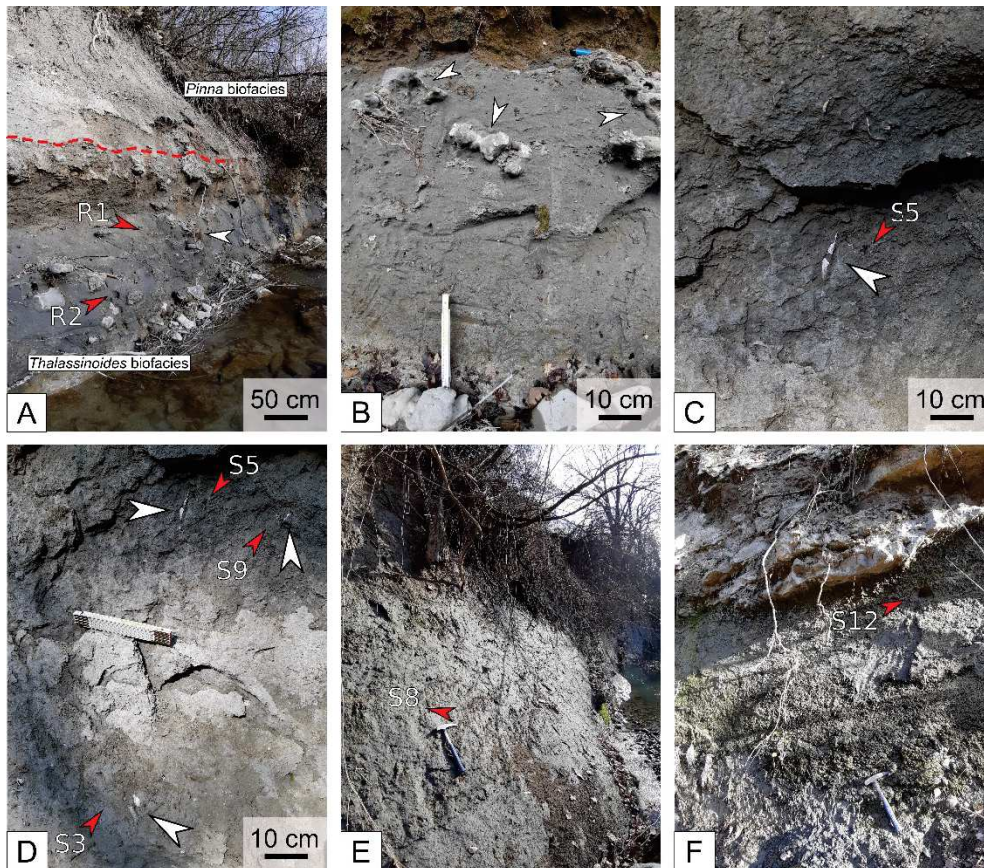


Figure 6.3 Field views and photos of the lower Pleistocene deposits cropping out at the Stirone River section, with location of some collected samples. A. Overview of the two analysed biofacies. The white arrow indicates a *Thalassinoides* burrow specimen. B. *Thalassinoides* biofacies. The white arrows indicate *Thalassinoides* specimens. C. *Pinna* biofacies. The arrow indicates a *Pinna nobilis* specimens in life position. D. *Pinna nobilis* specimens within the *Pinna* biofacies. E. *Pinna* biofacies outcropping on the southern side of the Stirone River. F. Stratigraphic contact between the upper level of the *Pinna* biofacies and the overlying biocalcarenes.

Agglutinated foraminifera (*Bannerella gibbosa*, *Sahulia* spp., *Spiroplectinella* spp., *Textularia* spp.) were counted as a single group. Miliolids (*Adelosina* spp., *Cycloforina* spp., *Miliolinella* spp., *Quinqueloculina* spp., *Siphonaperta* spp., *Spiroloculina* spp., *Triloculina* spp.) were also clustered as a single group. All other species identified are reported in the supplementary material (Appendix 6.1). The standardised abundance of benthic foraminifera presents the lowest values within the *Thalassinoides* biofacies (samples R1 and R2) with an average value of 16.858 specimens/100 g of sediment, whereas in the *Pinna* biofacies the values are one order of magnitude higher, with an average value of 134.466 specimens per 100 g of sediment. The abundance of broken tests shows no significant difference among the samples. The average abundances of the species (Table 6.3) in the *Thalassinoides* and *Pinna* biofacies were used to calculate the similarity matrix and to plot the corresponding dendrogram (Fig. 6.7). Two main sample groups are separated at 55% similarity. The first group corresponds to the *Thalassinoides* biofacies, and includes *A. beccarii*, *A. parkinsoniana*, *B. spathulata*, *Buccella* aff. *frigida*, *C. carinata*, *C. refulgens*, *C. pachyderma*, *E. translucens*, *G. subglobosa*, *N. boueanum* and *N. terquemi* as the most common taxa. The second group of samples

corresponds to the *Pinna* biofacies, and is characterized by the presence of *Planorbulina mediterranensis*, *C. carinata*, *C. refulgens*, *N. terquemi* (with a much higher abundance than in the *Thalassinoides* facies), and miliolids (except for samples S2, S3 and S7). Further subdivisions (Fig. 6.7) are based on the abundance of certain species in particular samples. For instance, S5, S6 and S8 contain frequent *Asterigerinata mamilla*; S1 and S12 are characterized by *L. lobatula*; S2 and S3 form a group with locally frequent *A. beccarii* and *B. spathulata*, *B. elongata*, *C. pachyderma*, *G. subglobosa*, *N. boueanum*, and scarce small miliolids. Within the *Thalassinoides* biofacies, the ammoniid group and the Boliviniidae are present with higher abundances (8.7%). Buliminidae display low values in both *Thalassinoides* and *Pinna* biofacies, whereas Cassidulinidae are abundant in both the biofacies (around 8%). Cibicididae constitute nearly 20% of the assemblage in both biofacies and are slightly more abundant within the *Thalassinoides* biofacies. Within Cibicididae, *L. lobatula* is slightly more abundant in the *Pinna* biofacies. The group of keeled *Elphidium* (morphotype K) is abundant in both facies, presenting a slightly higher value in the *Pinna* biofacies (7.4%) compared to the *Thalassinoides* biofacies (5.9%). Rosalinidae are much more abundant in the *Pinna* biofacies (18.6%). The rounded periphery group (morphotype R) is highly common within the *Thalassinoides* biofacies (22.1%). Uvigerinidae are rare in both levels. Agglutinated foraminifera are mostly not abundant but are slightly more common in the *Pinna* (3.7%) than in the *Thalassinoides* biofacies (2.5%). Miliolids are abundant in the *Pinna* biofacies (9.1%) and scarce in the *Thalassinoides* biofacies (0.8%). Epiphytic foraminifera were assigned to different morphotypes of Mateu-Vicens et al. (2010, 2014) (Table 6.4). Morphotype A* only contains *P. mediterranensis* and consequently its abundance is equal to the abundance of this species, which is absent in the *Thalassinoides* biofacies and present in every sample of the *Pinna* biofacies (but its abundance is low: 1.1%). No specimens belonging to morphotype SB have been observed. Morphotype B (*Ammonia* group, *A. mamilla*, *Aubignyna perlucida*, *B. aff. frigida*, Cibicididae, *Discorbinella bertheloti*, *Eponides repandus*, *Hanzawaia boueana*, Rosalinidae) are equally common in both biofacies, with values around 44%. Morphotype C (*A. stelligerum*, *Criboelphidium* sp., keeled *Elphidium* group) is slightly more abundant in the *Pinna* biofacies (7.7%) compared to the *Thalassinoides* biofacies (5.9%). Morphotype D* (agglutinated foraminifera and miliolids) is much more abundant in the *Pinna* biofacies (12.8%), and rather scarce in the *Thalassinoides* one (3.4%).

Morphotype	
A*	<i>Planorbulina mediterraneensis</i>
B	<i>Ammonia beccarii</i> ; <i>Ammonia parkinsoniana</i> ; <i>Ammonia tepida</i> ; <i>Asterigerinata mamilla</i> ; <i>Aubignyna perlucida</i> ; <i>Buccella</i> aff. <i>frigida</i> ; <i>Cibicides refulgens</i> ; <i>Cibicides</i> sp.; <i>Cibicoides pseudoungerianus</i> ; <i>Cibicoides pachyderma</i> ; <i>Discorbinella bertheloti</i> ; <i>Eponides repandus</i> ; <i>Gavelinopsis praegeri</i> ; <i>Hanzawaia boueana</i> ; <i>Lobatula lobatula</i> ; <i>Neoconorbina terquemi</i> ; <i>Neoconorbina</i> sp.; <i>Rosalina bradyi</i> ; <i>Rosalina globularis</i> ; <i>Rosalina</i> sp.; <i>Rosalina williamsoni</i> ; <i>Planulina ariminensis</i> ; <i>Planulina</i> sp.;
C	<i>Astrononion stelligerum</i> ; <i>Criboelphidium</i> sp.; <i>Elphidium aculeatum</i> ; <i>Elphidium advenum</i> ; <i>Elphidium crispum</i> ; <i>Elphidium fichtelianum</i> ; <i>Elphidium macellum</i> ; <i>Elphidium</i> sp.; <i>Elphidium</i> sp.1; <i>Elphidium</i> spp.(keeled);
D*	Agglutinated; Miliolids
K	Keeled <i>Elphidium</i>
R	Rounded elphidiids (<i>Criboelphidium</i> , <i>Elphidium translucens</i> , <i>Porosononion</i>), <i>Astrononion</i> , <i>Haynesina</i> , <i>Nonion</i> , <i>Pullenia</i> , <i>Valvulineria</i>
Group	
<i>Ammonia</i> group	<i>A. beccarii</i> ; <i>A. parkinsoniana</i> ; <i>A. tepida</i>
<i>Bolivina</i> group	<i>B. alata</i> ; <i>B. dilatata</i> ; <i>B. earlandi</i> ; <i>B. pseudoplicata</i> ; <i>B. spathulata</i> ; <i>B. striatula</i> ; <i>B. subspinescens</i> ; <i>B. sp.</i>
<i>Bulimina</i> group	<i>B. aculeata</i> ; <i>B. elongata</i> ; <i>B. marginata</i> ; <i>B. striata</i>
Cassidulinidae	<i>Cassidulina carinata</i> ; <i>Globocassidulina subglobosa</i>
Cibicididae	<i>Cibicides refulgens</i> ; <i>Cibicides</i> sp.; <i>Cibicoides pseudoungerianus</i> ; <i>Cibicoides pachyderma</i> ; <i>Lobatula lobatula</i>
Rosalinidae	<i>Gavelinopsis praegeri</i> ; <i>Neoconorbina terquemi</i> ; <i>Rosalina bradyi</i> ; <i>Rosalina globularis</i> ; <i>Rosalina</i> sp.; <i>Rosalina williamsoni</i> ; <i>Neoconorbina</i> sp.
Uvigerinidae	<i>Trifarina angulosa</i> ; <i>Uvigerina mediterranea</i> ; <i>Uvigerina peregrina</i> ; <i>Uvigerina</i> sp.

Table 6.4 Morphotype classification and foraminifera groups used in this study. Species were assigned to a specific morphotype as in literature (Langer, 1993; Mateu-Vicens et al., 2010, 2014; Mariani et al., 2022a).

Index_{EP} is higher for the *Pinna* biofacies, with an average value of 0.66, compared to the 0.53 of the *Thalassinoides* biofacies. FI' display the lowest values in sample R1 and R2 (*Thalassinoides* biofacies), with an average of 1.02, whereas the average value for the *Pinna* biofacies is slightly higher (1.27). I_{LS} index shows very low values in all samples, without clear trends. K/R_{EXT} presents higher values in the samples from the *Pinna* biofacies (average of 0.91), and distinctly lower values in the *Thalassinoides* biofacies (average of 0.27). The bivariate statistical model, considering the relationship between K/R_{EXT} and morphotype A* abundance, display a mild-strength linear correlation. Pearson and Spearman correlation coefficients are 0.54 and 0.53, respectively. R² display a statistically significant value of 0.29.

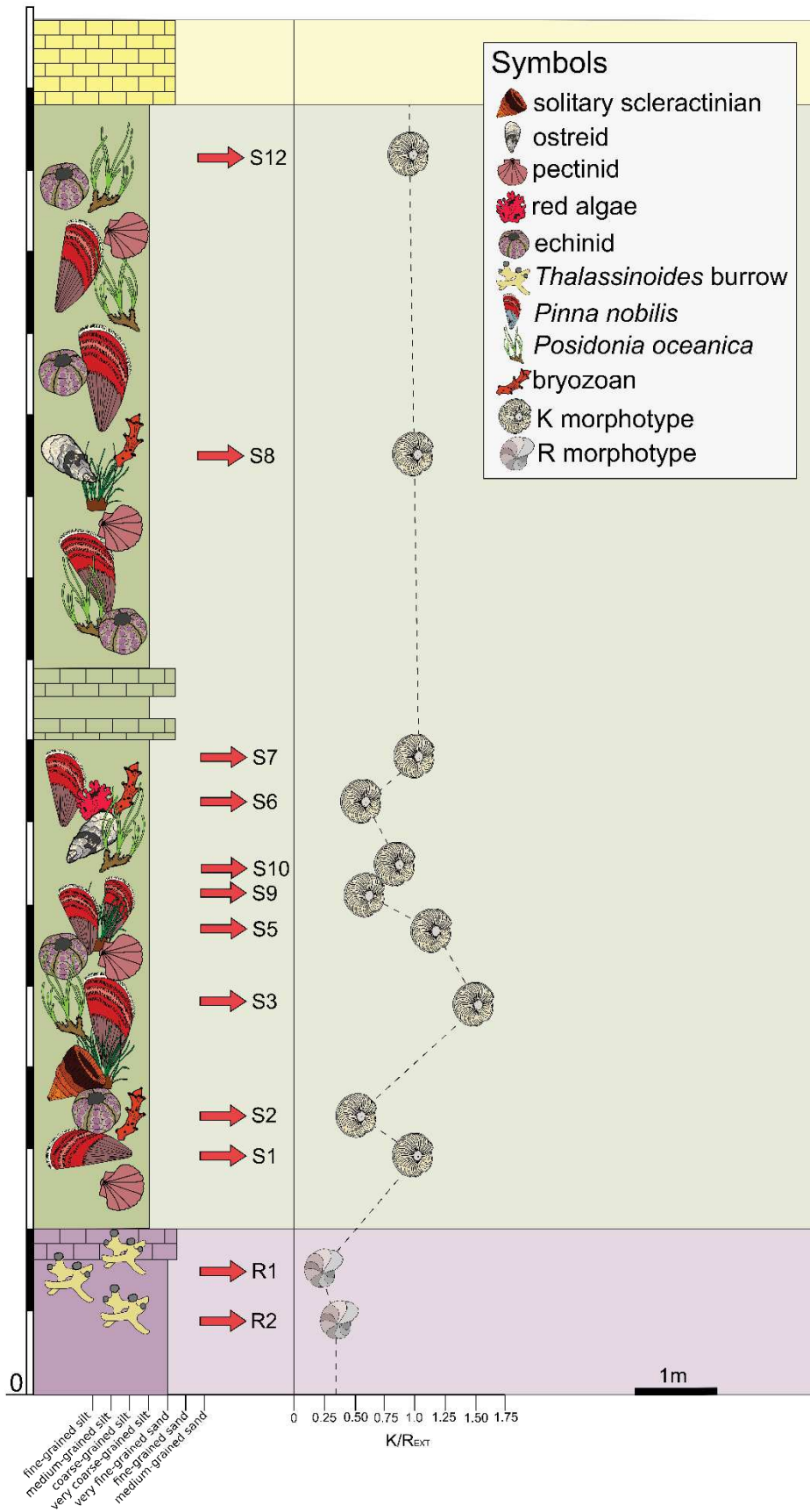


Figure 6.4 Stratigraphic log of the analysed section of the Stirone River. Is it possible to appreciate the contact between the *Thalassinoides* biofacies (in purple), the *Pinna* biofacies (in green) and the upper biocalcarenes (in yellow). The curve of the K/R_{EXT} values is also reported, showing the differences between the two biofacies. (For interpretation of the references to colour in this figure legend, the reader is referred to the Web version of this article).

6.6 Discussion

6.6.1 Foraminiferal assemblages in a seagrass-related environment

The preservation of seagrass remains within the fossil record is extremely rare and mainly related to processes such as silicification or rapid burial by fine-grained sediments (e.g., Ivany et al., 1990; Moissette et al., 2007; Van der Ham et al., 2007; Reich et al., 2015; Dilcher, 2016; Van der Ham et al., 2017; Bosio et al., 2021). On the other hand, seagrass related carbonate producing-organisms have a much higher fossilization potential. In the Stirone area, the presence of a palaeo-meadow is indicated by both direct (seagrass rhizomes reported by Raffi and Serpagli, 2003) and indirect observations (*Pinna nobilis* in life position reported by Bracchi et al., 2020). *P. nobilis* is a large endemic bivalve of the Mediterranean, occurring between 0 and 60 m of water depth and commonly associated with *Posidonia oceanica* and *Cymodocea nodosa* meadows (Pérès and Picard, 1964; Gómez-Alba, 1988; Lemer et al., 2014; Basso et al., 2015). Although due to its fragile shell this mollusc displays a relatively low preservation potential compared to other bivalves (Beesley et al., 1998), its occurrence in life position has been used as an IPSI (Reuter and Piller, 2011; Reuter et al., 2012; Reich et al., 2015b; Tomassetti et al., 2022). The *Pinna* biofacies of the Stirone River displays many *P. nobilis* specimens in life position and includes large amounts of tiny plant frustules. Based on these features and the molluscan assemblage of the facies, Bracchi et al. (2020) suggest the presence of a vegetated substrate, possibly *Cymodocea* meadow (although the occurrence of a patchy meadow with both plants cannot be excluded). Overall, the palaeoenvironmental reconstruction of the *Pinna* biofacies of the Stirone River suggests a shallow (less than 15 m) infralittoral seafloor, colonised by marine phanerogams, and characterised by periods of high terrigenous influx (Bracchi et al., 2020). Sedimentological evidence, especially grain size, suggest that the *Thalassinoides* biofacies also represents an infralittoral environment, even if bioturbation has obliterated most sedimentary structures (Crippa et al., 2019). *Thalassinoides* is a system of horizontal, unlined, cylindrical burrows possibly joined by vertical or oblique shafts (Pervesler et al., 2011), generally produced by crustaceans in shallow water settings (Curran et al., 1977; Belt et al., 1983; Ekdale et al., 1984; Frey et al., 1984; Kamola, 1984; Miller and Knox, 1985; Myrow, 1995; Pervesler and Uchman, 2009; De Araújo et al., 2021). Although not limited to shallow water settings (e.g., Crimes, 1977; Curran et al., 1977; Link and Bottjer, 1982; Ekdale and Bromley, 1984), *Thalassinoides* burrows are commonly reported in intertidal-subtidal deposits characterised by fine-grained sediments like those of the Stirone River (Table 6.1; Fig. 6.3), thus supporting the shallow-water interpretation of this biofacies. The benthic foraminiferal associations of the two studied facies is consistent with the interpretation based on molluscs (Bracchi et al., 2020) and ichnofacies (Pervesler et al., 2011), thus confirming that the analysed Stirone section displays a slightly deepening-upward

sequence (Crippa et al., 2019). High abundances of the foraminifera of the *Ammonia* group and associated taxa (e.g., *Buccella*) support this interpretation for the *Thalassinoides* biofacies, while the higher biodiversity associated to *Pinna* biofacies is consistent with a seagrass-related environment. Q-mode cluster analysis (Fig. 6.7) allows to recognize two groups corresponding to the two biofacies (*Thalassinoides* and *Pinna*) and to the lithozones described by Crippa et al. (2019). *Thalassinoides* biofacies is dominated by foraminiferal taxa grouped in low-oxygen foraminiferal assemblages (LOFA; Bernhard and Sen Gupta, 1999), which is consistent with high riverine terrigenous and nutrient input. The assemblage of the *Pinna* biofacies is instead representative of a seagrass environment, based on the presence of *P. mediterraneensis* and the abundance of small epiphytic foraminifera (*Planorbulinitum mediterraneensis* sensu Colom, 1942). Moreover, several sub-biofacies can be distinguished based on differences in the foraminiferal assemblages, mostly referring to the small miliolids and LOFA taxa. In particular, very abundant LOFA and scarce miliolids (samples S2 and S3) might indicate punctual episodes of high riverine influence or, alternatively, they may represent transitional settings between the terrigenous-dominated and the well-developed seagrass environments. $INDEX_{EP}$ displays higher average values within the *Pinna* biofacies as compared to the *Thalassinoides* biofacies (average value of 0.66 for the former and 0.53 for the latter; Table 6.2). This means that almost 70% of the species within the *Pinna* biofacies might have lived on a phytal substrate, compared to the 50% of potential epiphytes of the *Thalassinoides* facies. If *Ammonia* spp. (and related genera such as *Aubignyna* and *Buccella*) are excluded from the epiphytic association, since they are not exclusive of seagrass meadows, the difference is enhanced (0.39 of the *Thalassinoides* biofacies vs. 0.62 of the *Pinna* biofacies). Although *Ammonia* is often reported to be present within vegetated seafloors, especially in those characterised by a high content of organic matter (Frezza et al., 2011; Mateu-Vicens et al., 2014), this genus can populate a wide range of coastal, shallow-water environments (Murray, 2006). Nonetheless, here we have considered *Ammonia* group as part of the epiphytic taxa, following different authors (e.g., Mateu-Vicens et al., 2014; Mariani et al., 2022a), in order to facilitate comparisons with other sites. In modern environments, epiphytic photosymbiotic foraminifera (morphotype SB, e.g., *Amphistegina*, *Peneroplis*, *Sorites*) are indicative of shallow, well-illuminated environments and are usually, but not always, associated to flat, long-lasting, vegetated substrates (Langer, 1993; Murray, 2006; Mateu-Vicens et al., 2014; Reich et al., 2015). *Peneroplis* can be found on seagrass rhizomes and leaves (Hohenegger, 1994; Renema, 2006), but also on algal and sandy substrates (Hohenegger, 1994). Similarly, *Amphistegina* can be very abundant within seagrass meadows (Riordan et al., 2012), but its distribution is not exclusively related to the presence of a vegetated substrate. Both peneroplids and soritids are limited by the 14 °C (or even colder) isotherm (Langer and Hottinger, 2000; Beavington-Penney and Racey, 2004; Murray,

2006), while *Amphistegina* is limited by the 14 °C winter isotherm (Langer et al., 2012; El Kateb et al., 2018). Therefore, although the presence of morphotype SB foraminifera in the fossil record may be indicative for vegetated habitats (e.g., *Orbitolites* in the Eocene; Beavington-Penney et al., 2006; Tomassetti et al., 2016; Coletti et al., 2021), their absence is not necessarily evidence for the lack of phytal substrates. For the Stirone *Pinna* biofacies, the lack of this group is definitively more likely related to the cold climate of the early Pleistocene (Prista et al., 2015). Morphotype A*, represented here by *P. mediterranensis* only, is one of the most reliable IPSIs (Mariani et al., 2022a) and a useful indicator to distinguish between palaeo-seagrass meadows and other phytal substrates (e.g., macroalgae; Mateu-Vicens et al., 2010). Indeed, *P. mediterranensis* is present in every samples from the *Pinna* biofacies, whereas in the *Thalassinoides* biofaces it is absent (Tables 6.3 and 6.5; Fig. 6.8). Morphotype B* dominates in both biofacies, constituting about 45% of the entire epiphytic assemblage (Fig. 6.8; Table 6.5). According to Murray (2006) and Benedetti and Frezza (2016), morphotype B* usually constitutes 25–85% of vegetated seafloor assemblages (both seagrass and algae), suggesting its dependence on the presence of a vegetated substrate. However, its large frequency within the *Thalassinoides* biofacies indicates that its abundance cannot be solely related to the presence of seagrasses. Some species that belong to morphotype B are not directly related to a phytal substrate but can colonize a large variety of environments (e.g., *Ammonia*, *Buccella*), whereas other species, such as *Lobatula lobatula*, are generally more linked to marine vegetation (Jorissen et al., 1995), even if nowadays it is commonly found in almost vegetation-free environments in colder climates (e.g., Hald and Korsun, 1997). Also, Rosalinidae (e.g., *Rosalina* spp., *Neoconorbina terquemi*) and Asterigerinidae (*Asterigerinata mamilla*), are generally linked to vegetated sea-bottoms (Langer, 1988; Panieri et al., 2005; Frezza and Carboni, 2009). In our case, both Rosalinidae and *A. mamilla* are much more abundant within the *Pinna* biofacies (Tables 6.3 and 6.5). Morphotype C is slightly more abundant in the *Pinna* biofacies, but it also includes motile suspension feeders that are not strictly epiphytic taxa (Fig. 6.8; Tables 6.4 and 6.5). Murray (1991) suggested that elphidiids can range from epifaunal to infaunal, with elphidiids with an acute periphery, such as *Elphidium crispum* or *Elphidium aculeatum*, generally linked to phytal substrates (e.g., Langer, 1993; Mateu-Vicens et al., 2014), as this test shape seems to facilitate their motility on algae and plants. On the other hand, elphidiids with rounded periphery and other genera such as *Astrononion* or *Criboelphidium* are not solely epiphytes but can conduct an infaunal mode of life. Morphotype D* is constituted by stress-tolerant taxa with a short life-span, such as small miliolids and agglutinated foraminifera (Langer, 1993). These species could be adapted to nutrient-rich environments, such as seagrass rhizomes (Mateu-Vicens et al., 2014). In the Stirone River, samples from the *Pinna* biofacies display a larger abundance of morphotype D* specimens, especially miliolids (Fig. 6.8; Table 6.5). Miliolids are in

general very abundant in shallow water seagrass meadows (Frezza et al., 2011), but not exclusively. Moreover, their abundance must be carefully considered because, they are strongly affected by diagenetic processes due to their high-Mg-calcite tests (Budd and Hiatt, 1993). The FI' index is based on the abundance of epiphytic foraminifera and has been successfully implemented in the modern Mediterranean Sea as a proxy of water quality (e.g., El Kateb et al., 2020; Khokhlova et al., 2022). This index presents low values in both biofacies and display only a minor difference between the samples of the *Thalassinoides* and *Pinna* biofacies (Table 6.2). As suggested by Mariani et al. (2022a), the application of FI' to fossil context might be hindered by diagenesis (e.g., the preferential dissolution of miliolids). Similarly, I_{LS} (which is used to assess the ecological status of modern seagrass meadows) displays no significant differences between the samples of the two biofacies. Overall, the use of FI' and I_{LS} alone is not recommended as an IPSI but can be helpful for the palaeoenvironmental reconstruction of the seagrass-related deposits. Actually, their low values in the Stirone River deposits might suggest that the local palaeo-seagrass was growing under stressed conditions. The presence of mud-loving, deeper water, opportunistic foraminifera (e.g., *Bolivina*, *Bulimina*, Cassidulinidae), could be related to episodic pulses of fluvial discharge which are considered an important factor in the evolution of the Stirone environment by both Crippa et al. (2019) and Bracchi et al. (2020). Although some of these foraminiferal taxa are very common in cold climates (and thus their abundance could be related to the cold climate of the Calabrian), the overall distribution of *Ammonia* group and infaunal taxa (e.g., Bolivinidae, Buliminidae, Cassidulinidae, morphotype R foraminifera) within the Stirone River sediments could be also connected to river-related organic-matter input and not solely to seagrass distribution. K/R_{EXT} index confirms to be one of the most significant tools to perform this kind of palaeoenvironmental reconstructions, and its use as IPSI can be considered very important (Mariani et al., 2022a). Indeed, in the seagrass-related palaeoenvironment (*Pinna* biofacies), K/R_{EXT} displays remarkably higher values than in the *Thalassinoides* biofacies (Table 6.2).

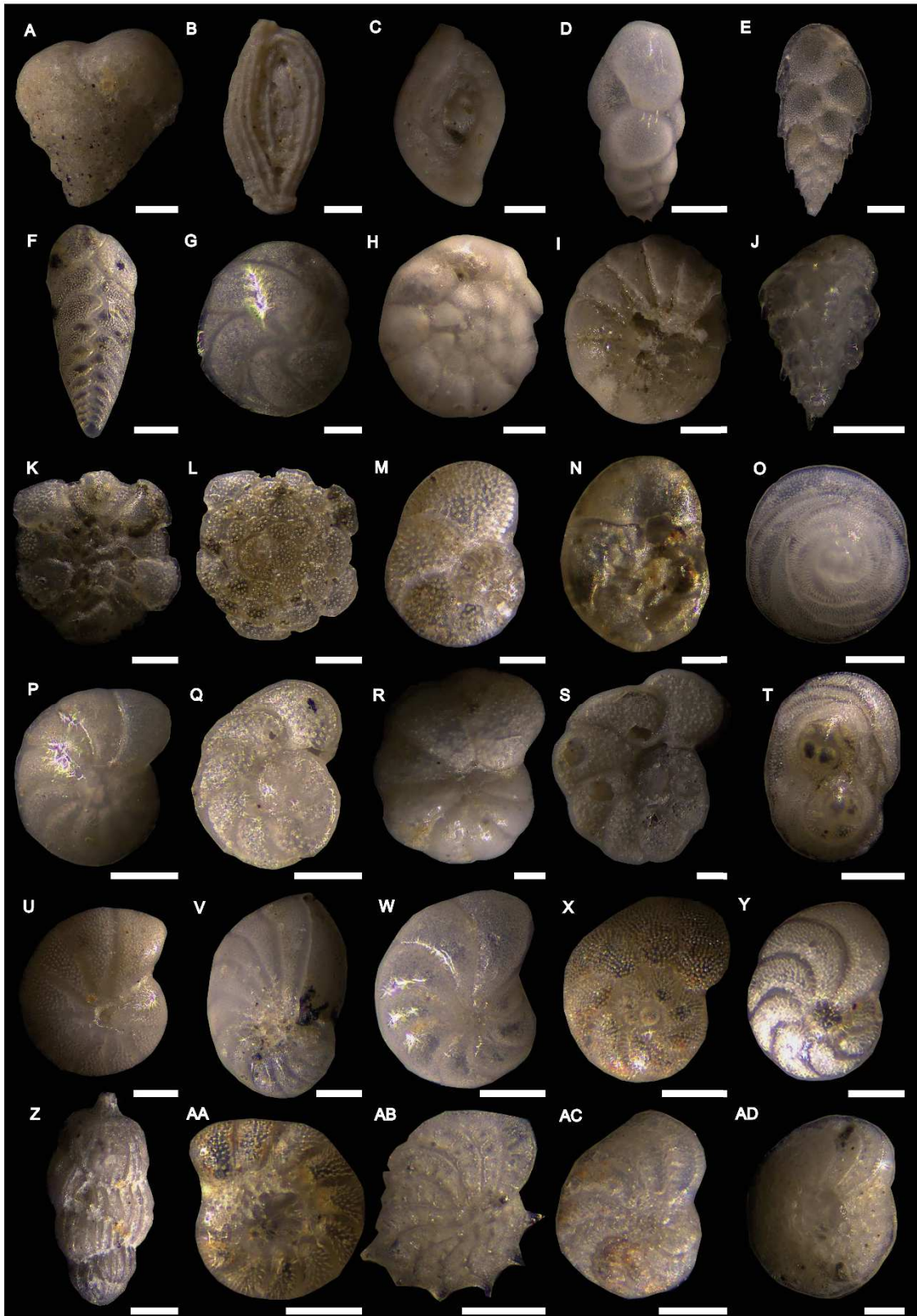


Figure 6.5 LM images of selected foraminifera species. A. *Sahulia conica*; B. *Cycloforina* sp.; C. *Spiroloculina* sp.; D. *Bolivina elongata*; E. *Bolivina alata*; F. *Bolivina spathulate*; G. *Cassidulina carinata*; H. *Ammonia beccarii*, spiral side; I. *A. beccarii*, umbilical side; J. *Reussella spinulosa*; K. *Planorbulina mediterraneensis*, spiral side; L. *P. mediterraneensis*, umbilical side; M. *Rosalina bradyi*, spiral side; N. *R. bradyi*, umbilical side; O. *Neoconorbina terquemi*, spiral side; P. *Cibicides refulgens*, spiral side; Q. *C. refulgens*, umbilical side; R. *Lobatula lobatula*, spiral side; S. *L. lobatula*, umbilical side; T. *N. terquemi*, spiral side. Specimen with two proloculus; U. *Melonis affinis*; V. *Nonion boueanum*; W. *Haynesina germanica*; X. *Valvulineria bradyana*; Y. *Hanzawaia boueana*; Z. *Uvigerina mediterranea*; AA. *Elphidium translucens*; AB. *Elphidium aculeatum*; AC. *Elphidium fichtelianum*; AD. *Elphidium crispum*. The white bars correspond to 100 μ m.

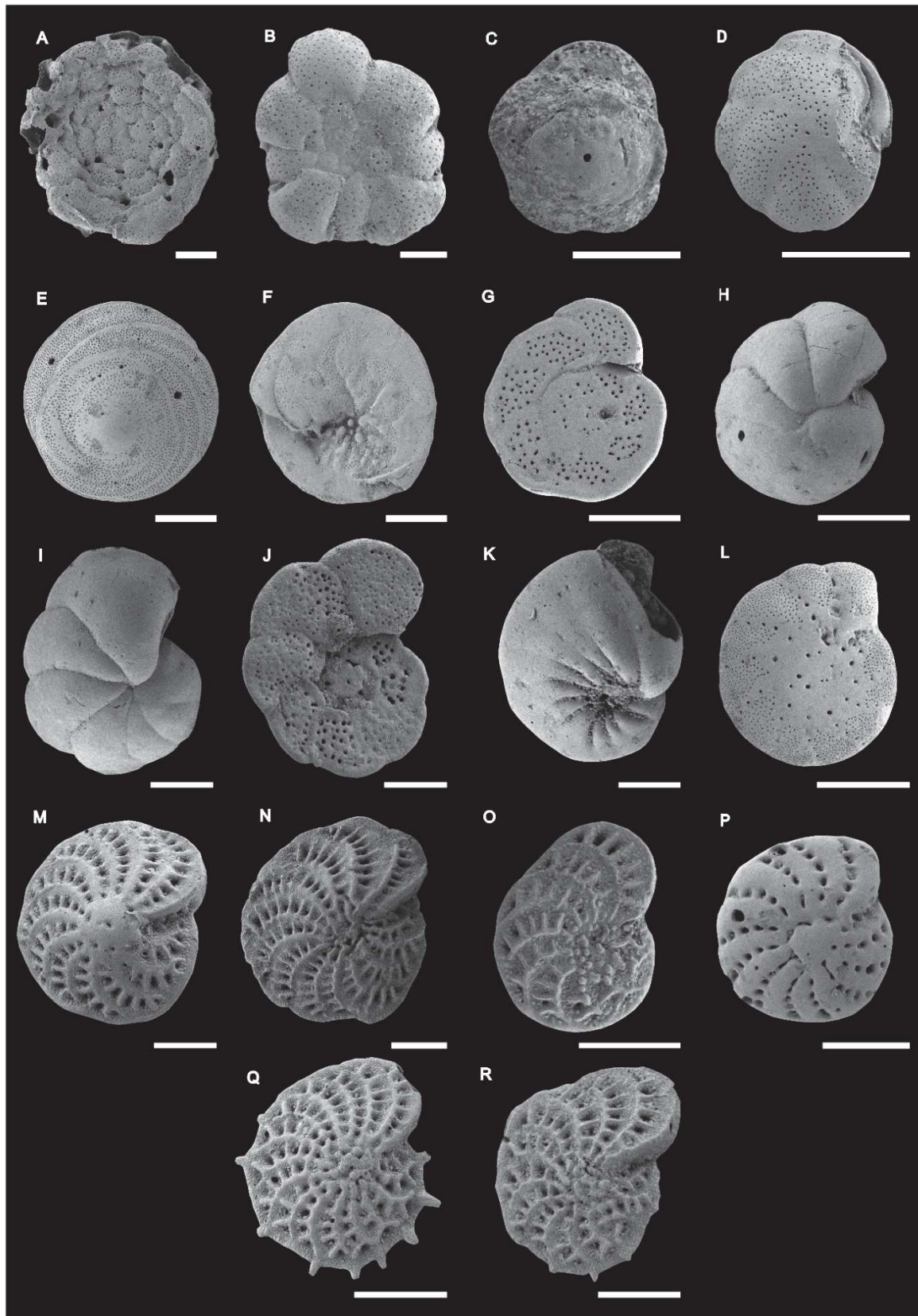


Figure 6.6 SEM images of selected foraminifera species and seagrass remains. A. *Planorbulina mediterraneensis*, umbilical side; B. *P. mediterraneensis*, spiral side; C. *Asterigerinata mamilla*, spiral side; D. *Cassidulina carinata*; E. *Neoconorbina terquemi*, spiral side; F. *N. terquemi*, umbilical side; G. *Cibicides refulgens*, umbilical side; H. *C. refulgens*, spiral side; I. *Lobatula lobatula*, spiral side; J. *L. lobatula*, umbilical side; K. *Nonion boueanum*; L. *Elphidium translucens*; M. *Elphidium crispum*; N. *Elphidium macellum*; O. *Elphidium fichtelianum*; P. *Elphidium advenum*; Q. *Elphidium aculeatum*; R. *E. aculeatum*. The white bars correspond to 100 μm .

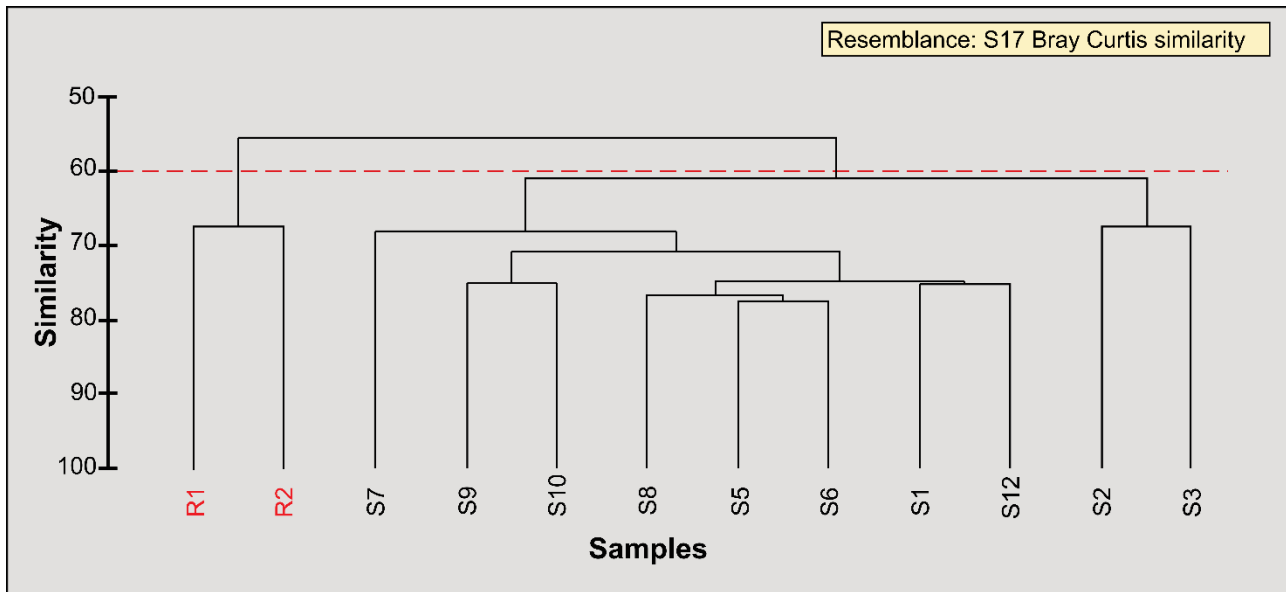


Figure 6.7 Q-mode cluster analysis.

Morphotype	R1	R2	S1	S2	S3	S5	S6	S7	S8	S9	S10	S12	R _{aver}	S _{aver}
A*	0.00	0.00	1.50	0.65	1.16	0.54	1.72	0.52	2.19	0.63	0.82	1.16	0.00	1.09
B	46.77	40.15	36.59	41.94	45.35	44.32	41.55	57.07	42.08	46.14	39.45	45.71	43.46	44.02
C	6.45	5.41	9.02	6.45	9.30	8.11	5.16	7.85	9.29	7.27	7.40	6.60	5.93	7.65
D*	3.23	3.47	14.20	7.74	8.14	20.18	14.61	4.97	17.49	13.41	15.07	11.72	3.35	12.75
D* - miliolids	1.61	3.47	3.34	5.81	6.98	4.14	4.58	3.40	2.73	0.14	1.92	3.96	2.54	3.70

Table 6.5 Morphotypes abundances within each sample and average abundance of each morphotype within the two lithozones of the Stirone river deposits.

6.6.2 Comparison with a similar study site: the case of Fauglia

To enhance the observations collected within the Stirone river deposits and strengthen the application of benthic foraminifera as IPSIs, in this section we compare the results from this case study with the fossil *P. oceanica* meadow of Fauglia (Tuscany, Italy). Both the successions belong to the Calabrian (lower Pleistocene) and are located at relatively close latitude, thus excluding large differences in climate. The Fauglia succession formed in a shallow, low-to moderate-energy, marine environment, as indicated by the presence of in situ *P. oceanica* rhizomes, a *Cladocora caespitosa* bank, an oyster reef and abundant foraminifera of the *Ammonia* group (Bosio et al., 2021; Mariani et al., 2022a). As for the Stirone River deposits, Fauglia benthic foraminiferal associations were analysed inside different deposits: within *Posidonia*-bearing layers and in a *C. caespitosa* bank. Based on the morphotypes analysis, morphotype B is the most abundant group in both sites. In particular, Cibicididae and Rosalinidae are the most abundant families in both the palaeo-meadows deposits. In Fauglia, Cibicididae display a higher frequency in the seagrass-related intervals, whereas in the *Cladocora* bank their abundance is much lower. On the other hand, in the Stirone outcrop, Cibicididae

are similarly distributed between vegetated and non-vegetated settings. In both sites, Rosalinidae displays higher abundance in the seagrass-related deposits, indicating Rosalinidae as one of the most clearly seagrass-related family. In both successions, morphotype A* foraminifera only occur in seagrass-related deposits, thus indicating the presence of morphotype A* foraminifera as a highly reliable IPSI. Also, the presence of foraminifera with a curved basal surface, such as Cibicididae and *P. mediterranensis* specimens, indicates that possibly they lived attached onto a firm substrate, which most likely consisted of seagrass leaves and rhizomes (Langer, 1993). Anyway, this feature is not undoubtedly diagnostic of a phytal substrate, as small benthic foraminifera could develop a curved attachment surface even in correspondence of non-phytal substrate (Mariani et al., 2022a). Morphotype C abundance is similar in both the study sites. In both sites morphotype K taxa are more common in seagrass related deposits, while morphotype R foraminifera are much more common in the layers that are not associated with seagrasses. This clearly testifies in favour of the usefulness of the K/R_{EXT} index as indirect indicator of the presence of a palaeo-seagrass meadow. Although other tests based on recent foraminiferal assemblages would be necessary, considering the data collected in this paper and in the study of the exceptionally well-preserved Pleistocene seagrass meadow of Fauglia (Bosio et al., 2021; Mariani et al., 2022a), values of K/R_{EXT} higher than 0.4 could be used as an indirect indicator of a seagrass-related palaeoenvironment (Table 6.2; Fig. 6.8). Indeed, in every samples collected within the seagrass-related layers the value of this index is higher than 0.4, whereas in the other samples is always lower than this threshold. The preferential dissolution of miliolids observed in Fauglia (Mariani et al., 2022a) further suggests evaluating Morphotype D* with caution. Indeed, miliolids and agglutinated foraminifera are more influenced by diagenesis than foraminifera with hyaline, pure calcite tests. However, this is not the case of the Stirone deposits, in which morphotype D* are well-preserved in all the samples and evidence of dissolution processes are not shown. If we do not consider miliolids, the morphotype abundances are similar in both study sites (Fig. 6.8), testifying that excluding the taxa that are mostly affected by diagenesis could be useful to identify fossil seagrass meadows. Finally, the higher abundance of foraminifera of the *Ammonia* group suggests that the Fauglia *Posidonia* meadow probably developed closer to the coastline than the Stirone River palaeo-seagrass meadow.

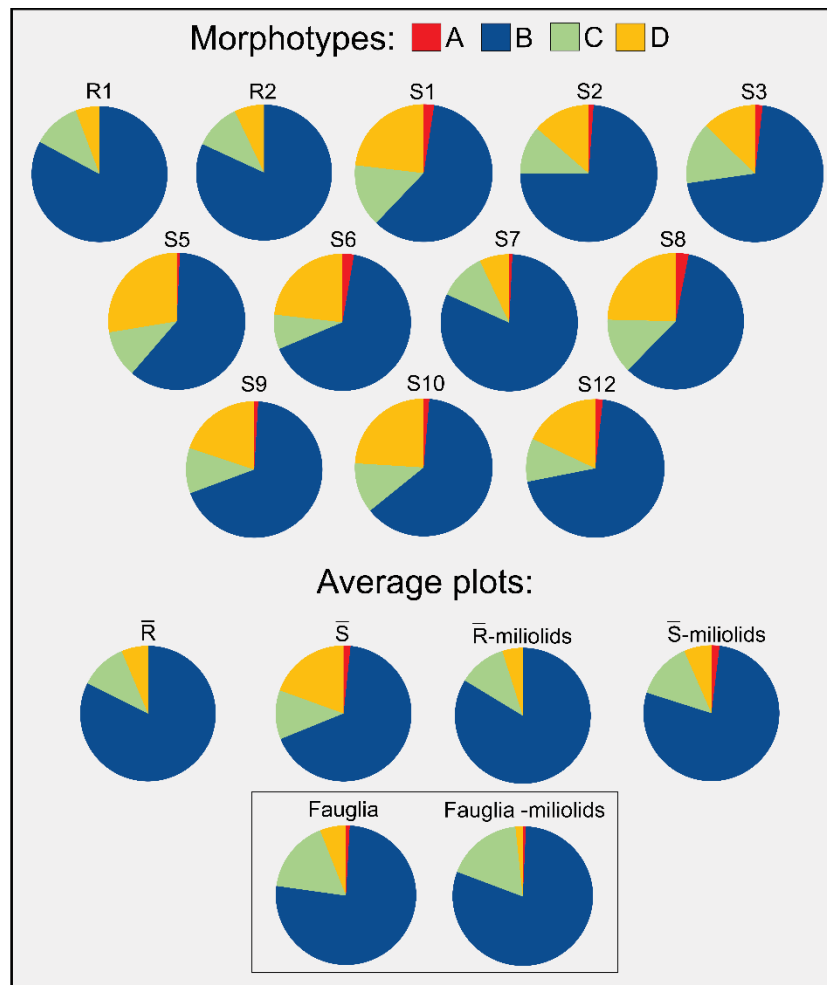


Figure 6.8 Pieplots resulting from the morphotype analysis for each studied sample. Average plots for the *Pinna* biofacies (S) and *Thalassinoides* biofacies (R), are present. Average plots for the two biofacies without considering miliolids are also present. Average pieplots from the Fauglia foraminiferal associations are also present (see Mariani et al., 2022a).

6.6.3 The usefulness of K/R_{EXT} index: insights and perspectives

Based on the evidence from known paleo-seagrass settings, such as those documented at the Fauglia and Stirone outcrops, the K/R_{EXT} index and the abundance of Morphotype A* foraminifera appear as the most promising indicators of such palaeo-environment. Both indices are based on morphological characters, more than species identifications. This means that they could be easily calculated even in more ancient successions than Stirone or Fauglia, where lowest-level taxonomical identification can be difficult to perform. Most likely, they could be calculated also in thin sections. This approach would also allow for the comparison of widely different sites, because even if the taxa are different, morphotypes can be recognized and the morphotype analysis could still be carried out. A bivariate statistical analysis was performed considering the relationship between K/R_{EXT} and the abundance of morphotype A* among all of the samples from the Stirone river deposits and the Fauglia successions (Fig. 6.9), with the exception of sample P11 from Fauglia, which was excluded from the analysis due to the very pervasive diagenetic processes. This analysis shows that the values from the two sites are comparable and that there is a weak positive correlation between the value of K/R_{EXT} and the

abundance of permanently attached foraminifera (Fig. 6.9). However, the occurrence of morphotype A* taxa is always indicative of fossil seagrass meadows, independently from its abundance. This model will be integrated in future with new data that will be collected from different fossil and modern foraminiferal associations, both in seagrass-related environments and in environments with no phytal substrate.

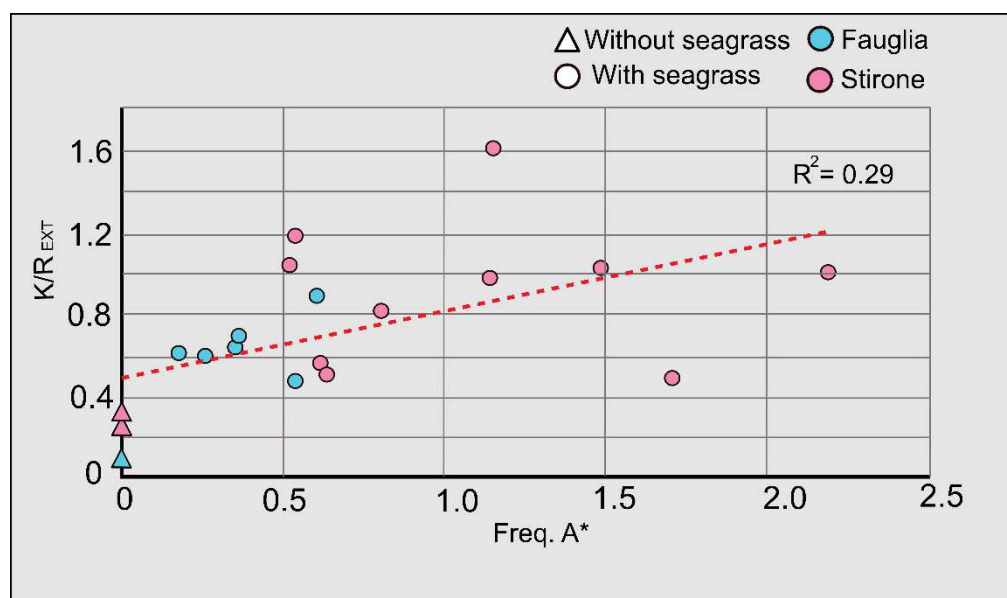


Figure 6.9 Bivariate analysis and linear regression model.

6.7 Conclusions

Benthic foraminifera were analysed from two different shallow water paleo-settings outcropping along the Stirone River. In particular, our results on the foraminifera confirm the occurrence of a vegetated marine palaeoenvironment in correspondence of the *Pinna* biofacies accordingly to Bracchi et al. (2020). On the other hand, the *Thalassinoides* facies represents a palaeoenvironment devoid of seagrass. The morphotype analysis of benthic foraminifera confirmed their effective application as Indirect Palaeo-Seagrass Indicators (IPSIs), as demonstrated from a similar vegetated palaeo-setting at Fauglia (Mariani et al., 2022a). In particular: i) when we exclude the taxa that are mostly affected by diagenesis (e.g., miliolids), it is possible to reproduce comparable signals in different fossil seagrass meadows. ii) the lack of photosymbiotic foraminifera (e.g., *Amphistegina*, *Sorites*, *Peneroplis*), was most likely related to the low early Pleistocene temperatures in this area, which did not allow the development of these species. iii) the presence of permanently attached, encrusting foraminifera, confirmed as one of the most reliable IPSI, as well as the abundance of Rosalinidae. iv) among the tested indexes, the K/R_{EXT} proved to be the most reliable in this kind of analysis, displaying values higher than 0.4 when calculated within seagrass-related environments. Further analyses are

required in order to improve the K/R_{EXT} index, making it comparable between different successions in terms of spatial and time distribution.

Data availability

Datasets related to this article can be found at <https://board.unimib.it/datasets/hrgfj7xfgs>, an open-source online data repository hosted at Mendeley Data (Mariani et al., 2022b).

Acknowledgments

We would like to thank the “Parco dello Stirone e del Piacenziano” for the permission to enter the conservation area. We would like to thank Nicoletta Fusi for her help with the laser granulometer analysis, Davide Coppa for his help with foraminifera picking and Simone Casati, Andrea Di Cencio and Alberto Collareta for the support and the stimulating discussions about the Fauglia site. We strongly acknowledge the two reviewers (Martin R. Langer and an anonymous one) for their comments and suggestions that have deeply improved the quality of the manuscript. This research did not receive any specific grant from funding agencies in the public, commercial, or not-for-profit sectors. This article is also an outcome of Project MIUR-Dipartimenti di Eccellenza 2018–2022.

Appendix 6.1. Supplementary data

Supplementary data to this article can be found online at <https://doi.org/10.1016/j.quaint.2022.10.005>.

References

- Alvarez, Z., Blackwelder, P.L., Hood, T., Nelsen, T.A. and Featherstone, C., 2000. Ostracods as indicators of natural and anthropogenically induced changes in coastal marine environments. In *Coasts at the Millennium. Proceedings of the 17th International Conference of The Coastal Society*. Portland: The Coastal Society, pp. 896-905.
- Arias-Ortiz, A., Serrano, O., Masqué, P., Lavery, P.S., Mueller, U., Kendrick, G.A., Rozaimi, M., Esteban, A., Fourqurean, J.W., Marbà, N., Mateo, M.A., Murray, K., Rule, M.J. and Duarte, C.M., 2018. A marine heatwave drives massive losses from the world's largest seagrass carbon stocks. *Nature Climate Change*, v. 8, pp. 338-344.
- Baceta, J.I. and Mateu-Vicens, G., 2021. Seagrass development in terrigenous-influenced inner ramp settings during the middle Eocene (Urbasa-Andia Plateau, Western Pyrenees, North Spain). *Sedimentology*, <https://doi.org/10.1111/sed.12937>.
- Backman, J., Raffi, I., Rio, D., Fornaciari, E. and Pälke, H., 2012. Biozonation and biochronology of Miocene through Pleistocene calcareous nannofossils from low and middle latitudes. *Newsletters on Stratigraphy*, v. 45, pp. 221-244.
- Barnes, R.S.K. and Barnes, M.K.S., 2012. Shore height and differentials between macrobenthic assemblages in vegetated and unvegetated areas of an intertidal sandflat. *Estuar. Coast. Shelf Sci.*, v. 106, pp. 112-120.
- Barras, C., Jorissen, F., Labrune, C., Andral, B. and Boissery, P., 2014. Live benthic foraminiferal faunas from the French Mediterranean Coast: Towards a new biotic index of environmental quality. *Ecological Indicators*, v. 36, pp. 719-743. [10.1016/j.ecolind.2013.09.028](https://doi.org/10.1016/j.ecolind.2013.09.028).
- Bernhard, J.M. and Sen Gupta, B.K., 1999. Foraminifera of oxygen-depleted environments, in *Modern Foraminifera*, Barun K. Sen Gupta (ed), Kluwer Academic Publishers, pp. 201-216.
- Basso, D. and Spezzaferri, S., 2000. The distribution of living benthic foraminifera in Iskenderun Bay A statistical approach. *Bollettino della Societa Paleontologica Italiana*, v. 39, pp. 359-379.

- Basso, L., Vázquez-Luis, M., García-March, J.R., Deudero, S., Alvarez, E., Vicente, N., Duarte, C.M. and Hendriks, I.E., 2015. The Pen Shell, *Pinna nobilis*: A Review of Population Status and Recommended Research Priorities in the Mediterranean Sea. In Curry B.E. (ed.), *Advances in Marine Biology*, Oxford: Academic Press, v. 71, pp. 109-160.
- Beavington-Penney, S. J. and Racey, A., 2004. Ecology of extant nummulitids and other larger benthic foraminifera; applications in palaeoenvironmental analysis. *Earth Science Reviews*, v. 67 pp. 219-265.
- Beavington-Penney, S.J., Wright, V.P. and Woelkerling, W.J., 2004. Recognising macrophyte-vegetated environments in the rock record: a new criterion using 'hooked' forms of crustose coralline red algae. *Sediment. Geol.*, v. 166, pp. 1-9. 10.1016/j.sedgeo.2003.11.022
- Beavington-Penney, S., Wright, V. and Racey, A., 2006. The Middle Eocene Seeb Formation of Oman: An Investigation of Acyclicity, Stratigraphic Completeness, and Accumulation Rates in Shallow Marine Carbonate Settings. *Journal of Sedimentary Research*, v. 76. 10.2110/jsr.2006.109.
- Beesley, P.L., Ross, G.J.B., and Wells, A., 1998. *Mollusca: The Southern Synthesis*. Fauna of Australia, v. 5, Part A-B. CSIRO Publishing, Melbourne.
- Belt, E.S., Frey, R.W. and Welch, J.S., 1983. Pleistocene coastal marine and estuarine sequences, Lee Creek phosphate mine, eastern North Carolina: in RAY, C.E., ed., *The Geology and Paleontology of the Lee Creek Mine, North Carolina: Smithsonian Contributions to Paleobiology*, n. 53, pp. 229-263.
- Benedetti, A. and Frezza, V., 2016. Benthic foraminiferal assemblages from shallow water environments of northeastern Sardinia (Italy, Mediterranean Sea). *Facies*, v. 62(2), p. 14.
- Betzler, C., Martín, J.M. and Braga, J.C., 2000. Non-tropical carbonates related to rocky submarine cliffs (Miocene, Almería, southern Spain). *Sediment. Geol.*, v. 131, pp. 51-65.
- Blanc-Vernet, L., 1969. Contribution a l'étude des foraminifères de Méditerranée. *Recueil des travaux de la Station Marine d'Endoume*, v. 64, pp. 1-279.
- Blanc-Vernet, L., Clairefond, P. and Orsolini, P., 1979. La Mer pelagienne: les foraminifères. *Géologie Méditerranéenne*, v. 61, pp. 171-209.
- Blott, S.J. and Pye, K., 2001. GRADISTAT: a grain size distribution and statistics package for the analysis of unconsolidated sediments. *Earth surface processes and Landforms*, v. 26(11), pp. 1237-1248.
- Bosio, G., Di Cencio, A., Coletti, G., Casati, S. and Collareta, A., 2021. Exceptionally preserved coral bank and seagrass meadow from the lower Pleistocene of Fauglia (Tuscany, Italy). *Alpine and Mediterranean Quaternary*, 34(2), 237-256.
- Boström, C. and Bonsdorff, E., 1997. Community structure and spatial variation of benthic invertebrates associated with *Zostera marina* (L.) beds in the northern Baltic Sea. *J. Sea Res.*, v. 37, pp. 153-166.
- Bracchi, V.A., Nalin, R. and Basso, D., 2014. Paleocology and dynamics of coralline dominated facies during a Pleistocene transgressive-regressive cycle (Capo Colonna marine terrace, Southern Italy). *Palaeogeography, Palaeoclimatology, Palaeoecology*, v. 414, pp. 296-309.
- Bracchi, V.A., Nalin, R. and Basso, D., 2016. Morpho-structural heterogeneity of shallow-water coralligenous in a Pleistocene marine terrace (Le Castella, Italy). *Palaeogeography, Palaeoclimatology, Palaeoecology*, v. 454, pp. 101-112.
- Bracchi, V.A., Bulegato, S. and Basso, D., 2020. Palaeoecology of the *Pinna nobilis* biofacies along the Stirone River (Early Pleistocene, Northern Italy). *Bollettino della Società Paleontologica Italiana*, v. 59, pp. 41-55. 10.4435/BSPI.2020.05.
- Brandano, M., Cuffaro, M., Gaglianone, G., Petricca, P., Stagno, V. and Mateu-Vicens, G., 2016. Evaluating the Role of Seagrass in Cenozoic CO₂ Variations. *Frontiers in Environmental Science*, v. 4, p. 72.
- Brandano, M., Tomassetti, L., Mateu-Vicens, G. and Gaglianone, G., 2019. The seagrass skeletal assemblage from modern to fossil and from tropical to temperate: insight from Maldivian and Mediterranean examples. *Sedimentology*, v. 66, pp. 2268-2296.
- Brasier M.D., 1975. An outline history of seagrass communities. *Palaeontology*, 18, 681-702.
- Brunetti, M.M. and Vecchi, G., 2005. *Rissoa quarantelli*, una nuova specie del Pleistocene inferiore italiano. *Bollettino Malacologico*, v. 41, pp. 60-65.
- Brunetti, M.M. and Vecchi, G., 2012. Nuove specie del genere *Alvania* (Caenogastropoda: Rissoidae) nel Pleistocene dell'Emilia occidentale (Nord Italia) *Bollettino Malacologico*, v. 48(1), pp. 42-50.
- Budd, D. and Hiatt, E., 1993. Mineralogical Stabilization of High-magnesium Calcite: Geochemical Evidence for Intracrystal Recrystallization Within Holocene Porcellaneous Foraminifera. *Journal of sedimentary petrology*, v. 63, pp. 261-274.
- Budd, A.F., Johnson, K.G. and Stemann, T.A., 1996. Plio-Pleistocene turnover and extinctions in the Caribbean reef-coral fauna. In: Jackson, J.B.C., Budd, A.F., Coates, A.G. (Eds.), *Evolution and Environment in Tropical America*. The University of Chicago Press, pp. 169-204.
- Buzas, M., 1990. Another look at confidence limits for species proportions. *Journal of Paleontology*, v. 64(5), pp. 842-843. doi:10.1017/S002233600001903X
- Calabrese, L. and Di Dio, G., 2009. Note Illustrative della Carta Geologica d'Italia alla scala 1:50.000, foglio 180 "Salsomaggiore Terme." Servizio Geologico d'Italia-Regione Emilia Romagna, Roma.
- Cau, S., Franchi, F., Roveri, M. and Taviani, M., 2015. The Pliocene age Stirone River hydrocarbon chemoherm complex (Northern Apennines, Italy). *Marine and Petroleum Geology*, v. 66, pp 582-595.
- Ceregato, A., Raffi, S. and Scarponi, D., 2007. The circalittoral/bathyal in the Middle Pliocene of Northern Italy: the case of the *Korobkovia oblonga-Jupiteria concava* paleocommunity type. *Geobios*, v. 40, pp. 555-572.
- Channell, J.E.T., Poli, M.S., Rio, D., Sprovieri, R. and Villa, G., 1994. Magnetic stratigraphy and biostratigraphy of Pliocene "argille azzurre" (Northern Apennines, Italy). *Palaeogeography, Palaeoclimatology, Palaeoecology*, v. 110, pp. 83-102.

- Ciangherotti, A.D., Crispino, P. and Esu, D., 1997. Paleocology of the non-marine molluscs of the Pleistocene Stirone River sequence (Emilia, Northern Italy). *Bollettino della Società Paleontologica Italiana*, v. 36, pp. 303-310.
- Cigala Fulgosi, F., 1976. *Dicerorhinus hemitoechus* (Falconer) del post-Villafranchiano fluvio lacustre del T. Stirone (Salsomaggiore, Parma). *Bollettino della Società Paleontologica Italiana*, v. 15, pp. 59-72.
- Cita, M.B., Gibbard, P.L., Head, M.J., the ICS Subcommittee on Quaternary Stratigraphy, 2012. Formal ratification of the GSSP for the base of the Calabrian Stage (second stage of the Pleistocene Series, Quaternary System). *Episodes*, v. 35, pp. 388-397.
- Coletti, G., Bracchi, V.A., Marchese, F., Basso, D., Savini, A., Vertino, A. and Corselli C., 2018. Quaternary build-ups and rhodalgal carbonates along the adriatic and ionian coasts of the italian peninsula: a review. *Riv. It. Paleontol. Strat.*, v. 124(2), pp. 387-406
- Coletti, G., Mariani, L., Garzanti, E., Consani, S., Bosio, G., Vezzoli, G., Hu, X. and Basso, D., 2021. Skeletal assemblages and terrigenous input in the Eocene carbonate systems of the Nummulitic Limestone (NW Europe), *Sedimentary Geology*, v. 425, 106005, ISSN 0037-0738, <https://doi.org/10.1016/j.sedgeo.2021.106005>.
- Colom, G., 1942. Una contribución al conocimiento de los foraminíferos de la bahía de Palma de Mallorca. *Notas y Resúmenes Ser. II, Instituto Español de Oceanografía*, v. 108, pp. 1-53.
- Cramer, M.D. and Hawkins, H.J., 2009. A physiological mechanism for the formation of root casts. *Palaeogeogr. Palaeoclimatol. Palaeoecol.*, v. 274, pp. 125-133.
- Crimes, T.P., 1977. Trace fossils of an Eocene deep-sea sand fan, northern Spain: in Crimes, T.P. and Harper, J.C., eds., *Trace Fossils 2*, Geological Journal Special Issue 9, Liverpool, Seel House Press, p. 71-90.
- Crippa, G., Azzarone, M., Bottini, C., Crespi, S., Felletti, F., Marini, M., Petrizzo, M.A., Scarponi, D., Raffi, S. and Raineri, G., 2019. Bio- and lithostratigraphy of lower Pleistocene marine successions in western Emilia (Italy) and their implications for the first occurrence of *Arctica islandica* in the Mediterranean Sea. *Quaternary Research*, v. 92, pp. 549-569.
- Cullen-Unsworth, L. and Unsworth, R., 2013. Seagrass meadows, ecosystem services, and sustainability. *Environment*, v. 55, pp. 14-28.
- Curran, H.A., and Frey, R.W., 1977. Pleistocene trace fossils from North Carolina (U.S.A.), and their Holocene analogues: in Crimes, T.P. and Harper, J.C., eds., *Trace Fossils 2*, Geological Journal Special Issue 9, Liverpool, Seel House Press, pp. 71-90.
- de Araújo, O.M.O., Aguilera, O., Coletti, G., Valencia, F.L., Buatois, L.A. and Lopes, R., 2021. X-ray micro-computed tomography of burrow-related porosity and permeability in shallow-marine equatorial carbonates: A case study from the Miocene Pirabas Formation, Brazil. *Marine and Petroleum Geology*, v. 127, 104966.
- De Falco, G., Simeone, S. and Baroli, M., 2008. Management of Beach-Cast *Posidonia oceanica* Seagrass on the Island of Sardinia (Italy, Western Mediterranean). *Journal of coastal research*, v. 24, pp. 69-75.
- De Leeuw, J.W., Frewin, N.L., Van Bergen, P.F., Sinninghe Damsté, J.S. and Colinson, M.E., 1995. Organic carbon as a palaeoenvironmental indicator in the marine realm. *Geol. Soc. Lond. Spec. Publ.*, v. 83, pp. 43-71.
- de los Santos, C.M., Olivé, I., Moreira, M., Silva, A., Freitas, C., Araújo Luna, R., Quental-Ferreira, H., Martins, M., Costa, M.M., Silva, J., Cunha, M.E., Soares, F., Pousão-Ferreira, P. and Santos, R., 2020. Seagrass meadows improve inflowing water quality in aquaculture ponds. *Aquaculture*, v. 528, 735502.
- Den Hartog, C., 1979. Seagrasses and seagrass ecosystems, an appraisal of the research approach. *Aquatic Botany*, v. 7, pp. 105-107.
- Debenay, J.P, Bénéteau, E., Zhang, J., Stouff, V., Geslin, E., Redois, F. and Fernandez-Gonzalez, M., 1998. *Ammonia beccarii* and *Ammonia tepida* (Foraminifera): morphofunctional arguments for their distinction, *Marine Micropaleontology*, v. 34, i. 3-4, pp. 235-244, [https://doi.org/10.1016/S0377-8398\(98\)00010-3](https://doi.org/10.1016/S0377-8398(98)00010-3).
- Debey, M.H., 1848. Übersicht der urweltlichen Pflanzen des Kreidegebirges überhaupt und der Aachener Kreideschichten insbesondere. *Verh. Nat. Hist. Ver. Preuss. Rheinl.*, v. 5, pp. 113-125.
- Debey, M.H., 1851. Beitrag zur fossilen Fauna der holländischen Kreide (Vaels bei Aachen, Kunraed, Maastricht). *Verh. Nat. Hist. Ver. Preuss. Rheinl.* v. 8, pp. 568-569.
- Deyanova, D., Gullström, M., Lyimo, L.D., Dahl, M., Hamisi, M.I., et al., 2017. Contribution of seagrass plants to CO₂ capture in a tropical seagrass meadow under experimental disturbance. *PLOS ONE*, 12(7): e0181386. <https://doi.org/10.1371/journal.pone.0181386>
- Di Martino, E. and Taylor, P.D., 2014. A brief review of seagrass-associated bryozoans, recent and fossil. *Stud. Tridentini. Sci. Nat. Acta Geol.*, v. 94, pp. 79-94 (IBA Conference 2013 Volume).
- Dilcher, D., 2016. Fossil plants from the Coon Creek Formation of Tennessee. In: *Paleontology of Cretaceous Coon Creek Formation* (eds Ehret D, Jr. TLH, Ebersole S). The Alabama Museum of Natural History, Tuscaloosa, Alabama, pp. 118-121.
- Dimiza, M. D., Koukousioura, O., Triantaphyllou, M. V. and Dermitzakis, M. D., 2016. Live and dead benthic foraminiferal assemblages from coastal environments of the Aegean Sea (Greece): Distribution and diversity, *Revue de Micropaléontologie*, v. 59, pp. 19-32.
- Dominici, S., 2001. Taphonomy and paleoecology of shallow marine macrofossil assemblages in a collisional setting (late Pliocene-early Pleistocene, western Emilia, Italy). *Palaios*, v. 16, pp. 336-353.
- Dominici, S., 2004. Quantitative taphonomy in sandstones from an ancient fan delta system (Lower Pleistocene, Western Emilia, Italy). *Palaios*, v. 19, pp. 193-205.
- Domning, D.P., 2001. Sirenians, seagrasses, and Cenozoic ecological change in the Caribbean. *Palaeogeogr. Palaeoclimatol. Palaeoecol.*, v. 166, pp. 27-50.

- Duarte, C.M., Losada, I.J., Hendriks, I.E., Mazarrasa, I. and Marba, N., 2013. The role of coastal plant communities for climate change mitigation and adaptation. *Nat. Clim. Change*, v. 3, pp. 961-968.
- El Kateb, A., Stalder, C., Stainbank, S., Fentimen, R. and Spezzaferri, S., 2018. The genus *Amphistegina* (Benthic foraminifera): Distribution along the southern Tunisian coast. *BioInvasions Records*, v. 7. 10.3391/bir.2018.7.4.06.
- El Kateb, A., Stalder, C., Martínez-Colón, M., Mateu-Vicens, G., Francescangeli, F., Coletti, G., Stainbank, S. and Spezzaferri, S., 2020. Foraminiferal-based biotic indices to assess the ecological quality status of the Gulf of Gabes (Tunisia): Present limitations and future perspectives. *Ecological Indicators*, v. 111, 105962
- Einsele, G., 2000. *Sedimentary Basins, Evolution, Facies, and Sediment Budget*: Springer, Berlin, Heidelberg, New York, 792 p.
- Ekdale, A.A. and Bromley, R.G., 1984. Comparative ichnology of shelf-sea and deep-sea chalk, *Journal of Paleontology*, v. 58, pp. 322-332.
- Ekdale, A.A., Bromley, R.G. and Pemberton, S.G., 1984. Ichnology: The use of trace fossils in sedimentology and stratigraphy: Society of Economic Paleontologists and Mineralogists Short Course 15, 317 p.
- Esu, D., 2008. A new species of *Tanousia* Servain (Gastropoda, Hydrobiidae) from the Early Pleistocene of Emilia-Romagna (Northern Italy). *Bollettino della Società Paleontologica Italiana*, v. 47, pp. 45-49.
- Esu, D. and Girotti, O., 2015. *Melanopsis wilhelmi* n. sp. and *Valvata ducati* n. sp., two new Pleistocene gastropods from a section of the Stirone River (Emilia, North Italy). *Archiv für Molluskenkunde*, v. 144, pp. 149-154.
- Eva, A.N., 1980. Pre-Miocene seagrass communities in the Caribbean. *Palaeontology*, v. 23, pp. 231-236.
- Fornos, J.J. and Ahr, W.M., 1997. Temperate carbonates on a modern, low-energy, isolated ramp: the Balearic Platform, Spain. *J. Sediment. Res.B.*, v. 67, pp. 364-373.
- Forsey, G.F., 2016. Ostracods as proxies for past seagrass: A review. *Palaeogeography, Palaeoclimatology, Palaeoecology*, v. 447, pp. 22-28.
- Frey, R.W., Curran, A. and Pemberton, S.G., 1984. Tracemaking activities of crabs and their environmental significance: The ichnogenus *Psilonichnus*, *Journal of Paleontology*, v. 58, pp. 333-350.
- Frezza, V. and Carboni, M., 2009. Distribution of recent foraminiferal assemblages near the Ombrone River mouth (Northern Tyrrhenian Sea, Italy). *Revue de Micropaléontologie*, v. 52, pp. 43-66. 10.1016/j.revmic.2007.08.007.
- Frezza, V., Mateu-Vicens, G., Gaglianone, G., Baldassarre, A. and Brandano, M., 2011. Mixed carbonate-siliciclastic sediments and benthic foraminiferal assemblages from *Posidonia oceanica* seagrass meadows of the central Tyrrhenian continental shelf (Latium, Italy). *Italian Journal of Geosciences*, v. 130, pp. 352-369.
- Gacia, E., Duarte, C., Marba, N., Terrados, J., Kennedy, H., Fortes, M. and Tri, N., 2003. Sediment deposition and production in SE-Asia seagrass meadows. *Estuarine Coastal and Shelf Science*, v. 56, pp. 909-919. 10.1016/S0272-7714(02)00286-X.
- Ghielmi, M., Minervini, M., Nini, C., Rogledi, S., Rossi, M. and 2013. Late Miocene-Middle Pleistocene sequences in the Po Plain-Northern Adriatic Sea (Italy): the stratigraphic record of modification phases affecting a complex foreland basin. *Marine and Petroleum Geology*, v. 42, pp. 50-81.
- Gómez-Alba, J.A.S., 1988. *Guía de campo de los fósiles de España y de Europa*. 925 pp. Ediciones Omega SA, Barcelona.
- Green, T.M., 2002. A Comparison of Paleocological Determinations Based on Vertebrate Faunas From the Moodys Branch Formation (Upper Eocene) of Louisiana and Mississippi. M.S. Thesis. The University of Louisiana, Monroe.
- Gunderson, K.L., Kodama, K.P., Anastasio, D.J. and Pazzaglia, F.J., 2012. Rock-magnetic cyclostratigraphy for the Late Pliocene-Early Pleistocene Stirone section, Northern Apennine mountain front, Italy. *Geological Society, London, Special Publications*, v. 373, pp. 309-323.
- Hald, M. and Korsun, S., 1997. Distribution of modern benthic foraminifera from fjords of Svalbard, European Arctic. *The Journal of Foraminiferal Research*, v. 27(2), pp. 101-122.
- Hallock, P., Lidz, B. H., Cockey-Burkhard, E. M., and Donnelly, K. B., 2003. Foraminifera as bioindicators in coral reef assessment and monitoring: the FORAM Index: Environmental Monitoring and Assessment, v. 81, pp. 221-238.
- Heck, K.L., Able, K.W., Fahay, M.P. and Roman, C.T., 1989. Fishes and decapod crustaceans of Cape Cod eelgrass meadows: species composition, seasonal abundance patterns and comparison with unvegetated substrates. *Estuaries*, v. 12, pp. 59-65.
- Hesse, M., Weber, M. and Halbritter, H.M., 1999. Pollen walls of Araceae, with special reference to their fossilization potential. *Grana*, v. 38, pp. 203-209.
- Hirst, J. A. and Attrill, M. J., 2008. Small is beautiful: An inverted view of habitat fragmentation in seagrass beds. *Estuarine, Coastal and Shelf Science*, v. 78, issue 4, pp. 811-818, ISSN 0272-7714, <https://doi.org/10.1016/j.ecss.2008.02.020>.
- Hohenegger, J., 1994. Distribution of living larger foraminifera NW of Sesoko-Jima, Okinawa, Japan. *Mar. Ecol.*, v. 15, pp. 291-334.
- Hosius, A. and Von der Marck, W., 1880. Die Flora der Westfälischen Kreideformation. *Palaeontographica*, v. 26, pp. 125-236.
- Howard, J.D. and Frey, R.W., 1975. Estuaries of the Georgia coast, U.S.A.: Sedimentology and Biology, II. Regional animal-sediment characteristics of Georgia estuaries, *Senckenbergiana Maritima*, v. 7, pP. 237-256.
- Hughes, R.G., Johnson, S. and Smith, I.D., 1991. The growth patterns of some hydroids that are obligate epiphytes of seagrass leaves. *Hydrobiologia*, v. 216, pp. 205-210.

- Ivany, L.C., Portell, R.W. and Jones, D.S., 1990. Animal–plant relationships and paleobiogeography of an Eocene seagrass community from Florida. *Palaios*, v. 5, pp. 244-258.
- Jorissen, F.J., de Stigter, H.C. and Widmark, J.G.V., 1995. A conceptual model explaining benthic foraminiferal microhabitats. *Mar. Micropal.*, v. 26, pp. 3-15.
- Jorissen, F.J., Fontanier, C. and Thomas, E., 2007. Chapter seven paleoceanographical proxies based on deep-sea benthic foraminiferal assemblage characteristics. In: Hillaire-Marcel, C., De Vernal, A. (Eds.), *Paleoceanography of the Late Cenozoic*. Developments in Marine Geology, Elsevier, pp. 263-325.
- Kamola, D.L., 1984. Trace fossils from marginal-marine facies of the Spring Canyon Member, Blackhawk Formation, (Upper Cretaceous), east-central Utah: *Journal of Paleontology*, v. 58, n. 2, pp. 529-541.
- Khokhlova, A., Gudnitz, M. N., Ferriol, P., Tejada, S., Sureda, A., Pinya, S. and Mateu-Vicens, G., 2022. Epiphytic foraminifers as indicators of heavy-metal pollution in *Posidonia oceanica* seagrass meadows, *Ecological Indicators*, v. 140, <https://doi.org/10.1016/j.ecolind.2022.109006>. Koriba, K. and Miki, S., 1931. On *Archeozostera* from the Izumi Sandstone. *Chikyū (The Globe)*, v. 15, pp. 165–201 (in Japanese).
- Koskeridou, E., Thivaoui, D., Giamali, C., Agiadi K. and Mantzouka, D., 2019. Seagrass-Associated Molluscan and Fish Communities from the Early Pleistocene of the Island of Rhodes (Greece), *IOP Conf. Ser.: Earth Environ. Sci.*, v. 221, 012050.
- Kusworo, A., Reich, S., Wesselingh, F.P., Santodomingo, N., Johnson, K.G., Todd, J.A., et al., 2015. Diversity and paleoecology of Miocene coral-associated mollusks from East Kalimantan (Indonesia). *Palaios*, v. 30, pp. 116-127.
- Langer, M. R., 1993. Epiphytic foraminifera. *Marine Micropaleontology*, v. 20, pp. 235–265.
- Langer, M. R., 1988. Recent Epiphytic Foraminifera from Vulcano (Mediterranean Sea). *Revue de Paléobiologie, Vol. Spéc. No. 2, BENTHOS*, v. 86, pp.827-832, 8 figs., Genève.
- Langer, M. R. and Hottinger, L., 2000. Biogeography of Selected “Larger” Foraminifera. *Micropaleontology*, v. 46, pp. 105-126.
- Langer, M. R., Weinmann, A. E., Lötters, S., and Rödder, D., 2012. “Strangers” in paradise: modeling the biogeographic range expansion of the foraminifera *Amphistegina* in the Mediterranean Sea. *The Journal of Foraminiferal Research*, v. 42(3), pp. 234-244.
- Lemer, S., Buge, B., Bernis, A. and Giribet, G., 2014. First molecular phylogeny of the circumtropical bivalve family Pinnidae (Mollusca, Bivalvia): evidence for high levels of cryptic species diversity. *Mol. Phylogenet. Evol.*, v. 75, pp. 11-23.
- Leonard-Pingel, J.S., 2005. Molluscan Taphonomy as a Proxy for Recognizing Fossil Seagrass Beds. M.S. Thesis. Louisiana State University, Baton Rouge.
- Letzsch, W.S. and Frey, R.W., 1980. Deposition and erosion in a Holocene salt marsh, Sapelo Island, Georgia. *Journal of Sedimentary Petrology*, v. 50, p. 529.
- Link, M.H. and Bottjer, D.J., 1982. Turbidites and slope facies association, Upper Cretaceous Holz Shale Member of the Ladd Formation, Santa Ana Mountains, California: in Bottjer, D.J., Colburn, I.P. and Cooper, J.D., eds., *Late Cretaceous Depositional Environments and Paleogeography*, Santa Ana Mountains, Southern California: Pacific Section Society of Economic Paleontologists and Mineralogists Guidebook, pp. 91-96.
- López-Belzunce, M., Blázquez, A.M. and Pretus, J.L., 2014. Recent benthic foraminiferal assemblages and their relationship to environmental variables on the shoreface and inner shelf off Valencia (Western Mediterranean). *Marine Environmental Research*, v. 101, pp. 169-183, <https://doi.org/10.1016/j.marenvres.2014.06.011>.
- Loubere, P. and Fariddudin, M., 1999. Benthic foraminifera and the flux of organic carbon in the seabed. In: *Foraminifera Modern* (ed) Sen Gupta BK. Kluwer Academic Publishers, Dordrecht, pp. 181-199.
- Malek, M.N.A., Omar, R. and Faiz, N.N., 2014. The distribution of benthic foraminifera on selected marine sediments in Pahang River estuary, Pahang, Malaysia: identification using SEM images. *Malaysian Journal of Microscopy*, v. 10, pp. 41-46.
- Mariani, L., Coletti, G., Mateu-Vicens, M., Bosio, G., Collareta, A., Khokhlova, A., Di Cencio, A., Casati, S. and Malinverno, E., 2022. Testing an indirect palaeo-seagrass indicator: benthic foraminifera from the Lower Pleistocene *Posidonia* meadow of Fauglia (Tuscany, Italy), *Marine Micropaleontology*, v. 73.
- [dataset] Mariani, L., Coletti, G., Bosio, G., Tentorio, C., Mateu Vicens, G., Bracchi, V.A., Basso, D. and Malinverno, E., 2022. “Benthic foraminifera as proxy for fossil seagrass from the Lower Pleistocene deposits of the Stirone River (Emilia-Romagna, Italy) - Raw Data”, Mendeley Data, V1, doi: 10.17632/hrgfj7xfgs.1
- Martini, P.I., Baker, V.R., and Garzon, G., 2002. Flood and megaflood processes and products: Recent and ancient examples: IAS Special Publication 32, Blackwell Science, Oxford, UK, 312 p.
- Mary, C., Iaccarino, S., Courtillot, V., Besse, J. and Aissaoui, D. M., 1993. Magnetostratigraphy of Pliocene sediments from the Stirone River (Po valley). *Geophysical Journal International*, v. 112, pp. 359-380.
- Mateu, G., 1970. Estudio sistemático y bioecológico de los foraminíferos vivientes de los litorales de Cataluña y Baleares. *Trabajos del Instituto Español de Oceanografía*, v. 38, pp. 1-84.
- Mateu-Vicens, G., Box, A., Deudero, S. and Rodríguez, B., 2010. Comparative analysis of epiphytic foraminifera in sediments colonized by seagrass *Posidonia oceanica* and invasive macroalgae *Caulerpa* spp. *Journal of Foraminiferal Research*, v. 40, pp. 134-147.
- Mateu-Vicens, G., Brandano, M., Gaglianone, G. and Baldassarre, A., 2012. Seagrass-meadow sedimentary facies in a mixed siliciclastic-carbonate temperate system in the Tyrrhenian Sea (Pontinian Islands, western Mediterranean). *Journal of Sedimentary Research*, v. 82, pp. 451-463.

- Mateu-Vicens, G., Khokhlova, A. and Sebastián-Pastor, T., 2014. Epiphytic foraminiferal indices as bioindicators in Mediterranean seagrass meadows. *The Journal of Foraminiferal Research*, v. 44, pp. 325-339.
- Mazzella, L. and Russo, G. F., 1989. Grazing effect of two *Gibbula* species (Mollusca, Archaeogastropoda) on the epiphytic community of *Posidonia oceanica* leaves. *Aquatic Botany*, v. 35, pp. 357-373.
- Miller, M.F. and Knox, L.W., 1985. Biogenic structures and depositional environments of a Lower Pennsylvanian coal-bearing sequence, northern Cumberland Plateau, Tennessee, U.S.A.: in Curran, H.A., ed., *Biogenic Structures: Their Use in Interpreting Depositional Environments: Society of Economic Paleontologists and Mineralogists Special Publication*, v. 35, pp. 67-97.
- Moissette, P., Koskeridou, E., Corneé, J.J., Guillocheau, F. and Lécuyer, C., 2007. Spectacular preservation of seagrasses and seagrass-associated communities from the Pliocene of Rhodes, Greece. *Palaios*, v. 22, pp. 200-211.
- Monesi, E., Muttoni, G., Scardia, G., Felletti, F., Bona, F., Sala, B., Tremolada, F., Francou, C. and Raineri, G., 2016. Insights on the opening of the Galerian mammal migration pathway from magnetostratigraphy of the Pleistocene marine-continental transition in the Arda River section (northern Italy). *Quaternary Research*, v. 86, pp. 220-231.
- Murray, J.W., 1991. *Ecology and paleoecology of benthic foraminifera*. Longman, Harlow, p. 397.
- Murray, J. W., 2006. *Ecology and Applications of Benthic Foraminifera*. Cambridge University Press, Cambridge, 426 p.
- Mutti, E., Davoli, G., Tinterri, R. and Zavala, C., 1996. The importance of ancient fluvio-deltaic systems dominated by catastrophic flooding in tectonically active basins. *Memorie di Scienze Geologiche*, v. 48, pp. 233-291.
- Myrow, P.M., 1995. *Thalassinoides* and the Enigma of Early Paleozoic Open-Framework Burrow Systems. *PALAIOS*, v. 10, n. 1, SEPM Society for Sedimentary Geology, pp. 58-74, <https://doi.org/10.2307/3515007>.
- Oishi, S., 1931. Discovery of Archeozostera and Sigillaria-like impressions in Hokkaido. *J. Geog. Tokyo*, v. 43, pp. 717-719 (in Japanese).
- Ondiviela, B., Losada, I.J., Lara, J.L., Maza, M., Galván, C., Bouma, T.J. and van Belzen, J., 2014. The role of seagrasses in coastal protection in a changing climate. *Coastal Engineering*, v. 87, pp. 158-168, ISSN 0378-3839, <https://doi.org/10.1016/j.coastaleng.2013.11.005>.
- Panieri, G., Gamberi, F., Marani, M. and Barbieri, R., 2005. Benthic foraminifera from a recent, shallow-water hydrothermal environment in the Aeolian Arc (Tyrrhenian Sea). *Marine Geology*, v. 218, pp- 207-229. [10.1016/j.margeo.2005.04.002](https://doi.org/10.1016/j.margeo.2005.04.002).
- Papani, G. and Pelosio, G., 1962. La serie plio-pleistocenica del Torrente Stirone (Parmense Occidentale). *Bollettino della Società Geologica Italiana*, v. 81, pp. 293-325.
- Parsons, K.M. and Brett, C.E., 1991. Taphonomic processes and biases in modern marine environments: an actualistic perspective on fossil assemblage preservation. In: Donovan, S.K. (Ed.), *The Processes of Fossilization*. Columbia University Press, New York, pp. 22-65.
- Pavia, G., Dulai, A., Festa, A., Gennari, R., Pavia, M. and Carnevale, G., 2022. Palaeontology of the Upper Pliocene marine deposits of Rio Vaccaruzza, Villalvernia (Piedmont, NW Italy). *Riv. It. Paleontol. Strat.*, 128(1): 129-210.
- Pelosio, G. and Raffi, S., 1974. Osservazioni su *Arctica islandica* ed altri lamellibranchi del Calabriano dell'Emilia occidentale. *Ateneo Parmense, Acta Naturalia*, v. 10, pp. 347-367.
- Pelosio, G. and Raffi, S., 1977. Preliminary remarks on mollusc assemblages of the Stirone River Pleistocene series (Parma Province, Northern Italy). In *X INQUA Congress, Birmingham*. 19 pp. International Union for Quaternary Research (INQUA), Norwich, UK.
- Pèrès, J.M. and Picard, J., 1964. *Nouveau manuel de bionomie benthique de la mer Méditerranée*, Edition revue et augmentée. *Recueil des Travaux de la Station Marine d'Endoume*, v. 31, pp. 1-137.
- Pergent-Martini, C., Leoni, V., Pasqualini, V., Ardizzone, G.D., Balestri, E., Bedini, R., Belluscio, A., Belsher, T., Borg, J., Boudouresque, C. F., Boumaza, S., Bouqueneau, J. M., Buia, M. C., Calvo, S., Cebrian, J., Charbonnel, E., Cinelli, F., Cossu, A., Di Maida, G., Dural, B., Francour, P., Gobert, S., Lepoint, G., Meinesz, A., Molenaar, H., Mansour, H.M., Panayotidis, P., Peirano, A., Pergent, G., Piazzzi, L., Pirrotta, M., Relini, G., Romero, J., Sanchez-Lizaso, J. L., Semroud, R., Shembri, P., Shili, A., Tomasello, A. and Velimirov, B., 2005. Descriptors of *Posidonia oceanica* meadows: Use and application, *Ecological Indicators*, v. 5, i. 3, pp. 213-230, <https://doi.org/10.1016/j.ecolind.2005.02.004>.
- Perry, C.T., 1999. Biofilm-related calcification, sediment trapping and constructive micrite envelopes: a criterion for the recognition of ancient grass-bed environments? *Sedimentology*, v. 46, pp. 33-45.
- Pervesler, P. and Uchman, A., 2009. A new Y-shaped trace fossil attributed to upogebiid rustaceans from Early Pleistocene of Italy, *Acta Palaeontologica Polonica*, v. 54, pp. 135-142.
- Pervesler, P., Uchman, A., Hohenegger, J. and Dominici, S., 2011. Ichnological record of environmental changes in early Quaternary (Gelasian-Calabrian) marine deposits of the Stirone Section, northern Italy. *Palaios*, v. 26, pp. 578-593.
- Pomel, A., 1849. Matériaux pour servir à la flore fossile des terrains jurassiques de la France. *Amt Ber 25ste Versamm Deutsch Naturf Ärzte, Aachenpp.*, pp. 331-354.
- Prista, G.A., Agostinho, R.J. and Cachão, M.A., 2015. Observing the past to better understand the future: a synthesis of the Neogene climate in Europe and its perspectives on present climate change. *Open Geosciences*, v. 7(1).
- Puga-Bernabéu, Á., Braga, J.C. and Martín, J.M., 2007. High-frequency cycles in Upper-Miocene ramp-temperate carbonates (Sorbas Basin, SE Spain). *Facies*, v. 53, pp. 329-345.
- Raffi, S. and Serpagli, E. 2003. *Introduzione alla Paleontologia*. Ed. UTET

- Reich, S., 2014. Gastropod associations as a proxy for seagrass vegetation in a tropical, carbonate setting (San Salvador, Bahamas). *Palaios*, v. 29, pp. 467-48
- Reich, S., Warter, V., Wesselingh, F.P., Zwaan, H., Renema, W., Lourens, L., 2015a. Paleoecological significance of stable isotope ratios in Miocene tropical shallow marine habitats (Indonesia). *Palaios*, v. 30, pp. 53-65.
- Reich S., Di Martino E., Todd J.A., Wesselingh, F.P. and Renema, W., 2015b. Indirect paleo-seagrass indicators (IPSIs): a review. *Earth-Science Reviews*, v. 143, pp. 161-186.
- Renema, W., 2006. Large benthic foraminifera from the deep photic zone of a mixed siliciclastic-carbonate shelf off East Kalimantan, Indonesia. *Mar. Micropaleontol.*, v. 58, pp. 73-82.
- Reuter, M. and Piller, W.E., 2011. Volcanoclastic events in coral reef and seagrass environments: evidence for disturbance and recovery (Middle Miocene, Styrian Basin, Austria). *Coral Reefs*, v. 30, pp. 889-899.
- Reuter, M., Piller, W.E., Harzhauser, M., Kroh, A., Roegl, F. and Coric, S., 2010. The Quilon Limestone, Kerala Basin, India: an archive for Miocene Indo-Pacific seagrass beds. *Lethaia*, v. 44, pp. 76-86.
- Reuter, M., Piller, W.E. and Erhart, C., 2012. A Middle Miocene carbonate platform under silici-volcanoclastic sedimentation stress (Leitha Limestone, Styrian Basin, Austria) depositional environments, sedimentary evolution and palaeoecology. *Palaeogeogr. Palaeoclimatol. Palaeoecol.*, 350-352, 198-211.
- Ribes, T., Salvadó, H., Romero, J. and Gracia, M. P., 2000. Foraminiferal colonization on artificial seagrass leaves. *Journal of Foraminiferal Research*, v. 30, pp. 192-201.
- Riordan, N.K., James, N.P. and Bone, Y., 2012. Oligo-Miocene seagrass-influenced carbonate sedimentation along a temperate marine palaeoarchipelago, Padthaway Ridge, South Australia. *Sedimentology*, v. 59, pp. 393-418.
- Roveri, M. and Taviani, M., 2003. Calcarene and sapropel deposition in the Mediterranean Pliocene: shallow-and deep-water record of astronomically driven climatic events. *Terra Nova*, v. 15, pp. 279-286.
- RStudio Team, 2020. RStudio: Integrated Development for R. RStudio, PBC, Boston, MA. URL <http://www.rstudio.com/>.
- Sanchez-Vidal, A., Canals, M., de Haan, W.P., Romero, J. and Veny, M., 2021. Seagrasses provide a novel ecosystem service by trapping marine plastics. *Sci Rep*, v. 11, p. 254.
- Spezzaferri, S., Basso, D. and Koral, H., 2000. Holocene palaeoceanographic evolution of the Iskenderun bay, South-Eastern Turkey, as a response to river mouth diversions and human impact. *Mediterranean Marine Science*, v. 1(1), pp. 19-44.
- Swinbanks, D.D. and Lutnerauer, J.L., 1987. Burrow distribution of thalassinidean shrimp on a Fraser Delta tidal flat, British Columbia: *Journal of Paleontology*, v. 61, n. 2, pp. 315-332.
- Tomassetti, L., Benedetti, A. and Brandano, M., 2016. Middle Eocene seagrass facies from Apennine carbonate platforms (Italy). *Sedimentary Geology*, v. 335, pp. 136-149. [10.1016/j.sedgeo.2016.02.002](https://doi.org/10.1016/j.sedgeo.2016.02.002).
- Tomassetti, L., Brandano, M. and Mateu-Vicens, G., 2022. 3D modelling of the upper Tortonian-lower Messinian shallow ramp carbonates of the Hyblean domain (Central Mediterranean, Faro Santa Croce, Sicily). *Marine and Petroleum Geology*, v. 135, <https://doi.org/10.1016/j.marpetgeo.2021.105393>.
- Unsworth, R.K.F., van Keulen, M. and Coles, R.G., 2014. Seagrass meadows in a globally changing environment. *Marine Pollution Bulletin*, v. 83, pp. 383-386.
- Van der Ham, R.W.J.M., van Konijnenburg-van Cittert, J.H.A. and Indeherberge, L., 2007. Seagrass foliage from the Maastrichtian type areas (Maastrichtian, Danian, NE Belgium, SE Netherlands). *Rev. Palaeobot. Palynol.*, v. 144, pp. 301-321.
- Van der Ham, R.W.J.M., van Konijnenburg-van Cittert, J.H.A., Jagt, J.W.M., Indeherberge, L., Meuris, R., Deckers, M.J.M., Renkens, S. and Laffineur, J., 2017. Seagrass stems with attached roots from the type area of the Maastrichtian Stage (NE 40 Belgium, SE Netherlands): Morphology, anatomy, and ecological aspects. *Review of Palaeobotany and Palynology*, v. 241, pp. 49-69.
- Vélez-Juarbe, J., 2014. Ghost of seagrasses past: using sirenians as a proxy for historical distribution of seagrasses. *Palaeogeogr. Palaeoclimatol. Palaeoecol.*, v. 400, pp. 41-49.
- Voigt, E., 1981. Upper Cretaceous bryozoan-seagrass association in the Maastrichtian of the Netherlands. In: Larwood, G.P., Nielsen, C. (Eds.), *Recent and Fossil Bryozoa*. Olsen & Olsen, Fredensborg, pp. 281-298.
- Voigt, E. and Domke, W., 1955. *Thalassocharis bosqueti* Debey ex Miquel, ein strukturell erhaltenes Seegrass aus der holländischen Kreide. *Mitt. Geol. Staatsinst. Hambg.*, v. 24, pp. 87-102.
- Wanless, H.R., 1981. Fining-upwards sedimentary sequences generated in seagrass beds. *J. Sediment. Res.*, v. 51, pp. 445-454.
- Zuschin, M. and Hohenegger, J., 1998. Subtropical coral-reef associated sedimentary facies characterized by molluscs (Northern Bay of Safaga, Red Sea, Egypt). *Facies*, v. 38, pp. 229-254.

7. Palaeoenvironmental and stratigraphic reconstruction of the Lower-Middle Eocene Foraminiferal Limestone of Pag Island (Croatia)

After discussing the importance of epiphytic foraminifera and stressing their significance as palaeo-seagrass proxies in more recent settings (the Pleistocene deposits of Fauglia and Stirone), the focus will be moved to five Eocene successions exposed at i) Pag Island (Croatia), ii) Western Liguria (Italy) and iii) South-Eastern France. The analysis of these successions will provide the palaeoenvironmental and stratigraphic reconstructions of the basins where they deposited. Moreover, it will be again emphasised the importance of the analysis of seagrass-related environments in palaeontology and the relationship between carbonate producers and terrigenous input.

This chapter is taken from the scientific paper in preparation for submission:

Mariani, L., Coletti, G., Bosio, G., Mateu Vicens, G., Ali, M., and Malinverno, E. (in preparation). Palaeoenvironmental and stratigraphic reconstruction of the Lower-Middle Eocene Foraminiferal Limestone of Pag Island (Croatia).

7.1 Abstract

This paper analyses and describes the Lower to Middle Eocene carbonate succession exposed at the Island of Pag (Croatia) in order to provide the palaeoenvironmental, palaeobathymetric, and stratigraphic reconstructions and clarify the dynamics of the carbonate factories in the Dinaric Foreland Basin. More than 100 samples have been collected within the Foraminiferal Limestone and the overlying Transitional beds units cropping out in the sites of Vrčići and Pago, in order to analyse quantitatively the skeletal assemblage and the foraminiferal association, taking into account both large benthic (LBF) and small benthic (SBF) foraminifera. Furthermore, samples were collected in the overlying Dalmatian Flysch, to constrain the age of the top of the succession through calcareous nanofossil (CN) biostratigraphy. Based on the analysed LBF and CN associations, the Foraminiferal Limestone has been dated to the Early Eocene (Ypresian) and the Middle Eocene (Late Lutetian/Early Bartonian). Thanks to the analysis of the skeletal assemblage and the foraminiferal assemblage, and multivariate statistics, seven main biofacies were identified within the Foraminiferal Limestone and one biofacies within the Transitional Beds. The *porcelaneous and agglutinated benthic foraminifera biofacies* (BF1) indicates a well-illuminated, oligotrophic to mesotrophic, shallow-water, lagoonal environment. The *hyaline SBF and encrusting benthic foraminifera biofacies* (BF2) developed in a shallow water, inner-ramp environment, and is related to a vegetated seafloor. The *nummulitid biofacies* (BF3) indicates a moderately high energy, shallow water environment, whereas the *comminuted bioclasts and nummulitid biofacies* (BF4) indicates a low-energy, shallow water environment, both deposited in inner-to-middle ramp settings. The *nummulitid and orthophragminid*

biofacies (BF5) indicates a moderate energy environment, deposited in middle ramp settings. The *nummulitid and serpulid biofacies* (BF6) consists of transported material from the inner ramp deposited in middle ramps settings. The *orthophragminid and nummulitid biofacies* (BF7) indicates a below-wave base, outer shelf setting and the *planktic foraminifera biofacies* (BF8), which is recorded in the Transitional Beds, deposited in hemipelagic environment. Based on the foraminiferal counting, quantitative parameters such as the orthophragminids/nummulitids ratio (O/N), the planktic/benthic foraminifera ratio (P/B), and the hyaline/porcelaneous foraminifera ratio (H/P) were calculated, indicating that the succession formed along a distally steepened ramp profile, with a progressively deepening of the depositional environment with the final drowning of the carbonate ramp. Quantification serves as a crucial instrument for precise and reliable palaeoenvironmental reconstruction, playing a pivotal role in comparing diverse successions.

7.2 Introduction

Reconstructing the paleoenvironment of carbonate ramps presents different challenges depending on the geological setting. While it may be relatively straightforward in passive-margin shelf environments (e.g., Read, 1985, Burchette and Wright, 1992, Pomar, 2001a), the complexity increases significantly in foreland basins (e.g., Read, 1980; Sinclair, 1998; Čosović et al., 2018). In these basins, the preservation of features is often compromised, and tectonic deformation complicates the interpretation of primary bathymetric gradients and paleogeographic context. In particular, this difficulty extends to the recognition and the distinction between eustatic and tectonic influences on the basin history.

Utilizing biota as a criterion for distinguishing paleobathymetric zones is a valuable approach in paleoenvironmental reconstructions. Taxonomic uniformitarianism, i.e., the application of recent biota analysis to reconstruct ancient palaeoenvironments, is an important and widely used tool in palaeontology. Nevertheless, the application of contemporary data to fossil faunal assemblages exhibits a diminishing efficacy over temporal scales (e.g., Breard et al., 2000). For instance, dynamic faunal turnover impairs the validity of Cenozoic models for the reconstruction of Mesozoic palaeobathymetry. This problem extends to encompass diverse taxa, including foraminifera, molluscs, corals, vertebrates and even trace fossils. Thus, taxonomic uniformitarianism is a substantive tool for interpretation in Cenozoic settings, albeit accompanied by some caveats. Thanks to insights from oceanography, sedimentology, ecological research and biology, it is possible to propose interpretations for distinctive features in fossil biofacies, e.g., the characterisation of large, flat specimens of benthic foraminifera in the fossil record (Hallock and Seddighi, 2020), or the

uniformitarian application of modern coral reefs has a keystone in interpreting ancient reefal successions (Pomar and Hallock, 2007).

Limited research has been conducted on carbonate ramps from the Cenozoic of the Tethys, particularly within Alpine foreland basins (Pomar, 2001b). Existing case studies are scarce (Scheibner et al., 2007, Scheibner and Speijer, 2008, Zamagni et al., 2008, 2012, Pomar et al., 2017, Čosović et al., 2018, Coletti et al., 2021).

To expand the knowledge on Palaeogene carbonate system and provide new quantitative data on Cenozoic carbonate ramps of the Tethys, the aim of this study is to reconstruct the Eocene carbonate succession in the Dinaric Foreland Basin of Pag Island (Croatia). To do this, different research approaches have been used: palaeontology, biostratigraphy, and sedimentological analysis, so as to decipher the depositional conditions of various carbonate depositional systems in an evolving foreland basin (e.g., Coletti et al., 2021). Large benthic foraminifera (LBF) and small benthic foraminifera (SBF), with their biostratigraphic and bathymetric significance (Hottinger, 1978, 1997; Serra-Kiel et al., 1998; Renema, 2005), play a key role in this investigation. LBF are useful as age indicators, recognizing shallow benthic biozones (SBZ; Serra-Kiel et al., 1998) and as palaeobathymetric proxies in carbonate ramp reconstruction (Beavington-Penney and Racey, 2004). This reflects how LBF assemblages contribute exceptionally to the analysis of carbonate successions. Furthermore, SBF and LBF are useful as palaeoecological indicators, providing reliable information about the depositional palaeoenvironments (e.g., Murray, 2006). However, evolutionary modifications in foraminiferal biofacies highlights the necessity of age-specific models in palaeoenvironmental interpretation (Breard et al., 2000). Thus, the quantitative analysis of foraminiferal assemblages and other components of the skeletal assemblage is essential to track the evolution of the Dinaric Foreland Basin and to understand the role of tectonics and eustatism in this context.

The significance of quantitative analysis also lies in the availability of numerical data derived from counts of various groups of foraminifera, or more broadly, carbonate producers. This facilitates a more accessible and standardized comparison between biofacies of different carbonate ramps at various sites, enabling direct comparisons and the creation of more reliable paleobathymetric models.

7.3 Geological setting

7.3.1 The Dinaric Foreland Basin

The Dinaric Foreland Basin is located in western Croatia and consists of a SE-oriented peripheral basin that developed between the Eocene and Oligocene (Ćosović et al., 2018). Its formation is a result of the structural evolution of the Dinarides, a fold-and-thrust belt containing sediments ranging from the Carboniferous to the Neogene (Pamić et al., 1998; Placer et al., 2010). The Dinarides developed during the Palaeogene as a consequence of the multiple phases of convergence between the Adria plate and the European plate (Stampfli, 2005; Placer et al., 2010). This convergence began in the Late Jurassic and is still ongoing (Aubouin et al., 1970; Schmid et al., 2008; Kastelic and Carafa, 2012; Kastelic et al., 2013). Changes in relative sea level occurred as a result of the interaction between global eustatic fluctuations and synsedimentary tectonics during the complex convergence between the Eurasia and Adria plates (Mitterpergher et al., 2019). The collision of these two tectonic plates started during the Late Cretaceous, leading to the emergence and erosion of the thick Adriatic Carbonate Platform (AdCP from this point onwards; Velić et al., 2002; Vlahović et al., 2002, 2005). The AdCP consists of Mesozoic units deposited on the Adria margin and its exposure has led to the development of a regional erosional unconformity surface, that sometimes includes bauxite deposits (Vlahović et al., 2005). This unconformity becomes less pronounced towards the southwest (Ćosović et al., 2004; Drobne et al., 2011; Babić & Zupanić, 2016). The AdCP, which represents the shallower part of the detached and highly deformed upper crust of the Adriatic plate (Korbar, 2009), constitutes the bedrock of the Dinaric Foreland Basin (Ćosović et al., 2018). Further south along the Croatian coast, in correspondence to Hvar Island and Brač Island (Martinuš et al., 2023), the subaerial unconformity runs through the Maastrichtian to Lower Palaeocene shallow-water carbonate deposits of the Sumartin Formation and is overlain by the Early Eocene succession of brackish water limestones (Kozina Member) passing into the open ramp foraminiferal limestones (Marjanac et al., 1998).

In the outer Dinaric Foreland Basin, sedimentation recommenced during the Early Eocene (Late Ypresian), with the deposition of the shallow carbonate unit called “Foraminiferal Limestone” (FL from this point onwards; Ćosović et al., 2018). The FL is interpreted as a carbonate ramp formed on a retreating forebulge flank (Babić and Zupanić, 2016; Ćosović et al., 2018). The FL is separated from the overlying middle to upper Eocene carbonate deposits by a subaerial unconformity, which is more prominent in the orogen-proximal zone (Mrinjek et al., 2012), and less defined in the outer foreland. Thus, the Dinaric foreland is a basin where sedimentation was significantly influenced by tectonic forces. As the Dinaric orogen developed, the inner foreland transformed into a wedge-top basin (De Celles & Giles, 1996) or a "piggyback" basin (Ori & Friend, 1984). Tectonic deeply

influenced the morphology of the basin, which is characterized by imbricate thrust sheets of folded bedrock, leading to the structuration of the distinct "ridge-and-swale" topography along the Dalmatian coast (Ćosović et al., 2018). Furthermore, in the outer foreland a foredeep zone is present, where the FL is overlain by the deposits of the "Dalmatian Flysch" (DF hereinafter). The DF consists of a 1-km-thick succession of subneritic turbidites (Ćosović et al., 2018), and its deposition was not synchronous across the basin, rejuvenating from the northern to the southern sectors. Indeed, the oldest deposits are recorded from the early Eocene in Slovenia, while the youngest deposits are found in southeastern Croatia and the offshore Adriatic. The latter consists of clastic hemipelagic sediments (Babić and Zupanić, 2008), deposited between the late Eocene (SE Croatia) and Oligocene-Miocene (offshore Adriatic), indicating the southward expansion and westward migration of the foredeep (Ćosović et al., 2018). Regarding the SE Croatia deposits, these are overlaid by the upper Eocene-lower Oligocene regressive molasse sequence known as the "Promina Beds" (Mrinjek, 1993; Tari Kovačić and Mrinjek, 1994; Vlahović et al., 2012; Zupanić and Babić, 2011), located tens of kilometers southeast of Pag Island.

Sedimentological investigations have demonstrated that the Promina Beds were deposited during fold growth, providing constraints on the imbrication and the folding in the southeastern part of the External Dinarides during the Late Eocene-Oligocene period (Ćosović et al., 2018; Vlahović et al., 2012). Another distinctive clastic unit in the External Dinarides is the Jelar Formation, a chaotic polymictic breccia composed mainly of carbonate clasts from the Jurassic to Cretaceous, with some clasts from the middle Eocene (Pamić et al., 1998; Korbar, 2009; Vlahović et al., 2012). The origin of this breccia is still not fully understood due to its unclear structural position and intense subsequent tectonic deformation, but it is interpreted as being associated with the gravitational collapse of early-stage anticlinal structures (Korbar, 2009; Vlahović et al., 2012). In the Late Oligocene to Miocene epoch, an extensional tectonic event occurred throughout the Dinaric chain (Ilić and Neubauer, 2005; van Unen et al., 2018), and during the same timeframe, a system of intramontane lakes formed, one of which is represented by lacustrine sediments preserved on Pag Island (Bulić and Jurišić-Polšak, 2009; Jiménez-Moreno et al., 2009). Following the Late Miocene, a contractional to strike-slip tectonic regime resumed due to the indentation and anticlockwise rotation of the Adria microplate (Ilić and Neubauer, 2005), which is still ongoing, as evidenced by GPS velocity studies and crustal stress patterns (e.g., Faccenna et al., 2014; Heidbach et al., 2016).

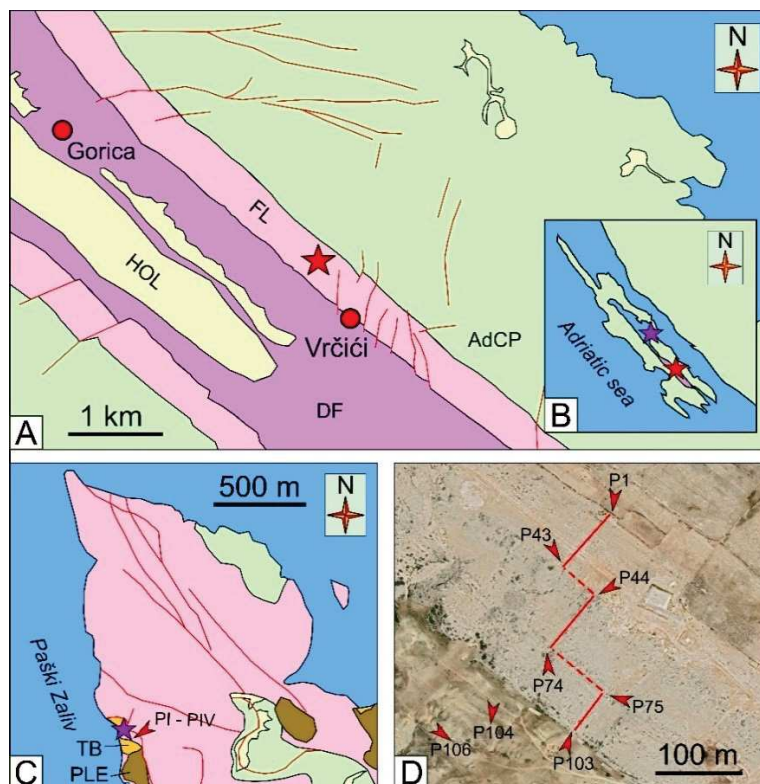


Figure 7.1 A. Geological map of the study site near the village of Vrčići, in southern part of the Island of Pag (after Mittempergher et al., 2019). B. Island of Pag, stars indicate the two analysed locations in A and C. C. Geological Map of the sector north of the town of Pago, with the location of the second analysed section. D. Location of the samples collected and the section followed during the sampling campaign, near the village of Vrčići. AdCP = Adriatic Carbonate Platform; FL = Foraminiferal Limestone; TB = Transitional Beds; DF = Dalmatian Flysch; PLE = Pleistocene deposits; HOL = Holocene deposits.

7.3.2 Pag Island sequence

The uppermost unit belonging to the AdCP, exposed in the Pag Island, consists of the Gornji Humac Formation. This unit consists of 250 -300 m-thick shallow water carbonates, Campanian to Santonian in age, characterized by remarkable lateral and vertical facies variability. Overall, it is mainly composed of coarse clasts of rudists, especially in the upper part of the formation (Mittempergher et al., 2019). The Gornji Humac Formation exhibits various facies that indicate shallow marine conditions, encompassing both low-energy environments like lagoons and peritidal/tidal flats, as well as high-energy environments such as shorefaces and tidal bars (Mittempergher et al., 2019). The upper 20-50 m of the Gornji Humac Formation consists of whitish to pinkish recrystallized limestones, located right below the erosive surface that separates the AdCP basement from the Paleogene units above. In the Pag area, this unconformity indicates a stratigraphic gap which lasted from the Coniacian-Santonian to the Ypresian (Jelaska et al., 1994; Korbar, 2009). Subsequently, sedimentation resumed with the deposition of the FL (Tišljarić et al., 2002; Čosović et al., 2004), that exhibits an angular unconformity of approximately 10° with the underlying Gornji Humac Formation (Mittempergher et al., 2019). The FL carbonates are described in the literature as wackestones-packstones rich in miliolids followed by floatstones-rudstones rich in alveolinids and nummulitids,

along with molluscs, echinoderms, and bryozoans (Mitterpergher et al., 2019), representing a typical inner-to-middle carbonate ramp. Locally, more confined lagoonal environment are also recorded (Ćosović et al., 2004, 2018; Španiček et al., 2017). In the southern region of Pag, the uppermost part of the FL is sharply juxtaposed by the overlying hemipelagic pelites and marls of the DF. The uppermost portion of the FL is characterized by iron oxide staining, intense burrowing, bioturbation and the presence of glauconite (Mitterpergher et al., 2019). The latter indicates that the top of the FL could be most likely interpreted as a drowning surface. Further northward in the island, the FL is overlain by marly limestones and greyish, glauconite-bearing marls, rich in planktonic foraminifera (Globigerinae), indicating a deepening of the depositional environment (Mitterpergher et al., 2019). Although this interval is only a few tens of meters thick, it is recognized in other regions and referred to as "Transitional Beds" (TB hereinafter; Ćosović et al., 2004; Marjanac and Ćosović, 2000). The TB are commonly found at the base of the DF and are characterized by a sudden increase in the terrigenous components relative to the bioclastic components. The DF primarily consists of greyish-blue coloured pelites and marls with occasional interbedded fine-grained sandstones and amalgamated yellowish-greyish sandstone beds that can reach several meters in thickness and is related to a deposition into a relatively shallow hemipelagic depositional environment influenced by fluvial activity (Mitterpergher et al., 2019). The deposition of DF has been dated, based on calcareous nannofossils, to the Lutetian-Bartonian boundary (more precisely 42.37–40.51 Ma; Persico et al., 2019).

The Quaternary deposits that crop out in the southeastern part of Pag Island consist mainly of Pleistocene alluvial deposits. These deposits contain typically angular, well-sorted, and cross-bedded subangular clasts, exhibiting reddish to yellowish coloration and being cemented by vadose calcite. These cemented sediments were formed under higher base level conditions compared to the present-day, and they are currently undergoing erosion. Based on various interpretations, they are believed to have formed during glacial and periglacial conditions during the Middle Pleistocene (Marjanac and Marjanac, 2004; Marjanac, 2012; Marjanac and Marjanac, 2016).

Holocene deposits predominantly consist of (i) colluvial sediments resulting from intense soil erosion, (ii) slope deposits near limestone cliffs, and (iii) lacustrine to marsh deposits found in larger valley floors.

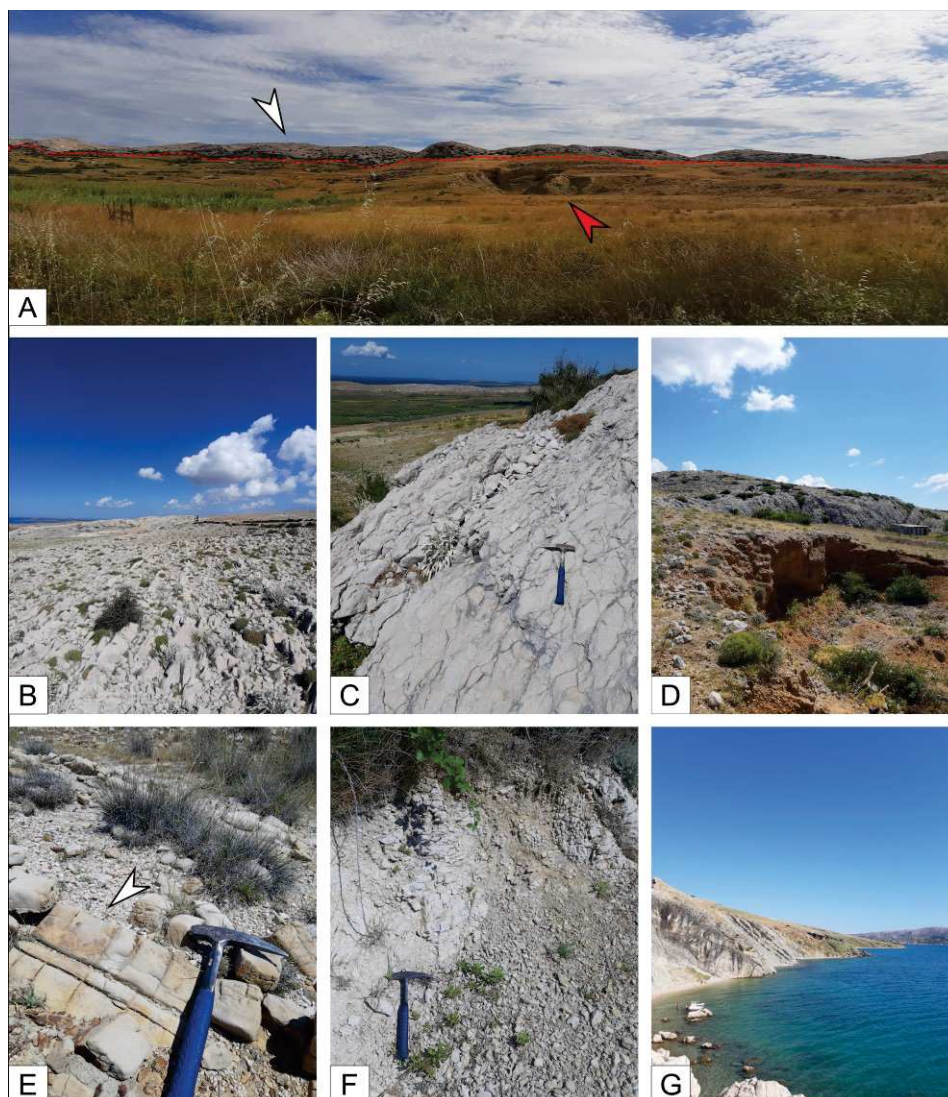


Figure 7.2 Stratigraphy of the Cenozoic deposits cropping out at the Island of Pag. A. Contact between Foraminiferal Limestone (FL; with arrow) and the Dalmatian Flysch (DF; red arrow). B. Lower part of the FL unit; C. Upper part of the FL unit; D. Pleistocene deposits. E. Dalmatian Flysch. F. Transitional beds. G. Outcrops in the area north to the town of Pago, it is possible to appreciate TB and DF.

7.4 Materials and methods

7.4.1 Field work

The analysis of the Dinaric foreland basin units cropping out in the Island of Pag was carried out on the field (by L.M and G.C.) along two successions, giving particular attention to major surfaces, macrofossil distribution, and sedimentary structures. The first succession is 350 m-thick and is exposed near to the village of Vrčići (from 44°23'27.30"N - 15° 8'27.90"E to 44°23'17.10"N - 15° 8'18.60"E). The second succession is less thick and is exposed northward from the town of Pago (44°28'8.27"N - 15° 2'45.98"E). The selection of the investigated area was determined by referring to the geological map and interpretative schemes provided by Mittempergher et al. (2019) and Persico et al. (2019). The analyses focused especially on the FL unit, in which sampling and detailed palaeontological and sedimentological analyses were performed. Moreover, samples were collected from the units that crops out below the FL (i.e., Gornji Humac Formation) and above (i.e., TB and

DF), to better characterise the entire carbonate succession. Since the TB unit is not cropping out in the Vrčiči section, samples of this unit were collected at the other section.

Initially, the exposed units were accurately measured and examined using hand lenses to make a preliminary assessment of the fossil content and sedimentological features. Significant structures and textures were also recorded. Subsequently, rock samples were collected from the Vrčiči section, approximately every 2-3 m, or with a higher resolution where significant changes in sedimentological patterns or palaeontological content were recorded. In total more than 100 samples (P1 to P106) were collected at the Vrčiči section. Within the Pago section, the studies focused on the TB, where four samples (from PI to PIV) were collected, and on the DF (sample P107). Samples PI to PIV were collected in the lower layers of the TB, which were easily accessible and rich in bioclasts.

7.4.2 Laboratory analysis

Thin sections of the collected samples were prepared at the laboratory of the Department of Earth and Environmental Sciences at Milano-Bicocca University by G.C., L.M and M.A. Initially, the rock samples were cut into manageable-sized pieces using a large blade. Where necessary, the samples were embedded in epoxy resin (ARALDITE DBF BD + REN HY 956; ratio of 5:1) to fill pores and strengthen the samples. The samples were then cut into thin-section-sized elements, and the designated surface, if necessary, was covered with epoxy resin (ARALDITE DBF BD + REN HY 956; ratio of 5:1) to eliminate porosity. Excess resin was removed using silicon carbide abrasive paper (Grit 600), and the surface was polished using silicon carbide powder (Grit 800). Once the surface was polished, the samples were cleaned in an ultrasound bath. After the surface dried, weakest samples were covered again with a thin layer of epoxy resin (ARALDITE DBF BD + REN HY 956; ratio of 5:1) to eliminate any remaining porosity, both original and related to the preparation process. After drying, excess resin was removed using silicon carbide abrasive paper (Grit 1000). At the end, the surface of all samples was polished with silicon carbide powder (Grit 1200). The samples were washed once more in an ultrasonic bath, and after drying, they were attached to standard thin-section glasses using UV-sensitive loctite (LOCTITE 3491). The excess material was removed using a Brumat thin-section saw. The thin sections were then reduced to a thickness of 150 µm using the diamond grinding cup-wheel end (Grit 400) of the Brumat thin-section saw. Further reduction to the desired thickness was achieved through hand-polishing, initially using silicon carbide powder (Grit 1000) and then Grit 1200. The final polishing step involved the use of aluminium oxide with a grain size of 1 µm. In total, 125 thin sections were prepared using this method. Thin sections were then examined at the University of Milano-Bicocca and at the University of the Balearic Islands under a transmitted light optical microscope to analyse microfacies and rock texture. For the classification of carbonate rocks, we relied on Dunham's (1962) classification, expanded by Embry and Klovan (1971) and refined by Lokier and Al Junaibi (2016).

The paleoenvironmental interpretation primarily relied on the quantitative analysis of foraminiferal assemblages. In each section, benthic foraminifera were identified at the lowest possible taxonomic level, grouped in categories with different ecological significance, and then counted. To avoid bias related to phenomena such as transport, only well-preserved and almost intact tests have been counted. We considered the following categories: large miliolids (*Orbitolites*, *Alveolina*, peneroplids), nummulitids (e.g., *Nummulites*, *Assilina*, *Operculina*), orthophragminids, asterigerinids/amphisteginids, other hyaline LBF, small miliolids, small rotaliids, small textulariids, large agglutinated, planorbulinids, rounded acervulinoidea (*Sphaerogypsina*, *Discogypsina*), *Fabiania*, victoriellidae, planktic foraminifera. To standardise the foraminifera counting, the area of every section has been measured with a micro-caliper and then, for each section, the number of foraminifera has been divided for the correspondent area. Foraminifera counts was used to assess different ecological parameters, e.g., the orthophragminids/nummulitids ratio (O/N), hyaline/porcelaneous ratio (H/P), and planktic/benthic foraminifera ratio (P/B), which are usually depth-related. These parameters, which generally increase with increasing water depth, have been studied by Hallock and Glenn (1986), Ćosović et al. (2004), and Beavington-Penney and Racey (2004).

For each section, the skeletal assemblages were examined and quantified using point-counting, following Flügel's (2010) method. This analysis utilized a 250 µm grid, with over 400 points identified in each analysed section. Full results of point-counting and foraminiferal counting analyses are included in Supplementary Table 7.1.

Data from foraminifera counting were processed also with multivariate statistical analysis. In particular, Q-mode cluster analysis was performed, in order to analyse similarities between the samples based on the foraminiferal content. MDS analysis was carried out to identify the similarity of different foraminiferal groups on the foraminifera counting dataset. Multivariate statistical analysis was performed with the software Primer v.6 and no data transformation was applied.

Large benthic foraminifera stratigraphy is based on Sartorio and Venturini (1988), Serra-Kiel et al. (1998), and BouDagher-Fadel et al. (2018).

Six samples from DF and TB were prepared as standard smear slides and analysed by E.M. for calcareous nannofossils using a polarised light microscope at 1000x. Calcareous nannofossil biostratigraphy is based on Martini (1971) NP biozones and Agnini et al. (2014) CNE biozones.

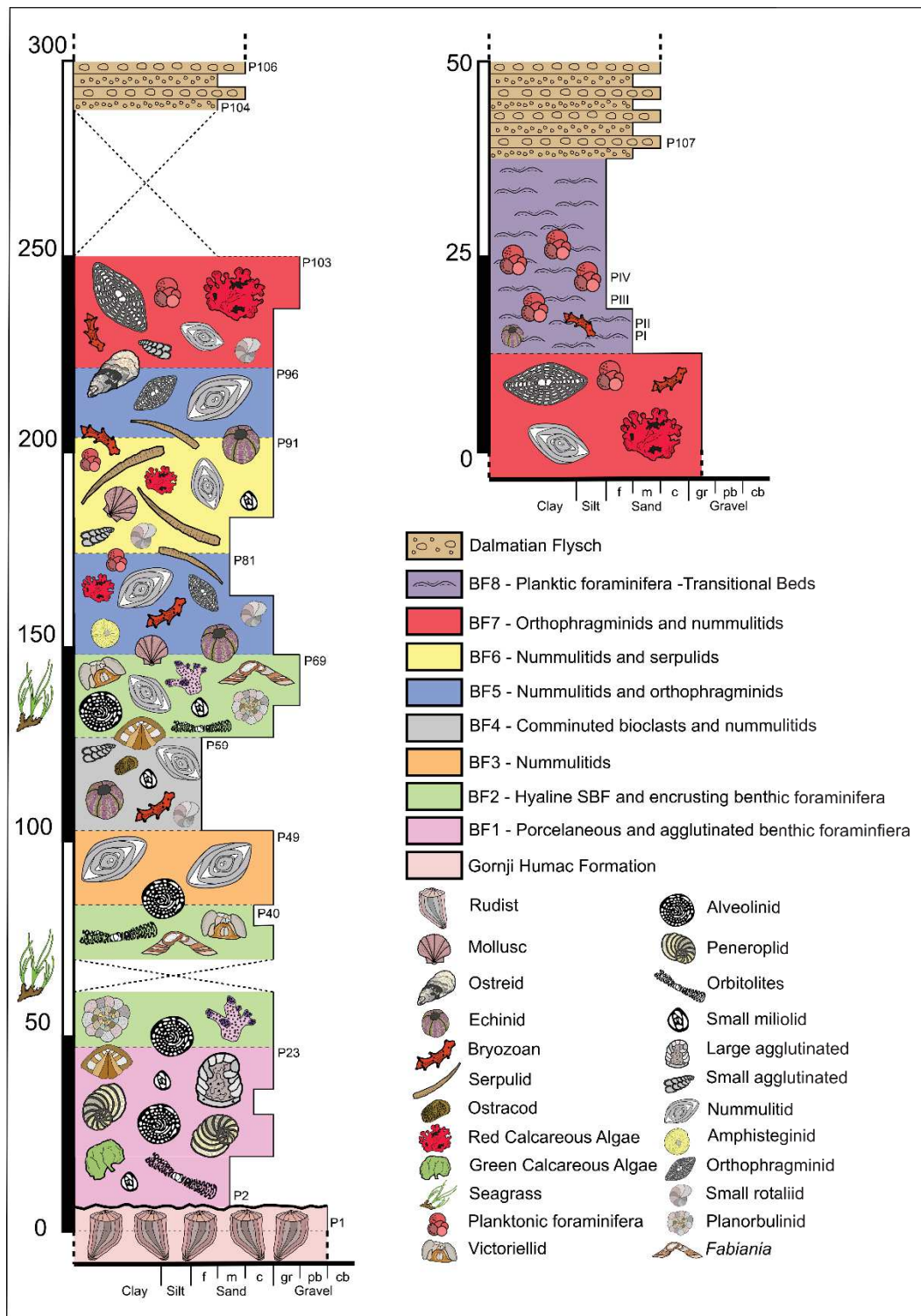


Figure 7.3 Stratigraphic log of the two analysed outcrop, showing different microfacies within the Foraminiferal Limestone unit.

7.5 Results

7.5.1 Field work

At the Vrčići site the succession is continuous and clearly exposed, and the entire sequence was followed avoiding the presence of faults and other tectonic features. The outcrops primarily comprise carbonate and carbonate-mixed deposits belonging to the FL. These deposits are characterized by a

steep stratification (average attitude of 225/80) and are exposed along the right flank of a NW-SE trending synclinal fold, which divides the Island of Pag into two sectors. The base of the succession is represented by the rudist-bearing heavily fractured and altered, pinkish limestone of the Gornji Humac Formation (Fig 7.4A). The FL lies on the Upper Cretaceous Gornji Humac Formation, with an angular unconformity of approximately 10°. The contact between these two units is well-defined and consists of an erosive surface.

The basal portion of the FL exhibits a high degree of fracturing, primarily attributed to tectonic activity but also influenced by surface alteration and karstification processes. Despite these features, it was possible to trace the entire succession relatively easily and collect well-preserved samples. From a mesoscale palaeontological point of view, the FL exposed in this site is rich in benthic foraminifera, along with subordinate echinoderms, molluscs, and occasional bryozoans. In the basal portion, the FL deposits consist of mostly greyish wackestones to packstones, featuring large benthic foraminifera, including common large miliolids (e.g., alveolinids), distinguishable at the mesoscale due to their morphology and their whitish colour, and large rotaliids (mainly nummulitids), accompanied by fragments of molluscs, green algae, and other small, indistinct bioclasts (Fig 7.4B). Continuing along the outcrop for approximately 12 meters (sample P8), the abundance of macroforaminifera increases, and microspheres with diameters exceeding one centimetre become recognisable, accompanied by molluscs, including recrystallized gastropods. At sample P11, foraminifera notably increase in size, and appear randomly oriented within the deposits. Small solitary corals and echinoid models are also observed (Fig 7.4C). Locally, there is a transition from packstones to grainstones composed almost entirely of bioclasts. From mesoscale observations up to sample P32 (covering a thickness of approximately 40 meters), no significant facies changes are noted, except for localized variations.

At this height, the succession is interrupted by a 10-m-wide dirt road, and the sequence resumes immediately after crossing it (44°23'25.8"N – 15°08'25.1"E). Here, the deposits are richer in LBF, particularly nummulitids, as compared to the previous deposits where large miliolids dominated (Fig 7.4D). Other hyaline LBF and fragments of echinoids and molluscs are also visible at the mesoscale. Moreover, LBF begin to increase in size, with more microspheres reaching centimetre-scale dimensions. Abundant echinoid internal moulds are observed in this facies, especially irregular ones, along with solitary corals. It is important to note the lateral variability characterising this facies, with LBF being abundant and highly concentrated in some areas, locally forming rudstones (Fig 7.4E). Additionally, microsphere tests often display a similar orientation.

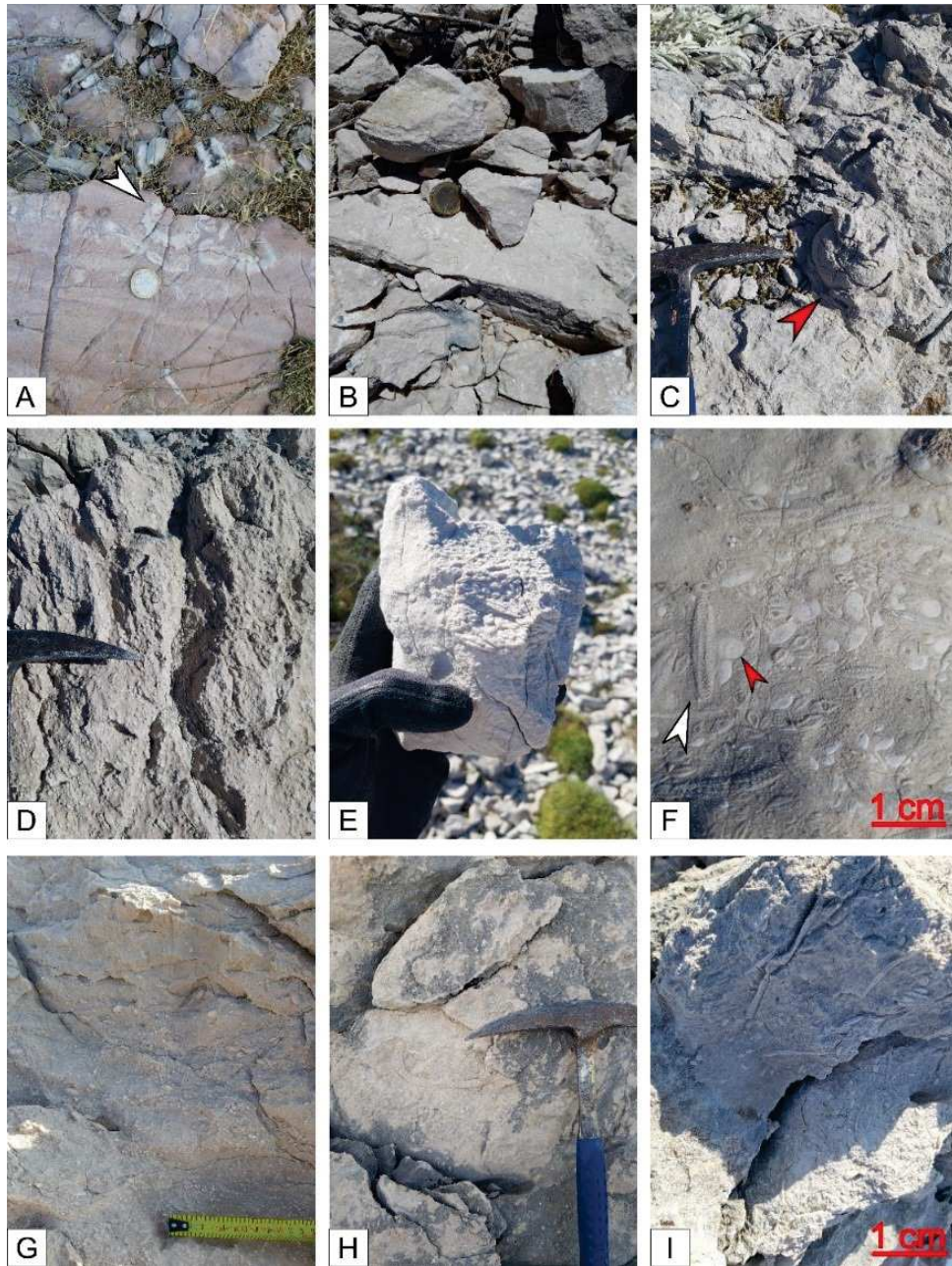


Figure 7.4 A. Greyish-to-pinkish carbonates of the Gornji Humac Formation. The white arrow indicates a rudist. B. Basal FL deposits. They consist of floatstones in which it is possible to appreciate large benthic foraminifera (primarily alveolinids). C. FL unit. The red arrow indicates a well-preserved echinoderm internal model. D. Karstification processes on the FL units. It is possible to appreciate the large abundance of benthic foraminifera. E. Sample from the FL unit. It is possible to appreciate the lateral variability of this deposits, even at small scale: the right side of the sample consists of a rudstone mainly composed by large benthic foraminifera; the left side consists of wackestone/floatstone less rich in allochems. F. Detail of a rudstone within the FL unit. The white arrow indicates a nummulitid; the red arrow points to an alveolinid. G. Rudstones/Floatstones from the middle part of the FL unit. H. Bioturbation trace fossil within the FL unit; I. Middle-upper part of the FL unit. It is possible to appreciate large benthic foraminifera tests with flat morphology, indicating deeper conditions.

Towards the top, karstification phenomena become more pronounced (Fig. 7.4G). Starting from sample P63 the FL generally displays a rudstone to floatstone texture with large benthic foraminifera microspheres exhibiting flat morphologies (Fig 7.4I). However, lateral variability remains high.

Moreover, in this part of the succession the first occurrences of *Assilina* microspheres are observed, and orthophragminids specimens are also noted.

From sample P76 the FL is characterized by a reduced abundance of foraminifera and the decrease in their size, along with a sharp increase of the abundance of serpulids of the genus *Ditrupa*. From sample P88 upwards the deposits are characterised by centimetre-scale orthophragminids and flat nummulitids, concentrated in unevenly-distributed lenses (Fig. 7.5B, C). Serpulids, *Pycnodonte gigas*, vermetids, articulated bivalves, and echinoids are also present (Fig. 7.5A, D). Bioturbation and similar orientation of the bioclasts were locally observed.

From sample P97 onwards the FL consists of rudstones/floatstones with large benthic foraminifera (including abundant *Assilina* and flat *Nummulites*) (Fig. 7.5E), irregular echinoids, red algae (forming rhodoliths) (Fig. 7.5F), and oysters.

The succession continues for about 18 meters and ends at in correspondence of sample P103 (Fig. 7.3). At this point, Pleistocene deposits, recent sediments, and anthropogenic activities prevent further tracking (Fig. 7.2). However, the Eocene deposits crop out again 40 m downslope, where the Dalmatian Flysch (DF) is exposed. The latter is characterized by alternating well-sorted marly and sandy layers, almost devoid of bioclasts.

The TD unit was sampled a few kilometres North on the island, near the town of Pago (Fig 7.1), where it is exposed in continuity with the upper part of the FL. The basal layers of the TB are relatively rich of bioclasts, including common echinoids and rare bryozoans (PI and PII). Bioturbation is also evident. Further above, the amount of bioclasts decrease and the amount of fine-grained material increases (sample PIII). At the top of the TB, bioclasts can no longer be observed on the outcrop surface (sample PIV) and the overlying DF, similarly to the Vrčići outcrop, consists of alternating layers of sandstones and marls.

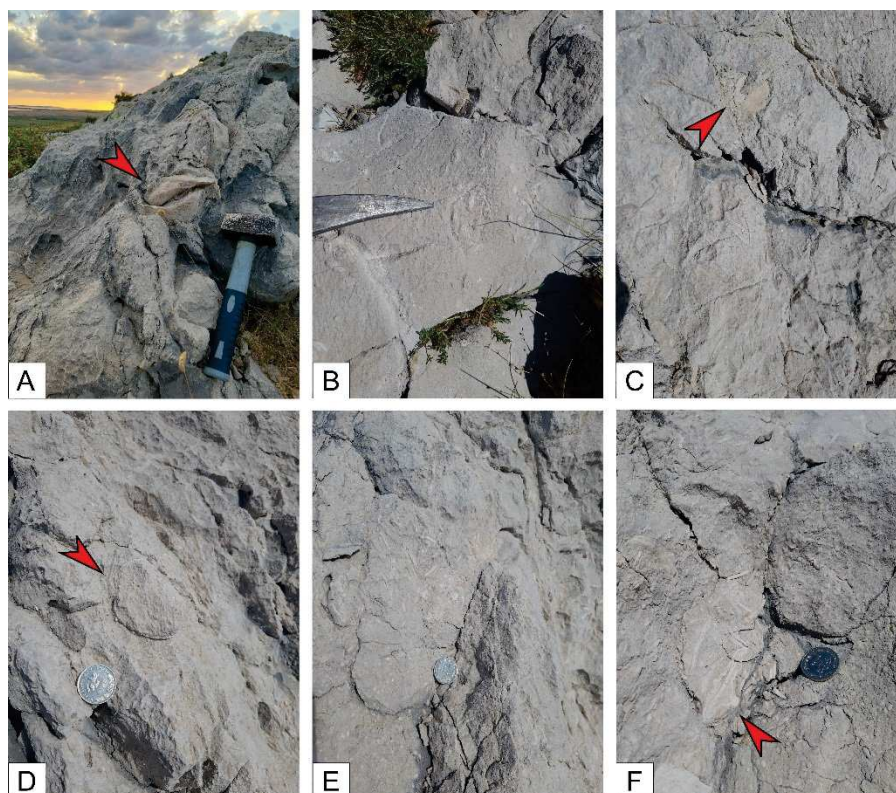


Figure 7.5 Outcrops of FL at Vrčici A. Red arrow indicates a *Pycnodonte gigas* specimens within the FL deposits. B. LBF rudstones/floatstones within the FL; C. LBF rudstones/floatstones within the FL, red arrow indicates a large nummulitid test. D. Red arrow indicates an articulated bivalve specimens within the LBF rudstones; E. Upper part of the FL. F. Upper part of the FL, red arrow indicates a red calcareous alga.

7.5.2 Microfacies analysis

Based on the quantitative analysis of the foraminiferal associations and the skeletal assemblages of the studied section, seven main biofacies have been recognized within the FL and one biofacies within the TB (Fig. 7.6; Table 7.1). These facies have been also constrained by multivariate statistics (Fig. 7.7):

1. *BF1 Porcelaneous and agglutinated benthic foraminifera biofacies*: this biofacies occurs at the base of the FL and lies above the Cretaceous Gornji Humac Formation. It comprises sample P2-P23, with total a thickness of about 45 m. It comprises mostly wackestones to floatstones, locally grainstones. Generally, the grains occur dispersed in a matrix consisting of mud-sized fragments of large miliolid tests. The terrigenous fraction, evaluated at the optical microscope, is very low. The skeletal assemblage is dominated by small benthic foraminifera (SBF; 52.45%) and LBF (32.81%); green calcareous algae (GCA), molluscs, echinoderms are common; ostracods and encrusting foraminifera (EBF) are rare. Non skeletal grains such as pellets and intraclasts also occur.

The foraminiferal association is characterised by large miliolids (5.52%), mostly alveolinids and peneroplids (e.g., *Peneroplis*, *Spirolina*), and *Orbitolites* to a lesser extent. Large,

agglutinated taxa (e.g., *Coskinon*, *Cribrbulimina*, *Pseudocrysalidina*, *Haddonia*) are also relevant (7.26%). Hyaline LBF (e.g., *Lockhartia*) are very-rare (0.66%). SBF are abundant along all the biofacies (44.19%); within them, small miliolids are the most abundant group (e.g., *Quinqueloculina*, *Spiroloculina*, *Triloculina*, *Idalina*, *Pyrgo*), followed by hyaline SBF (29%). Among hyaline SBF, the most common taxa are Bolivinitidae, Nonionidae, Reussellidae and Calcarinidae. Small, agglutinated taxa are abundant, too (13.23%). The preservation of the allochems is generally good; the taxa most affected by diagenesis are miliolids, especially alveolinids, that are commonly found with deformed, broken or partially dissolved tests.

2. *BF2 Hyaline SBF and encrusting benthic foraminifera biofacies*: this biofacies comprises samples P24 - P40 and samples P60 - P69, for a total thickness of about 50 m. It is mostly characterised by floatstones and rudstones in a packstone matrix. The matrix is constituted by micrite, bioclastic fragments and, less commonly, by sparite. The bioclastic fragments constituting the matrix generally consist of alveolinid fragments. The terrigenous fraction is low. The skeletal assemblage is dominated by LBF (44.15%) and SBF (27.99%); EBF (7.17%) are common and often display and hooked or tubular morphology; echinoderms and molluscs are common, too; red calcareous algae (RCA), bryozoans, serpulids and ostracods are rare. The foraminiferal association is characterised by the abundance of large miliolids (7.6%), especially alveolinids and *Orbitolites*, whereas peneroplids are present to a lesser extent. Large, agglutinated taxa are rare (1.26%), and consist mainly of *Cribrbulimina* specimens and very rare *Haddonia*. Hyaline LBF are common from sample P24 to P40 and consists mostly of Rotaliinae (e.g., *Rotalia*). From sample P60 to P69 nummulitids start to become abundant (16.80%; mainly *Nummulites*, but also *Assilina* and *Operculina*). Encrusting taxa such as *Fabiania*, *Eofabiania*, planorbulinids and victoriellids (e.g., *Gyroidinella*, *Eurupertia*) are common. Hyaline SBF are abundant (39.48%), and comprise a large amount of Cibicididae (e.g., *Lobatula*), Rosalinidae, Reussellidae, Calcarinidae and other infaunal taxa (e.g., *Bolivina*). In some cases, Cibicididae display a curved morphology. Small miliolids (e.g., *Quinqueloculina*, *Spiroloculina*) are abundant (21.09%). Small, agglutinated taxa are also common (7.50%). Dissolution processes affected the miliolids and it is common to find entire alveolinid tests completely deformed. Fragmented bioclasts are also common, especially from sample P69 to P69.
3. *BF3 Nummulitid biofacies*: this biofacies comprises samples P41 - P49, for a thickness of about 15 m. It is mostly characterised by floatstones with a micritic matrix. The dominant

components are LBF (46.3%) and SBF (26.53%); RCA, echinoderms, and molluscs are common; serpulids, GCA, EBF, ostracods, planktic foraminifera and bryozoans are rare.

The foraminiferal association is characterised by abundance of nummulitids (12.48%), especially *Nummulites*, but also *Assilina* and *Operculina* specimens are present. Other hyaline LBF are also present (4.74%), mainly asterigerinids and amphisteginids. Large miliolids are still present (3.85%), mostly alveolinids and *Orbitolites*. The latter are less common than in the previous biofacies. Hyaline SBF are very abundant (45.61%), and comprises Calcarinidae, Cibicididae, *Lenticulina*, and other infaunal taxa. Small miliolids (20.71%) are still abundant; small, agglutinated taxa (5.88%) are common. Moreover, this biofacies is characterised by the presence of some rounded acervulinoidea (e.g., *Sphaerogypsina*, *Discogypsina*; 2.90%). Dissolution on porcelaneous tests is still a common feature. This biofacies is also characterised by the presence of abundant bioeroded and/or broken bioclasts.

4. *BF4 Comminuted bioclasts and nummulitid biofacies*: this biofacies comprises samples P50 - P59, for a thickness of about 30 m. It is characterised by wackestones and mudstones, with an average matrix consisting of micrite, common sparite and rare unrecognizable bioclastic fragments. This biofacies is also characterised by the scarce presence of recognisable biogenic components. The skeletal assemblage is dominated by nummulitids (35.11%) and SBF (27.58%); rare serpulids, echinoderms, molluscs, bryozoans and planktic foraminifera (PF) are also present.

The foraminiferal assemblage is dominated by hyaline SBF (67.72%), mostly Calcarinidae, Cibicididae, Nonionidae, and Bolivinidae. Small miliolids are abundant, too (14.55%). Nummulitids, albeit large in size, are not very high in numbers and only represent a small part of the foraminiferal assemblage (9.88%). Small, agglutinated taxa (4.37%) are rare.

5. *BF5 Nummulitid and orthophragminid biofacies*: this biofacies comprises samples P70 - P81 and samples P92 - P96, with a total thickness of about 50 m. It consists mostly of floatstones to wackstones with an average matrix constituted by micrite and abundant unrecognizable bioclast fragments; sparite is rare. The skeletal assemblage is dominated by LBF (40%) and SBF (20%); PF (e.g., globigerinids, globorotaliid; 5.66%) are common, and their abundance is higher in samples P92 - P96; echinoderms, molluscs, serpulids and bryozoans are common; EBF and RCA are rare.

The foraminiferal association is characterised by the large abundance of nummulitids (20.06%), especially *Nummulites*, followed by *Operculina* and by *Assilina* to a lesser extent. *Nummulites* microspheres displaying a flat morphology are also common. Orthophragminids are abundant (e.g., *Discocyclina*, *Asterociclyna*; 14.91%), and their abundance is higher in

samples P92 - P96. Hyaline SBF are abundant (48.76%) and consists of *Lenticulina*, Calcarinidae, and infaunal taxa. Small miliolids (4.67%) and small, agglutinated taxa (3.40%) are present to a lesser extent. Rounded acervulinoidea and asterigerinids are also present. This biofacies is also characterized by the presence of broken bioclasts, that indicate a higher degree of transport. Bioturbation, bioerosion and bioencrustation phenomena are present.

6. *BF6 Nummulitid and serpulid biofacies*: this biofacies comprises samples P82 - P91 and covers a thickness of about 50 m. It is characterised by wackestones/floatstones in packstone matrix. The average matrix is constituted by micrite, abundant bioclastic fragments and rare sparite. The skeletal assemblage is dominated by serpulids (*Ditrupa*; 17.17%), LBF (27.32%) and SBF (21.14%); echinoderms (13.47%) are abundant, molluscs, bryozoans (6.32%) and planktonic foraminifera (5.28%) are common; RCA, EF, and ostracods are rare.

LBF are mostly constituted by nummulitids (19.36%), in particular *Nummulites* and *Operculina*, with the presence of *Assilina* specimens, too. Orthophragminids are almost absent. Large miliolids (0.83%) are very rare and consists mainly of alveolinids. Small rotaliids (60.96%) are abundant and comprise infaunal taxa like Bolivinitidae and Nonionidae, Cibicididae (*Cibicides*, *Cibicidoides* and *Lobatula*), Reussellidae and Calcarinidae, mostly. Small miliolids (e.g., *Quinqueloculina*, *Triloculina*, *Spiroloculina*; 5.68%) and small, agglutinated taxa (5.53%) are present to a lesser extent. Rounded acervulinidae are present, too. Dissolution on porcelaneous tests is still recognizable. Transport is common, highlighted by the presence of broken bioclasts. Bioturbation phenomena can be recognised, too.

7. *BF7 Orthophragminid and nummulitid biofacies*: this biofacies comprises samples P97 - P103 and its thickness is about 25 m. It consists of floatstones/rudstones in packstone matrix. The average matrix is constituted by a high abundance of micrite, and a lesser amount of bioclast fragments. The terrigenous fraction is scarce, but authigenic minerals, such as glauconite, are present. The skeletal assemblage is dominated by LBF (54.54%), and SBF (12.27%); bryozoans (11.43%), PF (8.32%), RCA (4.99%), echinoderms, molluscs and ostracods are common. Commonly, RCA form centimetre-size rhodoliths.

The foraminiferal assemblage is constituted by a large abundance of orthophragminids (e.g., *Discocyclina*, *Asterocyclina*; 28.26%). Nummulitids (14.12%) are also common and consist mainly of *Nummulites* (often displaying flat tests) and *Operculina*. Small rotaliids (35.78%) are very abundant, and consist of *Lenticulina*, and infaunal taxa. Small miliolids and small, agglutinated taxa are rare. Generally, bioclasts (and especially LBF tests) are iso-oriented. Bioencrustation, commonly by encrusting RCA, and bioerosion are common processes in this biofacies.

8. *BF8 Planktic foraminifera biofacies*: this facies comprises samples PI - PIV. These deposits consist of wackestones/mudstones with a micrite matrix. The skeletal assemblage is largely dominated by PF (33.48%) and SBF (17.90%), but also echinoderms (20.06%) and rare LBF (9.30%) are present.

The foraminiferal association is dominated by PF (50.82%). Small rotaliids (45.54%) are very abundant, whereas small miliolids and small, agglutinate taxa are rare. LBF consist mainly of few nummulitid and orthophragminid specimens.

Multivariate Q-mode statistic applied on the foraminiferal counting dataset displays a dendrogram that allows the identification of three main clusters, containing different samples. The distribution of the samples is visible in Fig. 7.7. MDS analysis made on the foraminiferal counting dataset produced a graphic showing the similarity among the different foraminifera groups considered in the analysis (Fig 7.8).

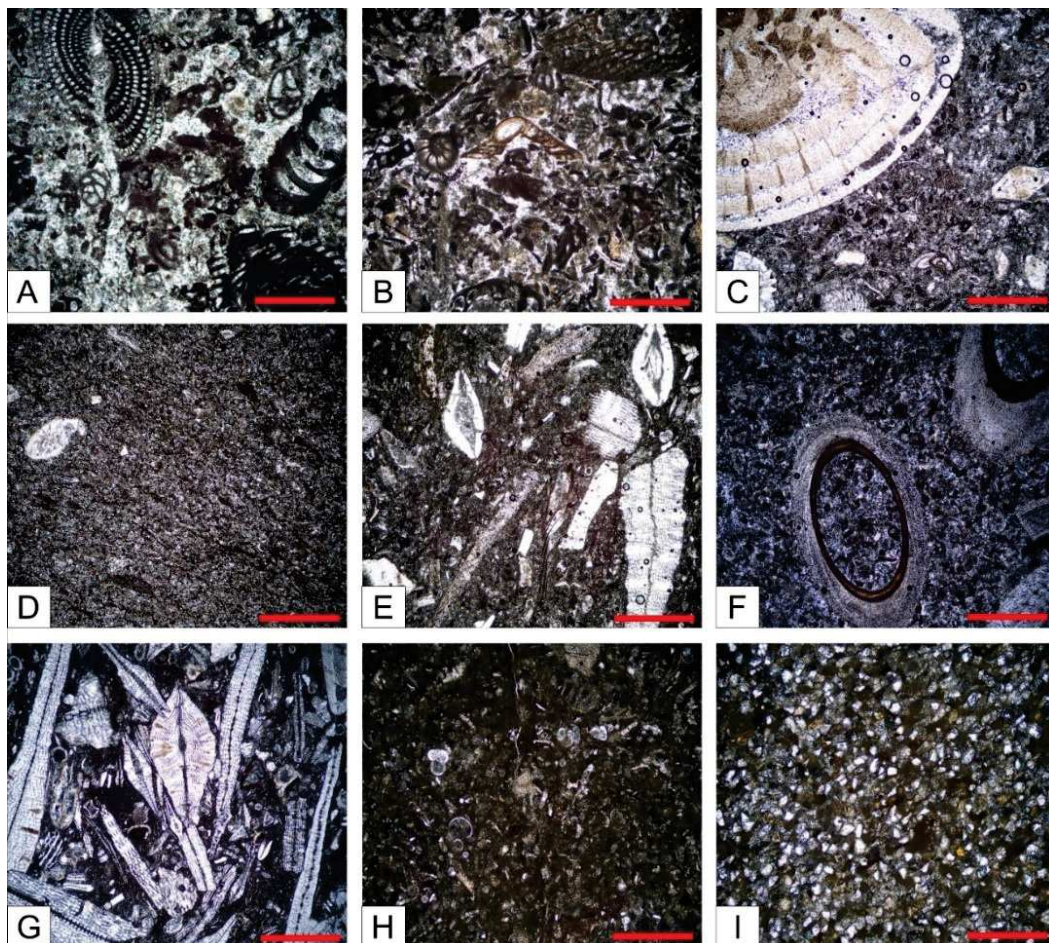


Figure 7.6 A. Porcelaneous and agglutinated benthic foraminifera biofacies (BF1); B. Hyaline SBF and encrusting benthic foraminifera biofacies (BF2); C. Nummulitids biofacies (BF3); D. Comminuted bioclasts and nummulitids biofacies (BF4); E. Nummulitid and orthophragminid biofacies (BF5); F. Nummulitid and serpulid biofacies (BF6); G. Orthophragminid and nummulitid biofacies (BF7); H. Planktic foraminifera biofacies (BF8); I. Dalmatian Flysch.

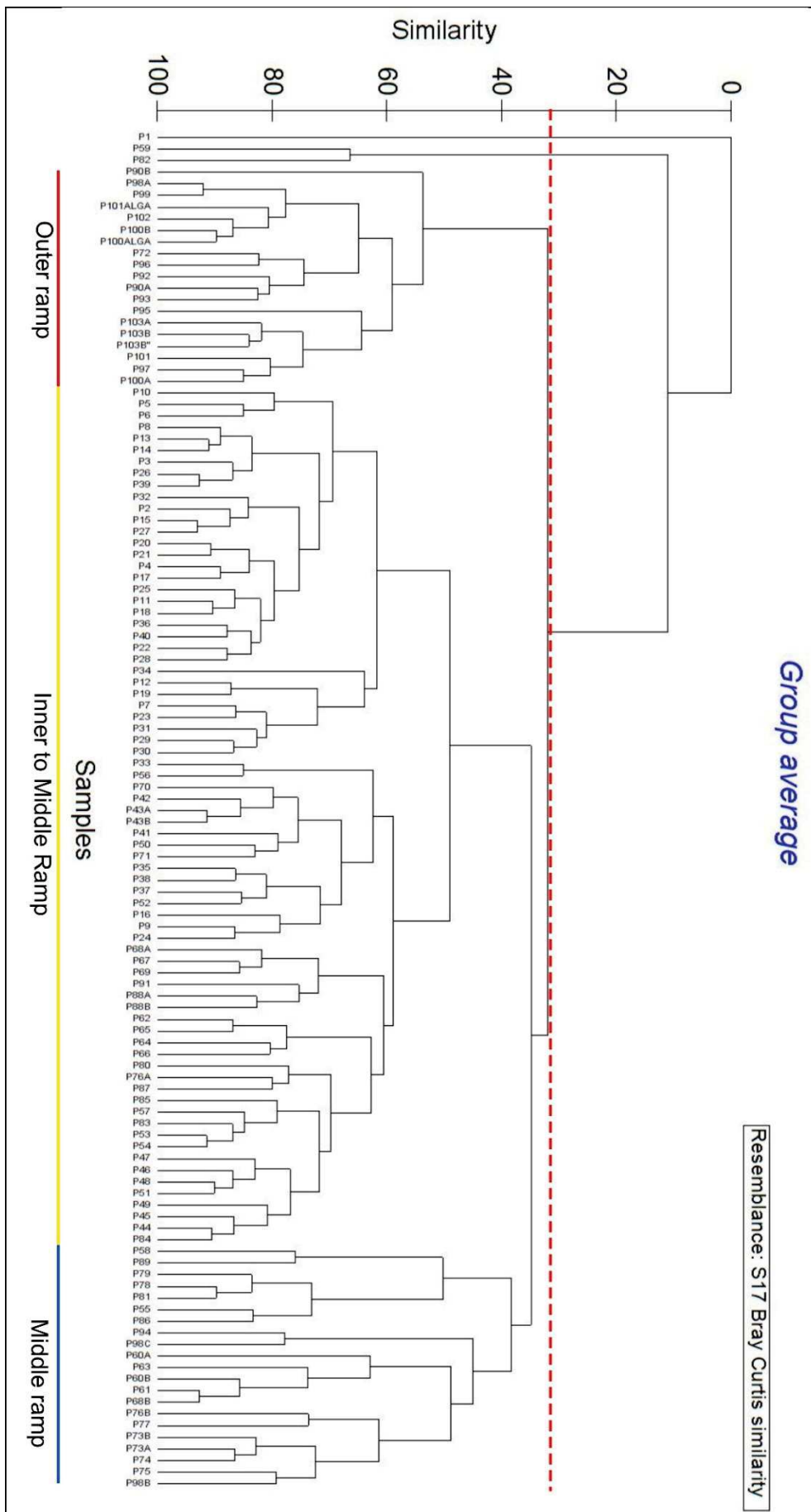


Figure 7.7. Q-mode cluster analysis on the foraminiferal counting dataset

Biofacies	BF1	BF2	BF3	BF4	BF5	BF6	BF7	BF8
Skeletal assemblage (point counting)								
RCA (encrusting + articulated)	0.00	2.43	3.82	1.16	1.31	2.74	4.99	0.00
Hyaline LBF	0.00	4.27	4.74	2.69	2.68	4.08	2.54	0.00
<i>Fabiania</i>	0.00	4.01	0.00	0.00	0.00	0.00	0.00	0.00
Nummulitids	0.00	13.23	27.10	35.11	20.23	19.36	19.69	2.01
Orthophragminids	0.00	0.00	0.00	0.00	17.16	1.18	32.31	7.29
Hyaline SBF	16.49	13.44	13.89	16.66	14.01	15.12	12.27	17.90
Encrusting Acervulinids	0.69	7.17	0.72	0.00	0.63	0.53	0.00	0.00
Alveolinids	12.81	12.21	9.00	0.00	0.00	0.96	0.00	0.00
Other Large Miliolids	6.19	7.38	5.46	0.00	0.35	1.74	0.00	0.00
Small Miliolids	24.56	10.08	8.49	5.25	3.17	4.23	0.00	0.00
Large Textulariids	13.81	3.05	0.00	0.00	0.00	0.00	0.00	0.00
Small Textulariids	11.40	4.47	4.15	5.67	2.39	1.79	0.95	4.70
Planktic foraminifera	0.39	0.00	2.10	0.64	5.66	5.28	8.32	33.48
Mollusks	1.93	3.52	4.10	7.77	4.22	3.76	0.48	2.32
Echinoids	4.26	11.32	7.64	9.14	13.16	13.47	5.64	20.06
Bryozoans	0.17	2.40	3.15	6.29	9.90	6.32	11.43	5.29
Serpulids	0.00	0.11	0.32	3.50	4.58	17.17	0.42	1.49
Ostracods	4.46	0.28	3.39	6.12	0.22	2.26	0.96	5.47
GCA	2.83	0.63	1.93	0.00	0.18	0.00	0.00	0.00
Corals	0.00	0.00	0.00	0.00	0.15	0.00	0.00	0.00
Foraminiferal assemblage (foraminiferal counting)								
<i>Orbitolites</i>	0.42	2.00	1.79	0.00	0.04	0.37	0.00	0.00
Alveolinids	2.85	4.55	1.94	0.32	0.06	0.46	0.00	0.00
Peneroplids	2.25	1.05	0.12	0.00	0.00	0.00	0.00	0.00
Nummulitids	0.00	16.80	12.48	9.88	20.06	18.88	14.12	0.33
Orthophragminids	0.00	0.00	0.00	0.00	14.91	0.06	28.26	0.47
Hyaline LBF	0.66	2.74	5.31	1.28	0.90	4.03	1.40	0.14
large agglutinated	7.26	1.26	0.44	0.00	0.00	0.00	0.00	0.00
<i>Fabiania</i>	0.00	1.19	0.00	0.00	0.00	0.00	0.00	0.00
Planorbulinids	0.00	0.58	0.00	0.00	0.00	0.00	0.00	0.00
Rounded acervulinoidea	0.00	0.00	2.90	0.39	0.66	0.55	0.06	0.00
Victoriellids	0.00	1.66	0.34	0.23	0.12	0.04	0.00	0.00
Hyaline SBF	29.06	39.48	45.61	67.72	48.76	60.96	35.78	45.54
Small miliolids	44.19	21.09	20.71	14.55	4.67	5.68	1.10	0.20
Small textulariids	13.23	7.50	5.88	4.37	3.40	5.53	2.62	2.50
Planktic foraminifera	0.08	0.12	2.48	1.26	6.42	3.42	16.66	50.82
Parameters								
O/N	\	\	\	\	0.7435	\	2.0017	1.4156
P/B	0.0008	0.0012	0.0255	0.0127	0.0686	0.0354	0.1999	1.0333
H/P	0.5979	2.1767	2.5953	5.3201	17.7673	12.8986	72.3272	232.40
Sedimentological observations								
Autigenic minerals	0.00	0.00	0.00	0.00	0.00	0.00	0.36	1.73
Sparite	9.21	5.77	2.99	1.69	2.11	0.84	0.74	0.19
Detrital Fraction	0.07	0.26	0.13	0.09	0.03	0.00	0.00	0.12

Micrite	18.47	0.03	5.94	2.98	2.81	0.21	10.53	10.90
Fine sand sized fraction 63 - 250 μm	33.07	34.17	52.41	85.82	57.41	69.42	31.80	67.77
Medium sand sized fraction 250 - 500 μm	0.54	4.62	0.00	0.00	3.97	2.16	0.27	0.00
Coarse sand sized fraction 500 μm - 2 mm	23.08	12.94	11.48	3.50	11.74	7.44	13.78	14.96
Gravel fraction > 2 mm	11.08	26.92	26.87	5.29	21.46	17.89	42.52	4.34
Non skeletal grains	4.47	15.30	0.18	0.62	0.46	2.03	0.00	0.00

Table 7.1. Quantitative dataset of the i) skeletal assemblage composition (point counting), ii) foraminiferal association (foraminifera counting), iii) calculated palaeoecological parameters (O/N: orthophragmids/nummulitids; P/B: planktic/benthic foraminifera; H/P: hyaline/porcelaneous foraminifera), and iv) sedimentological observations.

7.6 Discussion

7.6.1 Biostratigraphy

In the literature, the FL has been dated to the Early Eocene (e.g., Tišljarić et al., 2002; Čosović et al., 2004; Mittempergher et al., 2019). In the studied section, the FL has been dated based on the distribution of the LBF fauna, focusing on the most readily identifiable biological events (Sartorio and Venturini, 1988; Serra-Kiel et al., 1998). Based on the LBF assemblage the base of the FL, characterised by the BF1 biofacies, is dated at the Ypresian, most likely between SBZ10 and SBZ12 (Serra-Kiel et al., 1998). This is indicated by the presence of i) *Coskinon* (Hottinger and Drobne, 1980; BouDagher-Fadel et al., 2018), ii) large cylindrical and fusiform *Alveolina* specimens (Sartorio and Venturini, 1988), iii) the simultaneous presence of *Alveolina*, *Coskinon*, and *Pseudochrysalidina* (Sartorio and Venturini, 1988), iv) *Cribrbulimina*, which belong to Valvulininae subfamily and is a common feature from the Palaeocene to the Early Eocene (Sartorio and Venturini, 1988).

Ypresian-Lutetian boundary (SBZ12-SBZ13; Serra-Kiel et al., 1998) is placed at the boundary between BF1 and BF2 on the basis of the following observations: i) the presence of very elongated to subcylindrical forms of *Alveolina*, that started to appear in the upper part of the Early Eocene (Sartorio and Venturini, 1988; BouDagher-Fadel et al., 2018); ii) the absence of common *Coskinon* or other large agglutinated taxa (Sartorio and Venturini, 1988); iii) the occurrence of *Nummulites* displaying evident pillars, typical of Middle Eocene assemblages (Sartorio and Venturini, 1988); iv) the presence of *Eorupertia* and the abundance of victoriellids typical of the Middle Eocene (Sartorio and Venturini, 1988); v) the occurrence of abundant *Fabiania* (Sartorio and Venturini, 1988); vi) the simultaneous presence of abundant *Assilina*, *Discocyclina*, *Nummulites* and *Operculina*, which indicate most likely Middle Eocene age (Sartorio and Venturini, 1988).

The DF, instead, has been dated to the Middle Eocene by different authors (e.g., Babić and Zupanič, 2008). Previous analyses of calcareous nannofossils (Persico et al. 2019), along a section of the DF exposed at the site of Vrčiči (the same site analysed in this work), suggested deposition of the base of the DF within the CNE14 biozone (42.37–40.51 Ma) of Agnini et al. (2014), based on the lowest

common occurrence of *Reticulofenestra reticulata* and the highest occurrence of *Sphenolithus furcatolithoides* (Persico et al., 2019). Samples from the TB (PI-IV) showed rare and badly preserved calcareous nannofossils. Samples from the DF (P104-106 + P107) were barren, excluding one sample (P106) showing common and well preserved nannofossils. The latter sample is assigned to CNE14, based on the presence of *R. reticulata* along with other common middle-Eocene species (*Pontosphaera distincta*, *P. pulcheroides*, *P. pulchra*, *Reticulofenestra bisecta*, *R. wadeae*, *S. furcatolithoides*) and the absence of *R. stavensis* (FO 40.34 Ma).

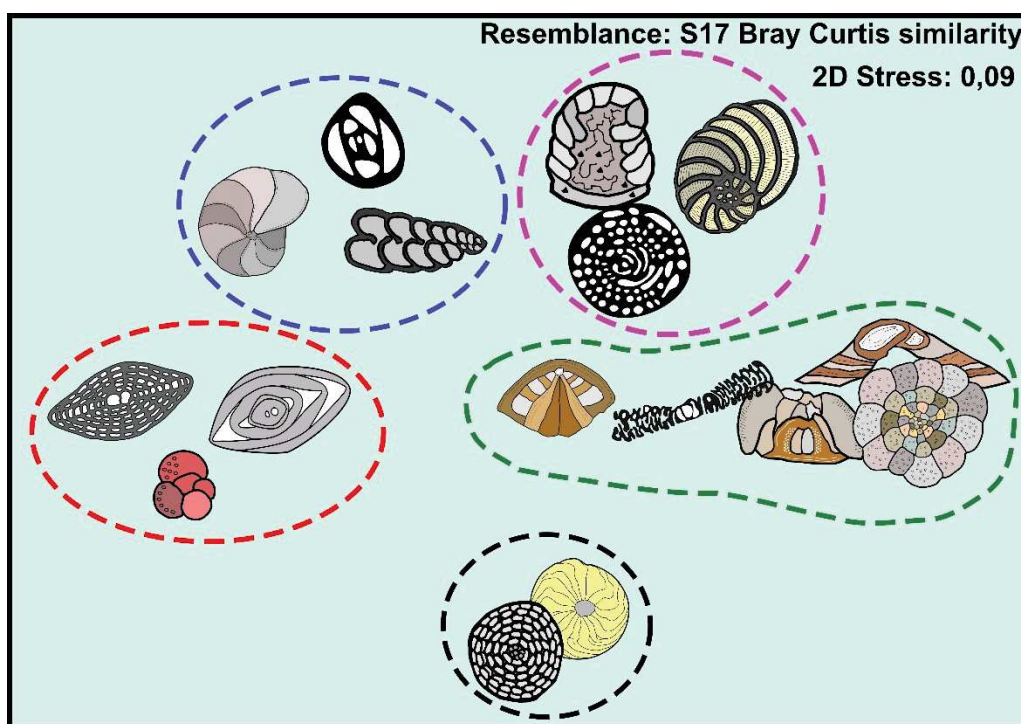


Figure 7.8 MDS analysis results. It is possible to identify 5 different clusters containing different foraminifera groups: i) large agglutinated foraminifera, peneroplids and alveolinids (pink); ii) *Orbitolites*, victoriellids, *Fabiania*, planorbulinids and hyaline LBF (green); iii) orthophragminids, nummulitids and planktonic foraminifera (red); iv) hyaline SBF, small miliolids and small textulariids (blue); and v) amphisteginids/asterigerinids and rounded planorbulinids (black).

7.6.2 Facies interpretation and palaeoenvironmental reconstruction

Microfacies analysis relies on the comparison between fossil and modern allochem assemblages. However, the distribution of allochems is not linear, and depends on different combinations of variables: depth, temperature and trophic state are interchangeable, implicating a level of non-uniqueness for palaeoenvironmental reconstructions (Bialik et al., submitted).

The skeletal assemblages of the Eocene FL of Pag Island indicate in all likelihood tropical conditions, being dominated by LBF and SBF adapted to oligo-mesotrophic conditions. Terrigenous input is scarce along all the FL sequence, with a slight increase in the TB and a significant input in the DF. Heterozoan organism, e.g., echinoderms, molluscs, serpulids, bryozoans, RCA, are present along the

entire succession but never become dominant, pointing to tropical, shallow-water, oligotrophic conditions.

A general model of LBF distribution in modern and fossil carbonate depositional environments has been developed by Hallock and Glenn (1986), from data on tropical settings (Brasier, 1975a, 1975b; Hallock, 1980, 1983, 1984; Glenn et al., 1981; Hottinger, 1983a; Reiss and Hottinger, 1984). This model has undergone refinement, strengthening through studies of modern assemblages, and application to diverse Cenozoic basins (e.g., Bassi, 1998; Moody, 1998; Accordi et al., 1998; Sinclair, 1998; Beavington-Penney and Racey, 2004). Čosović et al. (2004) proposed a depositional model of the Istrian Platform (northern Croatia), which is comparable with the other models proposed for other Eocene carbonate platforms. This model includes the following settings: i) inner ramp, characterised by medium to coarse-grained LBF-molluscs packstones (Drobne and Čosović, 1998), with the presence of larger miliolids (alveolinids, *Orbitolites*), larger agglutinated taxa (*Coskinolina*), *Nummulites* and *Assilina*; ii) middle ramp, characterised by foraminiferal packstones and floatstones dominated by *Operculina*, *Nummulites*, *Discocyclina*, *Orbitochypeus*, and *Asterocyclina*; iii) outer ramp, characterised by fine-grained wackestones dominated by orthophragminids and PF-dominated wackestones to mudstones (Čosović et al., 2004).

Overall, in shallow and restricted environments, such as sheltered back-shoal lagoon, up to 20 m of depth, miliolids are very abundant (e.g., soritids, alveolinids, small miliolids), and can dominate the foraminiferal assemblage. Large, agglutinated taxa are also common. Inner ramp, reef settings are characterized by the dominance of hyaline LBF displaying robust and thick tests. Thin and flat hyaline LBF, such as *Operculina*, or orthophragminids like *Discocyclina*, dominate communities in the lower photic zone, up to 200 m of depth, and are associated with common planktic foraminifera (Hallock and Glenn, 1986; Coletti et al., 2021).

These models can be applied to the analysis of the FL deposits outcropping at Pag Island, using our data on foraminiferal assemblage to constrain the environmental conditions during the deposition of each biofacies. The various biofacies in each section reveal a general and gradual deepening-upward trend and a continuum of depositional environments. The depositional system is thus characterized by a ramp profile, which is common in areas where carbonate factories mainly produce loose skeletal material rather than a rigid framework, such as a reef (Carannante et al., 1996; Schlager, 2005; Pomar, 2001; Pomar and Hallock, 2007; Pomar and Kendall, 2008; Williams et al., 2011), and typical of foreland basins settings (e.g., Sinclair, 1998; Coletti et al., 2021). Thus, Eocene ramps, lacking a marginal rim, are characterised by unimpeded downslope transport and reworking processes (e.g., Beavington-Penney et al., 2005; Coletti et al., 2016).

The palaeoenvironmental reconstruction of the different biofacies that characterise the Pag Island FL, starting from the shallowest to the deepest, is proposed thereafter. To further refine the palaeoenvironmental interpretation, three parameters that increase with the increasing of water depth (O/N, H/P, P/B), which will be discussed in the following chapter, have been used.

i) *BF1* is characterised by the abundance of small miliolids (e.g., *Quinqueloculina*, *Triloculina*, *Spiroloculina*, *Idalina*), hyaline SBF, large miliolids (alveolinids, *Orbitolites*, peneroplids), and large agglutinated taxa (e.g., *Coskinon*, *Pseudochrysalidina*). Small textulariids are also common. Conical coskinolinids (Fig. 7.9) typically indicate shallow and extremely restricted facies of Thethys (Vecchio and Hottinger, 2007). The abundance and the high diversity of miliolids suggest a well illuminated, oligotrophic to mesotrophic environment (Murray, 2006). Thus, common coskinolinids, abundant and diversified small miliolids, associated with large miliolids (especially peneroplids), suggest shallow water lagoonal conditions (Murray, 2006; Čosović et al., 2018). A lagoonal environment is also suggested by the presence of non-skeletal grains such as pellets (Coletti et al., 2019) and subtidal mud intraclasts. Overall, such observations might indicate a water depth above the mean fairweather wave base and possibly comprised between 0 and 10 m, within inner ramp settings. This facies is also characterised by a higher abundance of sparite than the other facies, that can derive also from processes of dissolution that affected mostly aragonitic and high-Mg calcite taxa, such as miliolids. Indeed, the matrix is composed by abundant bioclastic fragments most likely derived from the dissolution processes that affected miliolids (especially alveolinids), that is well visible under the microscope.

ii) *BF2* is characterised by a foraminiferal assemblage dominated by taxa that can be related to palaeo-seagrass meadows (Fig. 7.9). Seagrass occurrences documented in the Palaeogene predominantly formed in shallow warm-water habitats with oligo-mesotrophic conditions. These occurrences exhibit unique assemblages of small and larger benthic foraminifers that are well-adapted to environments with minimal terrigenous influence (Baceta and Mateu-Vicens, 2021). Hyaline SBF are the most abundant group, followed by small miliolids, and contain abundant specimens of Cibicididae (*Lobatula*) and Rosalinidae, typically related to vegetated seafloor (e.g., Langer, 1993; Mateu-Vicens et al., 2014; Baceta and Mateu Vicens, 2021). Large miliolids are abundant; the common presence of *Orbitolites*, which is similar to modern epiphytic soritids, is indicative of a vegetated substrate (Brasier, 1975c; Beavington-Penney et al., 2006; Tomás et al., 2016; Tomassetti et al., 2016; Coletti et al., 2021). The common presence of encrusting foraminifera displaying hooked morphology is also a common proxy for palaeo-seagrass meadow (e.g., Tomás et al., 2016; Reich et al., 2015; Tomassetti et al., 2016), such as the presence of other sessile taxa like *Fabiania* and victoriellids (Baceta and Mateu Vicens, 2021). Encrusting acervulinids are opportunistic foraminifera

that indicate conditions similar to those in which coralline algae flourish, and replacing the latter when the light intensity is reduced by increased water depth or turbidity (Bassi et al., 2007; Varrone & D'Atri, 2007; Bassi & Nebelsick, 2010), or the presence of vegetation. The presence of planorbulinids is also a major indicator of the occurrence of a vegetated substrate (e.g., Mateu Vicens et al., 2014; Mariani et al., 2022a; Mariani et al., 2022b). This biofacies is characterised by high biodiversity of the skeletal and foraminiferal assemblages, which is a marker for seagrass-associated environments (Steinker and Steinker, 1976; Murray, 2006). Furthermore, the poor selection of the deposits, with abundant silt, carbonate mud and coarse skeletal components, indicate the possible presence of vegetated environment (Fornos and Ahr, 1997). Among the other carbonate producers, echinoderms are abundant, suggesting an environment rich of food; possibly, some echinoderms taxa graze extensively on seagrass material (Larkum and West, 1990). The lower portion of BF2 lacks nummulitids specimens, which on the contrary are very abundant in the upper portion of this facies, as showed in the stratigraphic log (Fig. 7.3). Because modern seagrass meadows occur at a depth < 40 m (and mostly < 20 m; Duarte, 1991), the depth of deposition of the first cycle of BF2 was most likely around 20 m. The second cycle of BF2, which is characterised by the abundance of nummulitids, linked with the other observation on the skeletal and foraminiferal assemblage, and the lack of orthophragminids and planktonic foraminifera (Table 7.1), suggest a depth of deposition between 20 and 40 m. The occasional presence of flat tests of *Nummulites*, that are usually related to deeper settings (e.g., Cosovic et al., 2004, Beavington-Penney and Racey, 2004), could probably indicate an adaptation to low light, shadowed area, under the canopy of the seagrass meadow (Baceta and Mateu Vicens, 2021). Consequently, BF2 is interpreted as developed in proximity to seagrass meadows in a shallow, inner-ramp environment, between 10 and 40 m water depth.

iii) *BF3* is characterised by the large abundance of nummulitids, that dominate the LBF associations. Hyaline SBF are always abundant, such as small miliolids in a lesser extent. Small textularidiis are common. Taxa indicating shallower conditions are present in a lesser amount than the previous biofacies: large, agglutinated taxa are almost absent, whereas large miliolids abundance decrease. *BF3* is characterised by evidence of transport, consisting of fragmented tests of inner-ramp foraminifera (such as alveolinids) and micritized and encrusted allochems. Phenomena of downslope transport and reworking are typical of Eocene ramps, lacking a marginal rim (e.g., Beavington-Penney et al., 2005). This biofacies can also be interpreted as a lateral variation of *BF2*, in absence of vegetation on the seafloor. In this case, the transported inner-ramp bioclasts could have been canalised in channel-like structures formed near to seagrass meadows. The foraminiferal association indicates a moderately high energy, shallow water environment, with deposition in inner-to-middle ramp settings, indicatively between 20 and 40 m depth (Murray, 2006).

iv) *BF4* is characterised by the scarce abundance of bioclasts and scarce biodiversity, being mostly composed by fine sand-sized matrix. Hyaline SBF and nummulitids dominate the skeletal assemblage, small miliolids and small textulariids are common. Molluscs, echinoderm and bryozoans are common, too. Nummulitids are among the few recognised large bioclasts. Low biodiversity and scarcity of bioclasts, and common presence of infaunal taxa indicate a non-vegetated substrate. Also, transport from the inner-ramp is very low, consisting only of few large miliolids tests. *BF4* is similar to *BF3* except for low energy conditions: in *BF3* moderately high-energy allowed the deposition of coarse-sized bioclast, whereas in *BF4* low energy conditions allowed just the deposition of fine-sized bioclasts. Thus, *BF4* might indicate a low-energy, shallow water environment, deposited in inner-to-middle ramp settings, indicatively between 20 and 40 m depth (Murray, 2006), and located in between area colonised by seagrass meadows.

v) *BF5* is characterised by abundant nummulitids and orthophragminids. The nummulitids association comprises also a larger amount of *Operculina* and *Assilina*, and flat *Nummulites*. The orthophragminid association comprises *Discocyclus* and *Asterocyclus*. Hyaline SBF are abundant (e.g., *Lenticulina*), whereas small miliolids and small textulariids are present in a lesser extent than in the previous biofacies. Planktic foraminifera and bryozoans are common, amphisteginids are rare. This biofacies documents deeper water settings than the previous facies. Transport evidence from shallower settings are present: this is most likely due to the steepening of the carbonate ramp, related to the presence of a seagrass meadow in the interval above. Indeed, seagrass colonization of the sea bottom influence the carbonate production and the development of the carbonate ramp itself. Seagrass-dominated shallow carbonate production tends to result in steep slopes due to the low-transport characteristic imposed by seagrass trapping (O. Tella et al., 2022). This biofacies represents a deepening-upward trend, indicating middle ramp settings and a moderate energy, in a water depth interval comprised between 40 and 60 m.

vi) *BF6* is characterised by abundant serpulids (mainly *Ditrupa*), echinoderms, hyaline SBF and nummulitids. Bryozoans are common, such as planktonic foraminifera. Transport is a common feature within this biofacies, testified by the abundance of broken bioclasts and tests of foraminifera. Typically, this material comes from the previous facies, such as Cibicididae and alveolinids, that most likely derived from a setting typical of *BF2*, and broken nummulitids transported from inner-ramp settings. Bioturbation is also a common process, testifying the activity of organisms such as serpulids, that reworked the sediments. The abundance of serpulids indicates presence of food and instability of the deposits (Pérès and Picard, 1957). According to the literature, the modern distribution of *Ditrupa* ranges from 0 to 150 m (Gambi & Giangrande, 1985; Ten Hove & Smith, 1990) or even 200 m (Picard, 1965; Ben-Eliahu & Fiege, 1996). The lack of orthophragminids could indicate shallower

settings, whereas the common presence of planktic foraminifera and the abundance of bryozoans indicate deeper settings. Thus, this biofacies can be interpreted as middle ramp settings (40-80 m), consisting mainly of transported material from the inner ramp, especially from BF2 and BF3.

vii) *BF7* is characterised by the abundance of orthophragminids and nummulitids displaying flat tests. Planktic foraminifera are abundant. RCA and bryozoans are very common. SBF association is mainly composed of hyaline SBF, with common *Lenticulina* specimens. The skeletal assemblage and the foraminiferal association of this biofacies suggest a below-wave base, outer shelf setting, with a water depth comprised between 60 m and the lowest limit of the photic zone, around 100-130 m. The presence of authigenic minerals (e.g., glauconite), suggests low sedimentation rate and sediment starvation, testifying the beginning of the carbonate ramp drowning.

viii) *BF8* is characterised by the large abundance of planktic foraminifera and hyaline small benthic foraminifera. Echinoderms spines and plates are abundant, too. This biofacies consists mainly of marls deposits belonging to the TB unit, thus not comprised within the FL unit. This biofacies deposited in hemipelagic environment with limited clastic supplies, indicating the final drowning of the carbonate ramp.

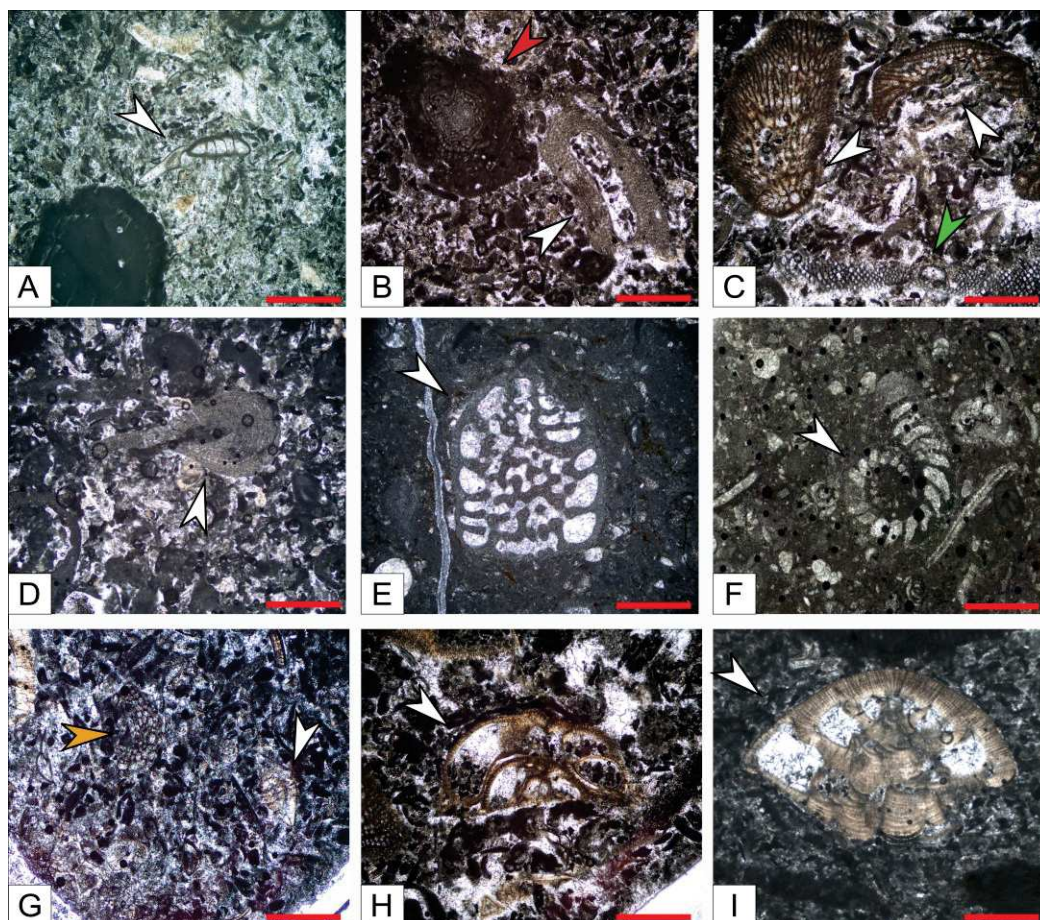


Figure 7.9 A. *Lobatula* (white arrow) and *Alveolina*; B. Hooked acervulinid (white arrow) and *Alveolina* (red arrow); C. *Fabiania* (white arrows) and *Orbitolites* (green arrow); D. Hooked acervulinid (white arrow); E. *Coskinon* (white arrow); F. *Spirolina* (peneroplid; white arrow); G. Planorbulinid (orange arrow) and hyaline SBF (white arrow); H. Victoriellid (white arrow); I. Hyaline LBF (*Rotalia*; white arrow). Bars 500 μ m.

7.6.3 Calculated parameters

The calculated foraminifera-based parameters (i.e., O/N, P/B, H/P; Table 7.1) demonstrated their reliability and efficiency for palaeoenvironmental purposes. Overall, their values increase from BF1 to BF8, testifying the deepening-upward trend of the Eocene carbonate ramp. However, it was not possible to calculate every parameters in each thin section (e.g., when lacking particular taxa), and it is preferable to consider the average value for each facies, taking into account the overall trend displayed. These parameters are also susceptible to biases related to transport and bioclast fragmentation, that can considerably modify the values. Indeed, to avoid this bias, it is essential to consider just the tests that do not present signs of transport such as the broken ones.

O/N (Ćosović et al., 2004; Beavington-Penney and Racey, 2004) has been calculated only in the biofacies that contain both orthophragminids and nummulitids, thus in BF5 (0.74), BF7 (2) and BF8 (1.4) (Table 7.1). O/N typically increases with depth (Ćosović et al., 2018) and this is the trend showed in the FL exposed in Pag Island. The value decreases when we consider BF8, but in this case it is based just on the little number of specimens that we found in the TB deposits, and so is not reliable as in the FL deposits.

P/B ratio typically increases with depth or with increasing distance from the coast (Van der Zwaan, 1990). This trend is reflected in the analysed section: P/B increases considerably along the stratigraphic log, passing from 0.0008 (BF1), to 0.07 (BF5), to 0.20 (BF7), until to 1.03 (BF8). This values clearly indicate the deepening-upward trend of the FL of Pag Island.

H/P (revised from Coletti et al., 2021) typically increases with depth. Indeed, miliolids and especially large miliolids, are more typical of shallower settings (e.g., Murray, 2006). The values of this parameter in the FL of Pag Island show an increasing trend, in agreement with the hypothesis of a deepening-upward section. They pass from 0.60 (BF1) to 72.3 (BF7), up to 232.4 (BF8). The increasing trend of this parameters is reversed only in BF6; however, this can be related to high-transport conditions that characterised this biofacies, and not to an effective decrease in depth. The trend showed by this parameter can be also seen in the ternary diagram that report the distribution of different foraminifera taxa based on the different test composition (i.e., hyaline, porcelaneous, agglutinated; Fig 7.10).

All the calculated parameters do not depict transgressive/regressive cycles, but they show a general deepening-upward trend along the analysed section, although influenced by the heterogeneity of the biofacies. Anyway, considering the values of these parameters for each samples (approximately every 3 m wherever possible) no cyclicity is evident, but a gradual deepening trend is always noticeable. Thus, no evidence of eustatism is displayed. This observation is confirmed by the analysis of the skeletal assemblage and the foraminiferal association, but the calculation of this parameters is

important because they can give us a quantitative reference that can be used in the future to compare different sections, using a standardised approach.

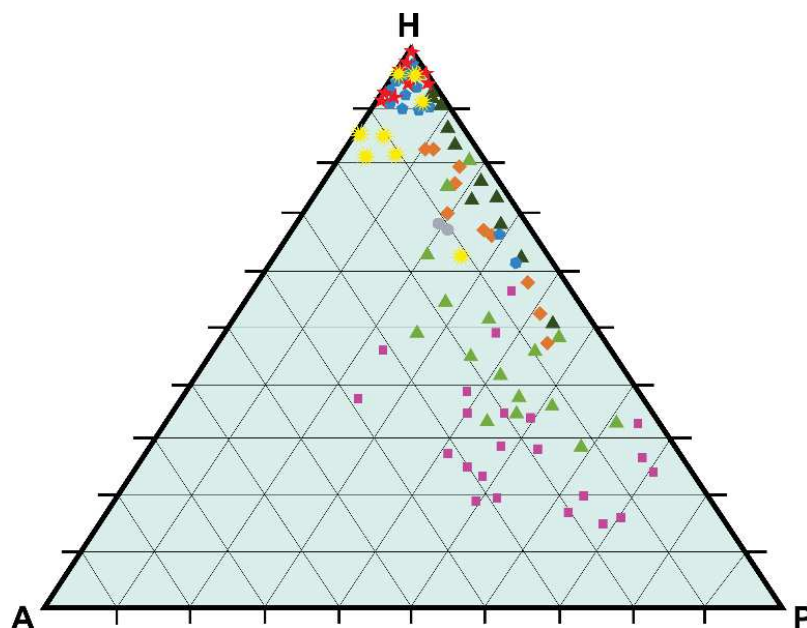


Figure 7.10 Ternary diagram showing the distribution of agglutinated (A), porcelaneous (P) and hyaline (H) foraminifera tests along the analysed section. Different colours refer to different biofacies, following the scheme proposed in the stratigraphic log (Fig. 7.3).

7.6.4 The advantages of quantitative analysis

Thanks to the analysis carried out it has been possible to build the paleobathymetry model of the FL exposed at Pag Island, within the Dinaric Foreland Basin. Sedimentation in the basin commenced during the late Ypresian with the deposition of the carbonate ramp of Foraminiferal Limestone. The controls on the deposition and the evolution of this carbonate ramp are attributed to tectonic activity, related to the formation of the Dinarides and the structuration of the foreland basin. Eustatism, as showed by the palaeobathymetric parameters, did not play a main role in this process, since eustatic cycles are not recorded in the succession. Indeed, ice caps were still not present in the Early-Middle Eocene on our planet (e.g., Zachos et al., 2001). The main influence on the evolution of the basin is, thus, related to tectonic processes, such as isostatic crustal adjustment in proximity to the collision zone (Ćosović et al., 2018), reverse faulting (Matenco et al., 2007, 2010), blind-thrust growth anticlines (on which carbonate ramps formed episodically; Mrinjek et al., 2012). During the Early to Middle Eocene, the persistence of the carbonate ramp formation indicates a net balance between subsidence and uplift of the basin, testified by the deepening-upward trend of the entire sequence. Furthermore, the lack of terrigenous material within the FL deposits of Pag Island indicates that the orogen was not completely developed at this time, disadvantaging the sediment influx toward the basin.

Within this context, it is critical to highlight the importance of quantification in microfacies analysis, that constitutes a powerful tool in providing more accurate palaeoenvironmental reconstructions. The point counting technique allows to obtain the detailed composition of all the skeletal assemblage and of the non-skeletal components. Being foraminifera one of the most relevant components of these assemblages, the foraminiferal counting permits the creation of a quantitative dataset of the abundance of different foraminiferal groups and to quantify their paleoecological significance, allowing comparisons with other geological sections. The quantitative data collected allowed the calculation of parameters (in this case mostly related to palaeobathymetry), that permit to characterise, with relative values, the evolution of the basin. Certainly, the collection of quantitative data from micropalaeontological analysis is biased by several processes. The point counting technique is exceptionally reliable to obtain information about the composition of the sediments and the abundance of every skeletal component, but tends to overestimate the larger components, that volumetrically dominate the deposits. Differently, the foraminiferal counting technique overcome this problem, because is based on the counting of every foraminiferal specimens present in the deposits. However, this second approach do not provide information on the skeletal assemblage and the non-skeletal components. Both the approaches require high specialised operator and are subject to human error. However, both the techniques are not strictly based on taxonomy, at least not at the highest level of taxonomical identifications, but are mostly based on palaeoecological significance. The creation of a large, standardised, and quantitative dataset, with all the data of composition (both the skeletal assemblage and the foraminiferal association) of different sections, will allow to shift from relative values to absolute values, and so trying to estimate the real depth of deposition of a determinate biofacies.

7.7 Conclusions

Based on the analysed LBF and nannofossil association, the Foraminiferal Limestone exposed at Pag Island deposited between the Early Eocene (Ypresian) and the Middle Eocene (Late Lutetian/Early Bartonian), with the Ypresian/Lutetian boundary identified at 45 m along the section.

Thanks to the analysis of the skeletal assemblage, the foraminiferal assemblage, and multivariate statistics, it was possible to identify seven main biofacies within the Foraminiferal Limestone and one biofacies within the overlying unit of the Transitional Beds: i) the porcelaneous and agglutinated benthic foraminifera biofacies (BF1), that indicate a well-illuminated, oligotrophic to mesotrophic, shallow water, lagoonal environment (0 - 10 m); ii) the hyaline SBF and encrusting benthic foraminifera biofacies (BF2), interpreted as developed in proximity to seagrass meadows in a shallow water, inner-ramp environment (10 - 40 m); iii) the nummulitid biofacies (BF3), that indicate a

moderately high energy, shallow water environment, deposited in inner-to-middle ramp settings (20 - 40 m); iv) the comminuted bioclasts and nummulitid biofacies (BF4), that indicate a low-energy, shallow water environment, deposited in inner-to-middle ramp settings (20 - 40 m); v) the nummulitid and orthophragminid biofacies (BF5), that indicate a moderate energy environment, deposited in middle ramp settings (40 - 60 m); vi) the nummulitid and serpulid biofacies (BF6), that consists of transported material from the inner ramp deposited in middle ramps settings (40 - 80 m); vi) the orthophragminid and nummulitid biofacies (BF7), that indicates a below-wave base, outer shelf setting, (60 - 100/130 m); and the planktic foraminifera biofacies (BF8), that deposited in hemipelagic environment, indicating the final drowning of the carbonate ramp. The Ypresian/Lutetian boundary has been placed between BF1 and BF2.

These biofacies formed along a distally steepened ramp profile, testifying the progressively deepening of the depositional environment. Furthermore, the analysis carried out allowed to characterize, even quantitatively, new deposits related to fossil seagrasses, which are commonly challenging to recognize in the geological record.

The quantitative parameters i) orthophragminids/nummulitids (O/N), ii) P/B (planktic/benthic foraminifera), and iii) H/P (hyaline/porcelaneous foraminifera) demonstrated their reliability and efficiency for palaeoenvironmental reconstruction, all quantitatively tracking the deepening-upward trend of the succession. No evidence of eustatism are detected.

Overall, quantification through point counting and foraminiferal counting constitutes a powerful tool in providing accurate and reliable palaeoenvironmental reconstruction and it is crucial to compare different successions. Hence, establishing a comprehensive, standardized, and quantitative dataset encompassing compositional data (including both skeletal assemblage and foraminiferal association) from various sections, might enable a transition from relative values to absolute values. This shift will facilitate the attempt to estimate the actual depth of deposition for a specific biofacies in the fossil record.

Supplementary material

The Supplementary Table 7.1 contains all the raw data derived from the foraminiferal counting and the point counting and is downloadable from the following link: <https://board.unimib.it/datasets/b96pxy8p9k/draft?a=38345214-3c6d-4e86-b2a2-7bd6a413f811>

References

Accordi, G., Carbone, F., Pignatti, J., 1998. Depositional history of a Paleogene carbonate ramp (Western Cephalonia, Ionian Islands, Greece). *Geol Romana* n.s. 34:131-205

- Agnini, C., Fornaciari, E., Raffi, I., Catanzariti, R., Pälke, H., Backman, J., & Rio, D., 2014. Biozonation and biochronology of Paleogene calcareous nannofossils from low and middle latitudes. *Newsletters on Stratigraphy*, 47, 131–181.
- Aubouin J., Blanchet R., Cadet J. P., Celet P., Charvet J., Chorowicz J., Cousin M., Rampoux J. P., 1970. Essai sur la geologie des Dinarides. *B. Soc. Geol. Fr.*, S7–XII (6), 1060–1095. <https://doi.org/10.2113/gssgfbull.S7-XII.6.1060>
- Babić, L., and Zupanić, J., 2008. Evolution of a river-fed foreland basin fill: the North Dalmatian flysch revisited (Eocene, Outer Dinarides). *Nat. Croat.*, 17, 357–374.
- Babić, L., and Zupanić, J., 2016. The youngest stage in the evolution of the Dinaric carbonate platform: the Upper Nummulitic Limestones in the North Dalmatian foreland, Middle Eocene, Croatia. *Natura Croatica*, 25(1), 55–71. <https://doi.org/10.20302/NC.2016.25.3>.
- Baceta, J.I., and Mateu-Vicens, G., 2021. Seagrass development in terrigenous-influenced inner ramp settings during the middle Eocene (Urbasa-Andia Plateau, Western Pyrenees, North Spain). *Sedimentology*, <https://doi.org/10.1111/sed.12937>.
- Bassi, D., 1998. Coralline Algal Facies and their paleoenvironmentals in the Late Eocene of Northern Italy (Calcarei di Nago, Trento). *Facies* 39:179–202
- Bassi, D., Hottinger, L. & Nebelsick, J.H., 2007. Larger foraminifera from the Late Oligocene of the Venetian area, northeastern Italy. *Palaeontology*, 50, 845–868.
- Bassi, D. and Nebelsick, J.H., 2010. Components, facies and ramps: Redefining Upper Oligocene shallow water carbonates using coralline red algae and larger foraminifera (Venetian area, northeast Italy). *Palaeogeogr. Palaeoclimatol. Palaeoecol.*, 295, 258–280.
- Beavington-Penny, S.J. & Racey, A., 2004. Ecology of extant nummulitids and other LBF: application in palaeoenvironmental analysis. *Earth-Sci. Rev.*, 67, 219–265.
- Beavington-Penney, S.J., Paul Wright, V., Racey, A., 2005. Sediment production and dispersal on foraminifera-dominated early Tertiary ramps: the Eocene El Garia Formation, Tunisia. *Sedimentology* 52, 537–569.
- Beavington-Penney, S.J., Wright, V.P., Racey, A., 2006. The middle Eocene Seeb Formation of Oman: an investigation of acyclicity, stratigraphic completeness, and accumulation rates in shallow marine carbonate settings. *Journal of Sedimentary Research* 76, 1137–1161.
- Ben Eliahu, M. Nechama and Fiege, D., 1996. Serpulid tube-worms (Annelida: Polychaeta) of the central and eastern Mediterranean with particular attention to the Levant Basin. *Senckenbergiana maritima*, 28(1/3): 1-51
- Bialik, O. M., Coletti, G., Mariani, L., Commissario, L., Desbiolles, F., Niyonkuru Meroni, A., 2023. Global neritic carbonate sediment distribution: allochem continuum along an energy gradient. *Scientific Reports*, submitted.
- Brasier, M.D., 1975a. Ecology of Recent sediment-dwelling and phytal foraminifera from the lagoons of Barbuda, West Indies. *The Journal of Foraminiferal Research* 5, 42–61.
- Brasier, M.D., 1975b. The ecology and distribution of recent foraminifera from the reefs and shoals around Barbuda, West Indies. *The Journal of Foraminiferal Research* 5, 193–210.
- Brasier, M.D., 1975c. An outline history of seagrass communities. *Palaeontology* 18, 681–702.
- Breard, S. Q., Callender, A. D., Denne, R. A., and Nault, M. J., 2000. Taxonomic Uniformitarianism in Gulf of Mexico Basin Cenozoic Foraminiferal Paleocology: Is the Present Always the Key to the Past? *Gulf Coast Association of Geological Societies Transactions*, v. 50, 725-736.
- Boudaughier-Fadel, M.K., 2018. Evolution and Geological Significance of Larger Benthic Foraminifera. UCL Press (693 pp.).
- Bulić J., Jurišić-Polšak Z., 2009. Macropalaeontology and stratigraphy of lacustrine Miocene deposits at Crnika beach on the Island of Pag (Croatia). *Geol. Croat.*, 62(3), 135–155. <https://doi.org/10.4154/gc.2009.16>
- Burchette, T.P. & Wright, V.P., 1992. Carbonate ramp depositional systems. *Sediment. Geol.*, 79, 3–57.
- Carannante, G., Severi, C., Simone, L., 1996. Off-shelf carbonate transport along foramol (temperate-type) open shelf margins: an example from the Miocene of the central-southern Apennines (Italy). *Mémoires de la Société géologique de France* 169, 277–288.
- Coletti, G., Vezzoli, G., Di Capua, A., Basso, D., 2016. Reconstruction of a lost carbonate factory based on its biogenic detritus (Ternate-Travedona Formation and Gonfolite Lombarda Group - northern Italy). *Rivista Italiana di Paleontologia e Stratigrafia* 122, 1–22.
- Coletti, G., Basso, D., Betzler, C., Robertson, A.H.F., Bosio, G., El Kateb, A., Foubert, A., Meilijson, A., Spezzaferri, S., 2019b. Environmental evolution and geological significance of the Miocene carbonates of the Eratosthenes Seamount (ODP Leg 160). *Palaeogeography Palaeoclimatology Palaeoecology* 530, 217–235.
- Coletti, G., Mariani, L., Garzanti, E., Consani, S., Bosio, G., Vezzoli, G., Hu, X., and Basso, D., 2021. Skeletal assemblages and terrigenous input in the Eocene carbonate systems of the Nummulitic Limestone (NW Europe). *Sedimentary Geology*, v. 425., <https://doi.org/10.1016/j.sedgeo.2021.106005>

- Ćosović, V., Drobne, K. & Moro, A., 2004: Paleoenvironmental model for Eocene foraminiferal limestones of the Adriatic carbonate platform (Istrian Peninsula). *Facies*. 50. 61-75.
- Ćosović, V., Mrinjek, E., Nemeč, W., Španiček, J. & Terzić, K., 2018: Development of transient carbonate ramps in an evolving foreland basin: *Basin Research*, v. 30, p. 746–765, <https://doi.org/10.1111/bre.12274>.
- DeCelles, G.P. & Giles, A.K., 1996: Foreland basin systems. *Basin Res.*, 8, 105–123.
- Drobne K., Ćosović, 1998. Repetitive order of appearance of larger Foraminifera and the ecological gradients preserved in Paleogene shallow benthic carbonate deposits. Tertiary to Recent larger Foraminifera. Their depositional environments and importance as petroleum reservoirs, conference and workshop: February 15-19th, 1998, Kingston Univ, 10 pp
- Drobne, K., Ćosović, V., Moro, A. & Bucković, D., 2011. The role of the Palaeogene Adriatic Carbonate Platform in the spatial distribution of Alveolinids. *Turkish J. Earth Sci.*, 20, 721–751.
- Duarte, C.M., 1991. Seagrass depth limits. *Aquatic Botany* 40, 363–377.
- Dunham, R.J., 1962. Classification of carbonate rocks according to depositional texture. In: Ham, W.E. (Ed.), *Classification of Carbonate Rocks*. American Association of Petroleum Geologist, Memoirevol. 1, pp. 108–121.
- Embry, A.F., Klovan, J.E., 1971. A Late Devonian reef tract on Northeastern Banks Island, NWT. *Bulletin of Canadian Petroleum Geology* 19, 730–781.
- Faccenna, C., Becker, T. W., Auer, L., Billi, A., Boschi, L., Brun, J. P., Capitanio, F., Funiciello, F., Horvát, F., Jolivet, L., Piromallo, C., Royden, L., Rossetti, F., Serpelloni, E., 2014. Mantle dynamics in the Mediterranean. *Rev. Geophys.*, 52(3), 283–332. <https://doi.org/10.1002/2013RG000444>
- Flügel, E. 2010: *Microfacies of Carbonate Rocks*, 2nd edn, 976 pp. Springer-Verlag, Berlin.
- J.J. Fornós, W.M. Ahr, 1997. Present-day temperate carbonate sedimentation on the Balearic Platform, western Mediterranean: compositional and textural variation along a low-energy isolated ramp H.M. Pedley, G. Carannante (Eds.), *Cool-Water Carbonates: Depositional Systems and Palaeoenvironmental Controls*, Special Publications, vol. 255, Geological Society, London (2006), pp. 121-135
- Gambi, M. C., and Giangrande, A., 1985. Distribution of soft bottom Polychaetes in two coastal areas of the Thyrrenian Sea (Italy): structural analysis. *Estuar. Coast. Shelf Sci.*, v. 23, pp. 847-862.
- Glenn, C., McManus, J.W., Talaue, L., Alino, P., Banzon, V., 1981. Distribution of live foraminifers on a portion of Apo Reef, Mindoro, Philippines. *Proceedings of the 4th International Coral Reef Symposium*, Manilavol. 2, pp. 775–781.
- Hallock, P., 1980. Application of ecologic studies of living, algal symbiont-bearing foraminifera to paleoecologic interpretation. *AAPG Bulletin* 64, 716–717.
- Hallock, P., 1983. Larger foraminifera as depth indicators in carbonate depositional environments. *AAPG Bulletin* 67, 477–478.
- Hallock, P., 1984. Distribution of selected species of living algal symbiont-bearing foraminifera on two Pacific coral reefs. *The Journal of Foraminiferal Research* 14, 250–261.
- Hallock, P., Glenn, E.C., 1986. Larger foraminifera: a tool for paleoenvironmental analysis of Cenozoic carbonate depositional facies. *Palaios* 1, 55–64.
- Hallock, P. and Seddighi, M., 2022. Why did some larger benthic foraminifera become so large and flat?. *Sedimentology*, 69: 74-87. <https://doi.org/10.1111/sed.12837>
- Heidbach, O., Custodio, S., Kingdon, A., Mariucci, M. T., Montone, P., Müller, B., Pirdominici, S., Rajabi, M., Reinecker, J., Reiter, K., Tingay, M., Williams, J., and Ziegler, M., 2016. Stress Map of the Mediterranean and Central Europe 2016. GFZ Data Services, 45. <https://doi.org/10.5880/WSM.EUROPE2016>
- Hottinger, L., 1978. Comparative anatomy of selected foraminiferal shell structures. In: *Foraminifera III* (Ed. by R.H. Headley, G. Adams), pp. 203–266. Academic Press, London.
- Hottinger, L., and K. Drobne, 1980. Early Tertiary conical imperforate foraminifera. Konične imperforatne foraminifere iz starejšega terciarja, Slovenska Akademija Znanosti in Umetnosti, *Classis IV Historia Naturalis, Dissertationes* 22(3): 187-276, page(s): p. 233, 253
- Hottinger, L., 1983a. Processes determining the distribution of larger foraminifera in space and time. *Utrecht Micropaleontological Bulletin* 30, 239–253.
- Hottinger, L., 1997. Shallow benthic foraminiferal assemblages as signals for depth of their deposition and their limitations. *Bull. Soc. g_eol. Fr.*, 168, 591–505.

- Ilić A., Neubauer F., 2005. Tertiary to recent oblique convergence and wrenching of the Central Dinarides: Constraints from a palaeostress study. *Tectonophysics*, 410(1–4), 465–484. <https://doi.org/10.1016/j.tecto.2005.02.019>
- Jelaska, V., Gušić, I., Jurkoviček, B., Ogorelec, B., Čosović, V., Sribar, L., and Toman, M., 1994. The Upper Cretaceous geodynamic evolution of the Adriatic-Dinaric carbonate platform. In *Perimediterranean carbonate platforms. First International Meeting. Marseille – France (5-8 septembre 1994)*, 21, 89–91.
- Jiménez-Moreno, G., de Leeuw, A., Mandić, O., Harzhauser, M., Pavelić, D., Krijgsman, W., and Vranjković, A., 2009. Integrated stratigraphy of the Early Miocene lacustrine deposits of Pag Island (SW Croatia): Palaeovegetation and environmental changes in the Dinaride Lake System. *Palaeogeogr. Palaeoclimatol.*, 280(1–2), 193–206. <https://doi.org/10.1016/j.palaeo.2009.05.018>
- Kastelic, V., and Carafa, M. M. C. (2012). Fault slip rates for the active External Dinarides thrust-and-fold belt. *Tectonics*, 31(3). <https://doi.org/10.1029/2011TC003022>
- Kastelic, V., Vannoli, P., Burrato, P., Fracassi, U., Tiberti, M. M., and Valensise, G., 2013. Seismogenic sources in the Adriatic Domain. *Mar. Petrol. Geol.*, 42, 191–213. <https://doi.org/10.1016/j.marpetgeo.2012.08.002>
- Korbar T., 2009. Orogenic evolution of the External Dinarides in the NE Adriatic region: a model constrained by tectonostratigraphy of Upper Cretaceous to Paleogene carbonates. *Earth-Sci. Rev.*, 96(4), 296–312. <https://doi.org/10.1016/j.earscirev.2009.07.004>
- Langer, M. R., 1993. Epiphytic foraminifera. *Marine Micropaleontology*, v. 20, pp. 235–265.
- Larkum, A.W.D., West, R.J., 1990. Long-term changes of seagrass meadows in Botany Bay, Australia. *Aquat. Bot.* 37, 55–70.
- Lokier, S.W., Al Junaibi, M., 2016. The petrographic description of carbonate facies: are we all speaking the same language? *Sedimentology* 63, 1843–1885.
- Mariani, L., Coletti, G., Mateu-Vicens, M., Bosio, G., Collareta, A., Khokhlova, A., Di Cencio, A., Casati, S. and Malinverno, E., 2022a. Testing an indirect palaeo-seagrass indicator: benthic foraminifera from the Lower Pleistocene *Posidonia* meadow of Fauglia (Tuscany, Italy), *Marine Micropaleontology*, v. 73.
- Mariani, L., Coletti, G., Bosio, G., Tentorio, C., Mateu Vicens, G., Bracchi, V. A., Basso, D., and Malinverno, E. (2022b). Benthic foraminifera as proxy for fossil seagrass from the Lower Pleistocene deposits of the Stirone River (Emilia-Romagna, Italy), *Quaternary International*, v. 640, pp. 73–87, <https://doi.org/10.1016/j.quaint.2022.10.005>.
- Marjanac, T., Babačić, D., Benić, J., Čosović, V., Drobne, K., Marjanac, L., Pavlovec, R. & Velimirović, Z., 1998. Eocene carbonate sediments and sea-level changes on the NE part of Adriatic carbonate platform (Island of Hvar and Pelješac peninsula, Croatia). In: *Paleogene Shallow Benthos of the Tethys*, 2 (Ed. by L. Hottinger & K. Drobne), pp. 243–254. Slovenian Academy of Sciences and Art, Ljubljana.
- Marjanac, T., and Čosović, V., 2000. Tertiary Depositional History of Eastern Adriatic Realm. *Pancardi 2000*, Dubrovnik, Croatia, 1 – 3.10.2000, 93–103.
- Marjanac, L., and Marjanac, T., 2004. Glacial history of the Croatian Adriatic and Coastal Dinarides. In: J. Ehlers and P. L. Gibbard (Eds.), *Quaternary Glaciations - Extent and Chronology* (pp. 19–26). Elsevier B. V.
- Marjanac L. (2012). Pleistocene glacial and periglacial sediments of Kvarner, northern Dalmatia and southern Velebit Mt. - Evidence of Dinaric glaciation. Doctoral thesis, University of Zagreb, Faculty of Science, Department of Geology.
- Marjanac, T., and Marjanac, L., 2016. The extent of middle Pleistocene ice cap in the coastal Dinaric Mountains of Croatia. *Quaternary Res.*, 85(3), 445–455. <https://doi.org/10.1016/j.yqres.2016.03.006>
- Martini, E., 1971. Standard Tertiary and Quaternary calcareous nannoplankton zonation. In: Farinacci, A. (Ed.), *Proceedings 2nd International Conference Planktonic Microfossils*. Tecnosci, Rome, pp. 739–785. Roma. Ed.
- Martinuš, M., Cvetko Tešović, B., Jurić, S. and Vlahović, I., 2023. Architecture and Palaeoecology of Coral–Stromatoporoid Patch Reefs in the Upper Maastrichtian and Lowermost Palaeocene Platform Carbonates, Adriatic Islands of Brač and Hvar (Croatia). Available at SSRN: <https://ssrn.com/abstract=4402242> or <http://dx.doi.org/10.2139/ssrn.4402242>
- Matenco, L., Bertotti, G., Leever, K., Cloetingh, S., Schmid, S.M., Tarpoancam, M. & Dinu, C., 2007. Large-scale deformation in a locked collisional boundary: Interplay between subsidence and uplift, intraplate stress, and inherited lithospheric structure in the late stage of the SE Carpathians evolution. *Tectonics*, 26, TC4011.
- Matenco, L., Krezsek, C., Merten, S., Schmid, S.M., Cloetingh, S. & Andriessen, P., 2010. Characteristics of collisional orogens with low topographic build-up: an example from the Carpathians. *Terra Nova*, 22, 155–195.
- Mateu-Vicens, G., Khokhlova, A. and Sebastián-Pastor, T., 2014. Epiphytic foraminiferal indices as bioindicators in Mediterranean seagrass meadows. *The Journal of Foraminiferal Research*, v. 44, pp. 325–339.
- Mitterpergher, S., Succo, A., Bistacchi, A., Storti, F., Bruna, P. & Meda, M. 2019. Geological and structural map of the southeastern Pag Island, Croatia: field constraints on the Cretaceous - Eocene evolution of the Dinarides foreland. *Geological Field Trips*. 11. 1-19. 10.3301/GFT.2019.06.

- Moody, R., 1998. Part 3: Background Information on Metloui Carbonates. In: Moody R, Brown A, Loucks R (eds) Tertiary to Recent larger Foraminifera: their depositional environments and importance as petroleum reservoirs. Field Trip Guide. Arco-BG plc-Carthago Oil-Chevron Kingston, pp 2-23
- Mrinjek, E., Nemeč, W., Pecinger, V., Miksa, G., Vlahović, I., Čosović, V., Velić, I., Bergant, S. & Matićec, D. (2012) The Eocene-Oligocene Promina Beds of the Dinaric Foreland Basin in northern Dalmatia. *J. Alpine Geol.*, 55, 409–451.
- Murray, J. W., 2006. Ecology and Applications of Benthic Foraminifera. Cambridge University Press, Cambridge, 426 p.
- Ori, G.G., and Friend, P.F., 1984. Sedimentary basins formed and carried piggyback on active thrust sheets. *Geology*, 12, 457–478.
- O. Tella, T., Winterleitner, G., Morsilli, M., and Mutti, M., 2022. Testing sea-level and carbonate production effects on stratal architecture of a distally steepened carbonate ramp (Upper Miocene, Menorca): A 3D forward modelling approach, *Sedimentary Geology*, Volume 441, <https://doi.org/10.1016/j.sedgeo.2022.106267>.
- Pamić J., Gušić I., Jelaska V., 1998. Geodynamic evolution of the Central Dinarides. *Tectonophysics*, 297, 251–268.
- Peres J.M., and Picard J., 1957. Note préliminaire sur une communauté benthique récemment mise en évidence: la biocoenose à *Dentalium rubescens* et *Lucina (Miltha) borealis* Rec. Trav. Stat. Mar. Endoume, 21 (12).
- Persico, D, Succo, A, Mittempergher, S, Storti, F, Piccinini, E, Villa, G., 2020. Calcareous nanofossil biostratigraphy of the External Dinarides flysch (Vrčić-Staravasa Pag Island, Croatia): A key to an Eocene tectono-stratigraphic and paleoenvironmental interpretation. *Geological Journal*; 55: 4656–4669. <https://doi.org/10.1002/gj.3673>
- Picard J., 1965. Recherches qualitatives sur les biocoenoses marines des substrats meubles dragables de la région marseillaise Rec. Trav. Stat. Mar. Endoume, 36 (52).
- Placer L., Vrabec M., Celarc B., 2010: The bases for understanding of the NW Dinarides and Istria Peninsula tectonics. *Geologija*, 53(1), 55–86. <https://doi.org/10.5474/geologija.2010.005>
- Pomar, L., 2001a. Types of carbonate platforms: a genetic approach. *Basin Res.*, 13, 313–334.
- Pomar, L., 2001b. Ecological control of sedimentary accommodation: evolution from a carbonate ramp to rimmed shelf, Upper Miocene, Balearic Islands. *Palaeogeogr. Palaeoclimatol. Palaeoecol.*, 175, 249–272.
- Pomar, L., and Hallock, P., 2007. Changes in coral-reef structure through the Miocene in the Mediterranean province: Adaptive versus environmental influence. *Geology*; 35 (10): 899–902. doi: <https://doi.org/10.1130/G24034A.1>
- Pomar, L., Kendall, C.G.StC, 2008. Architecture of carbonate platforms: a response to hydrodynamics and evolving ecology. *Controls on Carbonate Platform and Reef Development*. SEPM Special Publication vol. 89, pp. 187–216.
- Pomar, L., Baceta, J.I., Hallock, P., Mateu-Vicens, G. & Basso, D. 2017: Reef building and carbonate production modes in the west-central Tethys during the Cenozoic. *Mar. Pet. Geol.*, 83, 261–304.
- Read, J.F., 1980. Carbonate ramp-to-basin transitions and foreland basin evolution, Middle Ordovician, Virginia Appalachians. *AAPG Bull.*, 64, 1575–1612.
- Read, J.F., 1985. Carbonate platform facies models. *AAPG Bull.*, 69, 1–21.
- Reich S., Di Martino E., Todd J.A., Wesselingh, F.P. and Renema, W., 2015. Indirect paleo-seagrass indicators (IPSI): a review. *Earth-Science Reviews*, v. 143, pp. 161-186.
- Reiss, Z., Hottinger, L., 1984. The Gulf of Aqaba: Ecological Micropaleontology. Springer-Verlag (354 pp.).
- Renema, W., 2005. Depth estimation using diameter-thickness ratio in larger benthic foraminifera. *Lethaia*, 38, 137–141.
- Sartorio, D., Venturini, S., 1988. Southern Tethys Biofacies. Agip (235 pp.).
- Scheibner, C. & Speijer, R.P., 2008. Late Paleocene–early Eocene Tethyan carbonate platform evolution – a response to long- and short-term paleoclimatic change. *Earth-Sci. Rev.*, 90, 71–102.
- Scheibner, C., Rasser, M.W., and Mutti, M., 2007. The Campo section (Pyrenees, Spain) revised: implications for changing assemblages across the Paleocene-Eocene boundary. *Palaeogeogr. Palaeoclimatol. Palaeoecol.*, 248, 145–168.
- Schlager, W., 2005. Carbonate Sedimentology and Sequence Stratigraphy (No. 8). SEPM Society for Sedimentary Geology (206 pp.).
- Schmid, S. M., Bernoulli, D., Fügenschuh, B., Matenco, L., Schefer, S., Schuster, R., Tischler, M., and Ustaszewski, K., 2008. The Alpine-Carpathian-Dinaridic orogenic system: Correlation and evolution of tectonic units. *Swiss J. Geosci.*, 101(1), 139–183. <https://doi.org/10.1007/s00015-008-1247-3>

- Serra-Kiel, J., Hottinger, L., Caus, E., Drobne, K., Ferrandez, C., Jauhri, A., K., Less, G., Pavlovec, R., Pignatti, J., Samsó, J.M., Schaub, H., Sirel, E., Strougo, A., Tambareau, Y., Tosquella, J. & Zakrevskaya, E. 1998: Larger foraminiferal biostratigraphy on the Tethyan Paleocene and Eocene. *Bulletin de la Société géologique de France* 2, 281–299.
- Sinclair, H.D., Sayer, Z.R., & Tucker, M.E., 1998: Carbonate sedimentation during early foreland basin subsidence: the Eocene succession of the French Alps. Geological Society of London, Special Publication 149, 205–227.
- Španiček, J., Čosović, V., Mrinjek, E., and Vlahović I., 2017. Early Eocene evolution of carbonate depositional environments recorded in the Čikola Canyon (North Dalmatian Foreland Basin, Croatia). *Geol. Croat.*, 70(1), 11–25. <https://doi.org/10.4154/gc.2017.05>
- Stampfli, G.M., 2005. Plate tectonics of the Apulia-Adria microcontinents. In: CROP Project: Deep Seismic Exploration of the Central Mediterranean and Italy (Ed. by J.R. Finetti), pp. 747–766. Elsevier, Amsterdam.
- Steinker, P.J., and Steinker, D.C., 1976. Shallow-water foraminifera, Jewfish Cay, Bahamas Marit. Sediment. Spec. Publ., 1, pp. 171–180
- Tari Kovačić, V., and Mrinje, E., 1994. The role of Palaeogene clastics in the tectonic interpretation of Northern Dalmatia (Southern Croatia). *Geol. Croat.*, 47(1), 127–138.
- Ten Hove, H.A. and Smith, R. S., 1990. A re-description of *Ditrupa gracillima* Grube, 1878 (Polychaeta, Serpulidae) from the Indo-Pacific, with a discussion of the genus. *Records of the Australian Museum* 42(1):101–118.
- Tišljar, J., Vlahović, I., Velić, I., and Sokac, B., 2002. Carbonate platform megafacies of the Jurassic and Cretaceous deposits of the Karst Dinarides. *Geol. Croat.*, 55(2), 139–170.
- Tomás, S., Frijia, G., Bömelburg, E., Zamagni, J., Perrin, C., Mutti, M., 2016. Evidence for seagrass meadows and their response to paleoenvironmental changes in the early Eocene (Jafnayn Formation, Wadi Bani Khalid, N Oman). *Sedimentary Geology* 341, 189–202.
- Tomassetti, L., Benedetti, A., Brandano, M., 2016. Middle Eocene seagrass facies from Apennine carbonate platforms (Italy). *Sedimentary Geology* 335, 136–149.
- van Unen M., Matenco L. C., Nader F. H., Darnault R., Mandic O., Demir V., 2018. Kinematics of foreland-vergent crustal accretion : inferences from the Dinarides evolution. *Tectonics* 38. <https://doi.org/10.1029/2018TC005066>
- Varrone, D., and D'Atri, A., 2007. Acervulinid macroid and rhodolith facies in the Eocene Nummulitic Limestone of the Dauphinois Domain (Maritime Alps, Liguria, Italy). *Swiss Journal of Geosciences* 100, 503–515.
- Vecchio, E., and Hottinger, L. Agglutinated conical foraminifera from the Lower-Middle Eocene of the Trentinara Formation (southern Italy). *Facies* 53, 509–533 (2007). <https://doi.org/10.1007/s10347-007-0112-6>
- Velić, I., Vlahović, I., and Matičec, D., 2002. Depositional sequences and paleogeography of the Adriatic Carbonate Platform. *Mem. Soc. Geol. It.*, 57, 141–151.
- Vlahović, I., Tišljar, J., Velić, I., and Matičec, D., 2002. The Karst Dinarides are composed of relics of a single Mesozoic platform; facts and consequences. *Geol. Croat.*, 55(2), 171–183. <https://doi.org/10.4154/GC.2002.15>
- Vlahović, I., Tišljar, J., Velić, I., and Matičec, D., 2005. Evolution of the Adriatic Carbonate Platform: Palaeogeography, main events and depositional dynamics. *Palaeogeogr. Palaeoclimatol.*, 220(3–4), 333–360. <https://doi.org/10.1016/j.palaeo.2005.01.011>
- Vlahović, I., Mandic, O., Mrinjek, E., Bergant, S., Čosović, V., de Leeuw, A., Enos, P., Hratovic, H., Matičec, D., Miksa, G., Nemeč, W., Pavelić, D., Pencinger, V., Velić, I., and Vranjković, A., 2012. Marine to continental depositional systems of Outer Dinarides foreland and intra-montane basins (Eocene - Miocene, Croatia and Bosnia and Herzegovina). *Field Trip Guide. Journal of Alpine Geology*, 54, 405–470.
- Williams, H.D., Burgess, P.M., Wright, V.P., Della Porta, G., Granjeon, D., 2011. Investigating carbonate platform types: multiple controls and a continuum of geometries. *Journal of Sedimentary Research* 81, 18–37.
- Zachos, J., Pagani, M., Sloan, L., Thomas, E., Billups, K., 2001. Trends, rhythms, and aberrations in global climate 65 Ma to present. *Science* 292, 686–693.
- Zamagni, J., Mutti, M., and Kosir, A., 2008. Evolution of shallow benthic communities during the Late Paleocene–earliest Eocene transition in the Northern Tethys (SW Slovenia). *Facies*, 54, 25–43.
- Zamagni, J., Mutti, M., Ballato, P., and Kosir, A., 2012. The Paleocene-Eocene Thermal Maximum (PETM) in shallow marine successions of the Adriatic Carbonate Platform (SW Slovenia). *Geol. Soc. Am. Bull.*, 124, 1071–1086.
- Zupanič J., and Babić L. (2011). Sedimentary evolution of an inner foreland basin margin: Paleogene Promina Beds of the type area, Mt. Promina (Dinarides, Croatia). *Geol. Croat.*, 64(2), 101–120. <https://doi.org/10.4154/gc.2011.09>

8. Skeletal assemblages and terrigenous input in the Eocene carbonate systems of the Nummulitic Limestone (NW Europe)

This chapter is taken from the scientific paper:

Coletti, G., Mariani, L., Garzanti, E., Consani, S., Bosio, G., Vezzoli, G., Hu, X., and Basso, D. (2021). Skeletal assemblages and terrigenous input in the Eocene carbonate systems of the Nummulitic Limestone (NW Europe), *Sedimentary Geology*, v. 425., <https://doi.org/10.1016/j.sedgeo.2021.106005>

8.1 Abstract

Terrigenous input is often considered detrimental for carbonate producing organisms, however, the common occurrence of mixed siliciclastic-bioclastic deposits indicates that the relationship between carbonate factories and terrigenous fluxes is a complex issue. To investigate this subject, we analysed the skeletal assemblages of the Paleogene Alpine foreland basin in a wide area encompassing NW Italy and SE France. Four different sections, Mortola, Loreto, Braux and Lauzanier, deposited between the Bartonian and the Priabonian, were studied in detail and, based on microfacies analysis, six main biofacies were recognized: i) nummulitid biofacies and ii) acervulinid and coralline algal biofacies related to shallow water; iii) nummulitid and orthophragminid biofacies and iv) coralline-algal branches and large benthic foraminifera biofacies related to intermediate depth; v) orthophragminid biofacies and vi) orthophragminid and coralline algal biofacies related to deeper settings. Thin sections and X-ray diffraction analyses show that these biofacies can be related to two major carbonate factories. The former was dominated by free-living benthic foraminifera and was characterized by a relevant terrigenous fraction, indicating free-living benthic foraminifera as the most terrigenous-tolerant group of carbonate producers of the Nummulitic Limestone system. The latter was dominated by encrusting acervulinids and coralline algae and thrived far-off major terrigenous sources. Conversely, recent and Neogene coralline algae are known to be able to tolerate high sedimentation rates. The distribution of coralline-algal-rich skeletal assemblages in the Nummulitic Limestone thus hints that Eocene coralline algae might have been fundamentally different (probably less adaptable) than their more modern counterparts.

8.2 Introduction

It is a common opinion that clastic input is detrimental for marine carbonate producing organism. This is based on three major pieces of evidence. First, most carbonate producers either feed by catching food from the water column (either passively like bryozoans or actively like corals), and thus they can be damaged by sediment ingestion (e.g., James and Kendall, 1992), or are dependent on light (e.g., calcareous algae, symbiont-bearing corals), and therefore they dislike turbid water, and

even more being covered in sediment. Secondly, most of them are sessile or they have a limited mobility, and thus, if buried by sediment, neither escaping nor relocating is an option. Last but not least, many large present-day carbonate systems are located far away from major sources of terrigenous sediment (e.g., the Bahamas Bank Complex, Roberts, 1987; the Maldives Islands, Lüdmann et al., 2013). Although the detrimental effect of clastic sediment is undeniable, carbonate production can take place even in areas with significant sediment influx, as testified by the common occurrence of mixed siliciclastic-bioclastic deposits (e.g., Doyle and Roberts, 1988; Wilson and Lokier, 2002; Lokier et al., 2009). One explanation for this apparent exception is that clastic input may be seasonal or episodic and a period of high supply can be followed by low accumulation sufficiently prolonged for a carbonate factory to develop (e.g., Bernasconi et al., 1997; Tomassetti et al., 2013). Another reason is that some carbonate-producing organisms are able to deal with high sedimentation rate. Red calcareous algae can photosynthesize even in dim light (e.g., van den Hoeck et al., 1995) and withstand sediment-related turbidity (e.g., Lokier et al., 2009). Larger benthic foraminifera can excavate themselves following shallow burial (e.g., Lokier et al., 2009). Corals are capable of cleaning their surface and remove sediment particles from their oral disk (e.g., solitary fungiids, Heikoop et al., 1996; *Cladocora caespitosa*, Schiller, 1993). The grain size of clastic material is another important variable, because the self-cleaning capabilities of corals are strictly limited by particle grain-size (e.g., Lasker, 1980). Moreover, particle size affects micro-environmental dynamics (e.g., substrate stability, development of microbial biofilms) and consequently also affects the distribution of carbonate producers such as bryozoans and foraminifers (e.g., Smith, 1995; Du Châtelet et al., 2009). Because sediment supply has a significant impact on both the development of carbonate factories and their composition, favoring certain groups over others, the interplay between skeletal-assemblage composition and abundance of clastic material can provide important paleoenvironmental information. Furthermore, because human activities (e.g., dam building, land development, deforestation) exert a significant impact on the sediment load of rivers, and thus on the amount of clastic material delivered to the sea, a full understanding of the response of carbonate factories to terrigenous fluxes is essential to foresee the long-term dynamics of modern environments. This study aims at investigating the effects of terrigenous fluxes on carbonate-producing biota focusing on the Paleogene Alpine foreland basin. Foreland basins are created by dynamic forces related to continental subduction and by lithospheric flexure caused by the load of the orogen (Dickinson, 1974; DeCelles and Giles, 1996; Sinclair and Naylor, 2012; Garzanti, 2019a). The southwestern part of the Alpine foreland basin hosts extensive carbonate and mixed siliciclastic-carbonate successions, mainly deposited during the Eocene epoch and generally displaying an overall (and similar) deepening-upward trend controlled by tectonic subsidence

(Ravenne et al., 1987; Sinclair, 1997). These successions, developed in a relatively small area, display a wide variety of carbonate facies and a remarkably variable terrigenous fraction, representing an ideal setting to study the effects of clastic input on carbonate-producing biota and highlight differences and similarities between Paleogene systems and their modern counterparts.

8.3 Geological setting

The Alpine foreland basin formed mainly as a consequence of the convergence of the European continent with the Adria microplate that created the Alps and next the Apennines and extends from Liguria and southeastern France to Switzerland and Austria. In the study area, located at the political border between Italy and France (Fig. 8.1A, B), the strata underlying the foreland-basin succession consist of calcilutites, sandstones and minor microconglomeratic sandstones deposited by turbidity currents and debris flows in the quasi-oceanic Alpine Tethys seaway during the Late Cretaceous (Ravenne et al., 1987; Giammarino et al., 2010; Mueller et al., 2018) (Fig. 8.1C). These units are separated by a major angular unconformity from the overlying Paleogene deposits (Fig. 8.1C).

8.3.1 The Paleogene succession

The Paleogene succession can be broadly divided into six main units testifying to the evolution of the basin: 1) the Infrannummulitic, 2) the Nummulitic Limestone, 3) the *Globigerina* Marls, 4) the Sandstones, 5) the Mélanges, and 6) the Molasse (Fig. 8.1C).

1) The Infrannummulitic (locally named Infrannummulitic Formation, *Microcodium* Formation, or Poudingues d'Argens) is generally 10 to 50 m thick (Sturani, 1965; Sinclair et al., 1998; Varrone and Clari, 2003; Barale et al., 2016), but thicker deposits have been reported in the western stretches of the basin (Barrême area; Ford et al., 1999). It displays a remarkable variety of sedimentary deposits related to fluvio-deltaic and very shallow marine environments (e.g., Sturani, 1965; Ravenne et al., 1987; Gupta, 1997; Sinclair et al., 1998; Evans and Elliott, 1999; Varrone and Clari, 2003). In the studied area, from the bottom to the top, the most common ones are: i) *Microcodium*-bearing marly breccias usually separated from the underlying substrate by an erosive surface and characterized by poorly sorted angular fragments of Upper Cretaceous marlstone and reworked Upper Cretaceous planktonic foraminifera (Varrone and Clari, 2003); ii) *Microcodium*-bearing marly limestone, locally nodular, displaying reworked Upper Cretaceous planktonic foraminifera and rare terrigenous grains (Sturani, 1965; Sinclair et al., 1998; Varrone and Clari, 2003); iii) *Microcodium*-bearing conglomerates, consisting of clast-supported lenticular deposits, mainly characterized by pebbles related to the erosion of the underlying Upper Cretaceous substrate (chert pebbles and very rare nummulitic limestone pebbles also occur) (Sturani, 1965; Sinclair et al., 1998; Varrone and Clari,

2003; Sztrákos and Du Fornel, 2003). Sand lenses have also been reported. These conglomerates also include a small bioclastic fraction consisting of reworked *Inoceramus* and rare *Nummulites* (Sinclair et al., 1998; Varrone and Clari, 2003); iv) clast-supported conglomerates with *Microcodium*-bearing pebbles locally displaying remains of terrestrial vertebrates (including *Palaeotherium* that indicates an age not older than the middle Eocene; Sturani, 1965); v) fine-grained dark limestones (also called *Cerithium* marlstones), characterized by lenses of dark-chert, terrestrial, brackish and shallow-marine gastropods, remains of charophytes, terrestrial plants and shallow-water benthic foraminifera (Sturani, 1965; Sinclair et al., 1998; Varrone and Clari, 2003; Sztrákos and Du Fornel, 2003). Gastropod assemblages suggest a Bartonian age for these deposits (Sturani, 1965); vi) well-sorted, quartz-rich sands displaying rare large benthic foraminifera (mainly *Nummulites brongnarti*, *Nummulites puschi*, *Nummulites striatus* and *Orbitolites*; indicating a Bartonian age; Serra-Kiel et al., 1998; Varrone and Clari, 2003). Since *Microcodium* consists of microscopic aggregates of elongated calcite crystals related to the decomposing activity of either roots, fungi or bacteria within the soil (Klappa, 1978; Košir, 2004; Kabanov et al., 2008), i, ii, iii, and iv should have formed in a continental environment (most likely a river valley) (Sturani, 1965; Gupta, 1997; Sinclair et al., 1998; Varrone and Clari, 2003; Sztrákos and Du Fornel, 2003); v should represent the transition toward a brackish or shallow marine environment, and vi should indicate fully marine conditions (Sturani, 1965; Sinclair et al., 1998; Varrone and Clari, 2003). Overall, the facies succession of the Infranummulitic unit represents the initial phase of a marine transgression.

2) The Nummulitic Limestone, which represents the focus of this study, testifies to a widespread marine transgression. It is characterized by a variable thickness ranging between 10 and 100 m, generally greater in the external eastern part of the basin and decreasing westward (Sinclair et al., 1998; Evans and Elliott, 1999; Varrone and Clari, 2003; Sztrákos and Du Fornel, 2003), but it goes up to 150m in western Liguria (Loreto area; Varrone and D'Atri, 2007). The Nummulitic Limestone lies unconformably either onto the Infranummulitic or, more commonly, directly onto the Upper Cretaceous (e.g., Lickorish and Ford, 1998). Despite its name, the unit contains siliciclastic detritus. The facies succession indicates progressive deepening of the basin. The base is usually characterized by a lag deposit rich in pebbles commonly displaying *Gastrochaenolites* borings (Carbone et al., 1980; Gupta, 1997; Evans and Elliott, 1999; Gupta and Allen, 2000; Varrone and D'Atri, 2007). This initial transgressive ravinement surface is overlain by shallow-water limestones rich in nummulitids and, locally, in coralline algae (Ravenne et al., 1987; Sinclair et al., 1998; Varrone and D'Atri, 2007) (Fig. 8.1C). Further deepening of the depositional environment is testified by the transition toward deposits rich in orthofragminids large benthic foraminifera (LBF from here onward) and planktonic foraminifera (Fig. 8.1C). The top of the unit generally presents a drowning

(maximum flooding) surface with reworked bioclasts and abundant authigenic minerals, which testifies to the demise of the carbonate factory (Sinclair et al., 1998).

3) The overlying *Globigerina* Marls have a variable thickness ranging from few meters (Sturani, 1965; Barale et al., 2016) to 100-200m (Allen et al., 1991; Sztrákos and Du Fornel, 2003). They deposited in a hemipelagic environment characterized by a limited clastic supply (Fig. 8.1C). The unit may be subdivided into a lower part (Blue Marls), mainly calcareous and containing coquina layers (sensu Schaffer, 1972) rich in reworked shallow-water bioclasts, and an upper part (Brown Marls) characterized by an increased terrigenous fraction (Ravenne et al., 1987; Artoni and Meckel, 1998).

4) Heralded by the Brown Marls, siliciclastic supply culminates with the deposition of the Sandstones (locally called Grès d'Annot, Grès du Champsaur, Grès de Ville, Souloise Greywacke, or Ventimiglia Flysch) (Fig. 8.1C). This terrigenous unit is usually 500 to 1000 m thick (Ravenne et al., 1987; Ford et al., 1999; Sztrákos and Du Fornel, 2003; Mulder et al., 2010), but in the western stretches of the basin (Barrême area) is much thinner, around 50 m (Ford et al., 1999). Quartzofeldspathic to litho-feldspatho-quartzose petrographic composition (Hu et al., submitted; classification after Garzanti, 2019b) and paleocurrents suggest that the main source of the detritus was located to the south and represented by the Sardinia-Corsica block and/or the Massif de l'Esterel (Ravenne et al., 1987; Lickorish and Ford, 1998; Ford et al., 1999; Mulder et al., 2010).

5) In the eastern part of the basin, the succession is sealed by the Mélange, which includes chaotic accumulation of detritus (300 to 600 m thick) from the internal Alpine domain (Ravenne et al., 1987; Evans and Elliott, 1999; Ford et al., 1999; Perotti et al., 2012; Maino and Seno, 2016) (Fig. 8.1C).

6) In the western part of the basin, instead, the succession is unconformably covered by the “Molasse”. This name, once commonly used to define late orogenic clastic deposits accumulated in a foredeep basin (e.g., van Houten, 1973), is nowadays used in the Alpine region to indicate a widespread and thick unit consisting of clastic marine deposits accumulated in progressively shallower settings and finally overlain by fluvio-deltaic sediments (Evans and Elliott, 1999; Ford et al., 1999) (Fig. 8.1C).

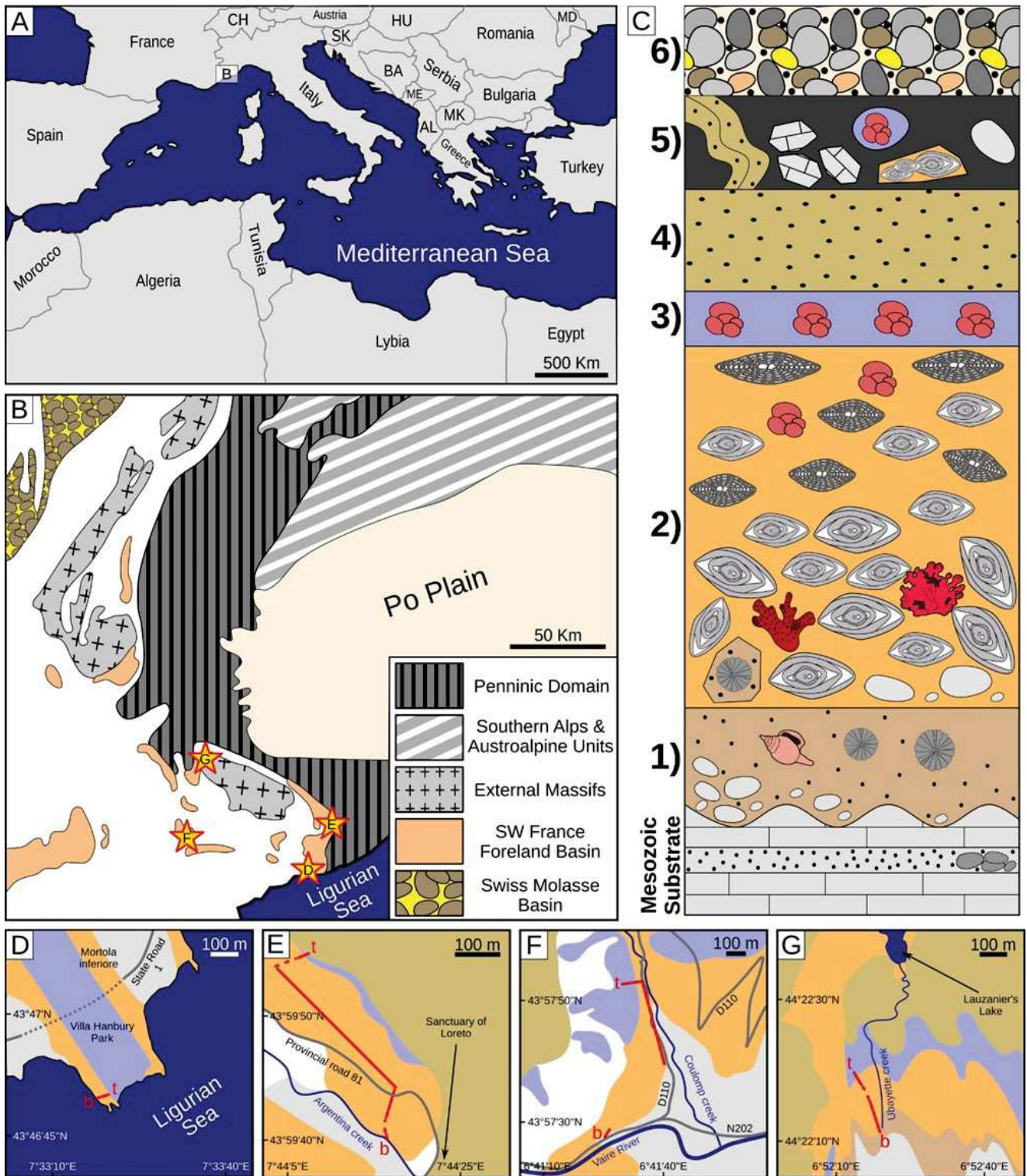


Figure 8.1 Geographical and geological setting of the four investigated successions. A) Location of the study area within the Mediterranean region. B) Main geological units of NW Italy and SE France. C) Simplified stratigraphic log of the Western Alpine foreland basin; 1=Infranummulitic; 2=Nummulitic Limestone; 3=*Globigerina* Marls; 4=Sandstones; 5=Mélanges; 6=Molasse; symbols as in Fig. 9.3. Simplified geological maps of: D) Mortola section; key colours as in panel C; b, t=base and top of section; E) Loreto section; F) Braux section; G) Lauzanier section.

8.3.2 Stratigraphic ages

The ages inferred for the Infrannummulitic Formation (1), in the study area, should be comprised between the Lutetian (based on the presence of *Palaeotherium*; Sturani, 1965) and the Bartonian (based on gastropod and LBF assemblages; Sturani, 1965; Varrone and Clari, 2003; Sztrákos and Du Fornel, 2003). A Priabonian age has also been proposed by Sinclair et al. (1998) based on a different interpretation of the association of the vertebrates and gastropods reported by Sturani (1965). It must be noted that the limited knowledge of the distribution of Paleocene terrestrial vertebrates and marine gastropods species limits their stratigraphic significance. On the other hand, Varrone and Clari (2003) reported the presence of *Orbitolites* (whose extinction occur at the Bartonian/Priabonian boundary; Sartorio and Venturini, 1988; Serra-Kiel et al., 1998; Nebelsick et al., 2005; Boudaughier-Fadel, 2018), thus indicating a pre-Priabonian age for the Infrannummulitic. Because of the inherent difficulties in dating shallow-water limestones, the age of the Nummulitic Limestone (2) is also imprecisely constrained. The onset of deposition is diachronous, with the oldest strata exposed in the central Swiss Alps (Fliegenspitze beds, Thanetian age) (Ravenne et al., 1987; Ford et al., 1999; Allen et al., 2001; Kempf and Pfiffner, 2004). Within the study area, the base of the Nummulitic Limestone was constrained by LBF assemblages to the Bartonian (Sztrákos and Du Fornel, 2003; Varrone and Clari, 2003; Varrone and D'Atri, 2007), although ages ranging from late Lutetian to Priabonian have also been proposed (Bodelle, 1971; Campredon, 1977; Varrone and D'Atri, 2007). A general younging trend from SE to NW has also been documented (Campredon, 1977; Ford et al., 1999; Sztrákos and Du Fornel, 2003). The overlying *Globigerina* Marls (3) are assigned, based on planktic foraminiferal and calcareous nannofossil assemblages, to the late Bartonian to early Priabonian in the eastern part of the study area, and to the Priabonian in the western part (Lickorish and Ford, 1998; Evans and Elliott, 1999; Sztrákos and Du Fornel, 2003; Varrone and D'Atri, 2007; Mulder et al., 2010). According to calcareous nannofossils, planktonic foraminifera and reworked LBF, Sandstones (4) sedimentation in the study area should have started between the uppermost Bartonian and the Priabonian, while westward, in the Barrême area, it should have started during the Rupelian (Ford et al., 1999; Sztrákos and Du Fornel, 2003; Mulder et al., 2010). This is substantially consistent with the $^{40}\text{Ar}/^{39}\text{Ar}$ and K-Ar ages of the volcanic pebbles of the Sandstones that range between 35 and 30 Ma (Féraud et al., 1995; Montenat et al., 1999).

8.4 Materials and methods

Four stratigraphic successions located in the area straddling the political border between NW Italy and SE France were accurately measured and sampled focusing on the Nummulitic Limestone and on immediately underlying and overlying intervals: Capo Mortola (NW Italy; 43°46'50.5"N

7°33'20.8"E), Loreto (NW Italy; 43°59'43.4"N 7°44' 18.8"E), Braux (SE France; 43°57'31.3"N 6°41'36.9"E), and Lauzanier (SE France; 44°22'55.1"N 6°52'18.7"E) (Fig. 8.1B, D–G). Strata were logged in detail in the field, giving particular attention to major surfaces, macrofossil distribution, and sedimentary structures. The Capo Mortola section follows the section measured and sampled by Carbone et al. (1980). The investigated carbonate rocks were classified based on Dunham's (1962) classification, expanded by Embry and Klovan (1971) and refined by Lokier and Al Junaibi (2016). Representative rock samples were taken for petrographic and paleontological analyses. Wherever possible, further samples of isolated LBF were collected for biostratigraphic analysis. A total of 147 thin sections were analysed (102 for skeletal assemblages, 25 dedicated to oriented sections of LBF, and 20 from units below and above the Nummulitic Limestone). Isolated LBF specimens were embedded in epoxy resin within a pill blister and abraded with silicon carbide to expose their equatorial plane (Coletti et al., 2019a). Subsequently, the specimens were prepared into thin sections. The taxonomy used for the classification of isolated orthophragminid specimens follows Less (1987). Skeletal assemblages and petrographic characteristics (including the amount of terrigenous material) were investigated by counting 350 points on each section and using a 250 µm mesh (Flügel, 2010). Full results of point-count analyses are included in Supplementary Table 8.1. Paleoenvironmental interpretation was based principally on foraminiferal assemblages. In each section, all LBF were identified at the lowest possible taxonomic level and counted; small miliolids and planktonic foraminifera were also counted. The orthophragminid/nummulitid ratio (O/N), the large rotaliid/miliolid ratio, and the abundance of planktonic foraminifera were thus obtained for each sample. These parameters are depth-related and generally increase with increasing water depth (Hallock and Glenn, 1986; Čosović et al., 2004; Beavington-Penney and Racey, 2004). The terrigenous fraction was further investigated by powder X-ray diffraction (PXRD) on 32 bulk samples from different microfacies, and from units underlying and overlying the Nummulitic Limestone. The samples were initially ground in an agate mortar. PXRD analysis was performed on zero-background silicon plates with a Philips PW1140 diffractometer equipped with CoK α radiation (K α 1 wavelength 1.789 Å) operating at 40 kV and 20 mA. The samples were scanned between 3° and 70° 2 θ with a step size of 0.02° 2 θ and an acquisition time of 1 s per step. Data treatment was carried out with Panalytical X'pert HighScore Plus to identify the main mineralogical phases and a semiquantitative analysis was carried out using the Reference Intensity Ratio (RIR) method (Chung, 1974).

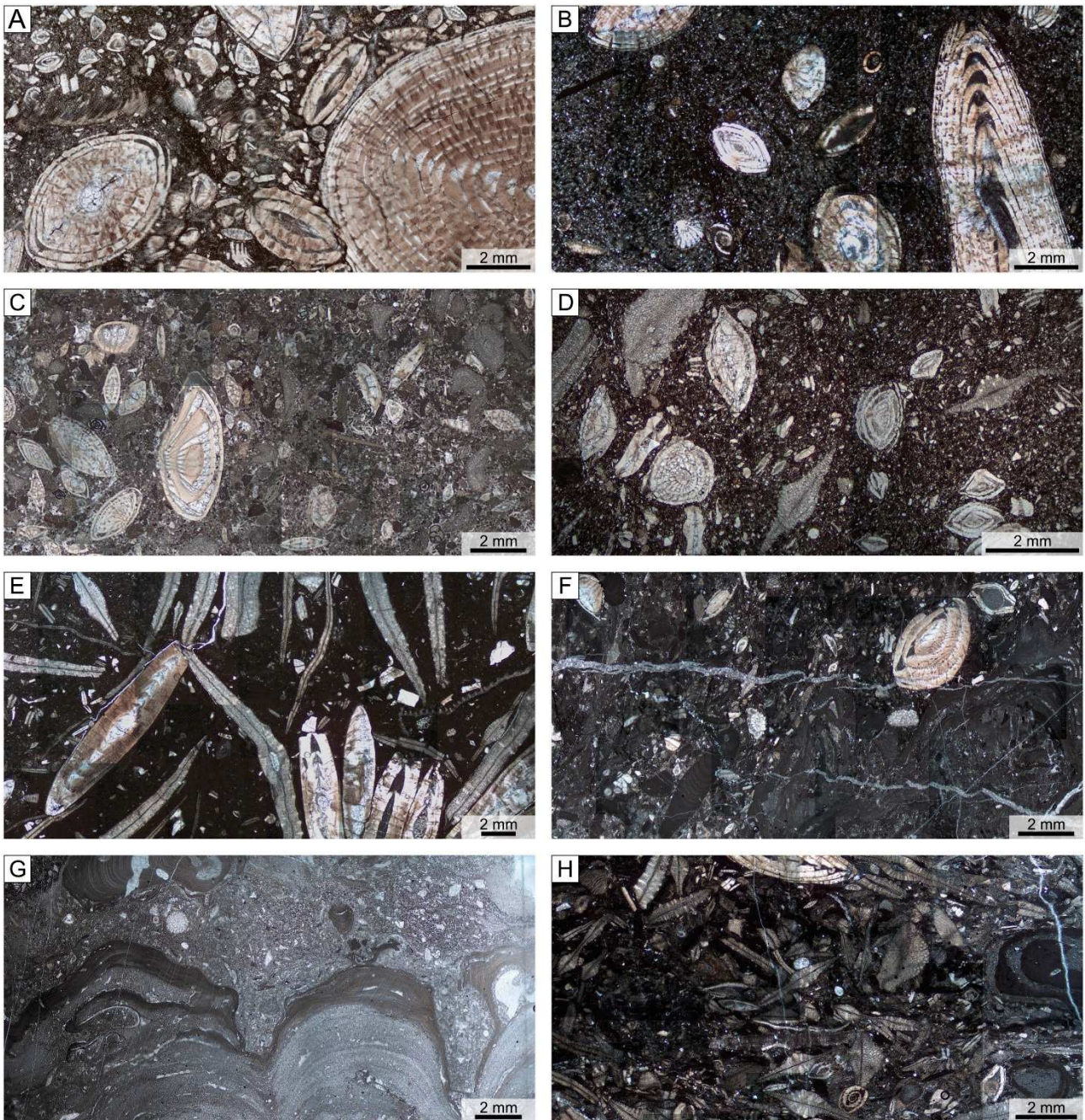


Figure 8.2 Overview of the main recognized biofacies of the Nummulitic Limestone. A) Nummulitid biofacies, Capo Mortola; B) *Orbitolites*-bearing nummulitid biofacies, Capo Mortola; C) acervulinid-bearing nummulitid biofacies, Braux; D) nummulitid and orthophragminid biofacies, Braux; E) orthophragminid biofacies, Capo Mortola; F) coralline algal branches and LBF biofacies, Loreto; G) acervulinid and coralline algal biofacies, Loreto; H) orthophragminid and coralline algal biofacies; Loreto.

8.5 Results

Based on the analysis of the skeletal and foraminiferal assemblages of the investigated sections, six main biofacies have been recognized:

i) Nummulitid biofacies, occurring at the base of Mortola and Braux successions and characterizing the whole Lauzanier section. The skeletal assemblage is largely dominated by nummulitids (Fig. 8.2A); echinoderms and molluscs are usually common; solitary corals can be

relevant. The foraminiferal assemblage is almost entirely consisting of benthic taxa and is dominated by the genus *Nummulites*; *Amphistegina* and small miliolids can be also common; planktic foraminifera are very rare or absent. The nummulitid biofacies can be further subdivided into the *Orbitolites*-bearing nummulitid biofacies (lowermost Mortola section; Fig. 8.2B) and the acervulinid-bearing nummulitid biofacies (lowermost Braux section; Fig. 8.2C).

ii) Nummulitid and orthophragminid biofacies, occurring above the nummulitid biofacies in both the Mortola and Braux sections. It is dominated by LBF (Fig. 8.2D), associated with common molluscs and echinoderms, and rare serpulids (mainly *Ditrupa*); solitary corals can be abundant. Nummulitids (*Nummulites*, *Assilina*, *Operculina*) and orthophragminids dominate the foraminiferal assemblage; *Amphistegina* is rare, while planktic foraminifera can be common.

iii) Orthophragminid biofacies, occurring above the nummulitid and orthophragminid biofacies in both the Mortola and Braux sections. The skeletal assemblage is almost entirely consisting of orthophragminids and planktic foraminifera (Fig. 8.2E). *Assilina*, *Operculina*, and rare *Nummulites* also occur (Fig. 8.2E).

iv) Coralline algal branches and LBF biofacies, occurring in the Loreto section. Its skeletal assemblage consists of red calcareous algae (mainly pebble to granule-sized branches and rhodoliths) and LBF, associated with echinoderms, bryozoans and molluscs (Fig. 8.2F). The foraminiferal assemblage includes acervulinids, nummulitids, orthophragminids, small rotaliids, and small miliolids.

v) Acervulinid and coralline algal biofacies, occurring in the Loreto section. It is characterized by pebble-sized macroids (i.e., coated grains created by the concentric growth of encrusting organisms) built by encrusting foraminifera and coralline algae (Fig. 8.2G). The macroids are associated with free-living LBF, echinoderms and molluscs. The foraminiferal assemblage is dominated by acervulinids, associated with *Nummulites*, orthophragminids, *Alveolina*, and small miliolids.

vi) Orthophragminid and coralline algal biofacies, occurring only in the uppermost part of the Loreto section. Differently from the orthophragminid biofacies of Mortola and Braux, it displays abundant coralline algae (Fig. 8.2H).

8.5.1 Mortola

In the Mortola section, the Nummulitic Limestone is roughly 55 m thick and overlies Upper Cretaceous pelagic marlstones (Fig. 8.1D). The contact is an erosive surface, punctuated by small traces of boring organisms (possibly endolithic bivalves), carved into the underlying marlstones and

filled with the coarser-grained bioclastic material of the Nummulitic Limestone. The basal layers of the Nummulitic Limestone contain common pebbles of dark chert, which do not occur up-section.

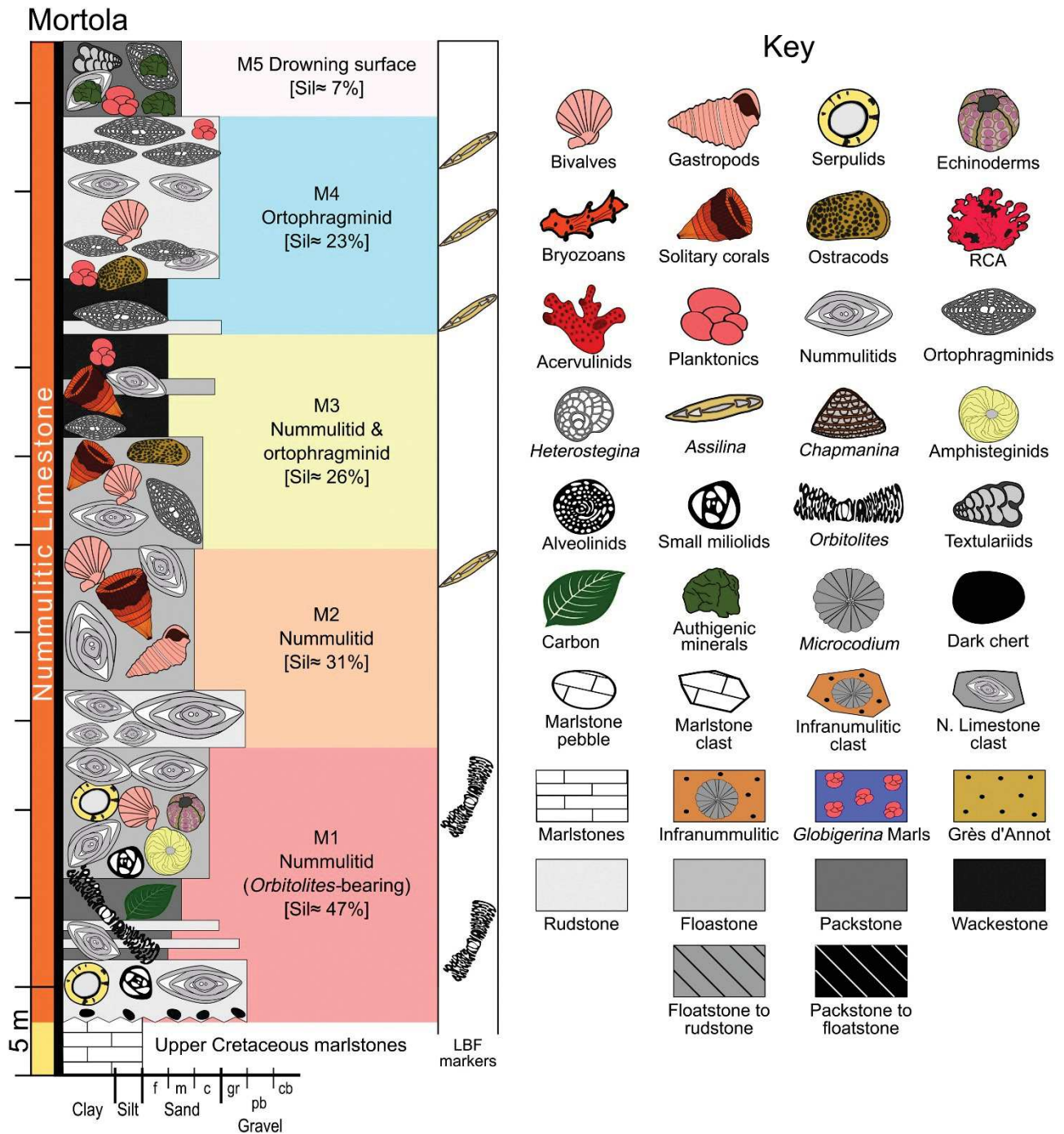


Figure 8.3 Stratigraphic log of Mortola section with information on skeletal assemblages, average grain-size, and key to symbols. Sil = siliciclastic fraction; sub. = subfacies; LBF= large benthic foraminifera; RCA = coralline algae; f = fine; m= medium; c = coarse; gr= granules; pb= pebbles; cb= cobbles.

Based on microfacies analysis, sedimentological features and macrofossil distribution, the measured section can be subdivided into five intervals (Figs. 8.3, 8.4).

Interval M1 (~17 m; *Orbitolites* bearing nummulitid biofacies). It consists of nummulitic rudstone layers (mainly lentil-sized megalospheric forms, associated with rarer microspheric forms

with diameter up to 5 cm) alternating with packstone layers with rare large oyster and charcoal fragments (Fig. 8.4B, C). These are overlain by a floatstone layer (packstone matrix), where nummulitids, locally concentrated in lenses, are associated with solitary corals, molluscs (mainly large specimens of *Pycnodonte*, but also cardiidae, pectinids, gastropods, and vermetid gastropods; Fig. 8.4D, E), serpulids, rare echinoderms, and very rare colonial corals (Fig. 8.4F). Small burrows lined with nummulitid tests also occur (Fig. 8.4G). Microfacies analysis indicates that the skeletal assemblage is overwhelmingly dominated by LBF, associated with, in decreasing order of abundance, echinoderms (mainly irregular echinoids), small benthic foraminifera, serpulids (mainly *Ditrupa*), and molluscs (Fig. 8.5A-G; Table 8.1). The benthic foraminiferal assemblage is dominated by *Nummulites* (Fig. 8.5A, B) with common *Orbitolites* (both whole specimens and fragments; Fig. 8.5A, C), *Amphistegina* (Fig. 8.5F), small rovaliids and small miliolids (Fig. 8.5G). The terrigenous fraction accounts for up to 50% of the rock (Fig. 8.3; Table 8.1) and is mainly represented by fine-sand-sized angular quartz grains, plagioclase and K-feldspar. The sparse heavy-mineral fraction chiefly consists of commonly euhedral zircon, tourmaline and rutile, with minor hornblende, staurolite, and garnet.

Interval M2 (~12 m; nummulitid biofacies). This interval starts with a 4 m-thick, nummulitic rudstone characterized by very common, thick megalospheric specimens associated with rarer gigantic microspheric specimens (diameter up to 5 cm; Fig. 8.4H, I), overlain by an 8 m-thick floatstone with a wackestone matrix displaying common nummulitids, solitary corals (Fig. 8.4J), gastropods, bivalves (mainly large *Pycnodonte* specimens and pectinids), scaphopods, rare serpulids, echinoderms (both spines and complete tests), and crab remains. Thin section analyses indicate that the skeletal assemblage is dominated by nummulitids (*Nummulites* and subordinate *Assilina*) with solitary corals, molluscs, small benthic foraminifera, echinoderms, serpulids, planktic foraminifera, and ostracods (Table 8.1). Terrigenous grains represent ~30% of the rock and mainly consist of fine-sand-sized angular quartz grains, plagioclase, K-feldspar, and rare muscovite (Fig. 8.3; Table 8.1).

Interval M3 (~12 m; nummulitid and orthophragminid biofacies). Floatstone (with a wackestone matrix) with nummulitids (mainly small specimens with diameter <1 cm), solitary corals, *Pycnodonte* (commonly occurring in groups of several specimens attached together), and gastropods, alternating with wackestones almost devoid of macrofossils. The skeletal assemblage is dominated by LBF, associated with solitary corals, molluscs, small benthic foraminifera, echinoderms, planktic foraminifera, serpulids, and ostracods (Fig. 8.5H; Table 8.1). The benthic foraminiferal assemblage is dominated by orthophragminids, *Nummulites* and small rovaliids including *Lenticulina*. The detrital fraction accounts for roughly 25% of the rock and mainly consists of coarse-silt-sized angular quartz grains, K-feldspar, plagioclase and rare muscovite (Fig. 8.3; Table 8.1).

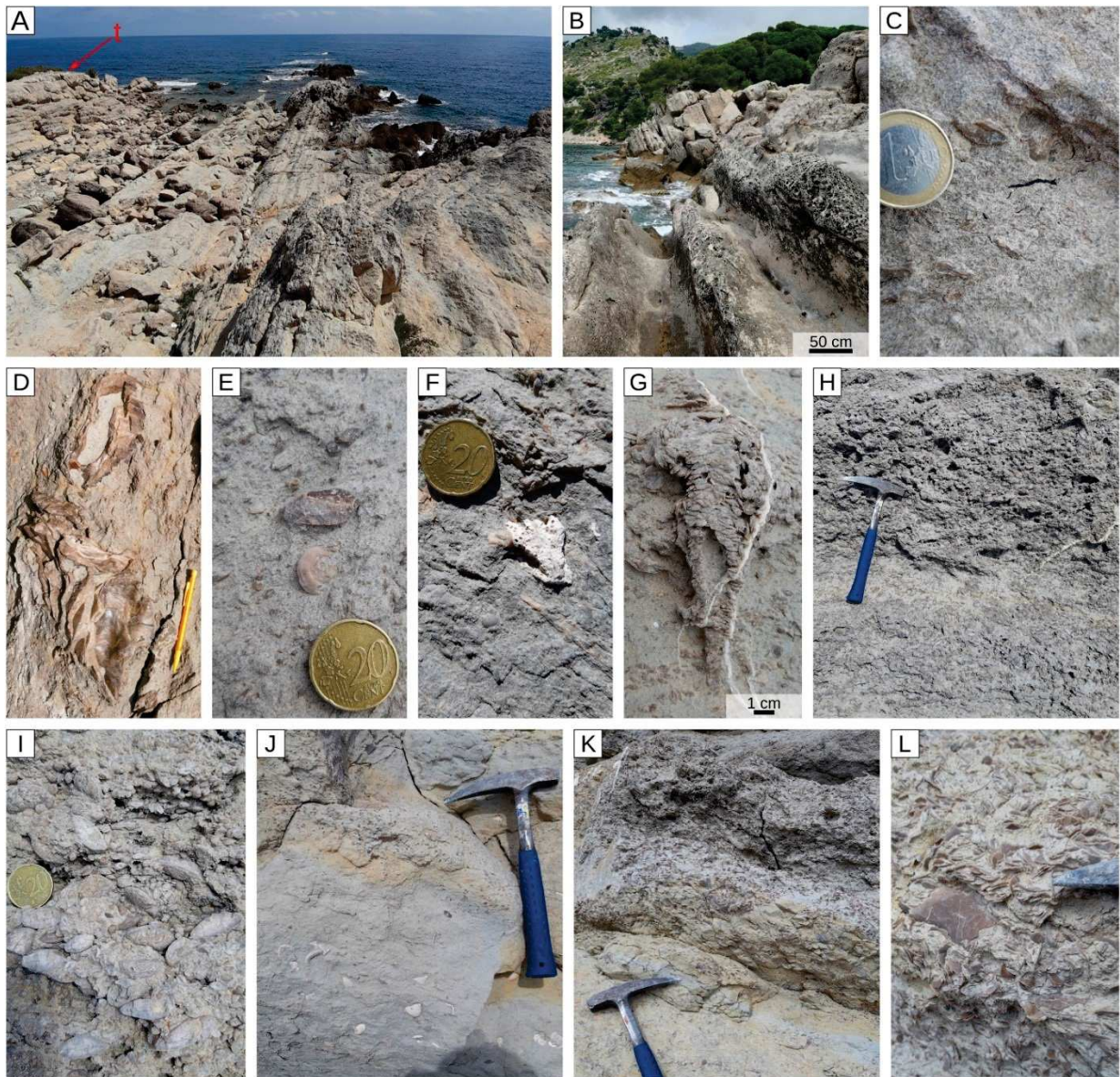


Figure 8.4 Mortola section. A) Outcrop overview (base of section to the right, top to the left). B) M1, nummulitid rudstone alternating with fine-grained packstones; C) M1, charcoal fragment D) M1, large *Pycnodonte* oysters; E) M1, vermetid gastropods; F) M1, colonial coral; G) M1, burrow lined with *Nummulites* tests; H) base of M2; I) M2, large-sized *Nummulites*; J) upper part of M2. K) Overview of M4; L) M4, thin and saddle-shaped orthoheragminids with a large-sized microspheric specimen.

Interval M4 (~13 m; orthoheragminid biofacies). The base of this interval consists of a rudstone, with a wackestone matrix, rich of flat and thin nummulitids (mainly *Assilina exponens*), and orthoheragminids including microspheric specimens up to several cm in diameter (Fig. 8.4K). This rudstone is overlain by a 50 cm-thick wackestone layer and further overlain by a rudstone characterized by densely packed, thin, and saddle-shaped orthoheragminids including microspheric specimens up to 5 cm in diameter (Fig. 8.4L). This layer also displays decimeter-long burrows lined by LBF. The skeletal assemblage almost entirely consists of LBF (orthoheragminids and subordinate nummulitids), associated with planktonic foraminifera, small rotaliids (including *Lenticulina* and

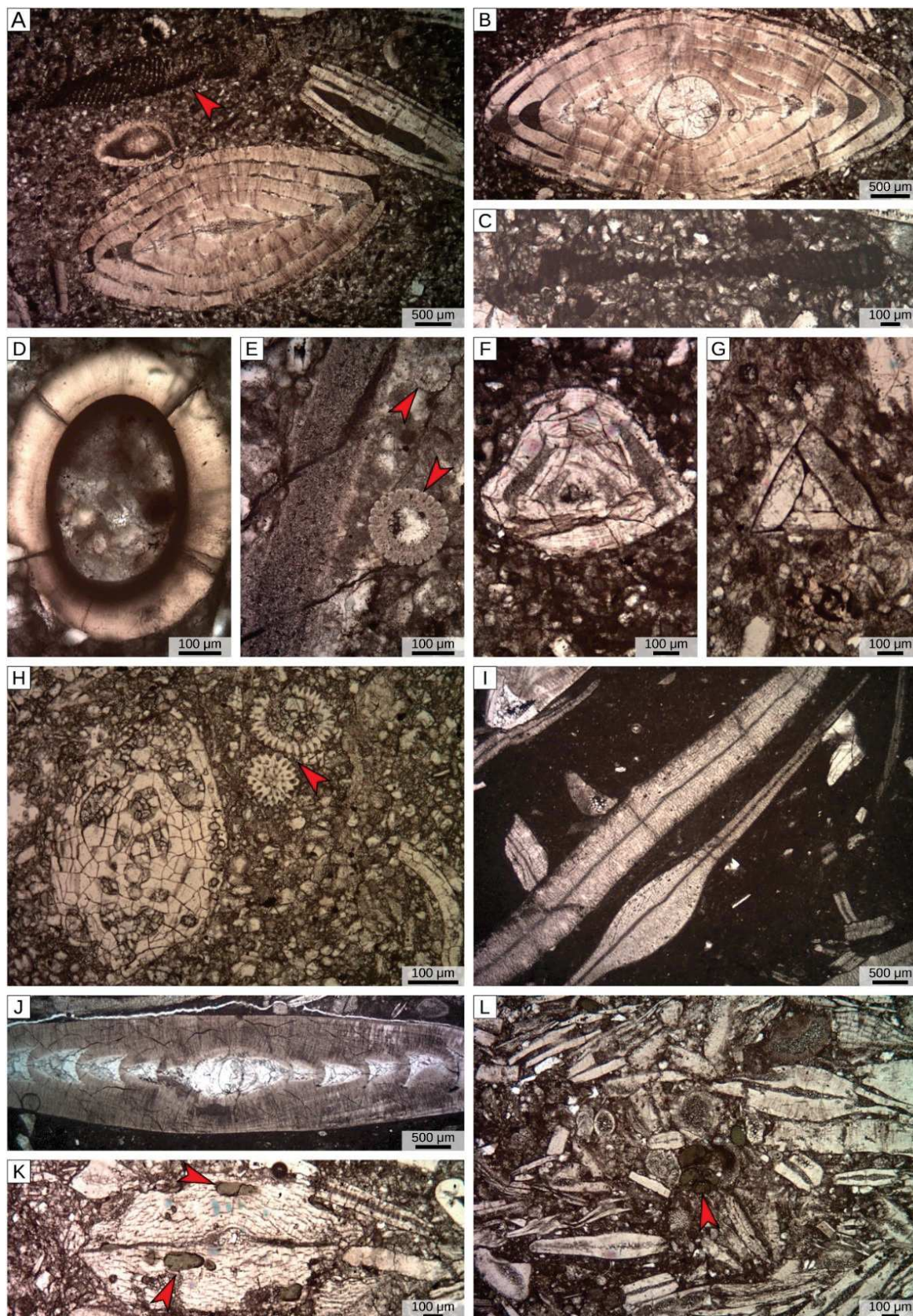


Figure 8.5 Skeletal assemblage and microfossils in the Mortola section. A) M1, *Orbitolites* (red arrow) bearing nummulitid biofacies; B) M1, *Nummulites*, axial section; C) M1, *Orbitolites*, axial section; D) M1, *Ditrupa*; E) M1, echinoderm fragments (red arrow points at spines of irregular echinoids); F) M1, *Asterigerina*; G) M1, *Triloculina*; H) M3, *Lenticulina* and planktonic forams (red arrow); I) M4, thin and flat orthofragminids; J) M4, *Assilina*; K) M4, glaucony-filled orthofragminid; L) M5, well-sorted and fragmented foraminifera (red arrow points at glaucony).

Stilostomella), echinoderms, and ostracods (Fig. 8.5I, J; Table 8.1). Coarse-silt-sized quartz grains represent the bulk of the terrigenous fraction, together with plagioclase, K-feldspar, and muscovite (Fig. 8.3; Table 8.1). Toward the top of the interval, foraminiferal chambers can be filled with glaucony (Fig. 8.5K).

Interval M5 (~1 m; drowning lag). The Nummulitic Limestone is capped by a drowning surface characterized by a well-sorted foraminiferal packstone containing molluscs, echinoderms, and glaucony commonly filling foraminiferal tests (Fig. 8.5L). The foraminiferal assemblage is dominated by nummulitids and orthophragminids, associated with common planktonic foraminifera, textulariids, small rotaliids (including *Lenticulina*), and rare miliolids. The minor siliciclastic fraction (Fig. 8.3) consists of fine-sand-sized angular quartz grains and includes a small heavy-mineral fraction displaying zircon, tourmaline, rutile, biotite, apatite, staurolite, and garnet.

8.5.2. Loreto

In the Loreto area (municipality of Triora; NW Italy; Fig. 8.1E), Upper Cretaceous pelagic marlstones are unconformably overlain by a 2 to 4 m-thick paraconglomerate comprising poorly sorted clasts of the marlstones and of the Nummulitic Limestone, together with loose Eocene bioclasts (mainly nummulitids and fragments of coralline algae) (Figs. 8.6, 8.7). The significant siliciclastic fraction, making up to ~30% of the rock, consists of coarse-silt-sized quartz grains with subordinate plagioclase, muscovite, and chlorite (Figs. 8.6, 8.7C). Angular and poorly sorted clasts of Nummulitic Limestone, ranging from granule to boulder-size (Fig. 8.7B, E, G), are mostly consisting of LBF (*Nummulites*, *Assilina*, orthophragminids, and *Sphaerogypsina*) and coralline algae. Rare fragments of encrusting acervulinids also occur. Coralline algae are poorly preserved, and the few recognizable fragments belong to the genus *Sporolithon*. Most of the Nummulitic Limestone material recovered from the paraconglomerate displays *Microcodium*-like alteration (Fig. 8.7G). The overlying 140-m thick Nummulitic Limestone, based on microfacies analysis, sedimentological features and macrofossil distribution, can be divided into five intervals (Figs. 8.6, 8.8A).

Interval L1 (~35 m; coralline-algal branches and LBF biofacies). The basal interval consists of floatstones to rudstones (with packstone matrix) dominated by coralline algae and LBF, including large microspheric specimens of *Nummulites* up to several centimeters in diameter. Rare large specimens of *Pycnodonte* also occur (Fig. 8.8B). The skeletal assemblage includes coralline algae (mainly *Sporolithon*, associated with *Hapalidiales* and *Corallinales*), LBF, associated with encrusting acervulinids, small benthic foraminifera, echinoderms, bryozoans, and molluscs (Fig. 8.9A–D; Table 8.1). The benthic foraminiferal assemblage includes *Nummulites*, *Assilina*, orthophragminids,

Sphaerogypsina, *Amphistegina*, small rotaliids, small miliolids and textulariids (Fig. 8.B, C). The terrigenous fraction is minor and quartz-rich (Fig. 8.6; Table 8.1).

Interval L2 (~50m; mass-transport deposits). Finely laminated, dark gray wackestones rich in organic matter, displaying dish structures related to dewatering, and characterized by fragmented and poorly preserved bioclasts, usually occurring in thin layers (1–2 cm) and displaying an imbricated fabric (Figs. 8.8C, 8.9E). Bioclasts include echinoderm fragments, planktic foraminifera, coralline algae, LBF (*Nummulites*, *Assilina*, orthophragminids), small rotaliids (including *Lenticulina*), textulariids, ostracods, bivalves, and rare small miliolids. Most of bioclasts are poorly preserved and fragmented except planktic foraminifera that are well preserved (Fig. 8.9F, G). Authigenic pyrite crystals may overgrow foraminiferal tests (Fig. 8.9H). The significant terrigenous fraction consists of coarse-silt-sized angular quartz grains together with chlorite, muscovite, and plagioclase (Fig. 8.6).

Interval L3 (~18 m; acervulinid and coralline algal biofacies). The central part of the section is characterized by dark-colored acervulinid macroid rudstones with a packstone matrix (Fig. 8.8D). Coralline algae commonly overgrow foraminiferal macroids. Gastropods and LBF are common, and solitary corals are rare. The skeletal assemblage is dominated by encrusting acervulinids and coralline algae, associated with LBF, small benthic foraminifera, echinoderms, and encrusting serpulids (Fig. 8.9I–L; Table 8.1). Green calcareous algae, bryozoans, molluscs, and ostracods are rare. Benthic foraminifera include common *Nummulites* and *Sphaerogypsina* associated with *Alveolina*, *Amphistegina*, *Eorupertia*, small rotaliids, small miliolids, textulariids, and rare *Orbitolites* and *Assilina* (Fig. 8.9J–L). Coralline algal assemblage is dominated by *Sporolithon* associated with *Hapalidiales* and *Corallinales* (including *Lithoporella*). The terrigenous fraction is negligible.

Interval L4 (up to 35 m-thick; coralline-algal branch and LBF biofacies). The upper part of the Loreto cliff is characterized by dark-coloured massive rudstones with a packstone matrix. Since the cliff is vertical, only the lower portion of this interval was extensively investigated. Coralline algae are slightly less abundant than in the L1 interval, while LBF and solitary corals are slightly more common. The foraminiferal assemblage is also similar, and the most noticeable difference is the lack of *Assilina*.

Interval L5 (3 m; orthophragminid and coralline algal biofacies). Only observable at the top of the cliff (Fig. 8.8A). It consists of a few meters of dark-gray rudstones with a packstone matrix dominated by thin and flat orthophragminids, whose abundance notably increases up section, coralline algae (including *Sporolithon* and *Hapalidiales*), associated with thin and flat nummulitids, molluscs, echinoderms, small benthic foraminifera, bryozoans, planktic foraminifera and acervulinids (Fig. 8.9M; Table 8.1). The benthic foraminiferal assemblage mostly consists of orthophragminids,

Nummulites, small rotaliids, textulariids, *Chapmanina*, *Sphaerogypsina* (Fig. 8.9N), and rare small miliolids. Quartz, muscovite, and plagioclase occur (Fig. 8.6; Table 8.1).

The Nummulitic Limestone is overlain by a thin layer of laminated *Globigerina* Marls, rich of sand-sized angular quartz grains and planktonic foraminifera, which is in turn overlain by the Ventimiglia Flysch (Figs. 8.8E, 8.9O). These fine-grained sandstones contain quartz and abundant plagioclase with common micas (chlorite, biotite, muscovite) associated with a sizable heavy mineral fraction including zircon, apatite, titanium oxides, tourmaline and hornblende (Figs. 8.6, 8.9P).

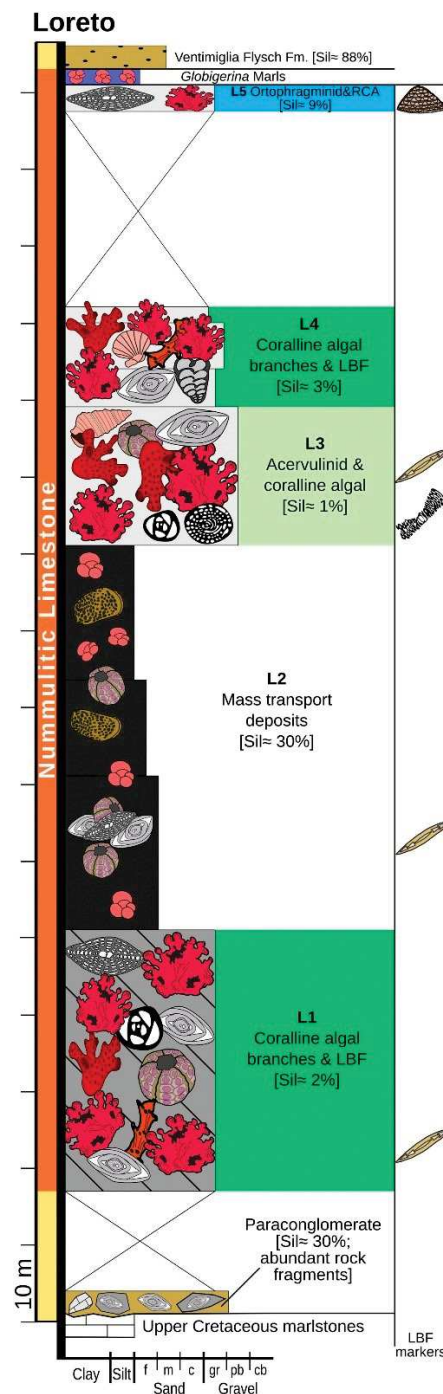


Figure 8.6 Stratigraphic log of Loreto section with information on skeletal assemblage and average grain-size. Symbols and abbreviations as in Fig. 8.3.

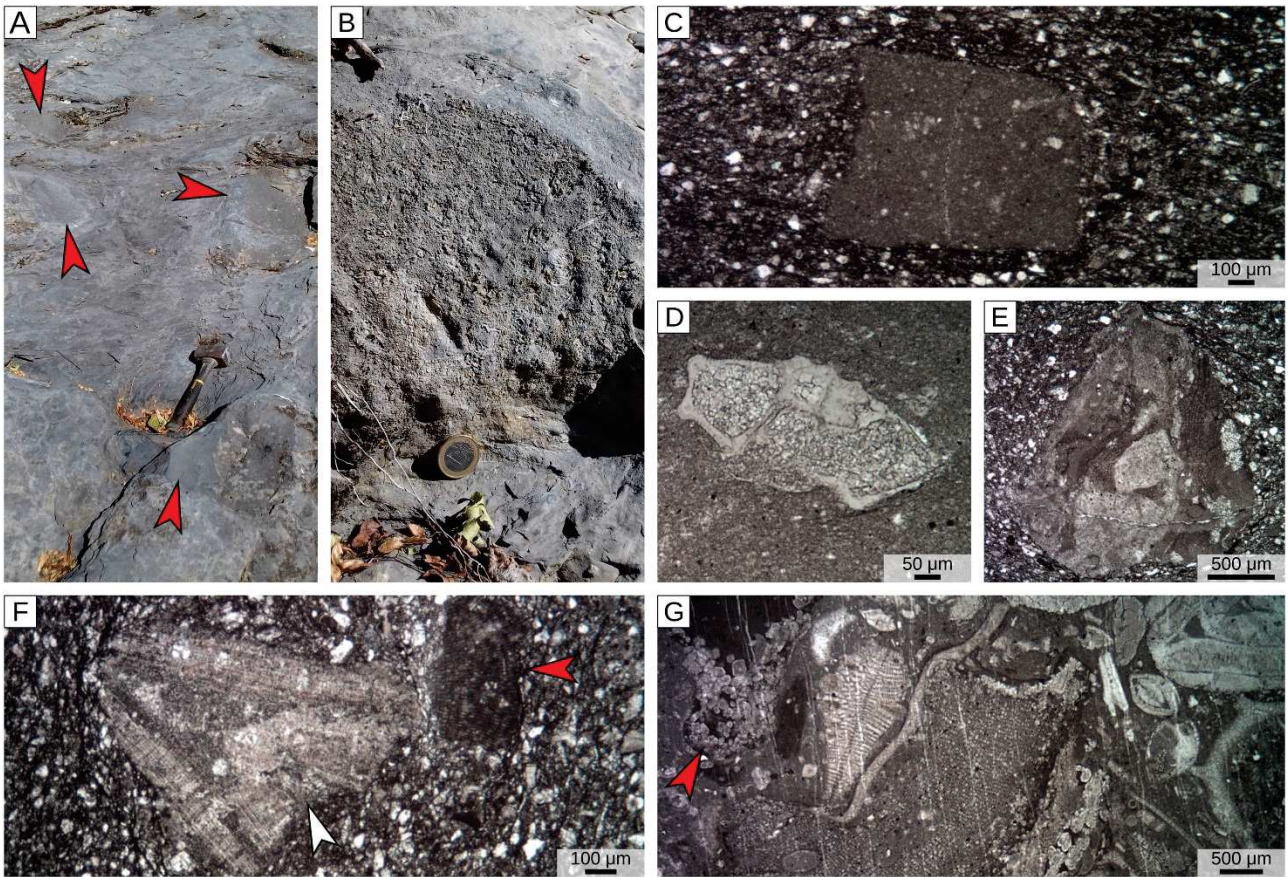


Figure 8.7 Paraconglomerate at the base of the Loreto section. A) Outcrop view of the paraconglomerate (red arrow points at clasts of Upper Cretaceous pelagic marls). B) Clast of Nummulitic Limestone. C) Angular clast of Upper Cretaceous pelagic marls embedded in paraconglomerate matrix. D) Specimen of *Globotruncana* contained in a clast of Upper Cretaceous pelagic marlstones. E) Angular clast of Nummulitic Limestone. F) Paleogene bioclasts embedded in the paraconglomerate matrix (white arrow points at *Nummulites* fragment, red arrow points at coralline alga). G) Detail of skeletal assemblage contained in a clast of Nummulitic limestone (red arrow points at an altered coralline alga).

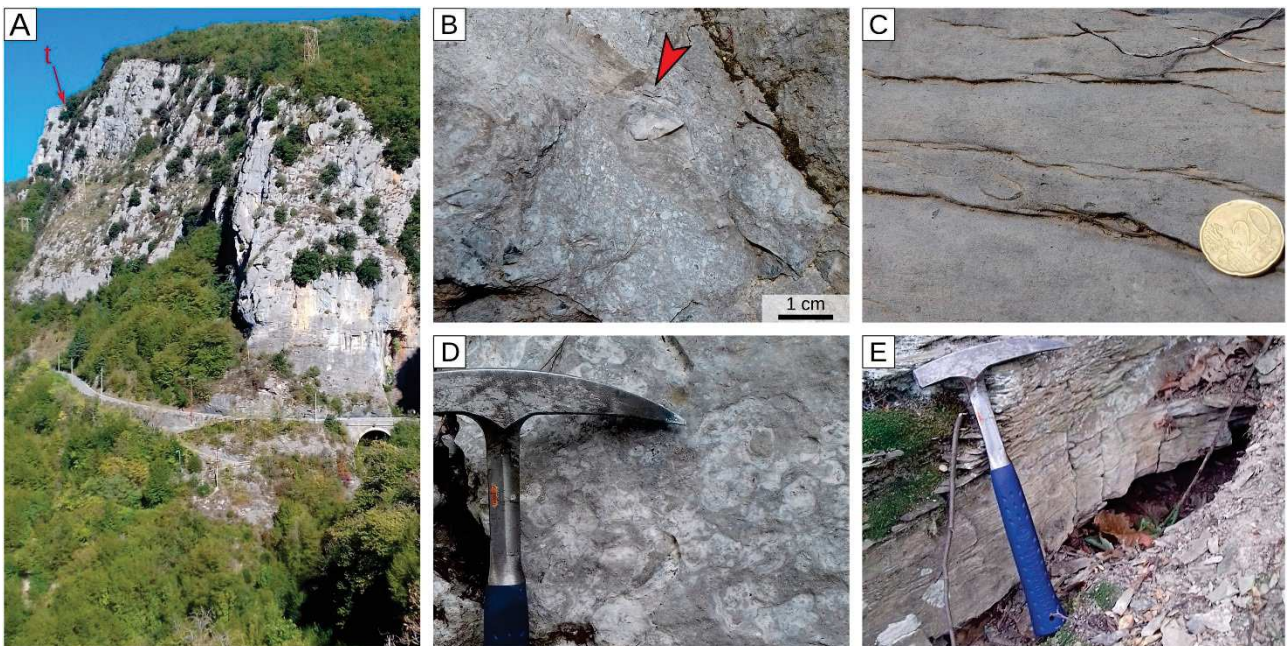


Figure 8.8 Loreto section. A) Outcrop overview (t = top of section); B) L1, *Pycnodonte* shell (red arrow); C) L2, dish structures; D) L3, overview of the acervulinids and coralline algal biofacies characterized by abundant acervulinid macroids; E) Ventimiglia Flysch Fm.

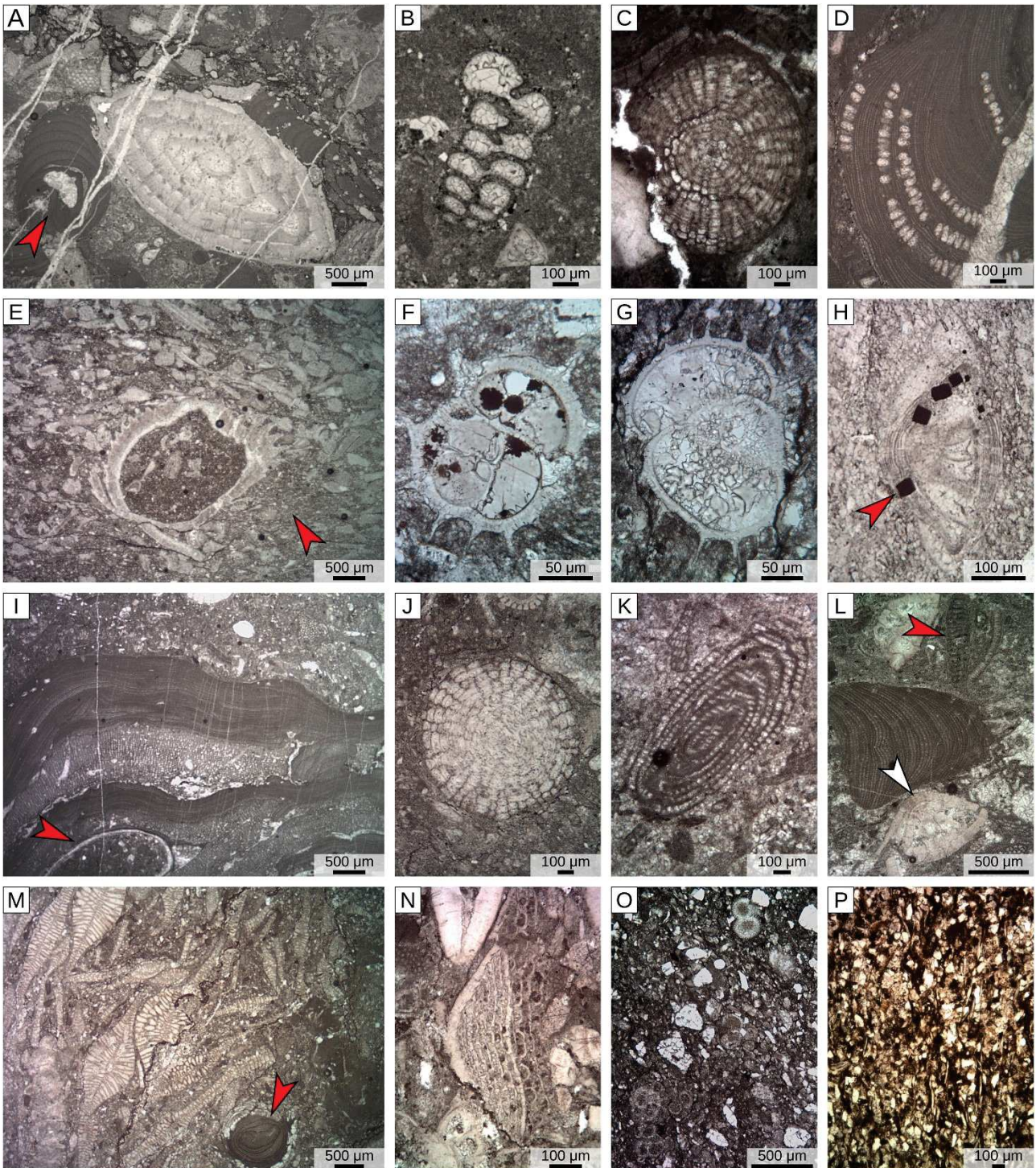


Figure 8.9 Skeletal assemblage and microfossils in the Loreto section; A) L1, coralline algal branches and LBF biofacies, corallinales=red arrow; B) L1, textulariid; C) L1; *Sphaerogypsina*; D) L1; *Sporolithon*; E) L2, imbricated fabric, the red arrow points at a bioclast-free area on the protected lee side of a large bioclast; F, G) L2, well preserved planktic foraminifera (possibly *Acarina*); H) L2, benthic foraminifera with authigenic pyrite growing from wall of chambers; I) L3, coralline algae and acervulinids growing together (red arrow points at encrusting serpulids); J) L3, *Sphaerogypsina*; K) L3, *Alveolina*; L) L3, *Amphistegina* (white arrow) and *Orbitolites* fragment (red arrow); M) L5, coralline algal fragment (red arrow); N) L5, *Chapmanina*. O) *Globigerina* Marls. P) Ventimiglia Flysch Fm.

8.5.3. Braux

In the Annot area, the Nummulitic Limestone is generally underlain by the Infrannummulitic. However, in the Braux section, the 35 m-thick Nummulitic Limestone directly overlies Upper Cretaceous marlstones (Figs. 8.1F, 8.10, 8.11A). The limestone can be subdivided into four intervals (Fig. 8.10).

Interval B1 (~13 m; acervulinid-bearing nummulitid biofacies). The lowermost interval of the section consists of layers of rudstones several meters thick (Fig. 8.11A). The skeletal assemblage is dominated by nummulitids that occur as lentil-sized megalospheric specimens and rare microspheric specimens with a diameter of ~1 cm (Fig. 8.12A; Table 8.1). Gigantic specimens (up to 3 cm in diameter) were observed only at the very base of the interval (Fig. 8.11B). Encrusting acervulinids are common and mainly occur as small nodules (≤ 1 cm in diameter), usually with a hooked morphology (Fig. 8.12B, C). Other bioclasts include small benthic foraminifera, echinoderms (locally as large test fragments), molluscs, coralline algae (small nodules of *Sporolithon* and articulated *Corallinales*), bryozoans, solitary corals, green calcareous algae, and serpulids (both encrusting taxa and free-living ones like *Ditrupa*) (Fig. 8.12D, E). The benthic foraminiferal assemblage includes common *Nummulites*, *Amphistegina*, *Chapmanina*, *Eorupertia*, *Triloculina*, *Quinqueloculina*, and small rotaliids; textulariids and orthophragminids are rare (Fig. 8.12F–J). Rock fragments eroded from the Upper Cretaceous pelagic marlstones and the *Microcodium*-bearing Infrannummulitic deposits are significant (Fig. 8.12A). Small charcoal fragments were frequently observed (Fig. 8.11C). Quartz grains represent ~4% of the rock (Fig. 8.10; Table 8.1).

Interval B2 (~11 m; nummulitid and orthophragminid biofacies). Packstones to floatstones dominated by LBF, associated with small benthic foraminifera, echinoderms, encrusting acervulinids, molluscs (mainly *Pycnodonte*), planktic foraminifera, rare bryozoans, serpulids (mainly *Ditrupa*), solitary corals, coralline algae, and ostracods (Fig. 8.12K, L; Table 8.1). Benthic foraminifera are mostly nummulitids (both *Operculina* and *Nummulites*), associated with orthophragminids, small rotaliids, rare *Amphistegina*, and small miliolids (Fig. 8.12M). The terrigenous fraction consists of fine-sand sized quartz grains and rare rock and charcoal fragments (Fig. 8.10; Table 8.1).

Interval B3 (~10 m; mass transport deposits; nummulitid and orthophragminid biofacies). The third interval of Braux section is separated from the underlying one by a markedly erosive surface (Fig. 8.11D). It consists of irregularly bedded packstones and floatstones (with a packstone matrix) and displays channelized features (Fig. 8.11D, E). Packstone layers mostly consist of comminuted bioclasts, while floatstone layers are usually characterized by coarse-grained bioclasts with an imbricated fabric (Fig. 8.12N). The skeletal assemblage is dominated by LBF associated with small

benthic foraminifera, echinoderms, molluscs, and solitary corals, *Ditrupa*, ostracods, and bryozoans. Rare coralline algae only occur in floatstone layers with imbricated bioclasts. Planktic foraminifera are common in packstone layers (Table 8.1). *Nummulites*, *Operculina*, orthophragminids and small rotaliids (including *Lenticulina*) dominate the benthic foraminiferal assemblage. Small miliolids are locally common, and textulariids are rare. *Amphistegina* and *Chapmanina* occur in floatstone layers. The terrigenous fraction mainly consists of coarse-silt-sized quartz grains (Fig. 8.10; Table 8.1). Rock fragments derived from Infrannummulitic lithologies and Upper Cretaceous marlstones occur in the floatstone layers (Fig. 8.12N).

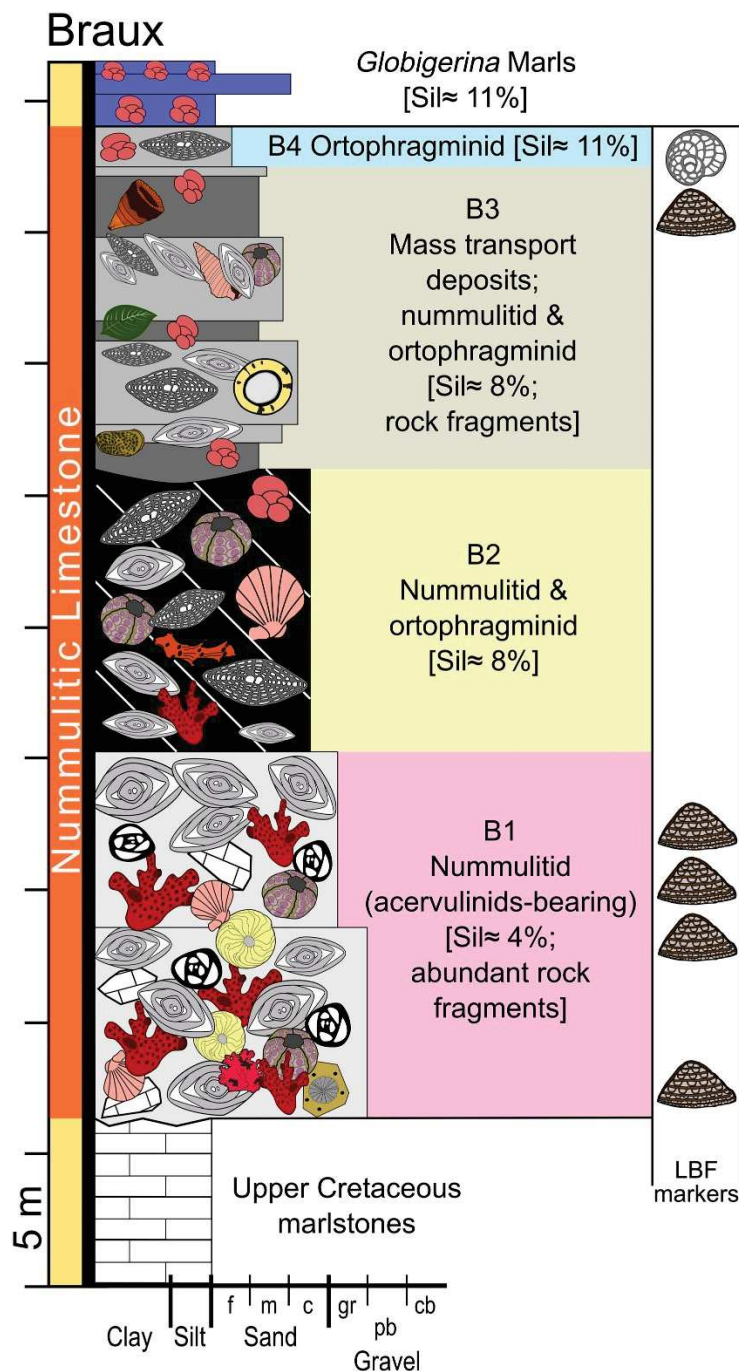


Figure 8.10 Stratigraphic log of Braux section with information on skeletal assemblage and average grain-size. Symbols and abbreviations as in Fig. 8.3.

Interval B4 (~2 m; orthophragminids biofacies). Poorly-lithified floatstone with a wackestone matrix, displaying a diversified orthophragminid assemblage (including *Discocyclina dispansa dispansa* and other discocyclinids), with subordinate nummulitids (*Nummulites*, *Operculina*, and *Heterostegina*), small benthic (*Lenticulina*, *Cibicides*, rare textulariids, very rare miliolids) and planktic foraminifera, rare echinoderms and ostracods (Figs. 8.11F, 8.13; Table 8.1). The quartzose terrigenous fraction represents ~11% of the rock (Fig. 8.10; Table 8.1).

The base of the overlying *Globigerina* Marls contains a resedimented layer of well-sorted fine-grained grainstone dominated by comminuted bioclasts including nummulitids and orthophragminids, rich in marly intraclasts, and with a significant terrigenous fraction (Fig. 8.11G). The *Globigerina* Marls are overlain by the Grès d'Annot (Fig. 8.11H).



Figure 8.11 Braux section. A) Unconformable contact between Upper Cretaceous pelagic marlstones and Nummulitic Limestone (red arrow); B) B1, large nummulitids and echinoderms; C) B1, charcoal seam; D) overview of Braux section, red arrow=Upper Cretaceous marlstones, white arrows=nummulitic limestone intervals, green arrow=boundary between B2 and B3; E) B3, channelized surfaces (red arrow); F) B4, orthophragminid biofacies; G) resedimented layer in the lower *Globigerina* Marls. H) Upper part of Braux section, white arrow= B4, blue arrow= *Globigerina* Marls (blue arrow); yellow arrow= Grès d'Annot.



Figure 8.12 Skeletal assemblage and microfossils in lower part of Braux section. A) B1, red arrows=clasts of Upper Cretaceous Marlstones; B, C) B1, large and small acervulinid nodules with hooked morphology; D) B1, *Sporolithon*; E) B1, bryozoan colony; F, G) B1, *Chapmanina*, axial and equatorial section respectively equatorial sections; H) B1, *Eorupertia*, equatorial section; I) B1, *Triloculina*; J) B1, *Quinqueloculina*; K) B2, nummulitid and orthophragminid biofacies; L) B2, *Nummulites*, axial section; M) B2, various specimens of *Operculina*; N) B3, imbricated fabric, red and white arrows point at clasts of Upper Cretaceous marls and of *Microcodium*, respectively.

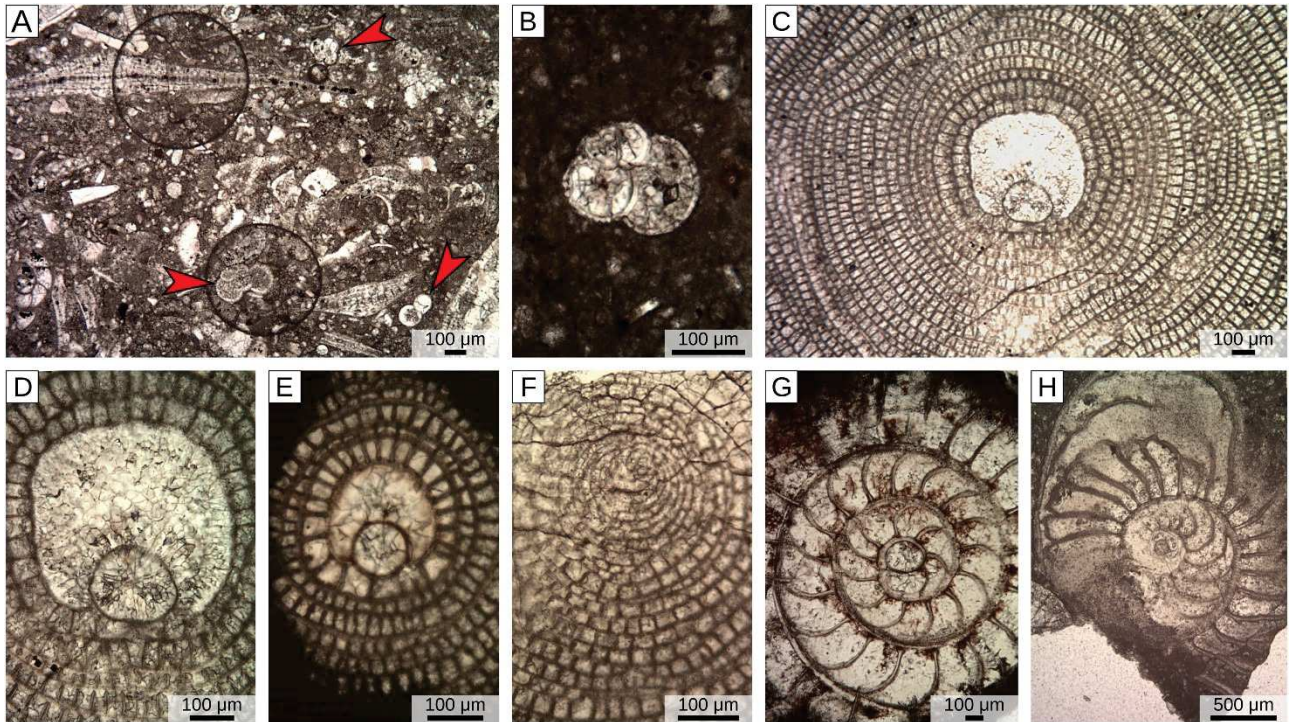


Figure 8.13 Skeletal assemblage, microfossils, and oriented LBF specimens of B4. A) Overview of the orthophragminid biofacies, red arrows=planktonic foraminifera. B) Detail of a planktonic foraminifer. C) *Discocyclina dispansa dispansa*, megalospheric specimen, equatorial section (detail of embryo in D); E) other orthophragminid taxa; F) microspheric orthophragminid specimen exposing its early spiral stage. G) *Nummulites*, equatorial section. H) *Operculina* (possibly *O. gomezi* group), equatorial section.

8.5.4. Lauzanier

In the Lauzanier valley, located in the Argentera Massif (Fig. 8.1G), the Upper Cretaceous and the Nummulitic Limestone are separated by the Infranummulitic (Figs. 8.14, 8.15A, B), which displays a remarkable facies variability and includes several distinct lithofacies: 1) *Microcodium*-bearing conglomerates with clasts derived from the Upper Cretaceous pelagic marlstones (ranging in thickness between 1 and about 10 m; Fig. 8.15C, D); 2) *Microcodium*-bearing nodular marly limestone with reworked globotruncanids (~4 m); 3) finely bedded, *Microcodium*-bearing, dark coloured limestones with conglomerate lenses (10 to 20 m of thickness); 4) conglomerates characterized by clasts issued from both the Upper Cretaceous marlstones and the *Microcodium*-bearing conglomerates (~2 m of thickness); 5) dark coloured marly limestones with vertebrate remains and pulmonate gastropods (~2 m of thickness); 6) pebble-rich limestones, with schizohaline and shallow marine gastropods (~2 m of thickness). The Nummulitic Limestone (12 m thick in the measured section) is relatively uniform and consists of finely and irregularly bedded floatstones with a packstone matrix characterized by the nummulitid biofacies (Figs. 8.14, 8.15E). Macrofossils include lentil-sized *Nummulites*, including rare microspheric specimens up to 1 cm in diameter. Solitary corals, orthophragminids, gastropods, and bivalves are common (Fig. 8.15F, G). The skeletal assemblage is consistently dominated by LBF associated with echinoderms, molluscs, solitary corals

and small benthic foraminifera (Fig. 8.16A, Table 8.1). *Nummulites* dominates the benthic foraminiferal assemblage and is associated with *Amphistegina* and *Operculina*; orthophragminids mainly occur in the upper part of the section (Fig. 8.16B, C). Small rotaliids and small miliolids are also present. Siliciclastic detritus including quartz, plagioclase, and abundant muscovite and chlorite increases up-section, whereas rock fragments (mainly reworked *Microcodium*) decrease (Fig. 8.14; Table 8.1). The overlying *Globigerina* Marls consist of planktic-foraminifera rich impure mudstones containing mainly silt-sized quartz and plagioclase grains together with common muscovite and chlorite (Figs. 8.14, 8.16D; Table 8.1). The marls are followed by the Grès d'Annot turbidites.

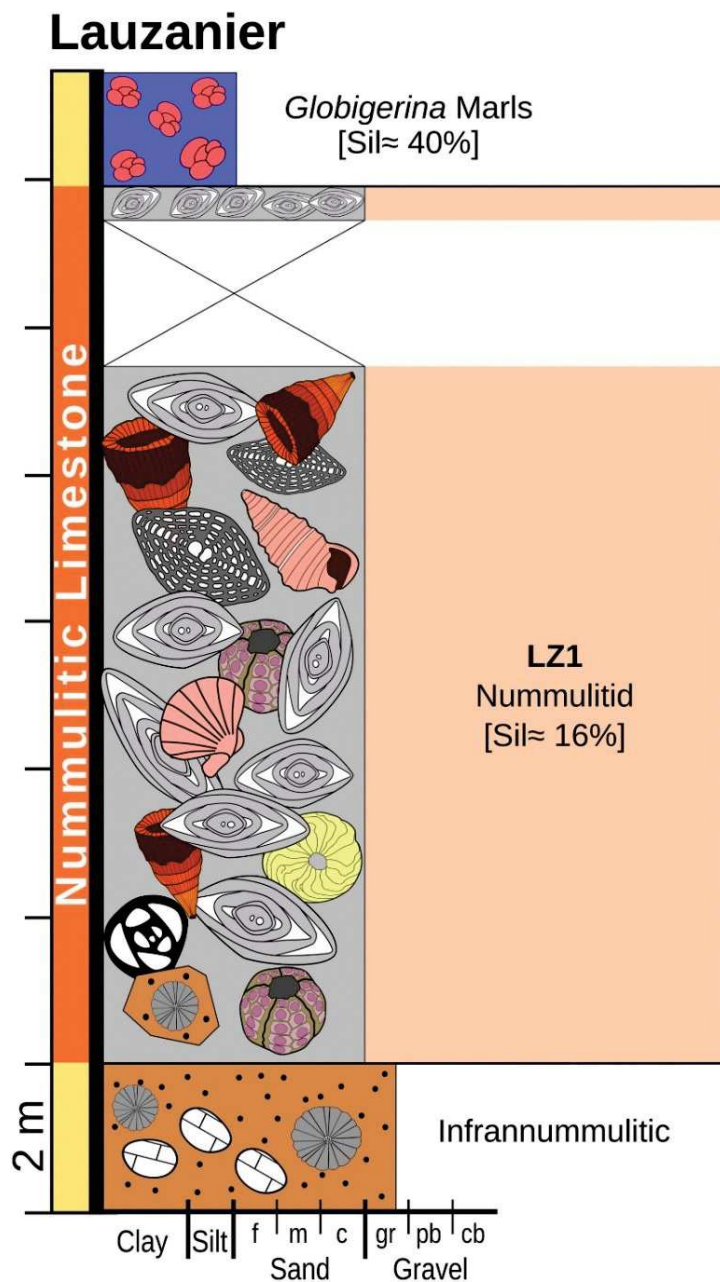


Figure 8.14 Stratigraphic log of Lauzanier section with information on skeletal assemblage and average grain-size. Symbols and abbreviations as in Fig. 8.3.

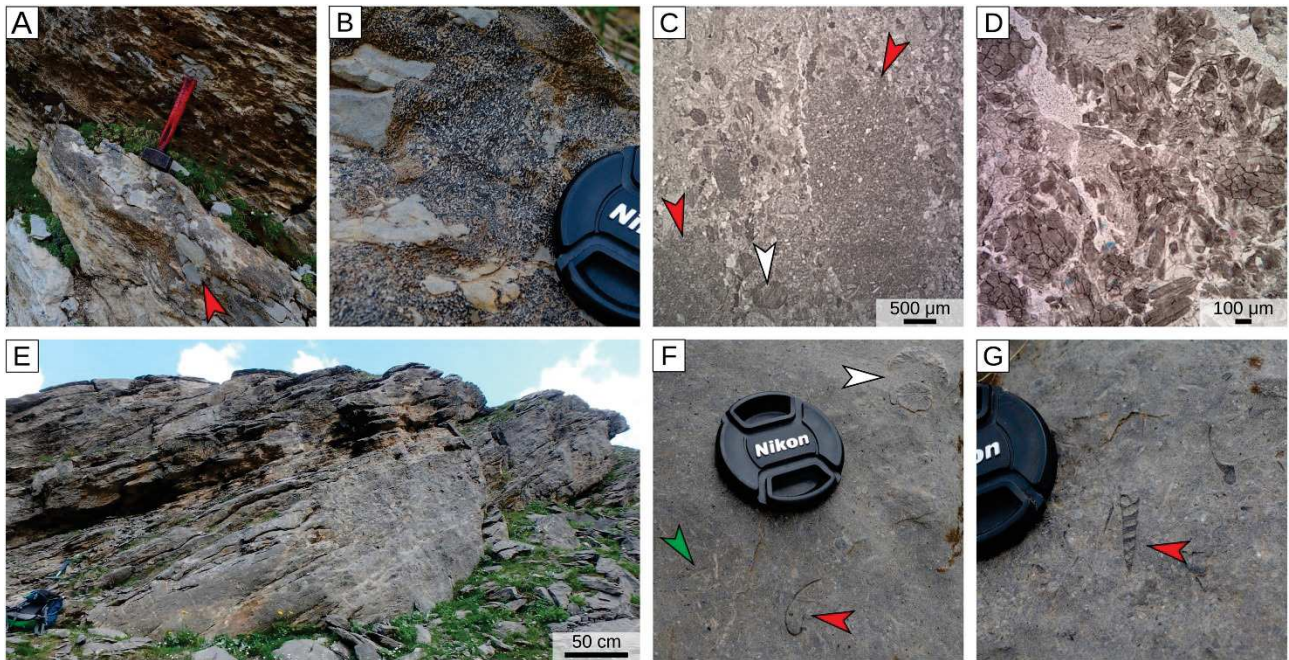


Figure 8.15 Lauzanier section. A) Infranummulitic, conglomerate with clasts of Upper Cretaceous marlstones (red arrow); B) detail showing *Microcodium*; C) thin section of the Infranummulitic rocks, white and red arrows point at *Microcodium* and clasts of Upper Cretaceous marlstones, respectively; D) Infranummulitic, *Microcodium* in thin section; E) overview of the Nummulitic limestone section; F) Nummulitic Limestone, green arrow = orthofragminids, white arrow = solitary corals, red arrow = bivalve; G) Nummulitic Limestone gastropod (red arrow).

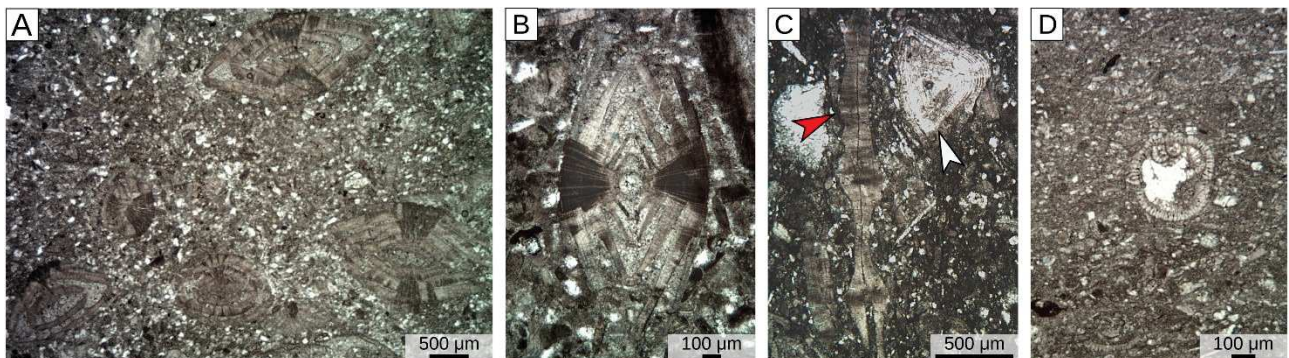


Figure 8.16 Skeletal assemblage and microfossils in Lauzanier section. A) Overview of Nummulitid biofacies. B) *Nummulites*, axial section. C) *Operculina* (red arrow) and *Amphistegina* (white arrow). D) *Globigerina* Marls.

8.6 Discussion

8.6.1 Biostratigraphy of the Nummulitic Limestone

The studied sections have been dated based on the distribution of the LBF fauna, focusing on the most readily identifiable biological events: a) the extinction of *Assilina*, which took place in the Bartonian plankton zone P14 (40.0-38.0Ma), following the 2011 calibration of Wade et al. (2011), Sartorio and Venturini (1988), Sztrákos and Du Fornel (2003), and Boudaughier-Fadel (2018); b) the common presence of *Chapmanina*, dated as within the shallow benthic zone SBZ18 of Serra-Kiel et al. (1998) (i.e., post-38 Ma); c) the extinction of giant-sized nummulitids, considered to have occurred at the Bartonian–Priabonian boundary (~37.7 Ma; Nebelsick et al., 2005; Less and Özcan, 2012; Boudaughier-Fadel, 2018; Özcan et al., 2019; Agnini et al., 2020); d) the extinction of *Orbitolites*,

also corresponding with the Bartonian-Priabonian boundary (Sartorio and Venturini, 1988; Serra-Kiel et al., 1998; Nebelsick et al., 2005; Boudaughier-Fadel, 2018); e) the first occurrence of *Heterostegina*, indicating the base of the Priabonian (Serra-Kiel et al., 1998; Boudaughier-Fadel, 2018). In the study area, the base of the Nummulitic Limestone was mainly considered as Bartonian (Sztrákos and Du Fornel, 2003; Varrone and Clari, 2003; Varrone and D'Atri, 2007). Thus, the presence of *Assilina*, *Orbitolites* and giant-size nummulitids indicates that the Mortola section deposited during the Bartonian and that the drowning of the carbonate factory here occurred before 38 Ma. The Loreto section also mostly deposited during the Bartonian, given the presence of not only giant-sized nummulitids, *Assilina* and *Orbitolites*, but also of large *Alveolina* specimens in the third interval. The large-sized representatives of this genus disappeared close to the end of the Bartonian (Serra-Kiel et al., 1998; Nebelsick et al., 2005; Less and Özcan, 2012). The presence of *Chapmanina*, however, indicates that the fifth interval of the Loreto section was deposited after 38 Ma. This is consistent with the local Upper Bartonian/Lower Priabonian planktic foraminiferal assemblage of the *Globigerina* Marls (Varrone and D'Atri, 2007). The presence of both *Chapmanina* and giant-sized nummulitids dates the base of the Nummulitic Limestone in the Braux section as latest Bartonian (close to 38 Ma). The presence of the Priabonian taxa *Heterostegina* and *Discocyclusina dispansa dispansa* (Less, 1987; Serra-Kiel et al., 1998) suggests a Priabonian age for the fourth interval. The Lauzanier section lacks diagnostic LBF taxa. The absence of either giant-sized nummulitids, *Assilina* and *Orbitolites* suggests deposition after 38 Ma, consistently with the Priabonian age proposed by Mulder et al. (2010) for the *Globigerina* Marls and the Grès d'Annot in this area.

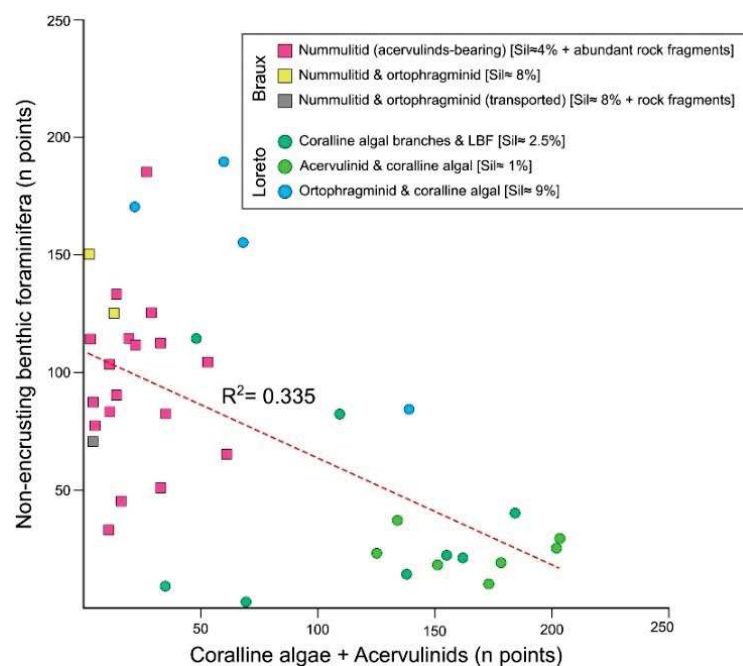


Figure 8.17 Correlation between encrusting carbonate producers (coralline algae and encrusting acervulinids), free-living benthic foraminifera and terrigenous supply in the study area. Only samples displaying both encrusting carbonate producers (intended as coralline algae and encrusting acervulinids) and free-living benthic foraminifera were plotted.

8.6.2 Facies interpretation and paleoenvironmental reconstruction

Hallock and Glenn (1986), based on data on foraminiferal assemblages from modern and fossil tropical settings (Brasier, 1975a, 1975b; Hallock, 1980, 1983, 1984; Glenn et al., 1981; Hottinger, 1983a; Reiss and Hottinger, 1984), provided a general model of LBF distribution in carbonate depositional environments. Flat and thin large rotaliids (e.g., *Operculina*, *Heterostegina*, or orthophragminids like *Discocyclusina*) dominate lower photic-zone assemblages, associated with common planktic foraminifera. Thick and more robust nummulitids and robust amphisteginids (e.g., *Nummulites*, several species of *Amphistegina*) thrive in middle-shelf environments especially closer to the inner shelf. Very robust large rotaliids (e.g., several species of *Amphistegina*, *Miogyopsina*) dominate reef settings, whereas in even shallower water miliolids (e.g., alveolinids, soritids) are more abundant and can dominate in restricted environments. This model has been refined (e.g., Geel, 2000; Beavington-Penney and Racey, 2004; Boudaughier-Fadel, 2018), strengthened based on studies of modern assemblages (Van der Zwaan et al., 1990; Hohenegger, 1994, 2000, 2004; Hohenegger et al., 1999, 2000; Renema and Troelstra, 2001; Renema, 2006, 2018; Mateu-Vicens et al., 2009), and applied to diverse Cenozoic basins (e.g., Čosović et al., 2004) including the Alpine foreland basin (Sinclair et al., 1998). Within this framework, we used our data on foraminiferal assemblages to constrain the environmental conditions in which each biofacies was deposited. The various biofacies of each section document a general deepening upward trend and a continuum of depositional environments with gradual transitions from one to another (e.g., nummulitid and orthophragminid biofacies). The depositional system was thus characterized by a ramp profile. Ramps are actually common wherever carbonate factories mainly produce loose skeletal material rather than a rigid framework (i.e., a reef; Carannante et al., 1996; Schlager, 2005; Pomar, 2001; Pomar and Hallock, 2007; Pomar and Kendall, 2008; Williams et al., 2011). Lacking a marginal rim, Eocene ramps are characterized by unimpeded downslope transport and reworking processes (e.g., Beavington-Penney et al., 2005; Coletti et al., 2016), as highlighted by the mass-transport deposits of the Loreto and Braux sections. The various biofacies can be ordered from shallowest to deepest. The nummulitid biofacies (Mortola, Braux and Lauzanier sections) is characterized by grain-supported texture, abundance of thick and robust specimens of nummulitids, common presence of *Amphistegina* and miliolids, and scarcity of orthophragminids and planktic foraminifera (Table 8.1), indicating a moderately high-energy, shallow-water environment (indicatively between 20 and 40 m water depth). *Orbitolites* is remarkably similar to modern epiphytic soritids, and its presence is thus deemed indicative of a vegetated substrate (Brasier, 1975c; Beavington-Penney et al., 2006; Tomás et al., 2016; Tomassetti et al., 2016). The *Orbitolites*-bearing nummulitid biofacies of the Mortola section (Figs. 8.2B, 8.3, 8.5A) thus developed around a macrophyte meadow and because modern seagrasses

occur in waters < 40 m and mostly <20 m deep (Duarte, 1991), water depth was probably around 20 m. The acervulinid-bearing nummulitid biofacies in the Braux section is characterized by hooked acervulinid crusts (Fig. 8.12B, C). Hooked and tubular morphologies in encrusting Eocene acervulinids have been linked to the presence of vegetated substrate (Tomás et al., 2016; Tomassetti et al., 2016), and seagrass encrusting acervulinids occurs in the recent (e.g., Langer, 1993; Wilson, 1998; Murray, 2006). Consequently, the acervulinid-bearing nummulitid biofacies of Braux are also interpreted as developed in close proximity to a vegetated substrate in a shallow environment (i.e., ~20 m water depth). The acervulinid and coralline algal biofacies of the Loreto section is dominated by nodules of encrusting foraminifera (Fig. 8.6; Table 8.1). Modern acervulinids forming large macroids have been reported from the clear waters of the Gulf of Aqaba between 25 and 60 m of water depth (maximum abundance between 40 and 60 m below sea level; Hottinger, 1983b; Rasser and Piller, 1997), from the Florida shelf (35-65 m b.s.l.; Prager and Ginsburg, 1989), and from the Ryukyu Islands, where they occur between 60 and 105 m b.s.l. associated with *Operculina* and *Cycloclypeus* (Bassi et al., 2012, 2019). Loreto macroids are associated with large alveolinids (Fig. 8.9K), which only occur in this biofacies. The presence of small miliolids, *Orbitolites*, thick amphisteginids, the low abundance of orthophragminids, and the lack of planktic foraminifera suggest deposition between 25 and 50 m of water depth. The nummulitid and orthophragminid biofacies (Mortola and Braux sections) contains more orthophragminids, flat nummulitids and planktic foraminifera, and less miliolids and amphisteginids than the nummulitid biofacies; grain size is finer, and textures mainly matrix supported (Table 8.1). This biofacies overlies the nummulitid biofacies, documenting a deepening-upward trend and a transition to a moderately low-energy, middle shelf setting at depths indicatively between 40 and 60 m. The coralline-algal branches and LBF biofacies in the Loreto section displays a foraminiferal assemblage similar to the nummulitids and to the nummulitid and orthophragminid biofacies (Table 8.1), indicating shallow to intermediate water depth. Similar skeletal assemblages, dominated by coralline algae but lacking either large rhodoliths or coralline algal bioconstructions, are common in the Eocene basins of eastern Italy and Austria and document inner to middle shelf environments (Nebelsick et al., 2005). A middle-shelf setting is also indicated by the diversified coralline algal assemblage including *Sporolithales*, *Corallinales*, and *Hapalidiales* (Adey, 1979, 1986; Minnery et al., 1985). Therefore, an environment with moderate hydrodynamic energy and water depth between 30 and 60 m is proposed. The orthophragminid biofacies (Mortola and Braux sections) overlies the nummulitid and orthophragminid biofacies in the Mortola and Braux sections and is characterized by orthophragminids and other thin and flat LBF, common planktic foraminifera, no miliolids, no amphisteginids, and abundant micrite (Table 8.1). This suggests a below-wave base, outer shelf setting between ~60 m and the lowest limit of the photic

zone (~100, 130 m maximum). Similarly to the orthophragminid facies, the orthophragminid and coralline algal biofacies of Loreto most likely developed in a similar outer shelf environment below wave base.

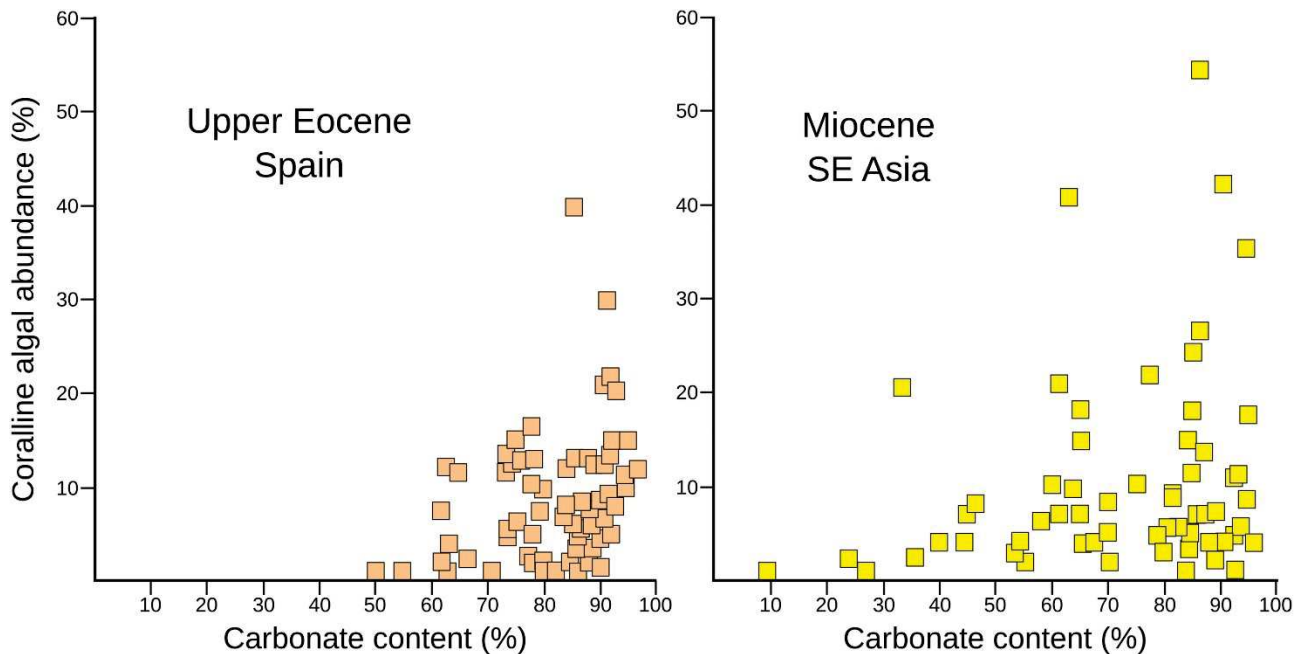


Figure 8.18 Relationship between carbonate percentage and coralline algal abundance in samples from the upper Eocene of Spain and the Miocene of SE Asia investigated by Lokier et al. (2009) (data from the Supplementary material of Lokier et al., 2009).

8.6.3 Controls on carbonate factories distribution

Sea-water temperature is considered a major control on the distribution of carbonate factories (e.g., Lees and Buller, 1972), however, the studied sections lie so close together that local temperature differences should not play a role in our case. The four sections were mostly deposited during the Bartonian (41.2-37.7 Ma), which was characterized by warm climate with a slow cooling trend culminated around the Eocene-Oligocene boundary (Zachos et al., 2001, 2008; Mosbrugger et al., 2005). The Bartonian also includes a warm peak, the Middle Eocene Climatic Optimum (c. 40.5-40.05 Ma; Zachos et al., 2008; Westerhold and Röhl, 2013). This event might have been recorded in the Mortola and Loreto sections. However, an overall large increase in thermophile taxa is not clearly documented in the skeletal assemblages. Nutrient availability is another important control, together with autotrophs and symbiont-bearing organisms (e.g., LBF, hermatypic corals, calcareous algae) favored by oligotrophic conditions and heterotrophs (e.g., bryozoans, barnacles) favoured by nutrient enrichment (Hallock and Schlager, 1986; Brasier, 1995a, 1995b). Such trend has been tested in both modern (Halfar et al., 2004; Reijmer et al., 2012; Reymond et al., 2016) and fossil carbonate systems (Coletti et al., 2017, 2019b). With the exception of the acervulinid and coralline algal biofacies, the

four studied sections are dominated by autotrophs and symbiont-bearing organisms, with heterotroph carbonate producers (bryozoans in particular) occurring only as minor components. Little is known about the trophic preferences of Eocene acervulinids as their modern relatives seem to harbour no symbionts (Leutenegger, 1984). Within the study area, acervulinids are mainly related to shallow-water facies and are associated with light-loving taxa (e.g., *Alveolina*), suggesting a preference toward clear water rather than toward turbid (and possibly nutrient rich) conditions. Overall, due to the abundance of terrigenous material (Table 8.1), it is likely that the foreland basin was enriched in nutrients in comparison to open oceanic conditions. However, by cross-comparing the various assemblage of the four sections there is no evidence indicating that nutrients exerted a primary control on the composition of the skeletal assemblages, possibly suggesting that if the basin was enriched in nutrients this enrichment was relatively uniform. Major effects are ascribed to varying terrigenous supply. The Mortola and Lauzanier sections contain more terrigenous detritus and are overwhelmingly dominated by free-living benthic foraminifera, whereas coralline algae and encrusting foraminifera are more common at Loreto and Braux where siliciclastic supply was more limited (Table 8.1). A manifest difference results when sections or biofacies deposited at similar water depth (e.g., *Orbitolites*-bearing nummulitid biofacies of Mortola vs. acervulinid-bearing biofacies of Braux vs. acervulinid and coralline algal biofacies of Loreto) are compared (Table 8.1). Furthermore, by plotting all the samples containing remains of acervulinids, coralline algae and free-living benthic foraminifera, a negative correlation ($R^2 = 0.335$) can be observed between free-living benthic foraminifera (more abundant in impure limestones) and encrusting carbonate producers (foraminifera and coralline algae; more abundant in pure limestones; Fig. 8.17). The dominance of free-living benthic foraminifera in settings characterized by siliciclastic supply has been documented in Cenozoic basins of SE Asia and Spain (Lokier et al., 2009), showing that free-living benthic foraminifera tolerate terrigenous input better than coralline algae and hermatypic corals (which are the least tolerant carbonate producers). While Lokier et al. (2009) indicated coralline algae as the second most tolerant group, the distribution of coralline algae in our study suggests that Eocene calcareous red algae were relatively sensitive and fared better in clear waters. However, it should be noted that, while in the Neogene basins of SE Asia coralline algae frequently occur in samples containing >50% of clastic material, in the late Eocene of Spain the majority of coralline-bearing samples have <50% of clastics (Fig. 8.18) (Lokier et al., 2009). During the late Eocene, coralline algae, *Hapalidiales* and *Corallinales* in particular, became more abundant and more diversified (Aguirre et al., 2000; Nebelsick et al., 2005; Pomar et al., 2017), but our research focuses on relatively primitive middle Eocene assemblages largely consisting of *Sporolithales*. Therefore, it is conceivable that the studied middle Eocene algae were less flexible than their late Eocene and Neogene

counterparts, and thus unable to flourish under very high rates of terrigenous sedimentation. Terrigenous supply exerted a significant influence also on secondary producers like solitary scleractinian corals, which are well adapted to high and persistent terrigenous input (Sanders and Baron-Szabo, 2005). This explains their common presence in the Mortola and Lauzanier sections that are rich in fine-grained terrigenous detritus (Table 8.1). The distribution of solitary corals, carefully investigated in the Mortola section by Carbone et al. (1980), has been shown to be dependent on the grain-size of terrigenous detritus: corals specialized in the removal of silt are more common in finer layers whereas species able to deal also with coarser particles prevail in coarser layers. Overall, two major carbonate factories, both dominated by benthic foraminifera, can be distinguished in the studied sections. Coastal areas closer to river outlets and thus characterized by greater terrigenous input and unstable substrates (e.g., Mortola, Braux and Lauzanier) were dominated by free-living LBF associated with other sediment-resistant taxa. Isolated banks (e.g., offshore shoals raised from the surrounding basin) characterized by limited terrigenous supply and more stable substrates (e.g., Loreto) hosted instead carbonate factories including more encrusting organisms (mostly foraminifera and coralline algae). The mineralogical analysis of the terrigenous fraction indicates the lack of minerals clearly related to high-grade Alpine metamorphic units, suggesting that the latter were probably not yet available for the erosion. This in turn might suggest a situation with limited relief around the basin during the development of the Nummulitic Limestone, with relatively localized input of material leading to the large differences in terrigenous content observed between the various outcrops.

8.7 Conclusions

Based on large benthic foraminiferal assemblages, the examined successions of the Nummulitic Limestone of Mortola, Loreto, Braux and Lauzanier deposited between the Bartonian and the Priabonian, with the former two depositing earlier. Thanks to the analysis of the skeletal assemblage it was possible to recognize six main biofacies: i) the nummulitid biofacies and ii) the acervulinid and coralline algal biofacies both related to high-energy, moderately shallow-water environment (20-40m and 25-50 m respectively); iii) the nummulitid and orthophragminid biofacies and iv) the coralline-algal branches and LBF biofacies, related to slightly deeper settings (40-60 and 30-60 m respectively); v) the orthophragminid biofacies and vi) the orthophragminid and coralline algal biofacies related to even deeper water (60-130 m). These biofacies formed along a ramp profile testifying a progressively deepening of the depositional environment. These biofacies can be related to two major carbonate factories, the former dominated by free-living benthic foraminifera (Mortola, Braux and Lauzanier sections), and the latter dominated by coralline algae and encrusting

foraminifera (Loreto section). Terrigenous supply exerted a primary control on these carbonate factories as encrusting organisms are significantly more common in pure limestones and free-living carbonate producers are much more common in areas characterized by a higher terrigenous supply like Mortola and Lauzanier. Free-living benthic foraminifera and solitary corals display more tolerance to clastic input than coralline algae and encrusting foraminifera. The distribution of coralline algae also suggests that Eocene algae might have been less tolerant to clastic input than their Neogene counterparts. Likewise, encrusting acervulinids seem to be mainly related to shallow-water settings in the studied successions, and, therefore, relatively different from their modern counterparts that usually prefer deeper settings. This analysis highlights several differences between Palaeogene and modern carbonate factories, but also indicates that, similarly to modern settings, terrigenous input represents a major controlling element of carbonate systems. Supplementary data to this article can be found online at <https://doi.org/10.1016/j.sedgeo.2021.106005>.

Declaration of competing interest

The authors declare that they have no known competing financial interests or personal relationships that could have influenced the work reported in this paper.

Acknowledgements

The authors are grateful to Prof. Stani Giammarino for his guidance in this research and for providing the samples, collected during the field work of 1980 and previous campaigns, which were used for the analysis of the Mortola section. The authors wish to thank Prof. Cristina Carbone for the access to the PXRD laboratory of the University of Genoa, Roberto Badano is also acknowledged for his great help with PXRD analyses. The authors are grateful to Prof. György Less of Miskolc University and Prof. Giorgio Basilici of UNICAMP University for their constructive and helpful revisions. The first author is also indebted to Dr. Silvia Spezzaferri, Dr. Irene Cornacchia, Prof. Elisa Malinverno, Prof. Sergio Andò, Prof. Marco Malusà and Prof. Antonino Briguglio for the fruitful discussions on Eocene foraminifera and carbonates, and to Dr. Wendong Liang, Dr. Marta Barbarano, Mara Soldi, Maura Lenzi for their help during the fieldwork and labwork. The first author would also like to thank Milano-Bicocca University for funding its pots-doc grant. Finally, G.C. and E.G. would like to thank Curzio Malinverno for his invaluable help in thin sections preparation. This research represents a scientific contribution to Project MIUR - Dipartimenti di Eccellenza 2018–2022.

References

- Adey, W.H., 1979. Crustose coralline algae as microenvironmental indicators in the Tertiary. In: Gray, J., Boucot, A.J. (Eds.), *Historical biogeography, Plate Tectonics and the Changing Environment. Proceedings of the Thirty-seventh Annual Biology Colloquium*, pp. 459–464.
- Adey, W.H., 1986. Coralline algae as indicators of sea-level. In: Van de Plassche, O. (Ed.), *Sea-level Research: A Manual for the Collection and Evaluation of Data*. Geo-Books, Norwich, pp. 229–280.
- Agnini, C., Backman, J., Boscolo-Galazzo, F., Condon, D.J., Fornaciari, E., Galleotti, S., Giusberti, L., Grandesso, P., Lanci, L., Luciani, V., Monechi, S., Muttoni, G., Pälke, H., Pampaloni, M.L., Papazzoni, C.A., Pearson, P.N., Pignatti, J., Premoli-Silva, I., Raffi, I., Rio, D., Rook, L., Sahy, D., Spofforth, D.J.A., Stefani, C., Wade, B.S., 2020. Proposal for the Global Boundary Stratotype Section and Point (GSSP) for the Priabonian Stage (Eocene) at the Alano section (Italy). Episodes <https://doi.org/10.18814/epiugs/2020/020074>.
- Aguirre, J., Riding, R., Braga, J.C., 2000. Diversity of coralline red algae: origination and extinction patterns from the Early Cretaceous to the Pleistocene. *Paleobiology* 26, 651–667.
- Allen, P.A., Crampton, S.L., Sinclair, H.D., 1991. The inception and early evolution of the North Alpine Foreland Basin, Switzerland. *Basin Research* 3, 143–163.
- Allen, P.A., Burgess, P.M., Galewsky, J., Sinclair, H.D., 2001. Flexural-eustatic numerical model for drowning of the Eocene perialpine carbonate ramp and implications for Alpine geodynamics. *GSA Bulletin* 113, 1052–1066.
- Artoni, A., Meckel, L.D., 1998. History and deformation rates of a thrust sheet top basin. The Barrem basin, western Alps, SE France. In: Mascle, A., Puigdefabregas, C., Luterbacher, H.P., Fernandez, M. (Eds.), *Cenozoic Foreland Basins of Western Europe*. Geological Society Special Publications vol. 134, pp. 213–237.
- Barale, L., Bertok, C., d'Atri, A., Martire, L., Piana, F., Domini, G., 2016. Geology of the Entracque–Colle di Tenda area (Maritime Alps, NW Italy). *Journal of Maps* 12, 359–370.
- Bassi, D., Iryu, Y., Humblet, M., Matsuda, H., Machiyama, H., Sasaki, K., Matsuda, S., Arai, K., Inoue, T., 2012. Recent macroids on the Kikai jima shelf, Central Ryukyu Islands, Japan. *Sedimentology* 59, 2024–2041.
- Bassi, D., Iryu, Y., Humblet, M., Matsuda, H., Machiyama, H., Sasaki, K., Matsuda, S., Arai, K., Inoue, T., 2019. Deep-water macroid beds of the Ryukyu Islands, Japan: encrusting acervulinids as ecosystem engineers. *Journal of Coastal Research* 35, 463–466.
- Beavington-Penney, S.J., Racey, A., 2004. Ecology of extant nummulitids and other larger benthic foraminifera: applications in palaeoenvironmental analysis. *Earth-Science Reviews* 67, 219–265.
- Beavington-Penney, S.J., Paul Wright, V., Racey, A., 2005. Sediment production and dispersal on foraminifera-dominated early Tertiary ramps: the Eocene El Garia Formation, Tunisia. *Sedimentology* 52, 537–569.
- Beavington-Penney, S.J., Wright, V.P., Racey, A., 2006. The middle Eocene Seeb Formation of Oman: an investigation of acyclicity, stratigraphic completeness, and accumulation rates in shallow marine carbonate settings. *Journal of Sedimentary Research* 76, 1137–1161.
- Bernasconi, M.P., Corselli, C., Carobene, L., 1997. A bank of scleractinian coral *Cladocora caespitosa* in the Pleistocene of the Crati valley (Calabria, Southern Italy): growth vs environmental conditions. *Bollettino della Società Paleontologica Italiana* 36, 53–61.
- Bodelle, J., 1971. Les formations nummulitique de l'arc de Castellane. Université de Nice (PhD Thesis)
- Boudaughier-Fadel, M.K., 2018. Evolution and Geological Significance of Larger Benthic Foraminifera. UCL Press (693 pp.).
- Brasier, M.D., 1975a. Ecology of Recent sediment-dwelling and phytal foraminifera from the lagoons of Barbuda, West Indies. *The Journal of Foraminiferal Research* 5, 42–61.
- Brasier, M.D., 1975b. The ecology and distribution of recent foraminifera from the reefs and shoals around Barbuda, West Indies. *The Journal of Foraminiferal Research* 5, 193–210.
- Brasier, M.D., 1975c. An outline history of seagrass communities. *Palaeontology* 18, 681–702.
- Brasier, M.D., 1995a. Fossil indicators of nutrient levels 1: eutrophication and climate change. In: Bosence, D.W.J., Allison, P.A. (Eds.), *Marine Palaeoenvironmental Analysis From Fossils*. Geological Society Special Publication vol. 83, pp. 113–132.
- Brasier, M.D., 1995b. Fossil indicators of nutrient levels 2: evolution and extinction in relation to oligotrophy. In: Bosence, D.W.J., Allison, P.A. (Eds.), *Marine Palaeoenvironmental Analysis From Fossils*. Geological Society Special Publication vol. 83, pp. 133–150.
- Campredon, R., 1977. Les formations paléogènes des Alpes Maritimes Franco-Italiennes. *Mémoires de la Société Géologique de France* vol. 9 (198 pp.).
- Carannante, G., Severi, C., Simone, L., 1996. Off-shelf carbonate transport along foramol (temperate-type) open shelf margins: an example from the Miocene of the central southern Apennines (Italy). *Mémoires de la Société géologique de France* 169, 277–288.
- Carbone, F., Giammarino, S., Matteucci, R., Schiavinotto, F., Russo, A., 1980. Ricostruzione paleoambientale dell'affioramento nummulitico di Capo Mortola (Liguria Occidentale). *Annali dell'Università di Ferrara, Scienze Geologiche e Paleontologiche* vol. VI, pp. 230–280.
- Chung, F.H., 1974. Quantitative interpretation of X-ray diffraction patterns of mixtures. I. Matrix-flushing method for quantitative multicomponent analysis. *Journal of Applied Crystallography* 7, 519–525.

- Coletti, G., Vezzoli, G., Di Capua, A., Basso, D., 2016. Reconstruction of a lost carbonate factory based on its biogenic detritus (Ternate-Travedona Formation and Gonfolite Lombarda Group - northern Italy). *Rivista Italiana di Paleontologia e Stratigrafia* 122, 1–22.
- Coletti, G., El Kateb, A., Basso, D., Cavallo, A., Spezzaferri, S., 2017. Nutrient influence on fossil carbonate factories: evidence from SEDEX extractions on Burdigalian limestones (Miocene, NW Italy and S France). *Palaeogeography Palaeoclimatology Palaeoecology* 475, 80–92.
- Coletti, G., Bosio, G., Collareta, A., Malinverno, E., Bracchi, V., Di Celma, C., Basso, D., Stainbank, S., Spezzaferri, S., Cannings, T., Bianucci, G., 2019a. Biostratigraphic, evolutionary, and paleoenvironmental significance of the southernmost lepidocyclinids of the Pacific coast of South America (East Pisco Basin, southern Peru). *Journal of South American Earth Sciences* 96, 102372.
- Coletti, G., Basso, D., Betzler, C., Robertson, A.H.F., Bosio, G., El Kateb, A., Foubert, A., Meilijson, A., Spezzaferri, S., 2019b. Environmental evolution and geological significance of the Miocene carbonates of the Eratosthenes Seamount (ODP Leg 160). *Palaeogeography Palaeoclimatology Palaeoecology* 530, 217–235.
- Ćosović, V., Drobne, K., Moro, A., 2004. Paleoenvironmental model for Eocene foraminiferal limestones of the Adriatic carbonate platform (Istrian Peninsula). *Facies* 50, 61–75.
- DeCelles, P.G., Giles, K.A., 1996. Foreland basin systems. *Basin Research* 8, 105–123.
- Dickinson, W.R., 1974. Plate tectonics and sedimentation. In: Dickinson, W.R. (Ed.), *Tectonics and Sedimentation*. Society of Economic Paleontology and Mineralogy, Special Publication vol. 22, pp. 1–27.
- Doyle, L.J., Roberts, H.H., 1988. Carbonate–clastic transitions. *Developments in Sedimentology*. vol. 42. Elsevier, Amsterdam (304 pp.).
- Du Châtelet, É.A., Bout-Roumazeilles, V., Riboulleau, A., Trentesaux, A., 2009. Sediment (grain size and clay mineralogy) and organic matter quality control on living benthic foraminifera. *Revue de Micropaleontologie* 52, 75–84.
- Duarte, C.M., 1991. Seagrass depth limits. *Aquatic Botany* 40, 363–377.
- Dunham, R.J., 1962. Classification of carbonate rocks according to depositional texture. In: Ham, W.E. (Ed.), *Classification of Carbonate Rocks*. American Association of Petroleum Geologists, Memoir vol. 1, pp. 108–121.
- Embry, A.F., Klován, J.E., 1971. A Late Devonian reef tract on Northeastern Banks Island, NWT. *Bulletin of Canadian Petroleum Geology* 19, 730–781.
- Evans, M.J., Elliott, T., 1999. Evolution of a thrust-sheet-top basin: the Tertiary Barreme basin. Alpes-de-haute-Provence, France. *GSA Bulletin* 111, 1617–1643.
- Féraud, G., Ruffet, G., Stéphan, J.F., Lapiere, H., Delgado, E., Popoff, M., 1995. Nouvelles données géochronologiques sur le volcanisme paléogène des Alpes occidentales: existence d'un événement magmatique bref généralisé. *Séance Spéciale de la Société géologique de France et de l' Association des Géologues du SE" Magmatismes dans le sud-est de la France"*, Nice, pp. 25–26.
- Flügel, E., 2010. *Microfacies of Carbonate Rocks: Analysis Interpretation and Application*. Springer, New York (984 pp.).
- Ford, M., Lickorish, W.H., Kuszniir, N.J., 1999. Tertiary foreland sedimentation in the Southern Subalpine Chains, SE France: a geodynamic appraisal. *Basin Research* 11, 315–336.
- Garzanti, E., 2019a. The Himalayan Foreland Basin from collision onset to the present: a sedimentary–petrology perspective. *Geological Society, London, Special Publications* 483, 65–122.
- Garzanti, E., 2019b. Petrographic classification of sand and sandstone. *Earth-Science Reviews* 192, 545–563.
- Geel, T., 2000. Recognition of stratigraphic sequences in carbonate platform and slope deposits: empirical models based on microfacies analysis of Palaeogene deposits in southeastern Spain. *Palaeogeography, Palaeoclimatology, Palaeoecology* 155, 211–238.
- Giammarino, S., Fanucci, F., Orezzi, S., Rosti, D., Morelli, D., 2010. Foglio 258–271 San Remo. Note illustrative della carta geologica d'Italia alla scala 1:50.000. Servizio Geologico d'Italia, Roma (136 pp.).
- Glenn, C., McManus, J.W., Talaue, L., Alino, P., Banzon, V., 1981. Distribution of live foraminifera on a portion of Apo Reef, Mindoro, Philippines. *Proceedings of the 4th International Coral Reef Symposium, Manilavol. 2*, pp. 775–781.
- Gupta, S., 1997. Tectonic control on paleovalley incision at the distal margin of the early Tertiary Alpine Foreland Basin, Southeastern France. *Journal of Sedimentary Research* 67, 1030–1043.
- Gupta, S., Allen, P.A., 2000. Implications of foreland paleotopography for stratigraphic development in the Eocene distal Alpine foreland basin. *GSA Bulletin* 112, 515–530.
- Halfar, J., Godinez-Orta, L., Mutti, M., Valdez-Holguin, J.E., Borges, J.M., 2004. Nutrient and temperature controls on modern carbonate production: an example from the Gulf of California. *Mexico. Geology* 32, 213–216.
- Hallock, P., 1980. Application of ecologic studies of living, algal symbiont-bearing foraminifera to paleoecologic interpretation. *AAPG Bulletin* 64, 716–717.
- Hallock, P., 1983. Larger foraminifera as depth indicators in carbonate depositional environments. *AAPG Bulletin* 67, 477–478.

- Hallock, P., 1984. Distribution of selected species of living algal symbiont-bearing foraminifera on two Pacific coral reefs. *The Journal of Foraminiferal Research* 14, 250–261.
- Hallock, P., Glenn, E.C., 1986. Larger foraminifera: a tool for paleoenvironmental analysis of Cenozoic carbonate depositional facies. *Palaaios* 1, 55–64.
- Hallock, P., Schlager, W., 1986. Nutrient excess and the demise of coral reefs and carbonate platforms. *Palaaios* 1, 389–398.
- Heikoop, J.M., Tsujita, C.J., Heikoop, C.E., Risk, M., Dickin, A., 1996. Effects of volcanic ashfall recorded in ancient marine benthic communities: comparison of a nearshore and an offshore environment. *Lethaia* 29, 125–139.
- Hohenegger, J., 1994. Distribution of living larger foraminifera NW of Sesoko Jima, Okinawa, Japan. *Marine Ecology* 15, 291–334.
- Hohenegger, J., 2000. Coenoclines of larger foraminifera. *Micropaleontology* 46, 127–151.
- Hohenegger, J., 2004. Depth coenoclines and environmental considerations of western Pacific larger foraminifera. *The Journal of Foraminiferal Research* 34, 9–33.
- Hohenegger, J., Yordanova, E., Nakano, Y., Tatzreiter, F., 1999. Habitats of larger foraminifera on the upper reef slope of Sesoko Island, Okinawa, Japan. *Marine Micropaleontology* 36, 109–168.
- Hohenegger, J., Yordanova, E., Hatta, A., 2000. Remarks on west Pacific Nummulitidae (foraminifera). *The Journal of Foraminiferal Research* 30, 3–28.
- Hottinger, L., 1983a. Processes determining the distribution of larger foraminifera in space and time. *Utrecht Micropaleontological Bulletin* 30, 239–253.
- Hottinger, L.K., 1983b. Neritic macroid genesis: an ecological approach. In: Peryt, T.M. (Ed.), *Coated Grains*. Springer-Verlag, Berlin, pp. 38–55.
- Hu, X., Garzanti, E., Li, J., BouDagher-Fadel, M.K., Coletti, G., Ma, A., Liang, W., Xue, W., 2021. The “underfilled trinity” from the western Alpine foreland basin: reality or myth? *Tectonics* (submitted).
- James, N.P., Kendall, P., 1992. Introduction to carbonate and evaporite facies models. In: Walker, R.G., James, N.P. (Eds.), *Facies Models: Response to Sea Level Change*. Geological Association of Canada, Ontario, pp. 265–275.
- Kabanov, P., Anadón, P., Krumbein, W.E., 2008. Microcodium: an extensive review and a proposed non-rhizogenic biologically induced origin for its formation. *Sedimentary Geology* 205, 79–99.
- Kempf, O., Pfiffner, O.A., 2004. Early Tertiary evolution of the North Alpine Foreland Basin of the Swiss Alps and adjoining areas. *Basin Research* 16, 549–567.
- Klappa, C.F., 1978. Biolithogenesis of *Microcodium*: elucidation. *Sedimentology* 25, 489–522.
- Košir, A., 2004. *Microcodium* revisited: root calcification products of terrestrial plants on carbonate-rich substrates. *Journal of Sedimentary Research* 74, 845–857.
- Langer, M.R., 1993. Epiphytic foraminifera. *Marine Micropaleontology* 20, 235–265.
- Lasker, H.R., 1980. Sediment rejection by reef corals: the roles of behavior and morphology in *Montastrea cavernosa* (Linnaeus). *Journal of Experimental Marine Biology and Ecology* 47, 77–87.
- Lees, A., Buller, A.T., 1972. Modern temperate-water and warm-water shelf carbonate sediments contrasted. *Marine Geology* 13, M67–M73.
- Less, G., 1987. Paleontology and stratigraphy of the European Orthophragminae. *Geologica Hungarica, series Palaeontologica* 51, 1–373.
- Less, G., Özcan, E., 2012. Bartonian–Priabonian larger benthic foraminiferal events in the western Tethys. *Austrian Journal of Earth Sciences* 105, 129–140.
- Leutenegger, S., 1984. Symbiosis in benthic foraminifera; specificity and host adaptations. *The Journal of Foraminiferal Research* 14, 16–35.
- Lickorish, W.H., Ford, M., 1998. Sequential restoration of the external Alpine Digne thrust system, SE France, constrained by kinematic data and synorogenic sediments. In: Mascle, A., Puigdefabregas, C., Luterbacher, H.P., Fernandez, M. (Eds.), *Cenozoic Foreland Basins of Western Europe*. Geological Society Special Publications vol. 134, pp. 189–211.
- Lokier, S.W., Al Junaibi, M., 2016. The petrographic description of carbonate facies: are we all speaking the same language? *Sedimentology* 63, 1843–1885.
- Lokier, S.W., Wilson, M.E.J., Burton, L.M., 2009. Marine biota response to clastic sediment influx: a quantitative approach. *Palaeogeography Palaeoclimatology Palaeoecology* 281, 25–42.
- Lüdmann, T., Kalvelage, C., Betzler, C., Fürstenau, J., Hübscher, C., 2013. The Maldives, a giant isolated carbonate platform dominated by bottom currents. *Marine and Petroleum Geology* 43, 326–340.
- Maino, M., Seno, S., 2016. The thrust zone of the Ligurian Penninic basal contact (Monte Frontè, Ligurian Alps, Italy). *Journal of Maps* 12, 341–351.
- Mateu-Vicens, G., Hallock, P., Brandano, M., 2009. Test shape variability of *Amphistegina* d’Orbigny 1826 as a paleobathymetric proxy: application to two Miocene examples. In: Demichuck, T., Gary, A. (Eds.), *Geologic Problems Solving With Microfossils*. SEPM Special Publication vol. 93, pp. 67–82.

- Minnery, G.A., Rezak, R., Bright, T.J., 1985. Depth zonation and growth form of crustose coralline algae: Flower Garden Banks, Northwestern Gulf of Mexico. In: Toomey, D. F., Nitecki, M.H. (Eds.), *Paleoalgology: Contemporary Research and Applications*. Springer, New York, pp. 237–246.
- Montenat, C., Leyrit, H., Gillot, P.Y., Janin, M.C., Barrier, P., 1999. Extension du volcanisme oligocène dans l'arc de Castellane (chaînes subalpines de Haute-Provence). *Géologie de la France* 1, 43–48.
- Mosbrugger, V., Utescher, T., Dilcher, D.L., 2005. Cenozoic continental climatic evolution of Central Europe. *Proceedings of the National Academy of Sciences* 102, 14964–14969.
- Mueller, P., Langone, A., Patacci, M., Di Giulio, A., 2018. Detrital signatures of impending collision: the deep-water record of the Upper Cretaceous Bordighera Sandstone and its basal complex (Ligurian Alps, Italy). *Sedimentary Geology* 377, 147–161.
- Mulder, T., Callec, Y., Parize, O., Joseph, P., Schneider, J.L., Robin, C., Dujonquoy, E., Salles, T., Allard, J., Bonnel, C., Ducassou, E., Etienne, S., Ferger, B., Gaudin, M., Hanquiez, V., Linare, F., Marches, E., Toucanne, S., Zaragosi, S., 2010. High-resolution analysis of submarine lobes deposits: seismic-scale outcrops of the Lauzanier area (SE Alps, France). *Sedimentary Geology* 229, 160–191.
- Murray, J.W., 2006. *Ecology and Applications of Benthic Foraminifera*. Cambridge University Press, Cambridge (426 pp.).
- Nebelsick, J.H., Rasser, M.W., Bassi, D., 2005. Facies dynamics in Eocene to Oligocene circumalpine carbonates. *Facies* 51, 197–217.
- Özcan, E., Less, G., Jovane, L., Catanzariti, R., Frontalini, F., Coccioni, R., Giorgioni, M., Rodelli, D., Rego, E.S., Kaygılı, S., Rostami, M.A., 2019. Integrated biostratigraphy of the middle to upper Eocene Kırkgeçit Formation (Baskil section, Elazığ, eastern Turkey): larger benthic foraminiferal perspective. *Mediterranean Geoscience Reviews* 1, 55–90.
- Perotti, E., Bertok, C., D'Atri, A., Martire, L., Piana, F., Catanzariti, R., 2012. A tectonically-induced Eocene sedimentary mélange in the Western Ligurian Alps, Italy. *Tectonophysics* 568–569, 200–214.
- Pomar, L., 2001. Ecological control of sedimentary accommodation: evolution from a carbonate ramp to rimmed shelf, Upper Miocene, Balearic Islands. *Palaeogeography, Palaeoclimatology, Palaeoecology* 175, 249–272.
- Pomar, L., Hallock, P., 2007. Changes in coral-reef structure through the Miocene in the Mediterranean province: adaptive versus environmental influence. *Geology* 35, 899–902.
- Pomar, L., Kendall, C.G.StC., 2008. Architecture of carbonate platforms: a response to hydrodynamics and evolving ecology. *Controls on Carbonate Platform and Reef Development*. SEPM Special Publication vol. 89, pp. 187–216.
- Pomar, L., Baceta, J.I., Hallock, P., Mateu-Vicens, G., Basso, D., 2017. Reef building and carbonate production modes in the west-central Tethys during the Cenozoic. *Marine and Petroleum Geology* 83, 261–304.
- Prager, E.J., Ginsburg, R.N., 1989. Carbonate nodule growth on Florida's outer shelf and its implications for fossil interpretations. *Palaios* 4, 310–312.
- Rasser, M.W., Piller, W.E., 1997. Depth distribution of calcareous encrusting associations in the northern Red Sea (Safaga, Egypt) and their geological implications. *Proceedings of the 8th international Coral Reef Symposium*, pp. 743–748.
- Ravenne, C., Vially, R., Riché, P., Trémolières, P., 1987. Sédimentation et tectonique dans le bassin marin Éocène supérieur – Oligocène des Alpes du Sud. *Revue de L'Institut Français du Pétrole* 42, 529–553.
- Reijmer, J.J.G., Bauch, T., Schäfer, P., 2012. Carbonate facies patterns in surface sediments of upwelling and non-upwelling shelf environments (Panama, East Pacific). *Sedimentology* 59, 32–56.
- Reiss, Z., Hottinger, L., 1984. *The Gulf of Aqaba: Ecological Micropaleontology*. Springer-Verlag (354 pp.).
- Renema, W., 2006. Habitat variables determining the occurrence of large benthic foraminifera in the Berau area (East Kalimantan, Indonesia). *Coral Reefs* 25, 351.
- Renema, W., 2018. Terrestrial influence as a key driver of spatial variability in large benthic foraminiferal assemblage composition in the Central Indo-Pacific. *Earth-Science Reviews* 177, 514–544.
- Renema, W., Troelstra, S.R., 2001. Larger foraminifera distribution on a mesotrophic carbonate shelf in SW Sulawesi (Indonesia). *Palaeogeography, Palaeoclimatology, Palaeoecology* 175, 125–146.
- Reymond, C.E., Zihrl, K.S., Halfar, J., Riegl, B., Humphreys, A., Hildegard, W., 2016. Heterozoan carbonates from the equatorial rocky reefs of the Galapagos Archipelago. *Sedimentology* 63, 940–958.
- Roberts, H.H., 1987. Modern carbonate-siliciclastic transitions: humid and arid tropical examples. *Sedimentary Geology* 50, 25–65.
- Sanders, D., Baron-Szabo, R.C., 2005. Scleractinian assemblages under sediment input: their characteristics and relation to the nutrient input concept. *Palaeogeography, Palaeoclimatology, Palaeoecology* 216, 139–181.
- Sartorio, D., Venturini, S., 1988. *Southern Tethys Biofacies*. Agip (235 pp.).
- Schaffer, W., 1972. *Ecology and Paleoecology of Marine Environments*. The University of Chicago Press, Chicago (568 pp.).
- Schiller, C., 1993. Ecology of the symbiotic coral *Cladocora caespitosa* (L.) (Faviidae, Scleractinia) in the Bay of Piran (Adriatic Sea): I Distribution and biometry. *Marine Ecology* 14, 205–219.

- Schlager, W., 2005. Carbonate Sedimentology and Sequence Stratigraphy (No. 8). SEPM Society for Sedimentary Geology (206 pp.).
- Serra-Kiel, J., Hottinger, L., Caus, E., Drobne, K., Ferrandez, C., Jauhri, A.K., Less, G., Pavlovec, R., Pignatti, J., Samsó, J.M., Schaub, H., Sirel, E., Strougo, A., Tambareau, Y., Tosquella, J., Zakrevskaya, E., 1998. Larger foraminiferal biostratigraphy of the Tethyan. *Bulletin de la Société géologique de France* 169, 281–299.
- Sinclair, H.D., 1997. Tectonostratigraphic model for underfilled peripheral foreland basins: an Alpine perspective. *Geological Society of America Bulletin* 109, 324–346.
- Sinclair, H.D., Naylor, M., 2012. Foreland basin subsidence driven by topographic growth versus plate subduction. *Bulletin* 124, 368–379.
- Sinclair, H.D., Sayer, Z.R., Tucker, M.E., 1998. Carbonate sedimentation during early foreland basin subsidence: the Eocene succession of the French Alps. In: Wrigth, V.P., Bruchette, T.P. (Eds.), *Carbonate Ramps*. Geological Society, London, Special Publications vol. 149, pp. 205–227.
- Smith, A.M., 1995. Palaeoenvironmental interpretation using bryozoans: a review. Geological Society, London, Special Publications 83, 231–243.
- Sturani, C., 1965. Presence de Palaeotherium et de pulmones dans l'Eocene Continental du Lauzanier. *Geologie Alpine* 41, 229–246.
- Sztrákó, K., Du Fornel, E., 2003. Stratigraphie, paléocéologie et foraminifères du paléogène des Alpes Maritimes et des Alpes de Haute-Provence (Sud-Est de la France). *Revue de Micropaléontologie* 46, 229–267.
- Tomás, S., Frijia, G., Bömelburg, E., Zamagni, J., Perrin, C., Mutti, M., 2016. Evidence for seagrass meadows and their response to paleoenvironmental changes in the early Eocene (Jafnayn Formation, Wadi Bani Khalid, N Oman). *Sedimentary Geology* 341, 189–202.
- Tomassetti, L., Bosellini, F.R., Brandano, M., 2013. Growth and demise of a Burdigalian coral bioconstruction on a granite rocky substrate (Bonifacio Basin, south-eastern Corsica). *Facies* 59, 703–716.
- Tomassetti, L., Benedetti, A., Brandano, M., 2016. Middle Eocene seagrass facies from Apennine carbonate platforms (Italy). *Sedimentary Geology* 335, 136–149.
- van den Hoeck, C., Mann, D.G., Jahns, H.M., 1995. *Algae: An Introduction to Phycology*. Cambridge University Press, Cambridge (623 pp.).
- Van der Zwaan, G.J., Jorissen, F.J., De Stigter, H.C., 1990. The depth dependency of planktonic/benthic foraminiferal ratios: constraints and applications. *Marine Geology* 95, 1–16.
- van Houten, F.B., 1973. Meaning of molasse. *Geological Society of America Bulletin* 84, 1973–1976.
- Varrone, D., Clari, P., 2003. Stratigraphic and paleoenvironmental evolution of the Microcodium Formation and the Numulitic Limestone in the French-Italian Maritime Alps. *Geobios* 36, 775–786.
- Varrone, D., D'Atri, A., 2007. Acervulinid macroid and rhodolith facies in the Eocene Nummulitic Limestone of the Dauphinois Domain (Maritime Alps, Liguria, Italy). *Swiss Journal of Geosciences* 100, 503–515.
- Varrone, D., D'Atri, D., 2007. Eocene larger foraminiferal biostratigraphy in the southernmost Dauphinois domain (Maritime Alps, France-Italy border). *Rivista Italiana di Paleontologia e Stratigrafia* 113, 257–267.
- Wade, B.S., Pearson, P.N., Berggren, W.A., Pälike, H., 2011. Review and revision of Cenozoic tropical planktonic foraminiferal biostratigraphy and calibration to the geomagnetic polarity and astronomical time scale. *Earth-Science Reviews* 104, 111–142.
- Westerhold, T., Röhl, U., 2013. Orbital pacing of Eocene climate during the Middle Eocene Climate Optimum and the chron C19r event: missing link found in the tropical western Atlantic. *Geochemistry, Geophysics, Geosystems* 14, 4811–4825.
- Williams, H.D., Burgess, P.M., Wright, V.P., Della Porta, G., Granjeon, D., 2011. Investigating carbonate platform types: multiple controls and a continuum of geometries. *Journal of Sedimentary Research* 81, 18–37.
- Wilson, B., 1998. Epiphytal foraminiferal assemblages on the leaves of the seagrasses *Thalassia testudinum* and *Syringodium filiforme*. *Caribbean Journal of Science* 34, 131–132.
- Wilson, E.J.W., Lokier, S., 2002. Siliciclastic and volcanoclastic influences on equatorial carbonates: insights from the Neogene of Indonesia. *Sedimentology* 49, 583–601.
- Zachos, J., Pagani, M., Sloan, L., Thomas, E., Billups, K., 2001. Trends, rhythms, and aberrations in global climate 65 Ma to present. *Science* 292, 686–693.
- Zachos, J.C., Dickens, G.R., Zeebe, R.E., 2008. An early Cenozoic perspective on greenhouse warming and carbon-cycle dynamics. *Nature* 451, 279–283.

9. Discussion and conclusions

The fundamental topic connecting all the various projects displayed in this thesis consists of the study and the application of benthic foraminifera, which have proven to be a valuable and reliable tool for paleoenvironmental reconstructions and stratigraphic analyses.

At the beginning of this thesis, two review papers were presented, offering a general overview and a quantitative analysis of different carbonate producers within the Cenozoic era. The first paper (Bialik et al., submitted) underscores the significance of a global, quantitative, and standardised analysis of skeletal assemblage compositions in shallow-water carbonate contexts. By combining literature data on skeletal assemblage compositions in modern carbonate sediments with satellite data on various abiotic factors (e.g., SST, WD, salinity), patterns in the distribution of carbonate producers relative to energy gradients, particularly solar and chemical energy, were identified. These findings suggest that similar skeletal assemblages may result from various combinations of factors. This is crucial for palaeoenvironmental analysis, as similar microfacies may be the result of diverse environmental conditions, or vice versa.

The second review paper (Coletti et al., 2022), based on an extensive literature dataset, demonstrates that foraminifera, particularly large benthic foraminifera, are the most voluminous carbonate producers during the Cenozoic, especially from the Palaeocene to the Miocene, with a peak in abundance during the Eocene. In simpler terms, volumetrically, most carbonate rocks within this time interval are composed of foraminifera. This implies that the study and analysis of these organisms are of paramount importance for advances in paleontological, ecological, and sedimentological research. Focusing on benthic foraminifera, it has been observed how they can be reliably used as paleoenvironmental and paleoecological proxies. Consequently, a research line regarding the use of benthic foraminifera as proxies for palaeo-seagrass has been developed. Since seagrass meadows are among the most important ecosystems in terms of ecosystem benefits and services, studying the evolution of these environments in light of current climate changes cannot disregard the analysis of their geological record. However, the fossil preservation of marine seagrasses is a rare process, as they are almost entirely composed of organic matter and thus prone to rapid decomposition. The study of epiphytic benthic foraminifera associations related to them has proven to be a powerful and reliable tool for this type of analysis. This has been observed and confirmed by studies conducted in Fauglia (Mariani et al., 2022a), and the Stirone River deposits (Mariani et al., 2022b). In particular, it has been possible to observe how the analysis of benthic foraminifera associations based on morphotypes, combined with the calculation of parameters such as the K/R_{EXT} ratio (which is simply a ratio between epiphytic and infaunal forms of similar morphology), can be used as a proxy to identify the presence of fossil seagrass meadows, thereby enhancing the resolution and reliability of palaeoenvironmental

reconstructions. However, preservation conditions of these associations and taphonomic and diagenetic processes that may have altered their composition, must always be considered.

In addition to relatively recent case studies (Pleistocene), chapters devoted to the study of older associations, particularly those related to the Eocene successions of Pag (Croatia) and the Alpine foreland basin (in western Liguria and southeastern France), have been presented.

Regarding the Eocene succession of Pag, through palaeontological and mesoscale sedimentological analysis of outcrops, as well as quantitative analysis of benthic foraminiferal associations and skeletal assemblages, a detailed understanding of the evolutionary dynamics of this foreland basin and the depositional environments that occurred simultaneously with the basin's structural development, was achieved. Benthic foraminifera proved to be highly reliable environmental indicators, enabling the differentiation of various facies within the succession. Moreover, a biofacies associated with fossil seagrass were recognised, identified through multiple IPSIs (Indirect Palaeo-Seagrass indicators, e.g., hooked acervulinids, planorbulinids, various types of encrusting foraminifera, rocks texture). Such a level of detail can only be attained through active observations of present-day environments (in this case, seagrass) and the study of exceptionally preserved fossils that can serve as reference points for the study of other sites (e.g., Fauglia).

Regarding the work centred on the Alpine foreland basin, in addition to the direct application of benthic foraminifera as environmental and stratigraphic indicators, an analysis of the role of terrigenous input in these contexts has been provided. Terrigenous input is commonly found within mixed carbonate-siliciclastic successions, particularly in foreland basin settings. Indeed, along with in-situ carbonate production, the transport of terrigenous material from the continental margin can reach significant levels. This allows us to understand how, in these cases, it is important to evaluate the effect of terrigenous input on carbonate producer associations within the basin. For some types of organisms (e.g., corals), terrigenous input can have a "destructive" effect on community development. However, this study has shown that free-living benthic foraminifera are among the carbonate producers that tolerate terrigenous input better. In contrast, encrusting foraminifera, with a sessile lifestyle, and coralline algae, tolerate terrigenous presence to a lesser extent. Nevertheless, these observations do not necessarily align with other studies on more recent environments, where it is demonstrated that coralline algae are among the groups that have developed significant tolerance to terrigenous input. This indicates how, over geological epochs, organisms may have developed tolerances to various ecological parameters and environmental factors.

This message must be clear when conducting environmental reconstructions. It is not sufficient to observe current associations and simply use the knowledge gained from them to describe fossil environments. One must consider all the possible complexities, and primarily three factors: i) space,

e.g., the type of basin within a specific fossil association is analysed, ii) time, e.g., the age of the deposits and consequently of the organisms in the geological record, and iii) the carbonate producers themselves. In fact, while they retain similarities to modern producers, they have undergone evolutionary processes that may have altered their adaptability to environmental stresses.

Within this thesis, various types of studies and applications have been explored, all unified by a common factor, namely benthic foraminifera. However, it is crucial to emphasize some key points in this research field that are essential for conducting reliable studies of benthic foraminifera communities and to apply them to palaeoenvironmental and stratigraphic reconstructions:

1. Taxonomy: correct taxonomic identification of foraminifera within the fossil assemblage is imperative. This does not mean that for every study or individual observed, species-level identification must be reached. Depending on the study's objectives, it is crucial to determine the minimum level of identification that provides detailed paleoecological or stratigraphic information, which depends significantly on the available material. When studying relatively recent sediments, it may be possible to achieve greater taxonomic detail compared to rocks thin-sections. In sediment studies, the foraminifera can be observed in three dimensions, and depending on their preservation state, all the details and morphological structures necessary for species identification can often be observed. However, it is worth considering that, depending on the type of study being conducted, it may not always be necessary to identify species. Correctly identifying a foraminifera species, especially for certain categories of them, can be time-consuming and, especially for fossil material, may always carry a degree of uncertainty. In certain cases, the identification of one species over another may not add significant palaeoecological insights to the study. In these cases, it might be more advantageous to settle for a less precise identification (e.g., at the genus level), as seen in the analysis of morphotypes. The analysis of morphotypes has proven to be highly reliable for paleoecological reconstructions, even if not all individuals are identified at the species level. However, it should be noted that the higher the level of taxonomic identification, the greater the reliability of the palaeoenvironmental reconstructions. Still, this only makes sense if the uncertainty in identifications is low. As can be easily deduced, the level of uncertainty in identifying individuals in thin-section is even higher. When it is not possible to provide a certain identification, it is more advantageous to stop at a less detailed level that can provide secure palaeoecological and stratigraphic indications. This was done for the works concerning the Dinaric and the Alpine foreland basins, where species identification was only performed when there were no uncertainties. However, the level of detail achieved allowed to obtain

reliable palaeoenvironmental reconstructions and possibly comparable with other case studies.

2. Comparison with modern associations: the study of fossil associations is intrinsically linked to the knowledge of modern associations. This does not mean that the principle of uniformitarianism should be applied irrationally when performing environmental reconstructions. Rational scrutiny is fundamental. Indeed, it is always essential to consider the differences that are present between modern and fossil environments. Moreover, it should be noted that each category of organisms has undergone evolutionary processes that have undoubtedly modified their adaptability to specific environments over geological epochs. Nevertheless, to achieve a correct interpretation of fossil microfacies, a comprehensive understanding of the dynamics governing current environments and ecosystems cannot be overlooked. This concept is very intuitive: we cannot interpret something that is no longer alive without a modern, current, and "living" reference point. The study of current environmental dynamics, the responses, and adaptations of carbonate producers to various biotic and abiotic factors within an ecosystem allows us to acquire tools that can be used to understand the geological record. However, it is essential to exercise caution when making paleoenvironmental reconstructions using this approach, as combinations of various factors can result in a similar skeletal assemblage, sediment texture, and, consequently, a similar microfacies. An additional and extremely powerful tool for comparison is the study of perfectly preserved fossil environments (as seen in the case of Fauglia), where it is possible to observe, within rocks and sediments, a precise snapshot of the environment when it was "alive." By carefully studying these rare case studies, we can obtain invaluable information about fossil carbonate producer communities without relying on indirect indicators. This is probably the most reliable tool at our disposal, but the disadvantage is that it is very difficult to observe this type of situation in the geological record due to various processes, such as transport, diagenesis, taphonomy, and even geodynamics, that contribute to altering the initial structure of an ecosystem.
3. Quantitative approach: undoubtedly, much of the information obtained about palaeoenvironmental reconstructions, stratigraphy, and palaeontology derived from qualitative/semiquantitative observations on fossils. The ability to observe and interpret is fundamental in every scientific discipline, but it is perhaps even more crucial when it comes to palaeontology. However, having quantitative data, such as individual counts, morphometric parameters, and faunal ratios, allows us to expand our palaeontological knowledge and perform more reliable paleoenvironmental reconstructions, that are also comparable with each

other. Having quantitative data, rather than a simple description of foraminifera associations in terms of observed species or present morphotypes, has provided the opportunity to calculate some parameters that have proven to be of significant paleontological importance. A clear example is the K/R_{EXT} ratio (Mariani et al., 2022a), which has allowed for a more "objective" assessment of environmental reconstructions in seagrass-dominated environments. These parameters are often relative, useful for comparing conditions across different sites rather than providing absolute values with specific ecological meanings. Nevertheless, having multiple parameters derived from counts (or measurements) allows us to say more about a particular type of environment. It also allows us to identify differences between situations that may not appear to differ based solely on qualitative observations or, conversely, to highlight similarities in cases where differences might be expected. Of course, the best approach to study involves both qualitative observations and quantitative analyses, enabling us to obtain the most detailed reconstructions as possible. Without quantitative data on skeletal assemblages, it would not have been possible to build the datasets on which the review papers presented in this thesis are based (Bialik et al., submitted; Coletti et al., 2022), nor would it have been possible to compare different sites to highlight differences and similarities. However, as well-known, statistics must be used with rigor and caution, and it should always be the scientist's judgment to determine whether correlations observed between two or more variables are indeed plausible and linked to the available data or simply the result of mathematical artifacts.

Much remains to be done within this field of research. Paleontology is a constantly evolving science, inexorably linked to new discoveries and technological advancements. Continuing to analyse different sites with a quantitative and standardized approach will enable the construction of a broader and more reliable database, allowing to achieve a more refined understanding of the distribution of carbonate producers throughout geological epochs. Furthermore, it is important to emphasize that this type of research is not an end in itself, as only by attaining a complete understanding of the evolution of fossil environments we can obtain insights into the possible evolution of these environments in the near future.